

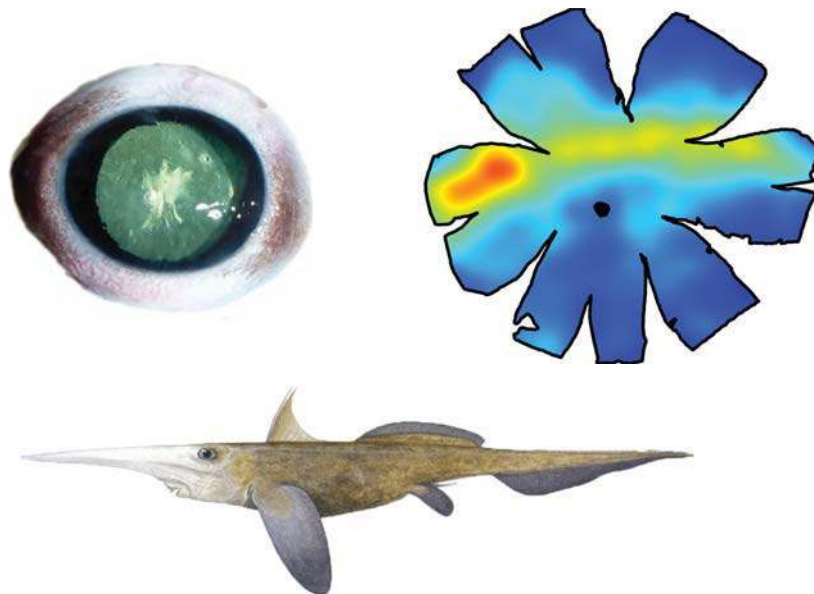


THE UNIVERSITY OF
**WESTERN
AUSTRALIA**

Visual Specializations and Light Detection in Chondrichthyes

Eduardo Garza-Gisholt

BSc (Marine Biology)
MAppSc



This thesis is presented for the degree of Doctor of Philosophy at
The University of Western Australia

School of Animal Biology
The Oceans Institute

2015

Summary

The visual ecology of representatives of the three groups of Chondrichthyes was analysed and compared to identify retinal and pineal specializations for photopic or scotopic vision in species from different habitats. The development of a new spatial analysis methodology to construct and analyse topographic retinal maps is also described. The typical arrangement of retinal photoreceptors and ganglion cells observed is a dorsal streak that affords the animal a high resolution panoramic view of the lower part of the visual field. The visual system in two species of deep-sea chimaeras: *Rhinochimaera pacifica* and *Chimaera lignaria* (rod-only retina specialized for scotopic vision with high sensitivity and high convergence of rods to ganglion cells) was compared to a demersal chimaera species *Callorhinchus milii* (duplex retina with both rods and cones). The visual system of the gummy shark, *Mustelus antarcticus*, another demersal species but from the Selachii, is similar to *C. milii*. Both *C. milii* and *M. antarcticus* show specializations to demersal habitats, where vertical migration markedly alters the ambient light conditions. Some photopic specializations (retinal duplicity) persist but the convergence between rods and ganglion cells is high, revealing adaptations for enhanced sensitivity. Five sympatric species of coral-reef dwelling stingrays from the Dasyatidae family (*Taeniura lymma*, *Neotrygon kuhlii*, *Himantura uarnak*, *Pastinachus atrus* and *Urogymnus asperrimus*) were compared and revealed specialisations for photopic vision with high numbers of cones and high spatial resolving power, in contrast to the other species of chondrichthyan examined (deep-sea and demersal species). The visual specializations within the stingrays reflect different ecological niches that may have promoted speciation or niche separation between the five sympatric species. An immunohistochemical analysis of cone photopigments using a long wavelength-sensitive (LWS) cone antibody in two species of ray (the bluespotted maskray, *Neotrygon kuhlii*, and the bluespotted fantail ray, *Taeniura lymma*) reveals that the proportion of labelled LWS cones to unlabelled cones is higher in *N. kuhlii* than in

T. lymma, which directly correlates to the amount of time spent in open sandy areas of the reef (*N. kuhlii*) versus resting under rocks and caves (*T. lymma*). The light conditions in shaded areas of the reef (with lower levels of long wavelength light) versus open, bright areas may place intense selection pressure on the type and density of retinal photopigment expressed within the retina. Immunohistochemical labelling of LWS cones in *C. milii* (in addition to populations of unlabelled cones) corroborates existing theories of the potential for colour vision. The detection of (non-image forming) light via the pineal organ in *N. kuhlii* and *C. milii* reveals a direct correlation between the morphology of the pineal and life history traits. Reproduction in *C. milii* might be triggered by increases in light intensity, as this species moves into shallow water, that is detected by the pineal, which is well developed compared to *N. kuhlii* and comprises a vesicle with multiple, long photoreceptors projecting into the lumen underlying a pineal window. The research fills a large gap in the visual ecology of the chimaeras and is the first comparative study of the morphology of the pineal organ between two species from different habitats.

Keywords

Visual ecology; retinal topographic maps; ganglion cell; cones; rods; photoreceptors; spatial resolving power; LWS cones; immunohistochemistry; Chondrichthyes; Holocephali; Elasmobranchii.

Abbreviations

CNS	Central nervous system
GCL	Ganglion cell layer
Gks	Gaussian kernel smoother
INL	Inner nuclear layer
IPL	Inner plexiform layer
IS	Inner segment
LWS	Long wave sensitive
MS222	Tricaine methane sulfonate
MWS	Medium wave sensitive
ONL	Outer nuclear layer
OS	Outer segment
PB	Phosphate buffer
PBA	Phosphate buffer azide
PFA	Paraformaldehyde
PR	Photoreceptor
RE	Retinal epithelium
RGC	Retinal ganglion cells
Rh1	Rhodopsin 1
Rh2	Rhodopsin 2
SRP	Spatial resolving power
SWS	Short wave sensitive
Tps	Thin plate spline

Table of Contents

Summary	I
Keywords	II
Abbreviations	III
Table of Contents	V
List of Figures	IX
List of Tables	XV
Acknowledgements	XVI
Declaration by Author	XIX
Statement of Contribution	XIX
Publications arising from work in this thesis	XIX
Chapter 1 Introduction	1
Chondrichthyes: chimaeras, sharks and rays	1
Vision in Chondrichthyes	3
Non-visual light detection.....	9
Species to be analysed.....	11
Aims	13
Hypotheses	14
Significance and expected outcomes	15
Chapter 2 A comparison of spatial analysis methods for the construction of topographic maps of retinal cell density	17
Abstract	17
Keywords	18
Introduction	18
Methods	23

Results	28
Choosing between different models	28
Choosing different smoothing parameters	30
Analysing different specializations	34
Special case - Fovea	40
Discussion	42
Acknowledgements.....	48
Chapter 3 Retinal topography in juvenile gummy sharks, <i>Mustelus antarcticus</i> : Implications for visual ecology and fisheries management	49
Abstract.....	49
Keywords	50
Introduction.....	50
Methods.....	54
Collection of animals	54
Eye dissection and visualization of photoreceptors and ganglion cells	54
Stereological assessment of cell density	56
Construction of iso-density contour maps	57
Retinal summation maps and calculation of spatial resolving power	58
Results	59
Discussion	64
Acknowledgements.....	68
Chapter 4 Retinal characteristics and visual specializations in three species of chimaeras, the deep sea <i>Rhinochimaera</i> <i>pacifica</i> and <i>Chimaera lignaria</i> , and the vertical migrator <i>Callorhinchus milii</i>	69
Abstract.....	69
Keywords	70
Introduction.....	70
Methods.....	75
Collection of animals	75

Eye dissection and visualization of photoreceptors and ganglion cells	75
Retinal summation maps and calculations of spatial resolving power	77
Histology of the retina and the calculation of optical sensitivity	78
Results.....	80
Photoreceptor morphology and topographic distribution	80
Ganglion cell characterization and topography	86
Summation maps	88
Spatial resolving power and optical sensitivity	89
Discussion	90
Acknowledgements.....	96
 <i>Chapter 5 Visual specializations in five sympatric species of stingrays from the family Dasyatidae from Ningaloo Reef, Western Australia</i>	 97
Abstract	97
Keywords	98
Introduction	98
Methods	103
Ethics Statement	103
Specimen Collection	103
Eye enucleation and retinal dissection	104
Average maps and transects	106
Spatial resolving power and retinal summation	107
Results.....	107
Discussion	118
Ganglion cell distribution	119
Focal length and spatial resolving power	121
Summation ratio of photoreceptors to ganglion cells	124
Visual ecology	126
Acknowledgements.....	128
 <i>Chapter 6 Immunohistochemical labelling of a long wavelength-sensitive cone opsin in the retina of three species of cartilaginous fishes (Chondrichthyes)</i>	 129

Abstract.....	129
Keywords	130
Introduction.....	130
Methods.....	133
Results	136
Discussion	139
Acknowledgements.....	143
Chapter 7 The morphology of the pineal organ in Chondrichthyes: a comparison between the elephant shark (<i>Callorhynchus milii</i> : Holocephali) and the bluespotted maskray (<i>Neotrygon kuhlii</i> : Elasmobranchii)	145
Abstract.....	145
Keywords	146
Introduction.....	146
Methods.....	148
Results	150
Discussion	155
Acknowledgements.....	158
Chapter 8 General Discussion	159
References	165
Appendix I	187
Original R Script to extract information from Stereoinvestigator in xml format, submitted for publication in PLOS one	187
Alternative method to extract information from .svg file	195
Hybrid method to combine thin plate spline with interpolation for a fovea from Chapter 2	196
Script to separate different population of cells (rods, cones of cone subtypes).	198
Method to combine and average multiple retinas	199
Method to calculate the summation ratio between photoreceptors and ganglion cells.	203
Method to save plots with Arial font for publications	207

List of Figures

Figure 1.1 Schematic diagram of a teleost eye and the direction of the incident light.	4
Figure 1.2 Schematic diagram of the position of the pineal organ in elasmobranchs	10
Figure 1.3 Diagram showing the light absorption in clear oceanic water at different depths and the relative depth range of each species analysed in this study.	13
Figure 1.4 Cladogram of the taxonomic position of the different species in the study.	14
Figure 2.1 Topographic maps of the ganglion cells in the retina of the Pacific spookfish, <i>Rhinochimaera pacifica</i> .	29
Figure 2.2 Topographic maps of the ganglion cells in the retina of the coral cod, <i>Cephalopholis miniatus</i> that show an area temporalis specialization.	31
Figure 2.3 Horizontal and vertical transects, and residual analysis of the two levels of smoothness for the coral cod, <i>Cephalopholis miniatus</i>	32
Figure 2.4 Topographic maps of the ganglion cells in the retina of the blue tusk fish, <i>Choerodon albigena</i> , that show a horizontal streak with a dorso-temporal area specialization ² .	33
Figure 2.5 Horizontal and vertical transects, and residual analysis of the two levels of smoothness for the blue tusk fish, <i>Choerodon albigena</i> .	34
Figure 2.6 Topographic maps of the ganglion cells in the retina of the staghorn damselfish, <i>Amblyglyphidodon curacao</i> , that show multiple areae specializations.	36
Figure 2.7 Topographic maps of the ganglion cells in the retina of the collared sea bream, <i>Gymnocranius bitorquatus</i> , that show a dorsal area specialization	37
Figure 2.8 Topographic maps of the ganglion cells in the retina of the sandperch, <i>Parapercis cylindrica</i> , that shows a horizontal streak with three areae specializations	39
Figure 2.9 Topographic maps of the ganglion cells in the retina of the smooth-head fish, <i>Conocara murrayi</i> , which shows a fovea ² .	41
Figure 3.1 Ganglion cell density maps in the gummy shark, <i>Mustelus antarcticus</i>	60
Figure 3.2 Rod cell density maps in the gummy shark, <i>Mustelus antarcticus</i>	62
Figure 3.3 Cone cell density maps in the gummy shark, <i>Mustelus antarcticus</i>	63
Figure 3.4 Summation maps between photoreceptor and ganglion cells in the retina of the gummy shark, <i>Mustelus antarcticus</i>	63
Figure 4.1 The eyes of chimaeras and their tapetal eyeshine	81
Figure 4.2 Retinal morphology of the elephant shark, <i>Callorhynchus milii</i>	82
Figure 4.3 Axial view of the wholemounted retina of the giant chimaera, <i>Chimaera lignaria</i> and the elephant shark, <i>Callorhynchus milii</i>	83
Figure 4.4 Topographic maps of the cone photoreceptor distributions in the elephant shark, <i>Callorhynchus milii</i>	85
Figure 4.5 Isodensity contour maps of the rod photoreceptor distribution in the three species of chimaeras	86

<i>Figure 4.6 Isodensity contour maps of the ganglion cell distribution in the three species of chimaeras.</i>	87
<i>Figure 4.7 Summation maps showing the ratio of rod cells per ganglion cell in the three species of chimaeras</i>	89
<i>Figure 5.1 Average retinal cell density maps in the bluespotted fantail ray, Taeniura lymma.</i>	108
<i>Figure 5.2 Average retinal cell density maps in the bluespotted maskray, Neotrygon kuhlii.</i>	110
<i>Figure 5.3 Average retinal cell density maps in the reticulated whipray, Himantura uarnak.</i>	111
<i>Figure 5.4 Average retinal cell density maps in the cowtail ray, Pastinachus atrus.</i>	113
<i>Figure 5.5 Average retinal cell density maps in the porcupine ray, Urogymnus asperrimus.</i>	114
<i>Figure 5.6 Transects across the retinal maps comparing cell density across the five species.</i>	115
<i>Figure 5.7 Ganglion cell, amacrine cell density distribution maps and amacrine cell proportions from the total cell numbers in the retina in the five species of rays</i>	117
<i>Figure 6.1 Petri dish set for change of solutions for the immunohistochemical protocol with the plastic mesh designed for handling the free floating retinal wholemounts.</i>	135
<i>Figure 6.2 Light micrographs of the positive immunolabelling for LWS opsin in the outer segments of the retinal cones in wholemount using CERN 956</i>	137
<i>Figure 6.3 Average topographic density maps of the cone distribution in the three species that showed LWS antibody labelling.</i>	138
<i>Figure 7.1 Position of the pineal gland in the brain of the elephant shark, Callorhinchus milii.</i>	151
<i>Figure 7.2 Position of the pineal gland in the ventral portion of the cartilage in the skull of the bluespotted maskray, Neotrygon kuhlii</i>	153
<i>Figure 7.3 Light micrographs of the pineal gland in a 2 μm thick transverse section of the pineal gland</i>	154

List of Tables

<i>Table 1-1. Ecological information of the species in the present study.</i>	12
<i>Table 3-1. Eye morphometrics and stereological data for the ganglion cells, rods and cones in the four retinas of the juvenile gummy shark, <i>Mustelus antarcticus</i>.</i>	61
<i>Table 4-1. Average total number of photoreceptors per retina and number of photoreceptors in the peak of the specialization..</i>	84
<i>Table 4-2. Average total number of ganglion cells per retina and number of ganglion cells in the peak of the specialization.</i>	88
<i>Table 4-3. Anatomical characteristics of the lens, spatial resolving power and optical sensitivity for the three species of chimaeras.</i>	90
<i>Table 5-1. Retinal data of the specializations of the ganglion cells, rods and cones in the five species.</i>	116
<i>Table 6-1. Size, depth range and cone photoreceptor data for three species with positive immunoreactivity to the LWS antibody: <i>Callorhinchus milii</i>, <i>Taeniura lymma</i> and <i>Neotrygon kuhlii</i> for each species</i>	139
<i>Table 7-1. Measurements of the pineal gland, pineal stalk and cartilage thickness in the two species of Chondrichthyes, the bluespotted maskray <i>Netorygon kuhlii</i> and the elephant shark, <i>Callorhinchus milii</i>.</i>	152

Acknowledgements

"Lord, you said that once I decided to follow you, you'd walk with me all the way. But I have noticed that during the most troublesome times in my life there is only one set of footprints. I don't understand why when I needed you most you would leave me."

The Lord replied: "My precious, precious child, I love you and would never leave you. During your times of trial and suffering, when you see only one set of footprints in the sand, it was then that I carried you." **(Mary Stevenson, 1936)**

This thesis is dedicated to my beautiful family that was with me during this time until the end. Mariana, I don't have words to thank you so much for your patience, unconditional support, hard work and especially for sharing this adventure with me even if it sounded crazy at the beginning. Danielle, baby you born during my first year of my PhD and you have grown so much since then. You are my biggest inspiration and motivation; one simple smile can make wonders.

I want to thank my supervisors Shaun and Nathan for everything; first for believing in me and my crazy ideas, and then for all your support and good advice. I really appreciate that even though you are busy researchers your door was always open for me and you were always available to discuss any aspect of my research as trivial as it sounded. It really amazes me how quickly you reviewed my work.

Caroline thanks so much for being always there. You helped me so much during my PhD that I can't thank you enough. Thanks for helping

with all the bureaucracy, paper work, for pushing me when I needed a push and for hugging me when I needed a hug. Michael, thank you for all your patience teaching me so much in the lab. So many times that I needed you to repeat the things that I forgot so quickly. Also thank you for keeping the flow of coffee during my research. Thanks to all the staff of the lab Jan, Wayne, Kara, David, Carl and all the “senior” researchers for all your input. Obviously thanks to all the staff of the School of Animal Biology, Graduate Research School and UWA in general. You were always helpful and friendly when I needed you.

Thanks to all the members of the neuroecology lab. I can't believe with how many friends I have at the end of the journey. I can't tell you guys how much I appreciate you, the good moments that we spent are unforgettable (well, maybe I already forgot some moments because of the alcohol). Joao Paulo first of all thank you buddy for everything. Thank you for showing me the secrets of the retinal topography and Stereology, thank you for all your good teaching and good example in the lab. I really owe you a great part of my research education. Ryan and Channing; thank you guys for being patient with me and all my bad jokes about veggies, pommies, greenies and more. The time that we spent in the field was some of the best moments of my PhD. Nicu and Lulu you have an amazing vibe, thank you for all the energy that you gave me. Nick, please, grow up but never change buddy. Rachael, Luke, Laura, Nick R., Tony and Carlitos, thank you so much for all the support, all the lunches together, all the talks and laughs that we shared but also thank you for being patient when I was having really bad moments and I needed some space. Fanny, Audrey, Marcin, Lee, Lauren P. Rebecca, Lauren B., Jess, Lars, Julien, Ugo, Vicky, Roland and I hope I don't forget anyone. Thanks so much for all the moments even if in some cases were too short, thanks so much for being part of this wonderful lab.

Thanks to all my Mexican friends, you were our family in Perth and I can't tell you how much I love you. Leo and Andrea, Monica and Cesar, Jior and Aletzin, Lasha and Luis, Paty and Hector, Cynthia and Jose Luis, Jorge and Susana, Angelica and Andrei and all the respective kids thanks so much for all the moments that we spent, all the food, drinks, laughs and experiences. Cuco, Cesar and Aletzin thanks so much for all the advice in how to finish this "thing". Monica, Jior, Paty, Cuca thanks for everytime that you took care of Danielle. And especially thanks for all the support during difficult moments, it hasn't been easy to finish but thanks to all of you I could make it!!!

Thanks to my parents and my sisters because even if we are far away, you are in my heart and you always make me feel so close. Ceci you are a wonderful sister and now you have a beautiful family. Tani you are stronger than I could imagine, you are my little sister but you are not that little anymore.

Thanks to all my friends and family in all the places that I have lived. I could write pages and pages but I think I have to finish. You all had an influence on who I am now so I really appreciate you even if the distance is large. I apologize because I am sure I didn't mention many people that I should but thank you for everything.

But special thanks to God for giving me life, for making me like I am with all my defects and virtues.

Declaration by Author

This thesis is result of my original work, and contains no material previously published or written by another person except where due reference has been made in the text. The material has not been submitted, either in whole or in part, for a degree at this or any other institution

Statement of Contribution

The work presented in this thesis is the original work of the author. This thesis contains work submitted for publication, some of which has been co-authored. The statistical analyses and manuscript preparation was carried out by the author of this thesis and discussed in extensive detail with the co-authors of the submitted paper W Prof Shaun Collin, Assoc Prof Jan Hemmi and Assoc Prof Nathan Hart before submission to the journal.

Eduardo Garza-Gisholt
September 2015

Publications arising from work in this thesis

- Chapter 2

Garza-Gisholt, E., Hemmi, J.M., Hart, N.S. and Collin, S.P. 2014 A comparison of spatial analysis methods for the construction of topographic maps of retinal cell density. PLOS One 9(4): e93485

- Chapter 3

Garza-Gisholt, E., Hart, N.S. and Collin, S.P. Retinal topography in juvenile gummy sharks, *Mustelus antarcticus*: Implications for visual ecology and fisheries management.

In preparation for Marine and Freshwater Research

- Chapter 4

Garza-Gisholt, E., Hart, N.S. and Collin, S.P. Retinal characteristics and visual specializations in three species of chimaeras, the deep sea *Rhinochimaera pacifica* and *Chimaera lignaria*, and the vertical migrator *Callorhinchus milii*.

Submitted and accepted with minor changes for Journal of Comparative Neurology

- Chapter 5

Garza-Gisholt, E., Hart, N.S., Kempster, R.M. and Collin, S.P. 2015 Visual specializations in five sympatric species of rays from the family Dasyatidae from Ningaloo Reef, Western Australia.

Brain, Behaviour and Evolution 85(4) 217-232

- Chapter 6

Garza-Gisholt, E., Hunt, D.M., Davies, W.I., Hart, N.S. and Collin, S.P. Immunohistochemical labelling of a long wavelength-sensitive cone opsin in the retina of three species of cartilaginous fishes (Chondrichthyes).

It will be combined with *in situ* molecular studies in the retina in collaboration with Davies and Hunt.

- Chapter 7

Garza-Gisholt, E., Leask, J., Hunt, D.M., Hart, N.S. and Collin, S.P. The morphology of the pineal organ in Chondrichthyes: a comparison between the elephant shark (*Callorhinchus milii*: Holocephali) and the bluespotted maskray (*Neotrygon kuhlii*: Elasmobranchii).

It will be combined with immunohistochemistry studies to label different types of opsin and with electron microscopy studies to describe the organization of the pineal in collaboration with Leask and Hunt.

Chapter 1 Introduction

Chondrichthyes: chimaeras, sharks and rays

Class Chondrichthyes is one of the most ancient groups of vertebrates. This diverse group originated from the first Gnathostomata or jawed vertebrates around 400 million years ago, during the late Silurian period. More than 1,200 species of chondrichthyans live in the water systems of the world today. This corresponds to approximately 5% of the total number of modern fish species (Lund and Grogan, 1997, Lamb et al., 2007, Last and Stevens, 2009). The two groups of cartilaginous fishes; Holocephali and Elasmobranchii are sister taxa within the Chondrichthyes (Ebert, 2003, Compagno et al., 2005, Grogan et al., 2012). These two groups are considered monophyletic subclasses of the Class Chondrichthyes (Arnason et al., 2001, Grogan et al., 2012)

The class Chimaeriformes (holocephalians) include less species than the Elasmobranchii (sharks and rays). There are only three families, containing six genera and about 47 species compared to the 630 species of rays and close to 500 species of sharks (Ebert, 2003, Compagno et al., 2005, Last and Stevens, 2009, Didier et al., 2012). The body of holocephalians is generally compressed with a silvery to dark coloration, possessing a gill cover that protects four gill openings. Chimaeras do not possess denticles on the body like sharks or rays and have a spine located rostral to the first dorsal fin. They also have large eyes with a golden coloured light reflex emanating from the eye in the dark-adapted condition. Most live mainly in deep water but some species found in relatively shallow water are considered commercially important (Compagno, 2001, Compagno et al., 2005, Last and Stevens, 2009, Didier et al., 2012).



Elasmobranchii is a group that includes sharks and rays. Sharks or Selachii can be divided into a primitive group (Squalomorpha) and a more recent group (Galeomorpha). Rays are members of the superorder Batoidei. The phylogenetic relationship between the Selachii and the Batoidei has been the subject of debate (Dunn and Morrissey, 1995, Naylor et al., 2005, Naylor et al., 2012, Aschliman et al., 2012a). The two major morphological differences between sharks and rays are centred on their gill openings and pectoral fins. Sharks typically possess between five and seven gill openings situated on the side of their head, whereas rays have only five, located ventrally. The pectoral fins of the sharks are paired structures, which originate behind the head and extend outwards, while those of the rays are fused to the head (Compagno, 2001, Compagno et al., 2005).

Chondrichthyes is a very diverse group of aquatic organisms that live mainly in the ocean with only some species residing in freshwater. They inhabit most marine ecosystems from estuaries and reefs to the deep-sea. Foraging behaviour and surveillance are directly related to their habitat. Consequently, members of the chondrichthyans have a wide range of feeding preferences from plankton feeders to active predators, and also possess morphological adaptations to cope with the environment in which they live and the behaviours they perform. Chondrichthyans, like all vertebrates, are highly complex animals that rely on different sensory systems to detect and interact with their surroundings (Bres, 1993). Chondrichthyans possess a range of sensory systems (besides vision) that have been studied, such as the mechanical senses i.e. the lateral line and audition (Roberts, 1978, Maruska, 2001, Peach and Marshall, 2009), the chemical senses i.e. olfaction and gustation (Hodgson and Mathewson, 1978, Schluessel et al., 2008, Meredith and Kajiura, 2010) and electroreceptive system (Fields and Lange, 1980, Kalmijn, 1982, Sisneros and Tricas, 2002, Freitas et al., 2006). Holocephali is an understudied group within the Chondrichthyes

and Lisney (2010) has recently published an excellent review of the current knowledge of the different senses.

Vision in Chondrichthyes

Light is a part of the electromagnetic spectrum and is detected by either the visual (image-forming eyes) or the non-visual (non-image forming pineal organs) systems. The light environment habitat is composed of spatial, temporal and spectral elements that define the quality of vision required by an animal to survive (Hueter, 1991a). The mechanism of detecting colour or contrast by the eyes of chondrichthyans (as in all vertebrates) is a complex process that is studied by different disciplines including anatomy, biochemistry, physiology, neurology and physics (Ripps and Weale, 1969).

Aquatic vertebrates use their eyes to detect light and form a focused image in a range of different light environments. Light passes through the cornea which, in chondrichthyans like other marine organisms, has a refractive index very similar to the surrounding water thereby nullifying its role in refraction. Therefore, the only refractive element in the aquatic eye is the crystalline lens, which enables a focused image to be formed on the retina (Figure 1.1) (Hueter and Gruber, 1980, Hueter, 1991a). After entering the eye, light passes through the retina to strike the photoreceptors. At the level of the photoreceptors, light is transformed from light energy to a biochemical signal by a process called phototransduction. Visual signals are then transmitted through to the inner retina via a series of interneurons (bipolar, horizontal and amacrine cells) to reach the ganglion cells, each of which possesses an axon that projects to the visual centres of the brain via the optic nerve (Ramon y Cajal, 1972, Glickstein, 1976).

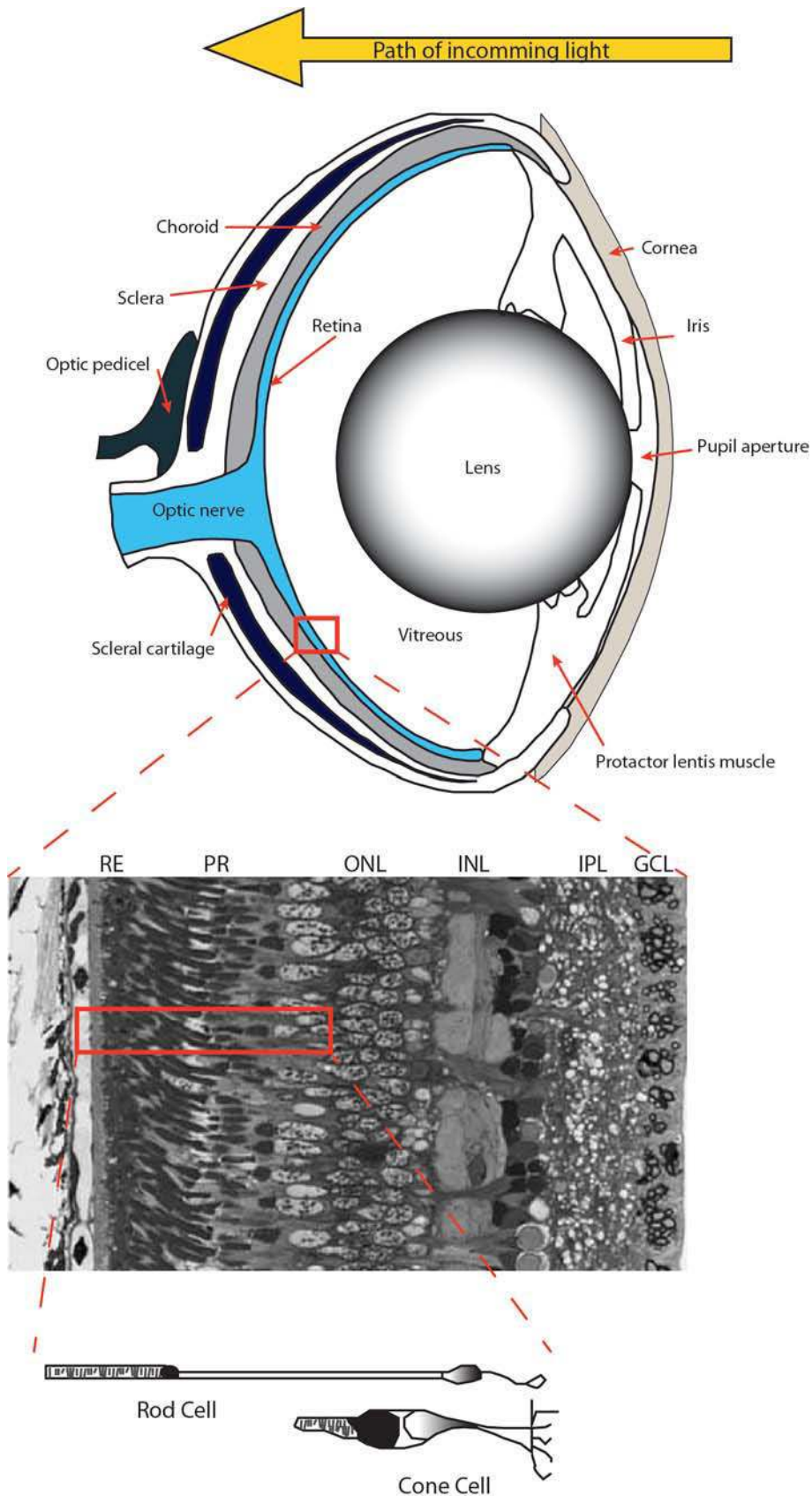


Figure 1.1 Schematic diagram of a teleost eye and the direction of the incident light. The light micrograph represents a higher power representation of the retina in cross section showing the variety of the retinal layers. The cellular schematic depicts the morphological differences between cone and rod photoreceptors. RE retinal epithelium, PR photoreceptors, ONL outer nuclear layer, INL inner nuclear layer, IPL inner plexiform layer, GCL ganglion cell layer
Modified from Walls (1942), Gilbert (1963) and Schieber et al. (2012).

Two major types of photoreceptor cells have been identified in vertebrates. According to their shape they are classified as cones and rods. The cones are adapted for bright light or photopic vision and the rods are adapted for dim light or scotopic vision (Bailes et al., 2006, Collin, 2008). The distribution of cones and rods in the retina changes according to the visual demands of each organism (Berkley, 1976). Localised increases in the density of photoreceptors indicate higher acuity or spatial resolving power in some specific area(s) of the visual field. A rod-based retina is less acute than a retina with a high proportion of cones and will convey high sensitivity (Lythgoe, 1979, Lythgoe, 1984). The outer segment of each photoreceptor houses a visual pigment that is chemically composed of an opsin protein coupled with a chromophore and it is this visual pigment that is responsible for absorbing light. There are two types of chromophores in vertebrates: the rhodopsins based on vitamin A₁ and porphyropsins based on vitamin A₂ (Bowmaker, 1995, Collin, 2010). In evolutionary terms, it seems that rods are more recent than cones (Bowmaker, 2008, Collin, 2009). There are five different visual pigment (opsin) genes in early vertebrates; LWS, SWS1, SWS2, RH1 and RH2 (Collin et al., 2003, Lamb et al., 2007), all of which were present in the last common ancestor of the jawed and jawless vertebrates. Colour vision is the capacity of an organism to discriminate between different wavelengths of light. Some organisms detect the ultraviolet (UV) part of the spectrum, while others are tuned to wavelengths in the visible range (400-700nm). In order to perceive colour, it is necessary to compare the outputs of more than one type of cone photoreceptor with a different spectral sensitivity. Some organisms are dichromatic (possess two spectrally different cone photoreceptor types such as many reef fish), while others are trichromatic (e.g. humans) or even tetrachromatic (e.g. birds and reptiles) (Carter, 1948, Vorobyev et al., 1998, Surridge et al., 2003, Hofer et al., 2005).



Several studies in elasmobranchs have investigated the number, type and distribution of photoreceptors. Elasmobranchs have a duplex retina, which means that they have both cones and rods (Gruber et al., 1975a, Dowling and Ripps, 1991, Gruber et al., 1991, Hart et al., 2006, Litherland and Collin, 2008). Using microspectrophotometry (MSP), Theiss et al. (2007) found that *Neotrygon kuhlii* (= *Dasyatis kuhlii*) possess three types of cone visual pigments. Other species of rays also have trichromatic vision (Hart et al., 2004). Recently, Davies et al. (2009) studied the molecular expression of the visual pigments in the elephant shark, *Callorhynchus milii*, and found a single rod pigment (RH1) and three cone pigments (RH2, LWSa, LWSb). However, the few species of sharks that have been studied only show one type of cone pigment (Hart et al., 2011, Theiss et al., 2012).

Other retinal cells have fundamental roles in light detection and transmission. Ganglion cells are important because they receive information from the photoreceptors and send these messages (via axons) to the brain as electrical impulses. Therefore, the ganglion cells act as somewhat of a bottleneck before conveying information centrally (Berkley, 1976, Collin and Pettigrew, 1989). The distribution of ganglion cells in the retinae of different species of chondrichthyans has been analysed and a greater density of cells has been found across the horizontal meridian (a specialization called a horizontal streak). This pattern indicates a higher acuity across a panoramic region of the visual field, a pattern that is common to almost all species of elasmobranchs examined thus far (Peterson and Rowe, 1980, Collin, 1988, Bozzano and Collin, 2000, Lisney and Collin, 2008, Litherland and Collin, 2008, Schieber et al., 2012). In some benthic species like the epaulette shark, *Hemiscyllium ocellatum*: the blue-spotted stingray, *Dasyatis kuhlii* and the ornate wobbegong, *Orectolobus ornatus*, the densities and topography of ganglion cells and photoreceptors are related to a benthic habitat. The densities are higher in the dorsal retina, which indicates an increase in spatial resolving power within the

lower lateral and frontal parts of the visual fields (Theiss et al., 2007, Litherland and Collin, 2008). In another study, which examined 10 species of elasmobranchs, Lisney and Collin (2008) found that all the ganglion cell distributions were heterogeneous in the different regions of the retina.

Spatial resolving power is the capacity to distinguish between two different objects and to create an image, whereas contrast sensitivity is the capacity to differentiate the lightest and the darkest part of an object and depends on the colour and the brightness of the object in the field of view (Gouras, 1991). The ganglion cell mosaic responds to the contrast of an object. The anatomical spatial resolving power of the retinal ganglion cell mosaic has been calculated for a large number of chondrichthyans and a direct correlation between habitat and visual acuity has been observed, where organisms that live in dim light have lower spatial resolving power and organisms that live in bright light require a higher spatial resolving power (Hart et al., 2006, Lisney and Collin, 2008, McComb et al., 2009, McComb et al., 2010). In the central area of the retina of some organisms, the responses of photoreceptors is conveyed to only a small number of ganglion cells (low convergence ratio), while in the periphery, photoreceptor responses are summed over many more receptors and converge onto a single ganglion cell (high convergence ratio). This trade-off between sensitivity and visual acuity depends on a range of ecological factors. It is not only important to identify a possible prey object from the background but also to identify it as a potential predator (Marshall and Vorobyev, 2003). The convergence information from the photoreceptor to the ganglion cells has been neglected in most of the topographic studies, but in four species of sharks studied by Litherland and Collin (2008), the densities of photoreceptors and ganglion cells were in register across the retina with high densities of both types of cells found in the visual streak of each species.



The environmental diversity in which chondrichthyans can be found plays an important role in the visual characteristics of each species. In general, organisms living in open environments have specializations for a panoramic view (mediated by an area of acute vision often termed a horizontal streak), while animals that live in more three dimensional environments such as a coral reef have specializations for a more concentrated zone of acute vision (Hughes, 1975, Hughes, 1977, Collin and Pettigrew, 1988b, Collin and Pettigrew, 1988c). In shallow waters, the animals should have visual specializations that take advantage of the higher levels of illumination. With increasing depth in the ocean, long and short wavelengths are differentially absorbed, leaving restricted parts of the visible spectrum available for colour vision (Lythgoe, 1979, Warrant and Locket, 2004). Below 100 m, the wavelengths of light are even more attenuated, predominantly leaving the blue-green parts of the visible spectrum. In addition, deep-sea organisms would be expected to possess adaptations that permit them to detect very low levels of light (Douglas et al., 2003, Warrant and Locket, 2004). Due to the lack of sunlight below 1000 m, many organisms have developed strategies to produce light flashes in the form of bioluminescence (Herring, 2000). Production of bioluminescence has different purposes: some animals use it to attract prey; while others use it to camouflage themselves using ventral photophores to confuse predators or to mediate intraspecific communication (Denton, 1963, Herring, 1977).

Some chondrichthyans have adaptations to increase or reduce the light entering the eye or stimulating the photoreceptors. The *tapetum lucidum* is a layer of cells that increases the quantity of light striking the photoreceptors. This layer is located behind the retina and acts like a mirror, reflecting the light back onto the photoreceptors to increase sensitivity and is usually found in animals that live in dim light environments (Kuchnow and Martin, 1970). Some elasmobranchs have an occlusible *tapetum* that can be occluded under bright light

conditions. This adaptation is very advanced in some sharks because it allows them to see in both bright light and dark conditions (Denton and Nicol, 1964, Heath, 1991, Dowling, 1997, Hart et al., 2006) by masking the reflective *tapetum* with melanophores. Other adaptations include the pigmentation of the retinal pigment epithelium behind the retina that absorbs excess light, especially where there is no *tapetum* present or when the light conditions are too bright (Fox and Kuchnow, 1965), and provides the photoreceptors with vitamin A (Braekevelt, 1994b). Pelagic or demersal organisms that live between the aphotic zone and the surface would have adaptations to detect different levels of illumination. The quantity of light that enters the eye, varies in species that migrate vertically in the water column from the deep, where they live in dim conditions, to the bright conditions closer to the surface, where many aspects of their life history i.e. reproductive migrations, are based on visual cues (Douglas et al., 2003).

Non-visual light detection

The pineal gland is an endocrine gland in the vertebrate brain that detects light and has some functions related to non-visual light detection (Figure 1.2). Photopigments involved in light detection are found in both the retina and in the pineal organ (Rudeberg, 1968, Vigh-Teichmann et al., 1983b, Vigh-Teichmann et al., 1990). Physiological responses in the body such as sexual development and circadian rhythms are triggered by light in the environment and are coordinated, or regulated, by both nerve activity and the production of hormones such as melatonin (Demski, 1991, Hankins et al., 2008, Davies et al., 2012). In some ancient vertebrates, the retinal photoreceptors and the pineal photoreceptors are very similar in structure and function i.e. melatonin biosynthesis, with higher levels produced in dark conditions and lower levels produced during day-time (Meissl and Yañez, 1994). Although some retinal ganglion cells produce melanopsin in mammals (Davies et al., 2010), melatonin levels can also control the colour of the



animal relative to a dark background. The photoreceptors detect the light available and this information is transferred to the dendritic epidermal melanosomes aggregating in the centre of the cell giving it a darker appearance (Fox and Kuchnow, 1965, Wilson and Dodd, 1973).

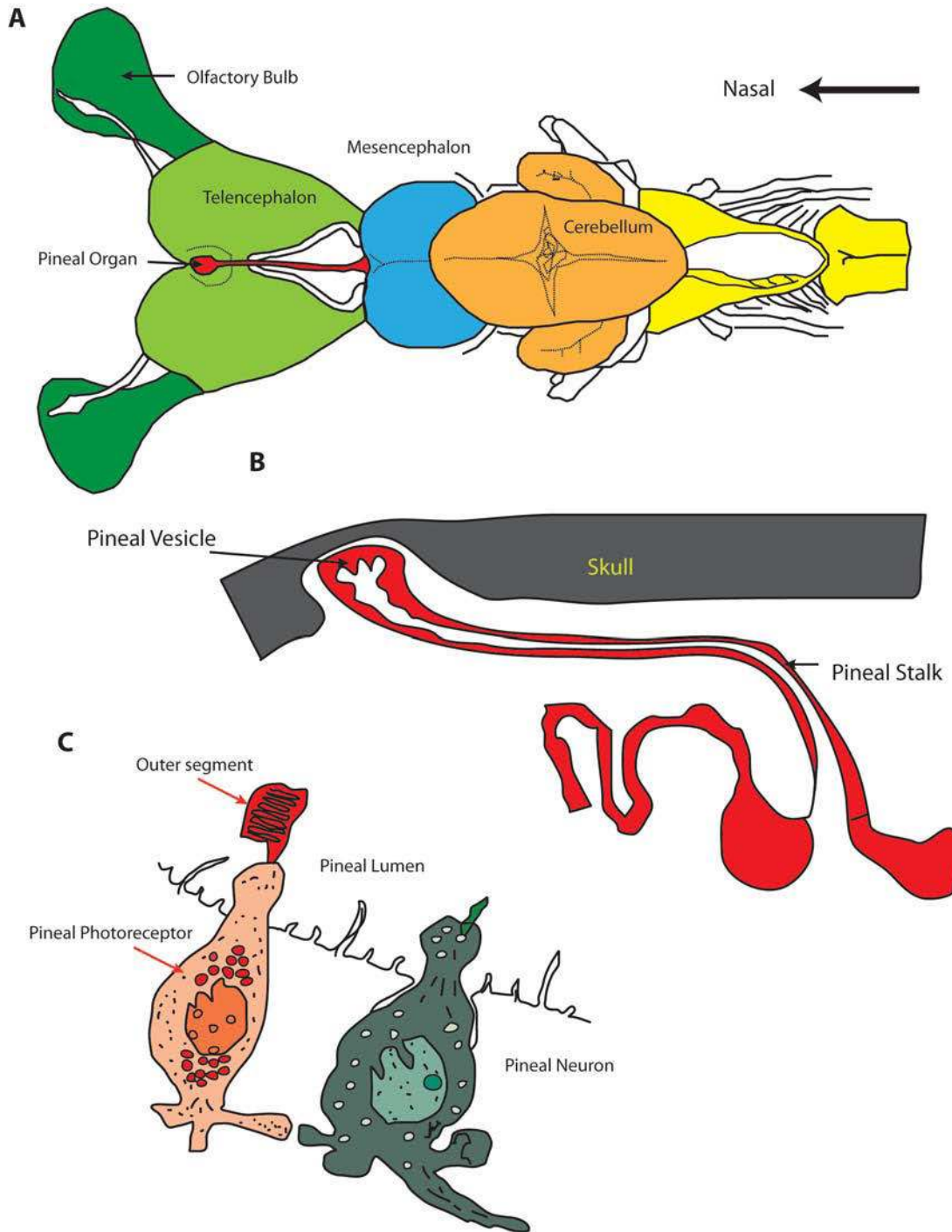




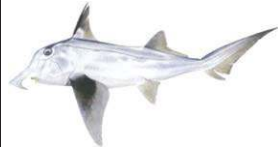

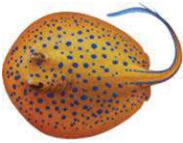

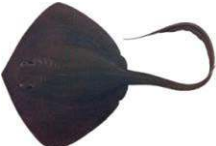


Figure 1.2 Schematic diagram of the position of the pineal organ in elasmobranchs. A. Dorsal view of an elasmobranch brain and the position of the pineal organ. B. Lateral view of the position of the pineal organ under the skull. C. Scheme of the pineal photoreceptors in the lumen and neural cells. Modified from Smeets (1998) and Vigh et al. (2002).

Species to be analysed

Chondrichthyans live in a diverse range of habitats and display many specializations in visual system morphology. However, in many cases the adaptive significance of these interspecific variations is poorly understood. Thus, in this thesis, the initial approach was to study the gummy shark, *Mustelus antarcticus*, which is a commercially important species of elasmobranch currently under fisheries management. Understanding of its visual ecology will reveal useful information regarding its habitat and behaviour that may assist in the conservation effort (Chapter 3). The second approach is to compare three species of chimaeras (Holocephali) that live in different habitats. Two deep-sea species: the Pacific spookfish, *Rhinochimaera pacifica* and the Carpenter's chimaera, *Chimaera lignaria*, are compared to the migratory elephant shark, *Callorhynchus milii* (Chapter 4). The third approach is to study the visual system in five species of sympatric reef-dwelling stingray from the same family (Dasyatidae): the bluespotted fantail ray, *Taeniura lymma*, the bluespotted maskray, *Neotrygon kuhlii*, the reticulated whipray, *Himantura uarnak*, the porcupine ray, *Urogymnus asperrimus* and the cowtail ray, *Pastinachus atrus* to identify differences in eye design that may have promoted or reflect niche separation and even speciation within the group (Chapter 5). Additionally, the different species might reveal information according to the habitat where they live. The deep-sea chimaeras live in the continental slope, where the sunlight is virtually non-existent but other sources of light like bioluminescence are present. The gummy shark and the elephant shark live in demersal habitats usually between 80 meters depth and the surface. The five species of stingrays spend most of their time in depths of no more than 20 meters (Table 1-1) (Figure 1.3).



Table 1-1 Ecological information of the species in the present study. Images modified from Last and Stevens (2009).

	Scientific Name Common Name	Taxonomic Group	Maximum size (cm)	Habitat Depth (m)	Distribution
	<i>Chimaera lignaria</i> Giant Chimaera	Holocephali	128 cm TL	Continental slope 400-1800	New Zealand and southern Australia
	<i>Rinochimaera pacifica</i> Pacific Spookfish	Holocephali	120 cm TL	Continental slope 760-1290	Pacific and Indian Oceans
	<i>Callorhynchus milii</i> Elephant Shark	Holocephali	120 cm TL	Demersal on continental shelf 0-200	New Zealand and southern Australia
	<i>Mustelus antarcticus</i> Gummy Shark	Elasmobranchii Euselachii	185 cm TL	Demersal on continental shelf 0-350	Temperate waters of Australia
	<i>Taeniura lymma</i> Bluespotted fantail ray	Elasmobranchii Batoidei	35 cm DW	Shallow coral reefs 0-20	Widespread Indo Pacific Ocean
	<i>Neotrygon kuhlii</i> Bluespotted maskray	Elasmobranchii Batoidei	47 cm DW	Inshore, reefs and estuaries 0-90	Indian and West Eastern Pacific Ocean
	<i>Pastinachus atrus</i> Cowtail Ray	Elasmobranchii Batoidei	200 cm DW	Inshore, reefs and estuaries 0-60	Northern Australia and New Guinea
	<i>Himantura uarnak</i> Reticulated whipray	Elasmobranchii Batoidei	160 cm DW	Inshore, reefs and estuaries 0-45	Widespread Indo Pacific Ocean
	<i>Urogymnus asperrimus</i> Porcupine ray	Elasmobranchii Batoidei	115 cm DW	Shallow coral reefs 0-20	Widespread Indo Pacific Ocean

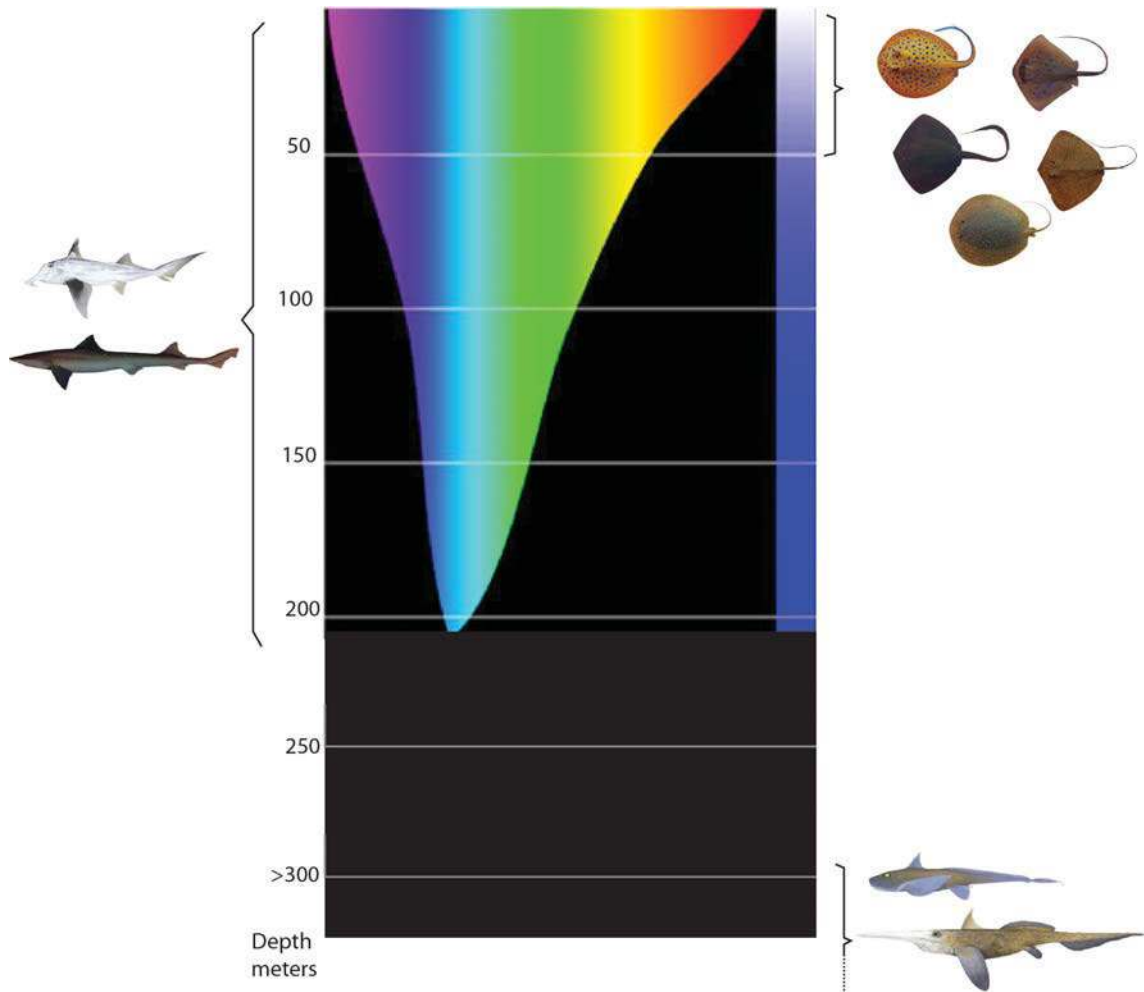


Figure 1.3 Diagram showing the light absorption in clear oceanic water at different depths and the relative depth range of each species analysed in this study. Modified from an image by Kyle Carothers in <http://oceanexplorer.noaa.gov/explorations/04deepscope/background/deelight/media/diagram3.html> and Last and Stevens (2009).

Aims

This thesis investigates anatomical aspects of the retina but also includes methodological advances, such as the use of novel methods to conduct the spatial analysis of cell densities in the retina and assess the most efficient method to construct topographic retinal maps (Chapter 2). The topographic distribution of photoreceptor and ganglion cells and other techniques to assess visual sensitivity, spatial resolving power and photoreceptor to ganglion cell convergence are applied to three species of chimaeras, one species of shark and five species of rays



(Figure 1.4). Immunohistochemistry was used to label different types of cones and to understand the role of photoreception in deep-sea, demersal and shallow water species of Chondrichthyes (Chapter 6). Additionally, a preliminary study compares the morphology of the pineal gland in the demersal elephant shark, *C. milii* with the bluespotted maskray *N. kuhlii* to identify possible trends in light sensitivity (Chapter 7).

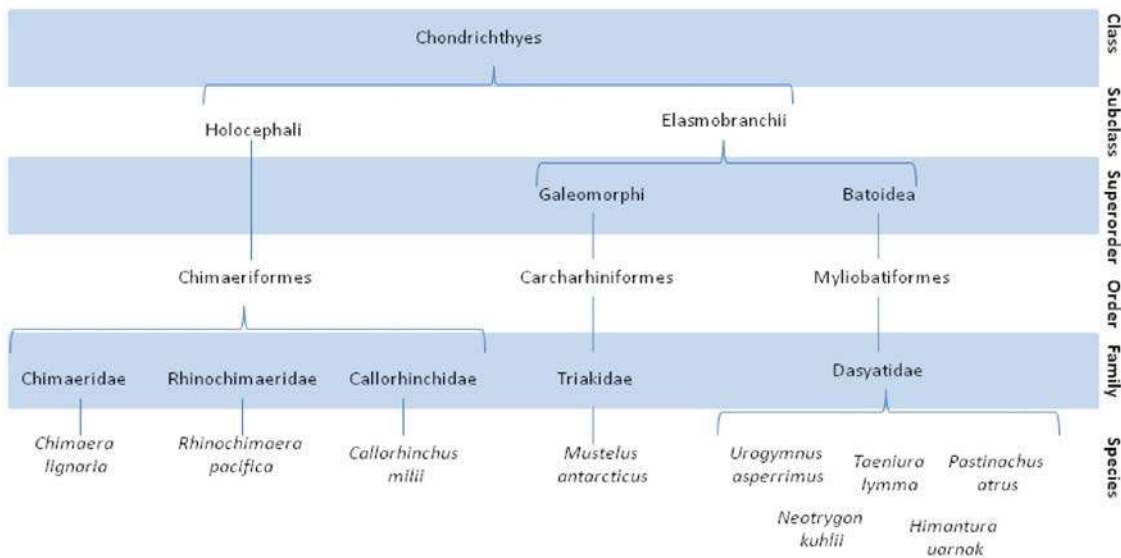


Figure 1.4 Cladogram of the taxonomic position of the different species in the study. Modified from Moyle and Cech (1988), Nelson (2006) and Last and Stevens (2009).

Hypotheses

- The species analysed will have a higher proportion of rods than cones in the retina with a high density region or streak adapted for panoramic vision across the horizontal meridian.
- In contrast to shallow water elephant fishes, the chimaeras from deep water will possess specializations or adaptations for scotopic vision, such as large eyes, with high rod to cone ratios and high summation of rod photoreceptors to ganglion cells ratio.

- The species that live in photopic conditions will show specializations to increase visual acuity, i.e. multiple types of cones, higher spatial resolving power and lower summation ratio.
- The demersal species will show a combination of adaptations for sensitivity and resolution because of the use of both types of habitats
- LWS opsin antibody will label cones in the retina of species living in photopic conditions.
- The pineal organ morphology will show higher specialization in the elephant shark for sensitivity, i.e. higher number of photoreceptors, longer outer segments in the photoreceptors, and increase in the lumen surface area.

Significance

The visual system in elasmobranchs has been studied for several decades. The information obtained by many researchers informs us that vision is a very important sensory system in sharks and rays. However, little information has been obtained in chimaeras. This study gives a better understanding of photoreception and vision in this important group. One of the unique aspects of chimaeras is that most of them live in deep water, that is considered one of the most common environments on the planet but rather extreme when compared to shallow water. The visual adaptations they use to live in conditions of very poor light, i.e. their relatively large eyes, by no means provides us with enough information to understand how they can survive at such depths and low light levels. This study on photoreception answers many questions such as: what parts of the visible light spectrum can they detect; how can a horizontal acute zone for panoramic vision assist them to detect food, mates and potential predators in their environment; and how do their eyes optimise the trade off between resolution and sensitivity. If we are able to better understand their natural history and sensory ecology, this information may aid in preventing overfishing.



This study compares the deep-sea chimaeras with the pelagic chimaera *C. milii*, which migrates to shallow water to reproduce. This study represents how important the roles of vision and the pineal gland are, in this peculiar reproductive migration. Very little is known about the role of the pineal organ in chondrichthyans and part of this study aims to examine the relative importance of image formation and light detection of photoreceptors in the retina and pineal, respectively. The capacity to live in two very different environments should reveal different adaptations in comparison to the chimaeras that live only in the deep ocean. The study of commercially important species, such as the gummy shark, contributes to our knowledge of the general biology and visual ecology of important indicator species that are often used for management. This species has vertical migrations between contrasting light conditions and this study gives information on sensory capabilities of the animals and how they can cope with the movements between the photopic and scotopic conditions. The information obtained in the present study represents the first stage in developing a by-catch reduction device for the juveniles of the gummy sharks, where a visual deterrent could be used in the fishing methods.

This study is the first to examine different sympatric species from a diverse family like Dasyatidae to compare their visual ecology and infer some possible causes of the use of different ecological niches in the same coral reef habitat that might be responsible for a shift in diet, a differential use of subregions in the reef and/or a temporal difference in activity pattern. This study also represents the first to use immunohistochemistry and compare different antibodies to label different opsins in the cones of Chondrichthyes and label their retinal distribution. This study is also the first to compare the pineal gland in species from different habitats i.e. species that live predominantly in bright light conditions and species that frequent the deep-sea but vertically migrate into shallow water to reproduce.

Chapter 2 A comparison of spatial analysis methods for the construction of topographic maps of retinal cell density

Garza-Gisholt, E., Hemmi, J.M., Hart, N.S. and Collin, S.P.

School of Animal Biology and The UWA Oceans Institute, The University of Western Australia, Crawley, 6009 W.A.

Abstract

Topographic maps that illustrate variations in the density of different neuronal sub-types across the retina are valuable tools for understanding the adaptive significance of retinal specialisations in different species of vertebrates. To date, such maps have been created from raw count data that have been subjected to only limited analysis (linear interpolation) and, in many cases, have been presented as iso-density contour maps with contour lines that have been smoothed ‘by eye’. With the use of stereological approach to count neuronal distribution, a more rigorous approach to analysing the count data is warranted and potentially provides a more accurate representation of the neuron distribution pattern. Moreover, a formal spatial analysis of retinal topography permits a more robust comparison of topographic maps within and between species. In this paper, we present a new R-script for analysing the topography of retinal neurons and compare methods of interpolating and smoothing count data for the construction of topographic maps. We compare four methods for spatial analysis of cell count data: Akima interpolation, thin plate spline interpolation, thin plate spline smoothing and Gaussian kernel smoothing. The use of interpolation ‘respects’ the observed data and simply calculates the intermediate values required to create iso-density contour maps. Interpolation preserves more of the data but, consequently includes outliers, sampling errors and/or other experimental artefacts. In



contrast, smoothing the data reduces the ‘noise’ caused by artefacts and permits a clearer representation of the dominant, ‘real’ distribution. This is particularly useful where cell density gradients are shallow and small variations in local density may dramatically influence the perceived spatial pattern of neuronal topography. The thin plate spline and the Gaussian kernel methods both produce similar retinal topography maps but the smoothing parameters used may affect the outcome.

Keywords

Retina; spatial analysis; fovea; area centralis; streak; topographic map; R language; interpolation; thin plate spline; Gaussian kernel smoother

Introduction

Topographic density maps are an informative and intuitive way of representing graphically the distribution of different types of cells in the retina. They are particularly useful for identifying retinal specialisations that may reflect an animal’s visual ecology and/or phylogeny. Topographic maps of retinal ganglion cell and photoreceptor distributions also provide crucial information about the limits of visual resolution and the degree of signal convergence (i.e. sensitivity). As a result, hundreds of maps have been produced in the last decades for a range of vertebrate and many invertebrate species (Collin, 1999, Collin, 2008). All species of vertebrates studied to date have some form of retinal specialization, rather than a uniform distribution of neurons, and each retinal specialization varies greatly in shape, size and number depending on the ecology and the phylogeny of the species. A retinal specialisation is usually defined as a localised area of increased cell density that affords increased spatial sampling of a specific region of an animal’s visual field (Collin and Shand, 2003).

A commonly observed retinal specialization is that of a radially symmetric gradient of increasing cell density. When the central zone of highest cell density (the 'area') is located in central retina, this specialisation is called an *area centralis* and when it is located in dorsal retina, it is called an *area dorsalis*, and so on. More than one retinal *area* may be present, as is common in many fishes and birds, which have both an *area centralis* and an *area temporalis* (Collin, 1999). Another form of specialization is an elongated band of high cell density that extends across a significant portion of the retina and is called a 'visual streak'. The primary axis of the streak may be oriented vertically or horizontally or even curved to form a 'dorsal arch' (Collin and Pettigrew, 1988c, Collin and Partridge, 1996, Coimbra et al., 2012b). This type of specialisation provides high acuity vision across an extended portion of the visual scene without the need for extensive scanning eye movements (Hughes, 1975, Hughes, 1977).

In some species of vertebrates, the zone of highest cell density within an *area* or a visual streak is characterised by an indentation of the retinal layers to form a pit or 'fovea' in the retina. Usually, the cell bodies of all but the photoreceptors are displaced to the sides of the foveal pit to provide unimpeded access of light to the rods and/or cones to mediate high acuity vision. The shape of the fovea may also provide some optical magnification of the image due to the difference in the refractive indices between the vitreous and the retinal tissue lining the fovea (Pumphrey, 1948, Locket, 1971, Collin and Collin, 1999). In some deep-sea species, the fovea in each eye may distort the image of bioluminescent light flashes enough to mediate some form of depth perception, while providing enhanced sampling with large numbers of tightly-packed rod photoreceptors (Locket, 1977, Collin, 1997, Warrant and Locket, 2004).



These retinal specializations can be found in various combinations and forms and show a marked interspecific variability. The position, shape, retinal coverage and centro-peripheral density gradient of each acute zone can be used to infer important information about the visual ecology of each species and their visual environment. Given the importance of topographic maps of retinal neurons for understanding the visual ecology of a species, it is critical that these distribution maps are as accurate as possible and that artefacts introduced by the techniques used, such as the preparation of the retinal wholemount (Chelvanayagam, 2000, Ullmann et al., 2012) and the staining and visualisation of the retinal neurons, are minimized as much as possible (Stone, 1981).

Traditionally, topography maps have been constructed from localised cell counts using a simple pairwise interpolation of adjacent points on the retina to calculate iso-density values that can be joined by contour lines (Hughes and Whitteridge, 1973, Beazley and Dunlop, 1983, Collin and Pettigrew, 1988b, Collin and Pettigrew, 1988c). However, this method does not consider or interpolate the distances between all points, but only the distances of adjacent points where the iso-density lines are constructed. The method also relies on the researcher's ability to discriminate the best interval of the contour lines, which can be subjective. More recent retinal studies use a variation of this method, where authors tend to employ a "smooth by hand or by eye" method that only means that some points might be arbitrarily removed or that the line might be "curved" to give a better visual appearance (Harman et al., 2001, Hart, 2002, Fritsches et al., 2003, Bailes et al., 2006).

Some authors have used computer methods to analyse the iso-density maps but, in some cases, the methodology is not clear and reproducible. The method used to determine the contour lines is often not stated so it is not possible to determine if any information is lost

because of any type of smoothing or whether maps can be compared if they use different kinds of spatial analyses. Some authors use a digital planimeter to digitize the iso-density contours and measure regions (Silveira et al., 1989, Do-Nascimento et al., 1991). Do-Nascimento *et al.* (1991) even include a different type of map, indicating differences in cell density with different sized dots. Mass and Supin (1992, 1995, 1999) have published a diversity of maps, where the contours were manipulated by computer and the number of cells were averaged (smoothed) in blocks of 3 X 3 samples. They have also devised an original method to transform the map into a continuous spherical representation.

Stone and Halasz (1989) used a dotted map to represent the magnitude of changes in cell density and a grey scale gradient with discrete steps generated using a computer-based paradigm in the elephant retina. Fischer and Kirby (1991) used the Golden software package (Surfer) to calculate the iso-density lines of the topographic maps in *Anubis* baboons. More recently, the geographic information system (GIS) has been used to analyse cell topography in retinas, where ArcGIS (Esri) systems like ArcView and ArcMap have been used to analyse retinal cell density gradients in birds (Coimbra et al., 2006, Coimbra et al., 2009, Dolan and Fernandez-Juricic, 2010). However, even with the use of powerful software packages i.e. Systat (Famiglietti and Sharpe, 1995) and graphical programs like DeltaGraph (Ahnelt et al., 2006, Schiviz et al., 2008, Rocha et al., 2009), the methodology used in most studies is insufficient to assess the accuracy of the spatial analysis although Hemmi and Grünert (1999) used a slightly smoothed thin plate spline interpolation and Coimbra et al. specified the use of a spline interpolation in penguins (Coimbra et al., 2012b) and giraffe (Coimbra et al., 2012a).



The statistical language 'R' is an inexpensive open access program (R Core Team, 2012) providing flexibility, a range of mathematical functions and online help including forums for experts to help users with specific questions. Spatial analysis using the R program has been applied in diverse fields. For example, the *spatstat* package was used to analyse the relationship between the population of tuna and the oceanographic conditions (Royer et al., 2004) and the insect distribution changes as a result of habitat loss (Zaviezo et al., 2006). R has recently been used to develop an extensive range of spatial analysis models for the examination of spatial patterns in animal disease (Stevenson, 2009). There are more than 30 different methods of interpolation and smoothing models that could create maps in R, making it a powerful tool for spatial analysis (Bivand et al., 2008, Hengl, 2007, Stevenson, 2009).

A comparison between different algorithms is necessary to identify which model can be adapted more easily to faithfully represent the topographic distribution of retinal cells. These algorithms come in two basic forms. Firstly, interpolation models interpolate the data to fill gaps and provide a sampling base for graphical representation. The observed data is not modified by the function so the resulting curve or surface will cross the sample locations at the exact observed value (Bivand et al., 2008). In contrast, spatial analysis that smoothes the data, uses the spatial position and the magnitude between the observed points to obtain a spatial function to calculate the cell densities in the different areas of the retina. The use of smoothing analysis removes outliers from the sampling and reduces local variation caused by potential artefacts (Baddeley, 2008, Furrer et al., 2012).

In this study, we present results comparing maps generated by different algorithms in R, and compare the resulting maps with previously published, hand-generated iso-density maps showing a range of

different retinal specializations. The algorithms provide an objective, reliable and improved representation of the topographic distributions of cells in the retina. The ability to automate map generation also saves significant time compared to traditional methods.

Methods

We analysed six different, previously published, topographic maps sampling retinal ganglion cell populations that were Nissl stained and counted under a compound microscope following the technique of Collin and Pettigrew (Collin and Pettigrew, 1988b, Collin and Pettigrew, 1988c). The topographic maps analysed were the reef fish: *Cephalopholis miniatus* with a temporal area, *Amplyglyphidodon curacao* with multiple areas, *Parapercis cylindrica* with a horizontal streak and two areas (Collin and Pettigrew, 1988b); *Choerodon albigena* with a horizontal streak and a dorso-temporal area, *Gymnocranius bitorquatus* with a dorsal area (Collin and Pettigrew, 1988c) and a deep sea fish *Conocara murrayi* with a fovea (Collin and Partridge, 1996). The original iso-density contour maps were based on cell counts that were interpolated by hand and were obtained with the permission of the authors. An additional iso-density contour map of ganglion cell distribution in the retina of the pacific spookfish, *Rhinochimaera pacifica*, illustrating the horizontal streak was analysed using the stereological method using *StereoInvestigator* software (Microbrightfield, USA) to sample the retina in an unbiased and automated way (Coimbra et al., 2009). Therefore, by including data collected and analysed using two different methods, it will be possible to objectively compare the neuronal distribution patterns generated by this new technique and how this may affect their interpretation.

Input data was generated either by digitising hand drawn counting maps or by reading in output files from the *StereoInvestigator* program. Original counting maps that show the position of each cell count and



the calibrated calculations of cells per square millimetre at each retinal locus were scanned and digitized using Adobe Illustrator CS5 (San Jose, Calif., USA). The outline of the retina, the position of the optic nerve head and any retinal artefacts were all digitised as *polyline* objects. To create a *polyline* object, we selected the *pen tool* and clicked on each point of the outline. The positions of the observations were placed like text inside the created outline. The outline of the retina and the outlines representing the optic nerve and other retinal artefacts should be of the type “*polyline*”. If they are saved as “*path*” then it means they are not straight lines and include curves. To convert a *path* to a *polyline*; it is possible to select the *path*, go to *Object>Path>Simplify* and select the straight lines option. Alternatively, *StereoInvestigator* can be used to generate the cell counts. The data needs to be saved in extensible markup language (.xml) format. The xml file includes the x and y coordinate positions and the type of marker for each object. For the spatial analysis, the script counts the cells and obtains the average position of the x and y coordinates for each site analysed. Additional modifications were necessary to obtain the correct value and the position of each site using the *plyr* (Wickham, 2011) and *stringr* packages in R (Wickham, 2012). More details can be found in the script attached in Appendix 1.

The data obtained was analysed spatially using R. Four different algorithms were used to spatially analyse the data, and construct iso-density maps: 1) an *akima* interpolation (*Akima* package), 2) a thin plate spline interpolation (*fields* package), 3) a thin plate spline (Tps, *fields* package), and 4) a Gaussian kernel smoother (Gks, *spatstat* package). The first two algorithms interpolate the data without modifying the observed values while Tps and Gks smooth the observed data.

The two interpolation models respect the original observations and only fill in empty spaces using different algorithms. Akima bivariate

interpolation is a fifth degree polynomial function in the x-y plane, which creates a series of triangles to estimate partial derivatives. This method is useful when some areas of the retina were not sampled due to damage, because it considers irregular-spaced samples (Akima, 1978, Akima et al., 2012). The second model uses a spline to obtain the interpolation. The thin plate spline is a geometric function that 'bends' the spatial arrangement to adjust to the values of the points. The smoothness of the thin plate spline can be adjusted in two ways: firstly, the thin plate spline uses a roughness penalty that is known as the penalized sum of squares, the strength of which can be adjusted through lambda (λ) and works as a smoothing parameter. If the smoothness parameter lambda is set to 0 then the data is not deformed and the original values are respected thereby creating a cubic interpolation (Duchon, 1977). The second way to adjust the smoothness is with the degrees of freedom that are the effective number of parameters used to fit the surface model. A lower number of degrees of freedom will increase the smoothing of the data (Hancock and Hutchinson, 2006, Furrer et al., 2012). For the present comparison, we used one third of the number of observations for the over-smoothed model and two thirds of the number of the observations for the under-smoothed model. Like the Tps, the Gaussian kernel smoother (Gks), smoothes the data locally and can adjust the observed data depending on neighbouring observations. The Gaussian kernel smoother, creates a series of Gaussian distributions to fit the spatial data. The smoothness can be controlled by the smoothing kernel bandwidth that can be modified with the use of the sigma value close to the distance between observations (Baddeley and Turner, 2005, Baddeley, 2008).

The resulting functions for each model were used to calculate the required points in the maps to construct the iso-density contours. A grid of 200 μm of resolution was created to input in the function to predict the values in each point of the grid. The iso-density contour levels were set to the original values presented in the published maps



and in some cases the number of levels was modified to compare the effects of using different iso-density lines. For each of the smoothing models, two parameters were compared giving an under-smoothed and an over-smoothed iso-density map. In the results of the paper, we present only a limited number of comparisons for each retina to illustrate different scenarios and enable a decision to be made as to the most appropriate type of analysis.

The foveal specialization (a very sharp peak of high cell density) represents a special case that required a different approach because of the magnitude of the cell density gradient. The interpolation model and the smoothed model were compared to a third approach. A hybrid of two models was used, where the foveal region was analysed as a subset of the data and isolated from the rest of the retina. The cell distribution in the fovea was analysed with a Tps interpolation and the Tps smoothed model was used to analyse cell distribution in the retinal periphery; the data was then superimposed and combined in a single topographic map.

To compare the models, we plotted the density function for all models (Wickham, 2009). This approach cannot however be used to compare the models to the original dataset, as the data is not normally evenly sampled across space, leading to a distortion in the density distribution. An alternative way to present the density distribution is to plot the cumulative distribution function. For retinal analysis, this is informative, because it allows one to easily read out how many cells a retina contains at different cell densities, which helps in comparing retinae across species. One way to analyse the change of the data from the smoother is to use a residual analysis. Residual values were obtained calculating the percentage of difference between the observed data and the modelled data. These residuals should be distributed randomly and with equal variance across the retina. The percentage

range gives an indication of how strongly the observed data was modified. Mapping the residuals in the same way we mapped the original density values, provides a graphical tool to check whether or not the data smoothing has affected the shape of the density distribution. Strong spatial structure in these plots indicates that the shape of the density distribution has been modified by the smoothing algorithm. Probably the most informative and direct way to assess the model fit (and at the same time reduce the dimensions of the spatial interpretation) is to plot the values along a transect line, i.e. horizontal and vertical transects across the maps, showing measured and estimated data points (Hijmans and van Etten, 2012).

R is a platform independent open source program (i.e. Windows, Mac, and Linux) that is available from the Comprehensive R Archive Network (CRAN), (<http://cran.r-project.org>)(R Core Team, 2012). We used the R Studio that is an Integrated Development Environment that helps novice users making R more user-friendly (<http://www.rstudio.com>)(R Studio, 2012). The R script for the extraction and analysis of the data presented here is included as electronic supplemental material and can be used and distributed freely as long as the authors, the creators of R and the different packages used in the script are all cited appropriately. There are two versions of the script; one version extracts the data in the form of an Extensible Markup Language (.xml) file that is suitable for exported files from *StereoInvestigator* and the other version extracts the values from a Scalable Vectors Graphic (.svg) file that can be obtained from *Adobe Illustrator*, *Corel Draw*, *Inkspace* and other vector graphics software packages.



Results

Choosing between different models

All four iso-density contour maps constructed using data obtained from the Pacific spookfish, *Rhinochimaera pacifica* using the four different analysis methods reveal a pronounced horizontal streak. These results are novel and the biological significance of the observed topographic distribution is discussed in Chapter 4. The interpolation models show more local variation in the retina (noise) with discontinuous iso-density areas; while the smoothed models show a similar overall topographic pattern but with less local variation. Comparing the two interpolation models, the main difference between the two interpolation algorithms is that the *Akima* interpolation (Figure 2.1A) uses a triangular calculation and so the nodes of the lines are sharp, while spline interpolation (Figure 2.1B) shows curved lines because the algorithm uses a cubic function to interpolate the data. The two smoothing algorithms give almost identical results. The only difference is that the output of the Gaussian kernel model (Figure 2.1D) gives an image from the calculated points, while thin plate spline model (Figure 2.1C) gives a series of equations that allows densities to be calculated for any point inside the retina. The comparison between the density lines of the models shows that the two interpolations and the two smoothing models are similar. The peak of the distribution curve reveals what cell density value is most abundant in the retina and does not represent the peak density; when the data is smoothed, the peak tends to narrow (Figure 2.1E). The cumulative distribution function is more intuitive to assess how broad or narrow the retinal area is. If we look at the cut-off density that contains the top 5% of density values, the shallower the curve at the top, the faster is the drop in density away from the peak. The cut-off value is higher in the spline model than the *Akima* interpolation model, while the smoothed models both have a lower value (Figure 2.1F), indicating that the area around the peak density has been slightly flattened out by the smoothing procedure.

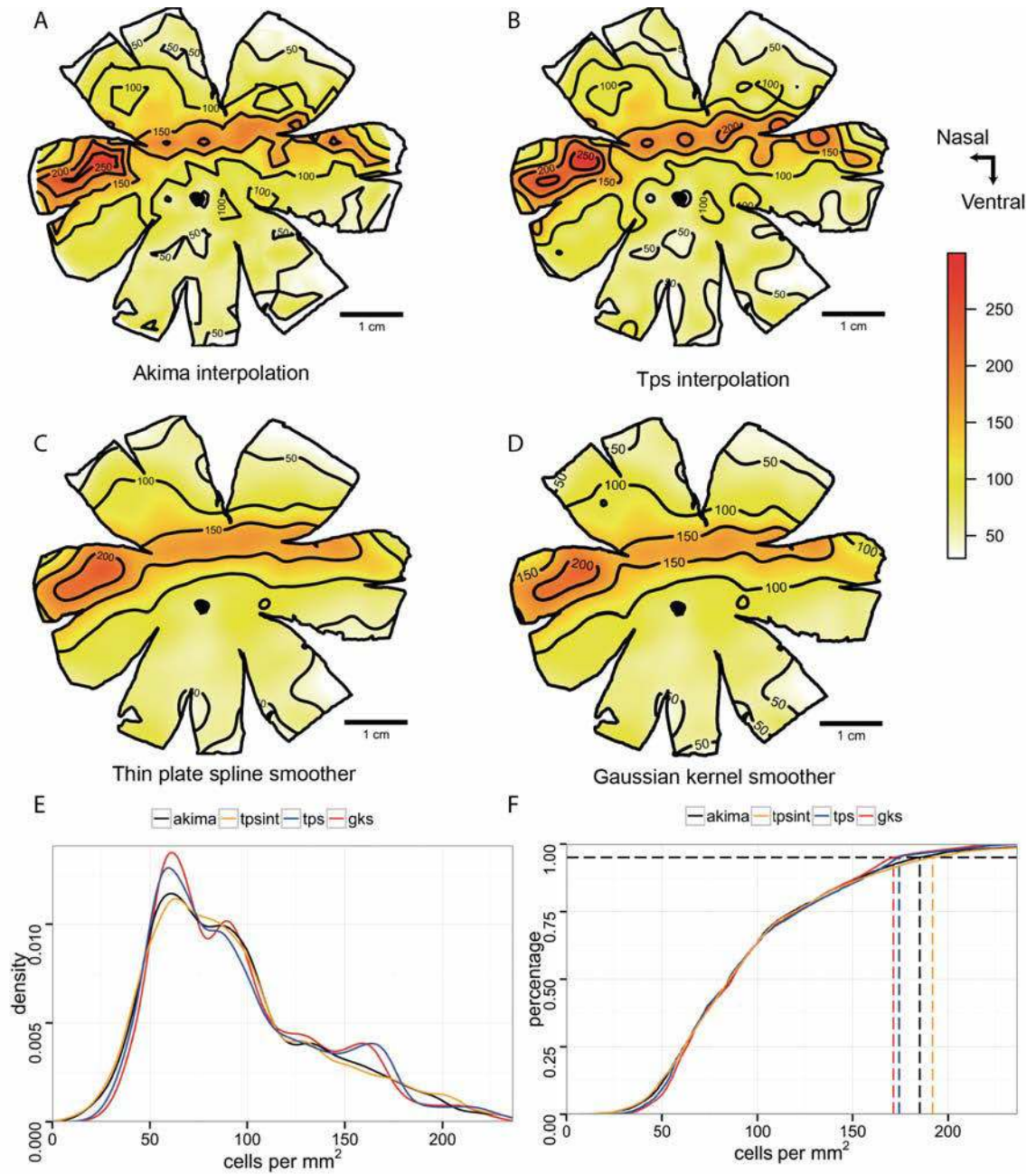


Figure 2.1 Topographic maps of the ganglion cells in the retina of the Pacific spookfish, *Rhinochimaera pacifica*. A. Akima interpolation. B. Thin plate spline interpolation. C. Thin plate spline smoother. D. Gaussian kernel smoother. E. Distribution density curves of the 4 models. F. Cumulative distribution functions for the four models; dash lines denote cell density higher of the 95% of the area of the retina. All the densities are in cells mm⁻². The maps were predicted with a distance of 200 μ m between points.



Choosing different smoothing parameters

We assessed all the retinas using the four models and concluded that the interpolation models are very similar, but the thin plate spline model has the advantage of a smoother appearance. The smoothed models are different to the interpolation models but show both the same general patterns. The Tps has the flexibility to manipulate the smoothness from a linear interpolation with no smoothness to an over smoothed analysis. Therefore, for the next six retinas, we present the figures for the thin plate spline (Tps) model only.

In the coral cod, *Cephalopholis miniatus*, an *area* is present in the ventro-temporal retina. The original map shows little variation in the iso-density contours, which emanate from the regions of highest cell density (predominantly spaced in 10,000 cells mm⁻² increments). In comparison, spline interpolation shows higher local variation that is underestimated in the traditional 'by hand' or 'by eye' interpolation model. Comparing the spline interpolation, an under-smoothed model and an over-smoothed model, the same *area* is present in all three maps. There is also a small *area* in the nasal retina present in the original map but the cell density is lower and it is not evident in the interpolation or the smoothing maps (Figure 2.2). The two transects crossing the retinal specialization, show higher variation in the curves in the low cell densities that is reduced with the smoothed models. The high density peak in the smoothed models is reduced in comparison to the observed models; in a higher degree in the over smoothed model. The residual maps show more variation in the ventral and temporal areas, i.e. the variation from the over-smoothed model is higher showing a similar pattern in the residuals of the specialization. The residual values for the under-smoothed model are lower and the area of more than 25% change from the observed data is very small compared to the over-smoothed model (Figure 2.3).

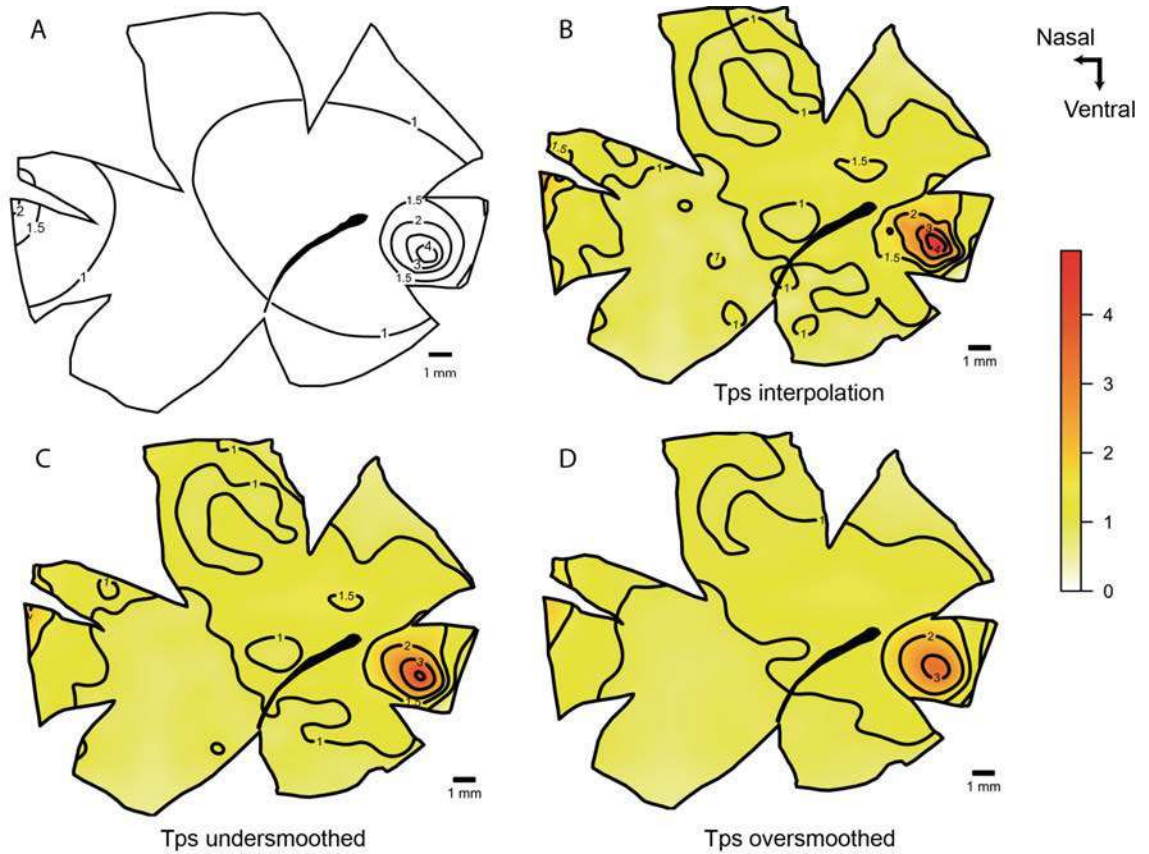


Figure 2.2 Topographic maps of the ganglion cells in the retina of the coral cod, *Cephalopholis miniatus* that show an *area temporalis* specialization. A. Modified map from Collin and Pettigrew, 1988a. B. Thin plate spline interpolation using a lambda value of 0. C. Thin plate spline under-smoothed with the 66% of count numbers for calculated degrees of freedom. D. Thin plate spline over-smoothed using the 33% of count numbers for calculated degrees of freedom. All the densities are $\times 10^4$ cells mm^{-2} . The maps were predicted with a distance of 200 μm between points.

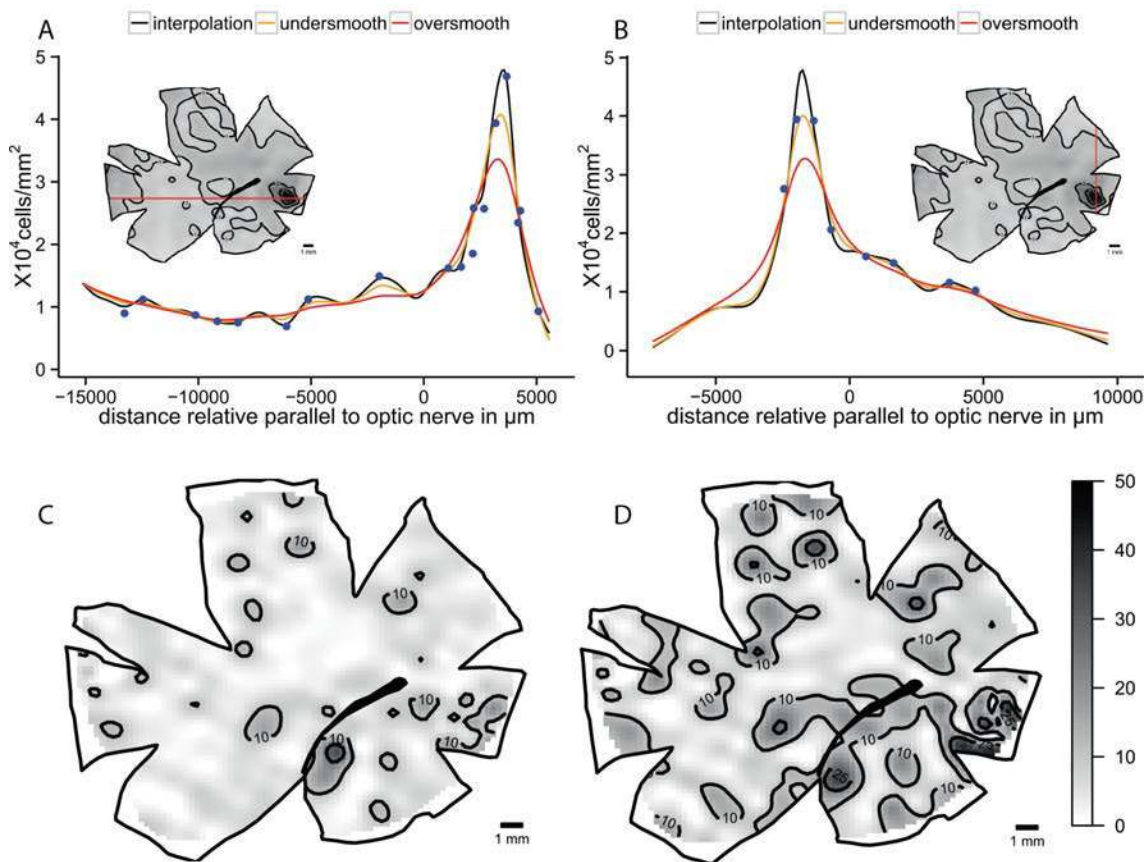


Figure 2.3 Horizontal and vertical transects, and residual analysis of the two levels of smoothness for the coral cod, *Cephalopholis miniatus*. A. Horizontal transect crossing the highest density area, the dots represent observed points that are in the transect or lie at a distance not more than 0.5 mm of the transect line. B. Vertical transect crossing the highest density area, the dots represent observed points that are in the transect or lie at a distance not more than 0.5 mm of the transect line. C. Residual map for the under-smoothed model showing percentage of variation between the calculated data and the observed data, the contour lines represent the areas that varied more than 10% and 25%. D. Residual map for the over-smoothed model showing percentage of variation between the calculated data and the observed data, the contour lines represent the areas that varied more than 10% and 25%.

The blue tusk fish, *Choerodon albigena*, presents a horizontal streak combined with an *area centralis* in the dorso-temporal retina. The linear interpolation shows the same specialization but the horizontal streak values of 40,000 cells mm^{-2} are discontinuous. The smoothed models show a similar pattern with a horizontal streak of more than 20,000 cells mm^{-2} that extends to the dorso-temporal retina. Additionally there is a dorso-temporal *area* with a peak of 80,000 cells mm^{-2} in the under-smoothed model that is not present in the over-smoothed model but the lower centro-temporal *area* with a peak of 60,000 cells mm^{-2} is present

in both models (Figure 2.4). The horizontal transect shows a high local variability in the streak affecting the continuity of the iso-density lines (Figure 2.4A). The high variability is reduced with the over-smoothing but the peak is lower than the interpolation line. The interpolation model shows that it is not a constant specialization and it has a lot of local variation. Along the vertical transect the observed cell densities are closely followed by the models and the smoothed models do not change the peak dramatically. The residual analysis shows a higher variation in the centre of the retina and the magnitude is higher but with no specific pattern revealed in the over-smoothed model (Figure 2.5).

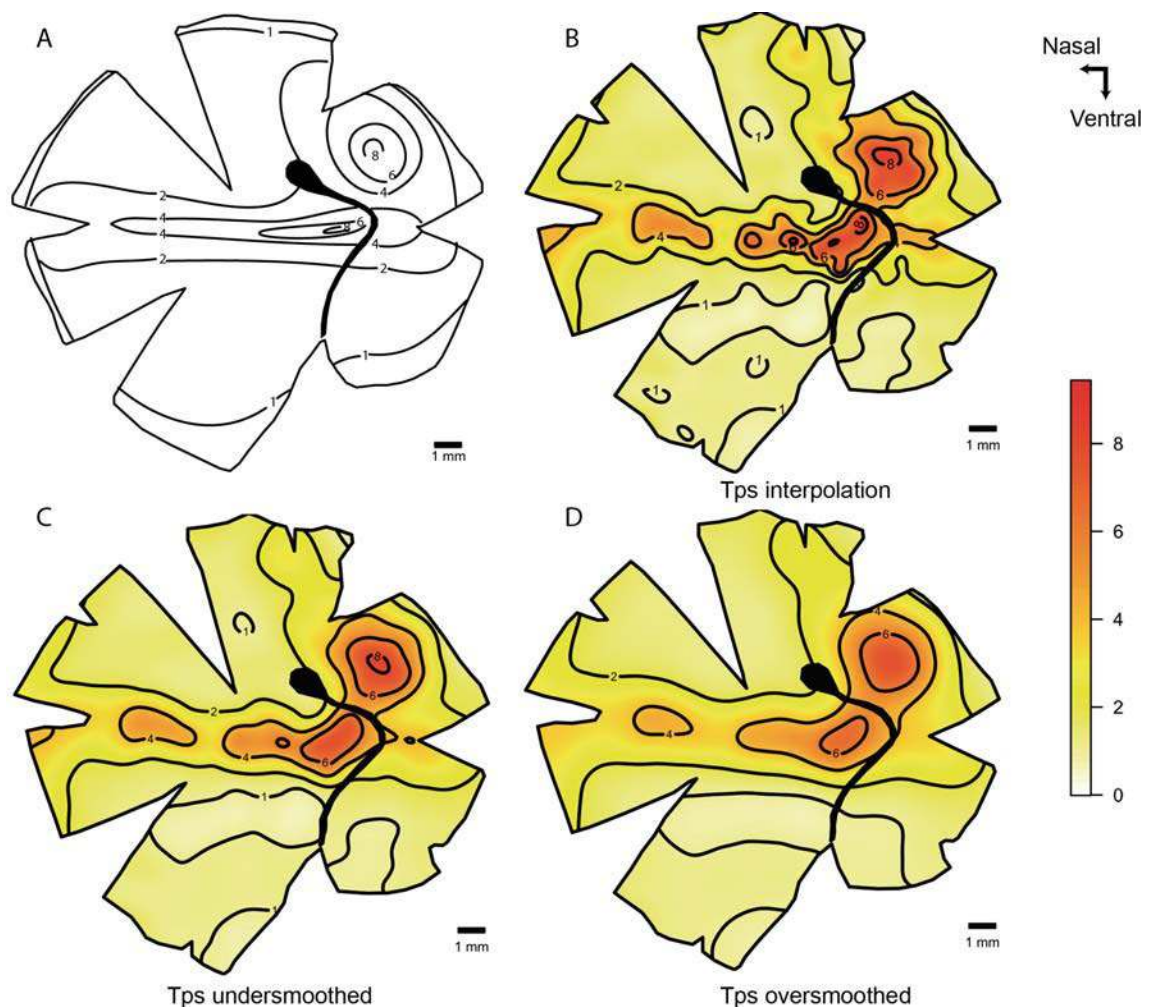


Figure 2.4 Topographic maps of the ganglion cells in the retina of the blue tusk fish, *Choerodon albigena*, that show a horizontal streak with a dorso-temporal *area* specialization. A. Modified map from Collin and Pettigrew, 1988b B. Thin plate spline interpolation using a lambda value of 0. C. Thin plate spline under-smoothed with the 66% of count numbers for calculated degrees of freedom. D. Thin plate spline over-smoothed using the 33% of count numbers for calculated degrees of freedom. All the densities are $\times 10^4$ cells mm^{-2} .

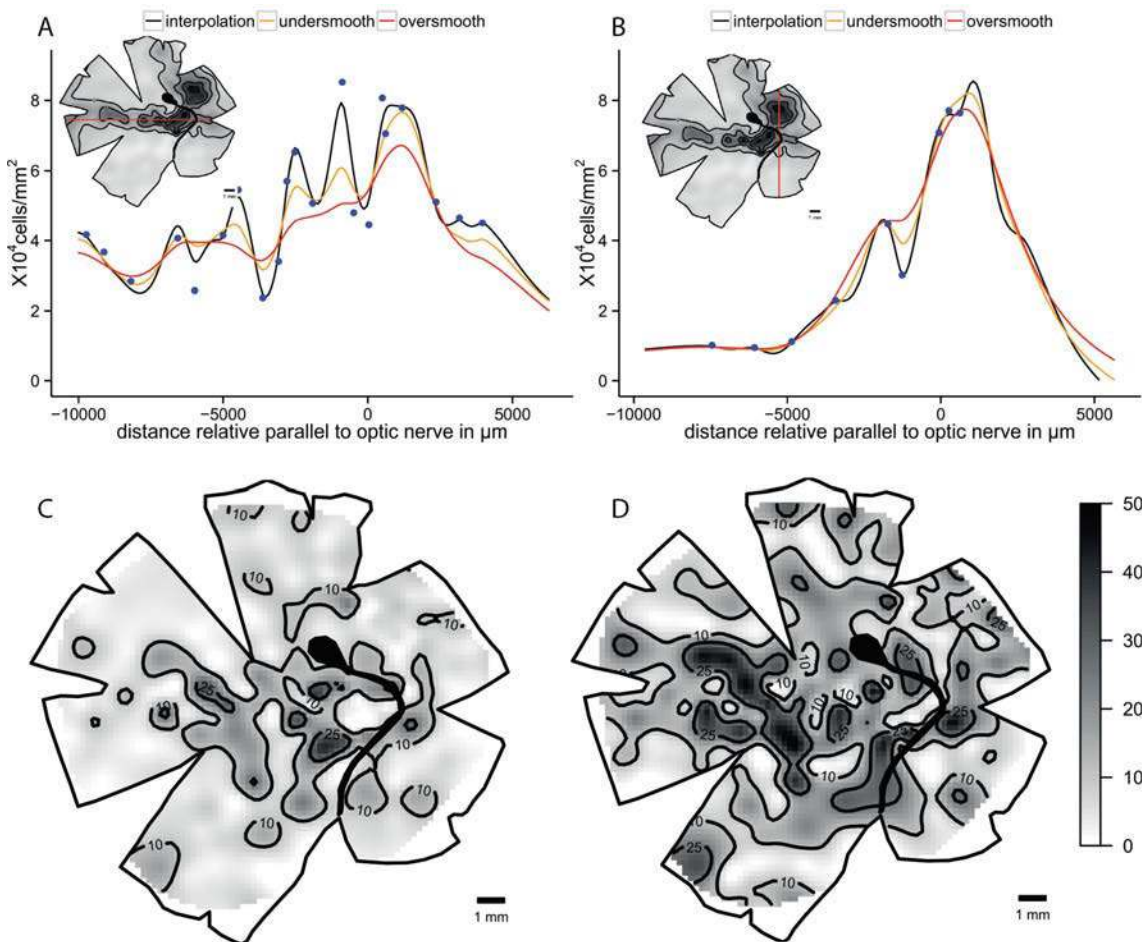


Figure 2.5 Horizontal and vertical transects, and residual analysis of the two levels of smoothness for the blue tusk fish, *Choerodon albigena*. A. Horizontal transect crossing the highest density area, the dots represent observed points that are in the transect or lie at a distance not more than 0.5 mm of the transect line. B. Vertical transect crossing the highest density area, the dots represent observed points that are in the transect or lie at a distance not more than 0.5 mm of the transect line. C. Residual map for the under-smoothed model showing percentage of variation between the calculated data and the observed data, the contour lines represent the areas that varied more than 10% and 25%. D. Residual map for the over-smoothed model showing percentage of variation between the calculated data and the observed data, the contour lines represent the areas that varied more than 10% and 25%.

Analysing different specializations

The under-smoothed version of the Tps, using two thirds of the number of observations for the degrees of freedom, is more appropriate to analyse the retinas because it maintains the peak values at a level closer to the observed values. The local variation is higher than the over-smoothed model but it is generally preferable to keep it as the variation might contain useful information and reflect real biological variation rather than sampling noise. Therefore, the results of the three

species presented below are analysed using the Tps interpolation and the under-smoothed Tps models.

The original map of the staghorn damselfish, *Amblyglyphidodon curacao*, shows a central plateau of more than 15,000 cells mm⁻² where three specializations are present in the dorsal, temporal and ventral areas. In contrast, the Tps model shows that the ventral *area* and the temporal *area* are evident with the contour interval of 25,000 cells mm⁻² in the periphery of the retina and a smaller dorsal *area* of 20,000 cells mm⁻². The lowest density areas of the retina are in the central retina showing values of less than 15,000 cells mm⁻². Only plotting the contour lines of 15,000, 20,000 and 25,000 cells mm⁻² shows the same colour pattern but the presence of the specialization is clearer. The vertical transect running through the ventral specialization shows that the smoothed model follows the same pattern as the interpolated model but there is a reduction in noise in the lower density area. The residual map shows that the variation of the calculated points doesn't follow a specific pattern and is not affecting the specialization (Figure 2.6).

The collared sea bream, *Gymnocranius bitorquatus* shows a dorsal specialization with a central *area* and a lower density horizontal streak of 20,000 cells mm⁻² in the centre of the retina. The interpolation model shows some isolated points but the streak lies within the 10,000 cells mm⁻² contour that is clearly represented in the smoothed model with less local variation. The horizontal transect shows this variation in the streak with the oscillations between 10,000 and 20,000 cells mm⁻². Note how the oscillations in the lines are reduced with the smoothed model indicating that the noise is reduced. The residual map shows that the highest level of variation is in the position of the horizontal streak. High fluctuations of the density values in the streak mean that the smoothing model will reduce these values (Figure 2.7)

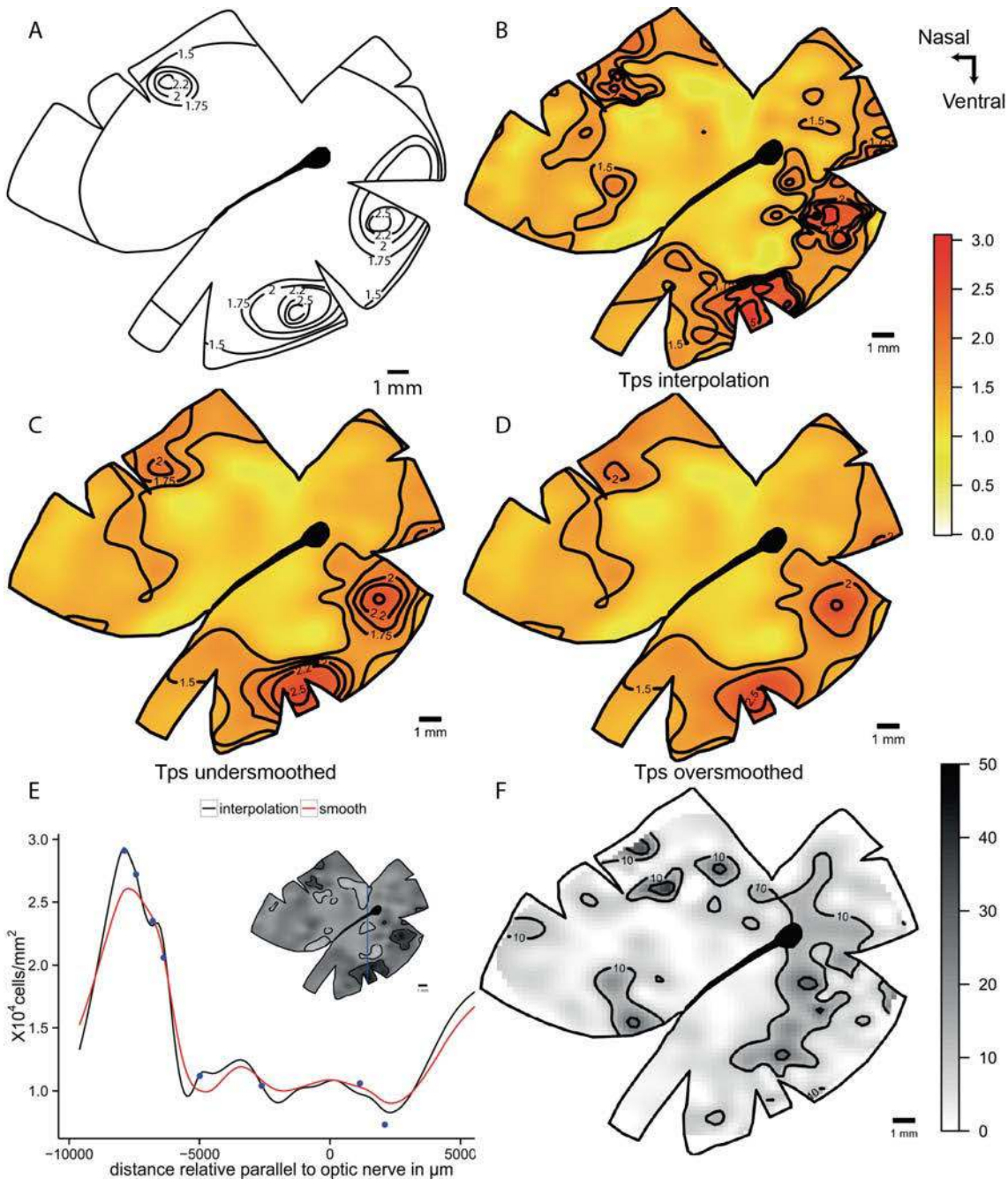


Figure 2.6 Topographic maps of the ganglion cells in the retina of the staghorn damselfish, *Amblyglyphidodon curacao*, that show multiple *areae* specializations. A. Modified map from Collin and Pettigrew, 1988a. B. Thin plate spline interpolation using a lambda value of 0. C. Thin plate spline under-smoothed map with the original isodensity contour levels. D. Thin plate spline under-smoothed map with lower number of isodensity contour levels. E. Horizontal transect crossing the highest density area, the dots represent observed points that are in the transect or lie at a distance not more than 0.5 mm of the transect line. F. Residual map for the over-smoothed model showing percentage of variation between the calculated data and the observed data, the contour lines represent the areas that varied more than 10% and 25%. All the densities are $\times 10^4$ cells mm^{-2} .

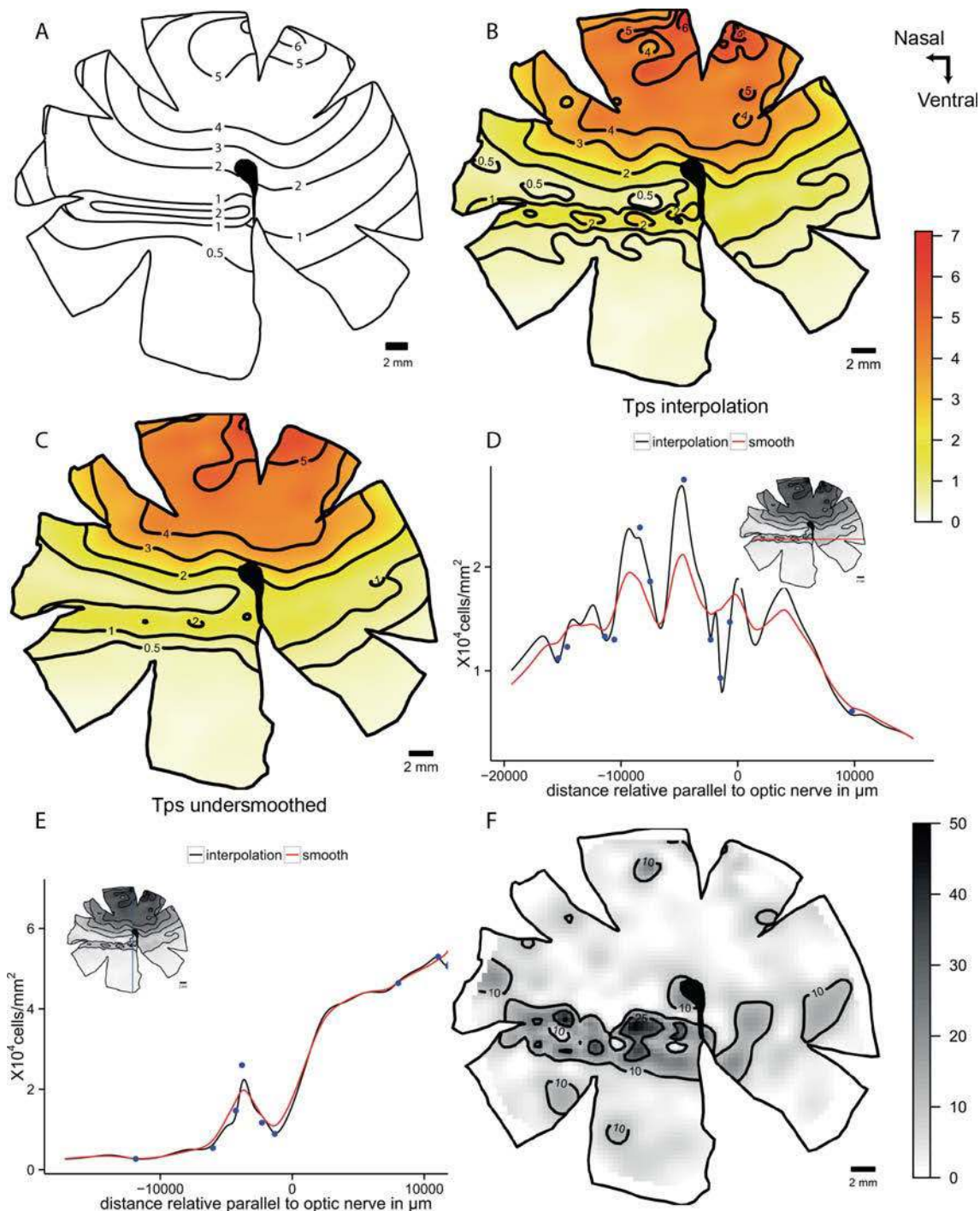


Figure 2.7 Topographic maps of the ganglion cells in the retina of the collared sea bream, *Gymnocranius bitorquatus*, that show a dorsal area specialization. A. Modified map from Collin and Pettigrew, 1988b. B. Thin plate spline interpolation using a lambda value of 0. C. Thin plate spline under-smoothed map. D. Horizontal transect crossing the supposed streak specialization, the dots represent observed points that are in the transect or lie at a distance not more than 0.5 mm of the transect line. E. Vertical transect crossing the highest cell density area, the dots represent observed points that are in the transect or lie at a distance not more than 0.5 mm of the transect line. F. Residual map for the over-smoothed model showing percentage of variation between the calculated data and the observed data, the contour lines represent the areas that varied more than 10% and 25%. All the densities are $\times 10^4$ cells mm^{-2} .



The original topographic map of the sandperch, *Parapercis cylindrica*, possesses a horizontal visual streak with two areas of elevated cell density, one that is located in the temporal retina and one that is located in the nasal retina. The Tps model shows the same overall pattern as the original map, but the interpolation method reveals a third peak in the centre of the streak. The smoothed model shows a similar distribution in the topographic map and it produces more radial iso-density contours for a more aesthetically pleasing result. On the other hand, we can observe from the line transects that the higher values within the specializations are lowered by this model. Specifically, the nasal and temporal peaks have a lower magnitude, while the central peak is slightly higher. The vertical transect shows a nice comparison between the two models. Most of the variation in the points can be observed in the central area as well as some subregions within the streak (Figure 2.8).

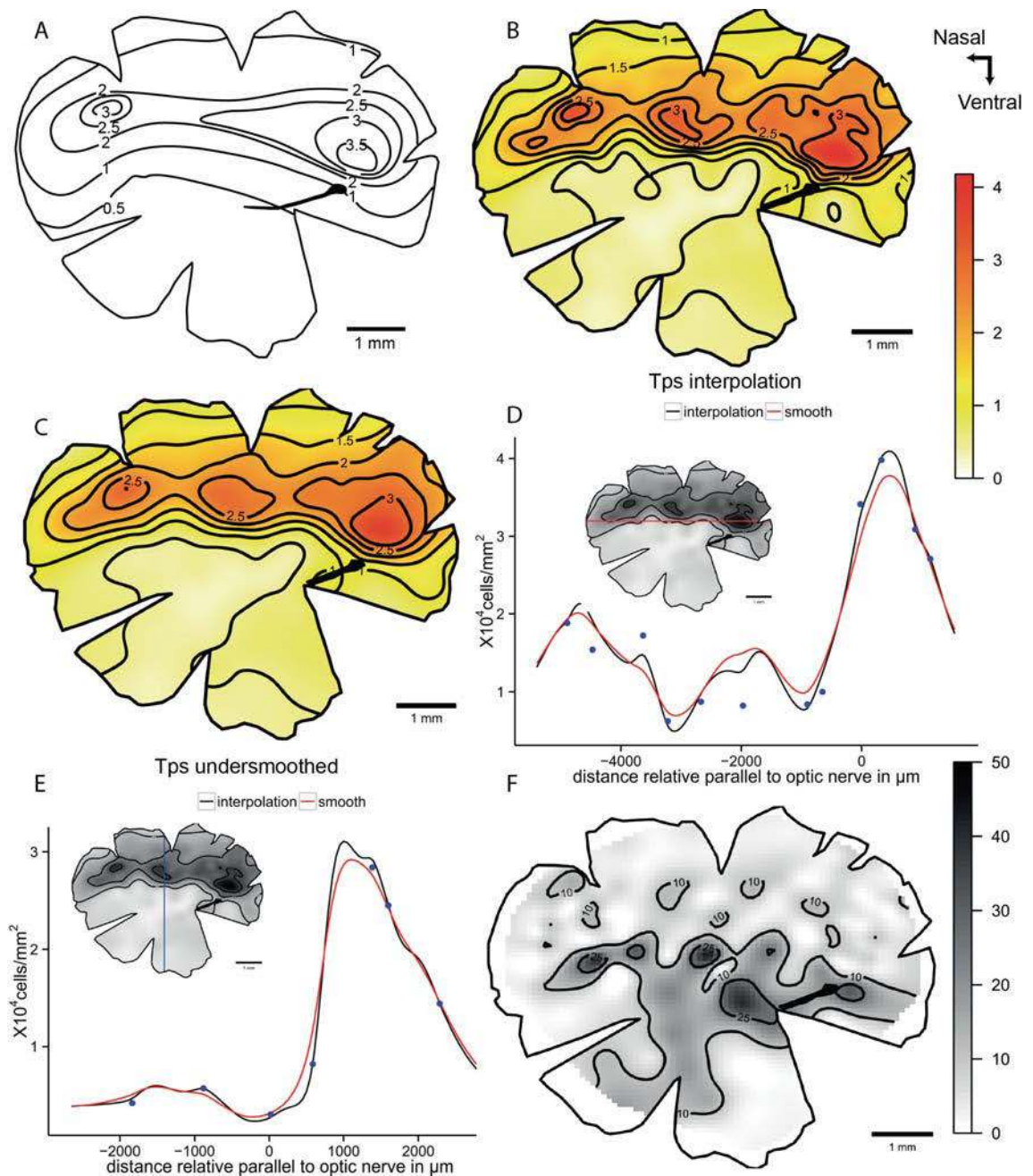


Figure 2.8 Topographic maps of the ganglion cells in the retina of the sandperch, *Parapercis cylindrica*, that shows a horizontal streak with three *areae* specializations. A. Modified map from Collin and Pettigrew, 1988a. B. Thin plate spline interpolation using a lambda value of 0. C. Thin plate spline under-smoothed. D. Horizontal transect crossing the horizontal streak specialization, the dots represent observed points that are in the transect or lie at a distance not more than 0.5 mm of the transect line. E. Vertical transect crossing the middle *area* specialization, the dots represent observed points that are in the transect or lie at a distance not more than 0.5 mm of the transect line. F. Residual map for the over-smoothed model showing percentage of variation between the calculated data and the observed data, the contour lines represent the areas that varied more than 10% and 25%. All the densities are $\times 10^4$ cells mm^{-2} .



Special case - Fovea

The deep-sea smooth-head fish, *Conocara murrayi*, possesses a temporal area with a fovea. It has approximately ten times higher densities of cells than are found in the retinal periphery. The graphical representation and the spatial analysis of this type of retina can be challenging. When the data is smoothed using the algorithms described above, the high density points are reduced by close to half of the observed values. On the other hand, if an interpolation algorithm alone is used the maps display local fluctuations in the lower density areas that probably represent 'noise' in the count data. The hybrid method of smoothing the data in the periphery but interpolating the data in the fovea optimizes the assessment of cell density in these two different regions independently in order to accurately characterise a major specialization (fovea) while still reducing the noise in the retinal periphery. The transect line that crosses the fovea shows how the hybrid model uses interpolation to preserve the high values present in the fovea but it uses the smoothed algorithm to reduce low density fluctuations from the periphery. The difference between the values obtained by the smoothing and the interpolation methods is evident in the horizontal transect (Figure 2.9).

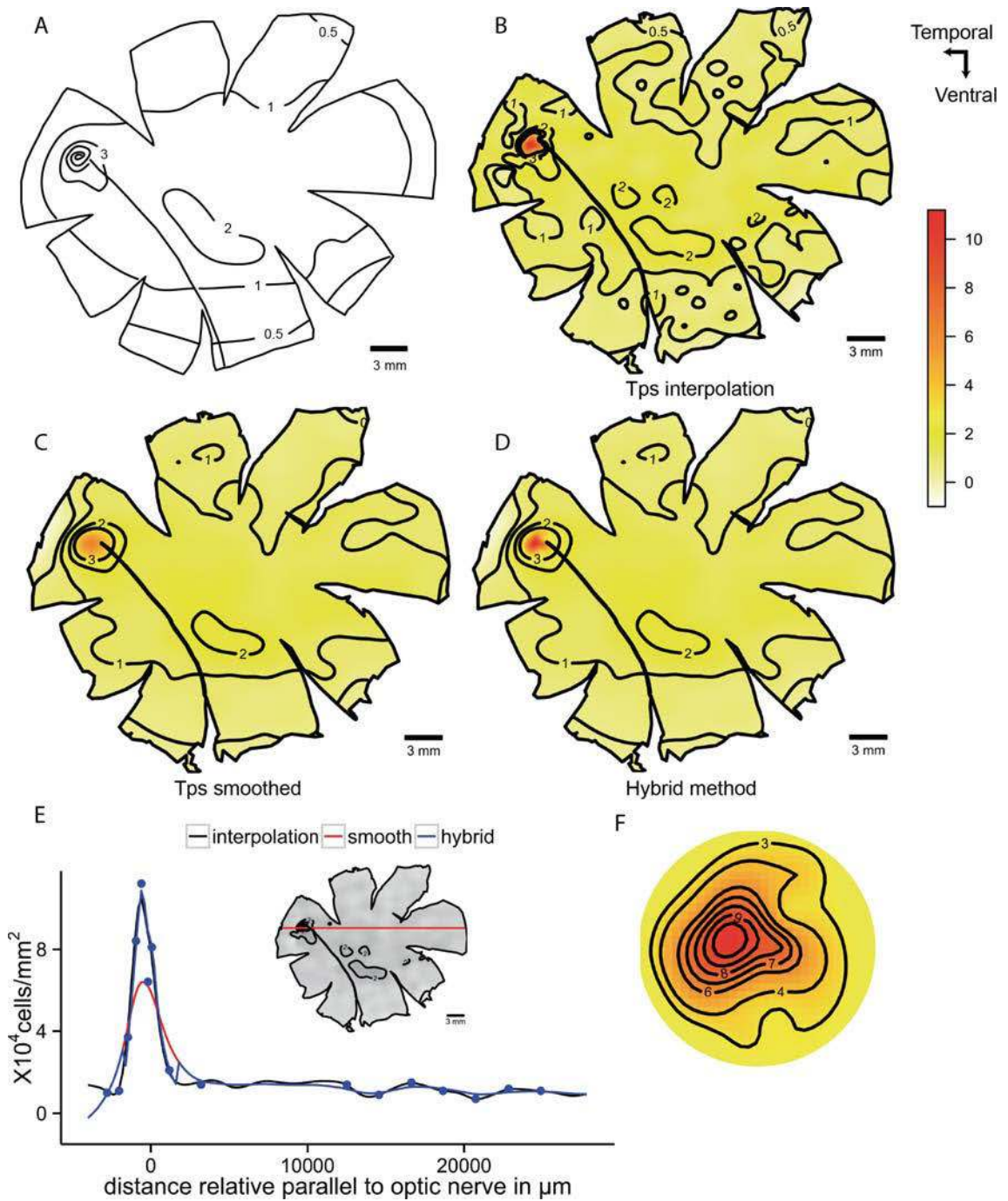


Figure 2.9 Topographic maps of the ganglion cells in the retina of the smooth-head fish, *Conocara murrayi*, which shows a fovea. A. Modified map from Collin and Patridge, 1996. B. Thin plate spline interpolation using a lambda value of 0. C. Thin plate spline under-smoothed. D. Hybrid model with Tps smoothed to GCV in the periphery and cubic interpolation in the fovea region. E. Horizontal transect crossing the fovea, the dots represent observed points that are in the transect or lie at a distance not more than 0.5 mm of the transect line. F. Detail of the fovea region using Tps interpolation. All the densities are $\times 10^3$ cells mm^{-2} .



Discussion

We have confirmed that the use of different models does not change the representation of the main retinal specializations, where the option of interpolate the data show an accurate map without modifying any value and the use of a smoother method (it is Gaussian kernel smoother or thin plate spline) will give a similar representation but reduces the noise and effects of potential outliers. The variation in the application of the smoothing parameters does affect the accuracy of the data presented and potentially its interpretation. The great diversity of retinal specializations constitutes a challenge to adopt a single model to compare the retinas but is highly important the use of an objective spatial analysis. The flexibility in the use of R allows the user to conduct the spatial analysis of retinal neuron distribution in different ways. This applies equally to the traditional method where retinal loci are examined using a compound microscope and manual counts of cell density are drawn onto a map, calibrated and iso-density contours constructed manually using limited linear interpolation or the more automated methods such as the software StereoInvestigator. This R script also gives the flexibility to change between different models of spatial analysis and to modify the smoothing parameters in order to optimize the accuracy of the final map. It also provides a faster, more reliable way to calculate and represent the topographic distribution of retinal neurons.

There are more than 30 different ways to analyse this type of data including the use of interpolations, kernel smoothers and spline methods to represent spatial distributions while taking into account things like clustering, independence of the areas, and nearest neighbour distances (Bivand et al., 2008). However, we found that for retinal analyses, where the sampling is relatively homogeneous and the distance between the observations is independent to cell density; the use of different smoothers does not alter the results. The smoothing models presented here help not only the interpretation of the data but

lends visual support to which model to use in addition to improving the aesthetic appeal of the maps. The models analyse the relationship between the different observation points assessing the spatial position and magnitude of each observation to detect a spatial pattern and reduce possible outliers (Simonoff, 1996). Smoothing models also help to reduce artefactual variation caused by retinal dissection and whole mounting (Stone, 1981). The cuts used to flatten the retina, physically modify the cell densities close to the retinal edges. Removal of the retinal pigmented epithelium, the choroid and/or the vitreous humour might also stretch or damage the tissue and therefore alter local cell density. The use of a smoothing algorithm is a very effective way of reducing the 'noise' caused by such artefactual variations by analysing the spatial distribution of the observations. If the author does not know the source of natural or artefactual variation, it is always recommended to run the models with the default parameters (Baddeley and Turner, 2005, Furrer et al., 2012) and then compare those using residuals analysis or transects.

This is the first study that compares the use of different spatial analysis algorithms to assess the topographic distribution of neurons in the retina. It is important to consider the characteristics of the retina when choosing the right smoothing parameters because of the possibility of under- or over- smoothing, where the densities can change and consequently the representation and characterisation of the specialization. Each retina should be treated independently according to its morphological characteristics. For example, a retina that might be damaged during dissection and handling will produce high artefactual variation and should be slightly over-smoothed, thereby reducing the noise and showing the natural topographic variation. This, however, always comes at the cost of under-representing the peak density. In some cases, one might expect high natural variation and the minor fluctuations in the topographic distribution could be important. In this case, under-smoothing the retina would be a better approach as



performed on the retinal data for the blue tusk fish, *Choerodon albigena*, where the under-smoothed model shows clearly the dorso-temporal specialization is evident and the horizontal streak is clearly present (Collin and Pettigrew, 1988c). The type of the study might also require a different level of smoothness; a comparative study between different species might not be affected by over-smoothing the retina while a study to identify small variability within organisms of the same species might use under-smoothing parameters.

The numerical output of each model for subsequent assessment of the maps depends on the type of algorithm used to analyse the data. Gaussian kernel smoothing using the *spatstat* package analyses only the points inside the retina, i.e. it creates a window, where the points are analysed and the cuts used to flatten the retina are considered to be empty spaces. It is possible to make very complex windows with holes and multiple polygons, which is particularly useful for the spatial analysis of the retina. The function in *spatstat* also has an edge corrector to fill the gaps between the last observed points in the periphery and the edge of the retina. It also gives a nice graphical representation because the final output is an image object instead of a numerical function, but this reduces the ability to perform subsequent statistical analyses (Baddeley and Turner, 2005, Hijmans and van Etten, 2012). However, the values calculated by the model can be extracted from the image using a raster model.

Thin plate spline, is a very powerful model that provides a *kriging* object as an output, which can predict the value at any coordinate. We prefer this model because it allows one using linear interpolation with a lambda value of 0 to assess different levels of smoothness. The use of degrees of freedom to modify the smoothness is more interpretative than the use of different lambda values. One of the disadvantages of this model is that it has to be masked to obtain the contour of the retina

and can be computationally-intensive and thus slow to run when constructing high resolution maps with thousands of points because each point is a pixel that represents a value. The Tps model has the advantage that the data frames obtained can be used easily for both statistical and graphical analyses (Furrer et al., 2012). The study of the retinal specializations requires the analysis of the highest density areas (Hughes, 1977, Collin and Pettigrew, 1988c). Most of the smoothing models tend to pull the highest and lowest values towards the mean of the population. Nevertheless, the models tend to provide complex spatial analysis, where local variation is analysed and higher values are respected. However, the use of a lower level of smoothness will give a more realistic value for the streak while, at the same time, maintaining natural local variability.

Comparing traditional methods of creating topographic maps, where the limitation of calculating the interpolation between some specific points over a spline interpolation using all the sampled points, can give slightly different results with more resolution obtained with the spline interpolation. In *P. cylindrica*, only two zones are described in the original paper (Collin and Pettigrew, 1988b) but using the thin plate spline model described here, it clearly shows a horizontal streak with three zones. Similarly, in *G. bitorquatus* there is a well defined dorsal area with similar values obtained in the original map and the smoothed model. However, the original map shows a horizontal streak of higher cell density than the thin plate spline model. This is due to the streak not being continuous so the points cannot be connected in a streak. On the contrary, the smoothing model places more emphasis on the spatial arrangement of the cells, which consequently means that the horizontal streak has a lower cell density (Collin and Pettigrew, 1988c).



The unbiased construction of iso-density contour lines, which may be effective in helping to characterise a retinal specialisation, can be obtained by the thin plate spline models. Without the most accurate data (especially within the regions of highest cell density) and without the use of colour gradients, it may be difficult to assess the spatial arrangement and relative importance of a retinal acute zone. In *C. miniatus*, the nasal and temporal specialisations have marked differences in cell density. In the original map, the iso-density contour lines for the nasal specialisation include a 15,000 cells mm⁻² and a 20,000 cells mm⁻² contour in contrast to the temporal specialisation, which shares these same contours but peaks with a density of 40,000 cells mm⁻². This may confound the importance of the two acute zones. The text of the original paper recalls this difference but readers looking for quick reference might look only for the graphical representation (Collin and Pettigrew, 1988b).

The fovea represents a special case because it has a high natural gradient in addition to the presence of a localised invagination, where the interpolation model gives a lot of noise in the periphery (Collin and Partridge, 1996). The subsampling of the foveal region and the analysis using cubic interpolation respects the high values of the fovea and reveals the real density values for the specialization. It is, therefore, possible to represent the fovea independently and plot the iso-density contour lines separately and combine the data by removing the points from the smoothed model in the area of the fovea and merging the interpolated predictions (Figure 2.9D).

Previous studies have analysed topographic densities using statistical software that might be expensive or inaccessible. The current script runs in a freely available open source program (R) and can be edited as required for specific purposes. The use of a continuous colour gradient is innovative and improves the interpretation of the variation inside the

contour intervals. The current study uses a 'heat gradient' representation that goes from white at low densities to red at high densities. This is useful because heat colours when transformed to black and white still present the same light to dark gradient. Additionally there are two colour gradients in the script that can be used in different circumstances: 1) The rainbow gradient from the *timcolours* package, where blue represents low values and red represents high values, which shows a nice representation of the densities that might be useful for visual presentations and 2) The grey gradient that might be used for black and white publications (Furrer et al., 2012, Neuwirth, 2012). The use of the R script has additional advantages, such as the easy manipulation of the maps. The commands are quick and any parameter can be changed easily with no need to repeat the whole process. Some parameters can be modified for better representation of the data including the number of contour lines and the intervals between the contours, the colour gradients of the map, the size of the text and lines and the x, y and z coordinate limits that are useful for creating the correct representation of the maps. The process to standardize the topographic maps to make them comparable (Moore et al., 2012) could be greatly improved by the use of the current script. If future studies give information in the observations and the position in the maps, more statistical analysis can be applied to extract more information on a global scale.

We consider that the main benefits of this method are in identifying specialisations that might be missed using conventional techniques and/or in reducing noise in the map patterns that are the result of random fluctuations or artefacts. This method also formalizes the analysis such that statistical comparisons can be made to robustly represent topographic data, which is both accurate and reproducible. Each retinal map should be analysed by a formal spatial analysis but it should be tested against transects or residuals to show that the smoothing parameter is accurate to the observed data.



Acknowledgements

We would like to express our gratitude to Adrian Baddeley and Duncan Temple Lang for their invaluable help in the use of the spatstat and Xml packages. We also would like to thank Bruno Buzatto and John Fitzpatrick for their excellent feedback and discussion in the use of R. We would like to express our gratitude to Joao Paulo Coimbra and Caroline Kerr for their help in the lab work and invaluable support in the use of the Stereology technique. This research was supported by the Australian Research Council and the Western Australian State Government. E.G.G. was supported by the Mexican scholarship for Postgraduate studies (CONACyT) and the Ad-Hoc Top-Up Scholarship by the University of Western Australia.

Chapter 3 Retinal topography in juvenile gummy sharks, *Mustelus antarcticus*: Implications for visual ecology and fisheries management

Garza-Gisholt, E., Hart, N. S., Collin, S. P.

School of Animal Biology and The UWA Oceans Institute, The University of Western Australia, Crawley, 6009 W.A.

Abstract

The gummy shark, *Mustelus antarcticus*, represents a high proportion of the total commercial catch of sharks in Australian fisheries. In addition to this targeted fishing effort, the species may be under additional pressure because juveniles are also caught as bycatch in other fisheries. Understanding the sensory ecology of the gummy shark would help to design and develop better bycatch reduction devices and, therefore, help to protect vulnerable gummy shark populations. Vision is one of many senses that sharks use to interpret their environment. Analysis of the topographic distribution of neurons in the retina can provide important information regarding the region/s of the visual field that are of critical importance and the spatial resolving power of the eye. In this study, we quantified the topographic distribution of both rod and cone photoreceptors and ganglion cells in the retina of the gummy shark. Maps of neuronal density contours revealed an elongated horizontal band or dorsal streak of elevated cell density in both the ganglion (1,350 peak of cells mm⁻²) and photoreceptor (rod peak of 130,000 cells mm⁻² and cone peak of 2,700 cells mm⁻²) cell populations. Such a horizontal streak would be optimal for scanning the visual horizon at increased spatial resolution. The retina of the gummy shark is duplex, containing both rods and cones, but the peak rod:cone



ratio—located in the streak—is approximately 50:1, which implies that the gummy shark retina is by-and-large adapted to provide enhanced sensitivity in dim light conditions. Maps of calculated summation ratios (i.e. the convergence of photoreceptors onto ganglion cells) reveal two retinal specializations: one area in the mid-dorsal retina with a high (300:1) rod:ganglion cell ratio and the other area in the mid-ventral retina with a low (3:1) cone:ganglion cell ratio. These two retinal specialisations would subserve high sensitivity in dim light and increased spatial acuity in brighter light, respectively.

Keywords

Gummy shark; *Mustelus antarcticus*; Triakidae, visual ecology; ganglion cells; photoreceptors; summation map; spatial resolving power; retinal topographic maps

Introduction

Sharks have been fished intensively in the last century (Holts, 1988, Williams and Schaap, 1992, Walker, 1998). Although in many cases sharks are targeted specifically for their fins, (Hoelzel, 2001, Fong and Anderson, 2002, Barker and Schluessel, 2005, Clarke et al., 2005), many fisheries also target sharks for their meat. In Australia, two shark species have been fished intensively since the 1920's: the school shark, *Galeorhinus galeus*, and the gummy shark, *Mustelus antarcticus* (Williams and Schaap, 1992). Gummy sharks are an important part of the Southern Shark Fishery (Victoria, South Australia and Tasmania) and the South Western Australia Fishery (Gardner and Ward, 1998). The gummy shark constitutes almost 55% of the total catch in the southern region of Australia with a peak of 3,450 tons in 1993 that corresponds to revenue of AU\$15.6 million (Stevens et al., 2000, Last and Stevens, 2009). According to different reports, numbers of gummy shark are stable and it is one of the few species with sustainable

catches (Kirkwood and Walker, 1986, Walker et al., 1994, Walker, 1998, Stevens et al., 2000, Pribac et al., 2005). It was reported that the population was almost depleted in the 1980s but improved management beginning in 1988 saw the population recover with steady increases in biomass over the next decade (Kirkwood and Walker, 1986, Walker et al., 1994). The ecology of elasmobranchs with low fecundity and slow growth rates make them susceptible to overfishing. However, gummy sharks grow relatively quickly compared to other elasmobranchs and achieve maturity within five years, reaching lengths of approximately 100 to 130 cm (Lenanton et al., 1990, Moulton et al., 1992, Last and Stevens, 2009).

Juvenile gummy sharks have a higher mortality rate than adults possibly because they are more susceptible to predators, i.e. other species of larger sharks, and have to compete for resources with both different species of sharks but also some species of bony fishes such as snapper (Walker et al., 1994). When gummy sharks are young, their diet is comprised of mainly crabs and octopus, with a diet shift to lobsters and bony fishes as they grow larger (Simpfendorfer et al., 2001). The distribution of juvenile gummy sharks is similar to that of the adults; this differs from the school shark, where juveniles congregate in nursery areas that provide additional protection against predators (Williams and Schaap, 1992, Heupel et al., 2007). One of the main risks for gummy shark populations is the indiscriminate bycatch of juveniles by other fisheries like trawl nets, which often represent more than 50% of the sharks caught generally often only recorded as generic “sharks”. It is also highly likely that juvenile gummy sharks are caught in seine nets and longlines (Williams and Schaap, 1992, Stevens et al., 2000) and caught by recreational fishermen that target other species such as snapper, whiting and mulloway in Western Port Bay, Victoria. (Stevens et al., 2000).



It is important to understand the ecology of species that are considered sustainable. Sensory systems represent the means that sharks use to perceive their environment, govern their distribution, predatory behaviour and even reproductive success (Myrberg Jr, 1991, Kim, 2007). By obtaining a clearer understanding of each species' perception of the environmental cues in its specific habitat, it may be possible to predict the impacts of biophysical parameters on each species perception of bycatch reduction devices and whether these can be modified to alleviate some of the environmental management pressures on juvenile sharks. The gummy shark is a demersal species (lives close to the bottom in the continental shelf) that is found in temperate waters of Australia in depths of 0-80 m but can be found down to 350 m (Last and Stevens, 2009).

Absorption by dissolved organic matter within the water column in the ocean means that light intensity falls off rapidly with increasing depth. The water also spectrally filters the incident light, absorbing more strongly at long wavelengths (Jerlov and Nielsen, 1974, McFarland, 1991). Some deep-living species have adapted to the ambient light environment by shifting the peak sensitivity of their rod pigment towards shorter wavelengths, which penetrate deeper into the water. (Crescitelli et al., 1985, Douglas and Partridge, 1997, Hart et al., 2006). Demersal species live in a wide range of light conditions and may have adaptations for scotopic (rod predominant) and photopic (cone predominant) vision. Many species of elasmobranchs are active at both dawn and dusk when low light levels are present. Some diurnal prey with visual adaptations for bright light conditions, may become more vulnerable to predators with scotopic visual adaptations (McComb et al., 2010).

The gummy shark may have different types of specializations, given the wide range of depths it inhabits. The proportion of rods and cones in

the retina is related to each species' ability to see under bright (higher number of cones) or dim (higher number of rods) light conditions (see review by Hart, 2006). The proportion of rods and cones correlates with their temporal activity (diurnal or nocturnal) and their depth distribution (Walls, 1942, Lythgoe, 1979). Topographic maps of photoreceptors reveal information of high density areas of cells that correlates to the retinal projections but only a few species of elasmobranchs have been studied (Litherland and Collin, 2008, Theiss et al., 2010). The ganglion cells in the retina send information about the image collected by the photoreceptors (via the bipolar cells) to the visual centres of the brain (Bozzano and Collin, 2000, Lisney and Collin, 2008, Litherland and Collin, 2008). The rod pathway to the central nervous system includes a high convergence of information from rod photoreceptors to bipolar cells to ganglion cells. This summation of information represents a bottleneck of information transmitted from the retina to the brain (Collin and Pettigrew, 1988a), where a high summation ratio indicates high sensitivity and a low summation ratio means increased resolving power or acuity (Bozzano and Collin, 2000, Lisney and Collin, 2008, Litherland and Collin, 2008).

The study of the topographic distribution of the photoreceptor and ganglion cell populations and its implications for the visual ecology of the gummy shark gives the fundamentals to understand and develop a possible way to avoid bycatch. Regulation of gummy shark populations is important because it is a species that is being exploited commercially in Australia and the fishing pressure on the juveniles might affect the health of the population. An understanding of any specializations in the retina will reflect the activity patterns and how this species perceives objects within its visual field (including fishing gear). Some kind of visible fishing gear targeting the juvenile sharks or some mechanism to visually repel them might be useful for reducing juvenile bycatch, thus maintaining a sustainable fishery.



Methods

Collection of animals

Four juvenile gummy sharks, *Mustelus antarcticus*, (54-62 cm total length, TL) were collected in shallow water off the coast of Victoria, Australia. The fishing method used was rod and reel from a commercial fishing vessel (Reel Time Fishing Charters) in Western Port Bay, Victoria according to guidelines of the Department of Fisheries (Permit RP1041). The animals were euthanized in the field by severing the spinal cord following the protocol approved by the Ethical guidelines of the University of Western Australia (AEC RA/3/100/917).

Eye dissection and visualization of photoreceptors and ganglion cells

The eyes of each individual were measured longitudinally (rostro-caudally) and axially (medio-laterally) using a pair of digital calipers. A small lesion was made in the ventral part of the eyecup (prior to eye removal) for orientation. The eyes were then enucleated and the cornea, lens and iris removed to expose the fundus. The eyecup was submerged in 4% paraformaldehyde in 0.1 M sodium phosphate buffer (pH 7.2-7.4) for a maximum of 14 days and then transferred to a mixture of 0.1 M phosphate buffer and 1% sodium azide (pH 7.2-7.4) and stored at 4°C. The retinas were carefully dissected free of the eyecup and radial cuts made to flatten the retina and aid in the removal of the scleral and choroidal layers. The pigment epithelium was removed using fine forceps and a fine natural-hair paint brush.

The retina was first flattened onto a glass slide, photoreceptor layer facing up, and mounted whole under a cover slip in 100% glycerol. The cover slip was sealed using nail polish to prevent the retina from drying out. After two to three days, the retina had cleared sufficiently in the glycerol that the morphology and topographic density distribution of the

photoreceptors could be analysed using conventional transmitted light microscopy. The cones and rods were visible in axial view and could be distinguished (based on their position and size) by changing the fine focus on the microscope at a magnification of 600X.

After the completion of the topographic analysis of the photoreceptors, the coverslip was removed and the retina resuspended and washed in 0.1 M phosphate buffer (twice for five minutes and a third time for 12 hours) to remove the glycerol. The retina was then mounted ganglion cell layer upwards on a gelatinized slide and allowed to dry slowly overnight in a closed chamber with formaldehyde vapors at room temperature to fix the retina to the slide and improve differentiation during the subsequent Nissl staining procedure (Stone, 1981, Coimbra et al., 2006, Coimbra et al., 2009). The retina was then rehydrated through a series of alcohols (90%, 70% 50% ethanol and 5% glacial acetic acid in distilled water) for five minutes each. The retina was then stained for two minutes using an aqueous solution of 0.1% cresyl violet (Sigma; pH 3.8). After staining, the retina was rinsed in a series (distilled water, 70% ethanol, 90% ethanol with the addition of three drops of glacial acetic acid). Finally, the retina was dehydrated in two solutions of absolute ethanol, a 1:1 mixture of ethanol and xylene and cleared with two changes of xylene (3 minutes each). The retina was cover slipped with Entellan (Merck Millipore) and allowed to set for 24 hours before counting (Stone, 1981, Coimbra et al., 2006).

Ganglion cells were distinguished by their large and irregularly-shaped somata and the granular appearance of the Nissl substance present in the cytoplasm as opposed to the glial cells, which have a darker coloration and elongated shape (Collin and Pettigrew, 1988a, Bozzano and Collin, 2000). Some amacrine cells were hard to distinguish from ganglion cells particularly in the centre of the retina (or the more specialised region) where cells are more densely packed. Nevertheless,



the total percentage of distinguishable amacrine cells was lower than 20% of the total cell counts, which will have only a small effect on the topographic distribution and the estimates of spatial resolving power.

Stereological assessment of cell density

The optical fractionator method was implemented to assess the density of ganglion cells in the ganglion cell/inner plexiform layers, rods and cones (West et al., 1991, Coimbra et al., 2006) using the StereoInvestigator (Microbrightfield Inc., USA). The section sampling fraction was 1 because the retina was also considered as a single section. The retina was considered as a flat single layer so the thickness sampling factor was 1. Therefore, the only fraction considered to be relevant for this method is the area sampling fraction. The total number of cells was estimated with the formula:

$$N_{total} = \sum Q \cdot \frac{1}{asf}$$

Where N_{total} is the total number of cells, Q is the number of cells counted in each sampling site and asf is the area sampling fraction, which is the ratio of the counting frame and the sampling grid. The counting frame was adjusted to 30 x 30 μm for rods, 100 x 100 μm for cones and 100 x 100 μm for the ganglion cells. The sampling grid size was around 200 counting frames, which is a recommended sampling number for the retina (Coimbra et al., 2009) but this varied between retinas according to eye size. The optical fractionator divides the sampling area in a random, systematic way that reduces bias by allowing all the possible locations to have the same probability to be sampled. The total number of cells is estimated by the fraction of the total grid without being affected by the distribution of cells. The correct number of sites and the accuracy of the estimated cell population were assessed using the Schaeffer Coefficient of Error, which should be <0.01 .

Construction of iso-density contour maps

Using StereoInvestigator software on a compound microscope (Olympus BX50) connected to an automatic motorized stage (MAC200, Ludl Electronic Products, USA), the outline of the retina, including the peripheral incisions, was traced using a x4 NA 0.13 objective. The outline of the acellular optic nerve head was also traced and excluded from the counting area. The retinal outline data and the cell counts were exported in an Extensible Markup Language (.xml) format file and analyzed using the open source program 'R' (R Core Team, 2012) and additional packages (Baddeley and Turner, 2005, Wickham, 2009, Furrer et al., 2012, R Core Team, 2012, R Studio, 2012, Wickham, 2012) using custom script for the construction of retinal topographic maps (Garza-Gisholt et al., submitted). The uncalibrated cell counts were transformed to a density value of cells per mm² with the formula:

$$\text{Cells}\cdot\text{mm}^{-2} = Q \cdot \frac{1,000,000}{cf}$$

where Q is the number of cells counted in each sampling site and cf is the counting frame in μm^2 . Topographic maps for the spatial distribution of cell density were obtained using an under-smoothed thin plate spline (Garza-Gisholt et al., 2014) (Chapter 2).

Three topographic maps were constructed for each type of cell. Since the size of all the individuals was similar with no more than a 5% variation in the total retinal area, all maps were standardized to the largest retina by aligning the position of the optic nerve head as a reference and then using the proportional distance to the edge to calculate the new set of coordinates for the contour and the observed data. The total number of cells was not calculated from the corrected map but for each single stereological procedure. A grid of retinal loci (every 200 μm in the x and y axes) was used to calculate the cell density values for each retina in the same position. The mean of each cell density was calculated to obtain an average topographic map. The final map was outlined using



an oval of the dimensions of the largest retina. This map does not represent a hemispherical orientation but simply removes the radial cuts made to flatten the retina (since cuts were not placed in the same position). The spline method adjusts the values that are close to the edge of the cuts using a spatial algorithm to correct any artefacts due to shrinkage, etc. A surface representation of the spatial arrangement of points was obtained with the contour lines representing areas of equal cell density.

Retinal summation maps and calculation of spatial resolving power

Summation ratios comparing the density of rod photoreceptor cells and ganglion cells at each retinal locus were calculated using the average maps (see above). The three topography maps were aligned with the optic nerve head as a reference point, where the grid of calculated average cell densities was then used to obtain the number of rods per ganglion cell. These summation ratios were plotted and iso-density contours constructed using the same technique as for the single cell type maps.

Spatial resolving power (SPR) was calculated assuming a hexagonal ganglion cell distribution as performed in previous studies (Hart, 2002, Theiss et al., 2007):

$$d = \frac{2\pi f}{360}$$

$$S^2 = \frac{2}{D\sqrt{3}}$$

$$v = \frac{1}{S\sqrt{3}}$$

where d is the distance on the retina subtended by one degree, f is the focal length calculated by multiplying the axial radius of the lens along the optical axis by 2.55 according to Matthiessen's ratio (Matthiessen, 1880), D is the peak ganglion cell density in the area centralis, S is the cell to cell spacing and ν is the maximum spatial frequency. The theoretical spatial resolving power in cycles per degree is then given by $\nu * d$ (Hart, 2002, Theiss et al., 2007).

Results

The analysis of the topographic distribution of ganglion cell densities in the gummy shark (*Mustelus antarcticus*) reveals a dorsal streak delineated by a density contour of 700 cells mm⁻² with a peak of more than 900 cells mm⁻² close to the middle of the retina (Figure 3.1D). The retinal regions bounded by the 700 cells mm⁻² contour were discontinuous in two of the three retinas but when the average map was formed, the density values stabilized, thereby creating a continuous streak (Figure 3.1A). The positions of the smaller, more localised, retinal regions of higher density (900 cells mm⁻²) were consistent in the three retinas. The density of ganglion cells differed by a factor of two between retina 6 RE and 2 RE, with the peak density in retina 2 RE reaching 1,600 cells mm⁻². The total number of ganglion cells in the retina varied between 243,000 cells in retina 6 RE to 510,000 in retina 2 RE (Table 3-1).

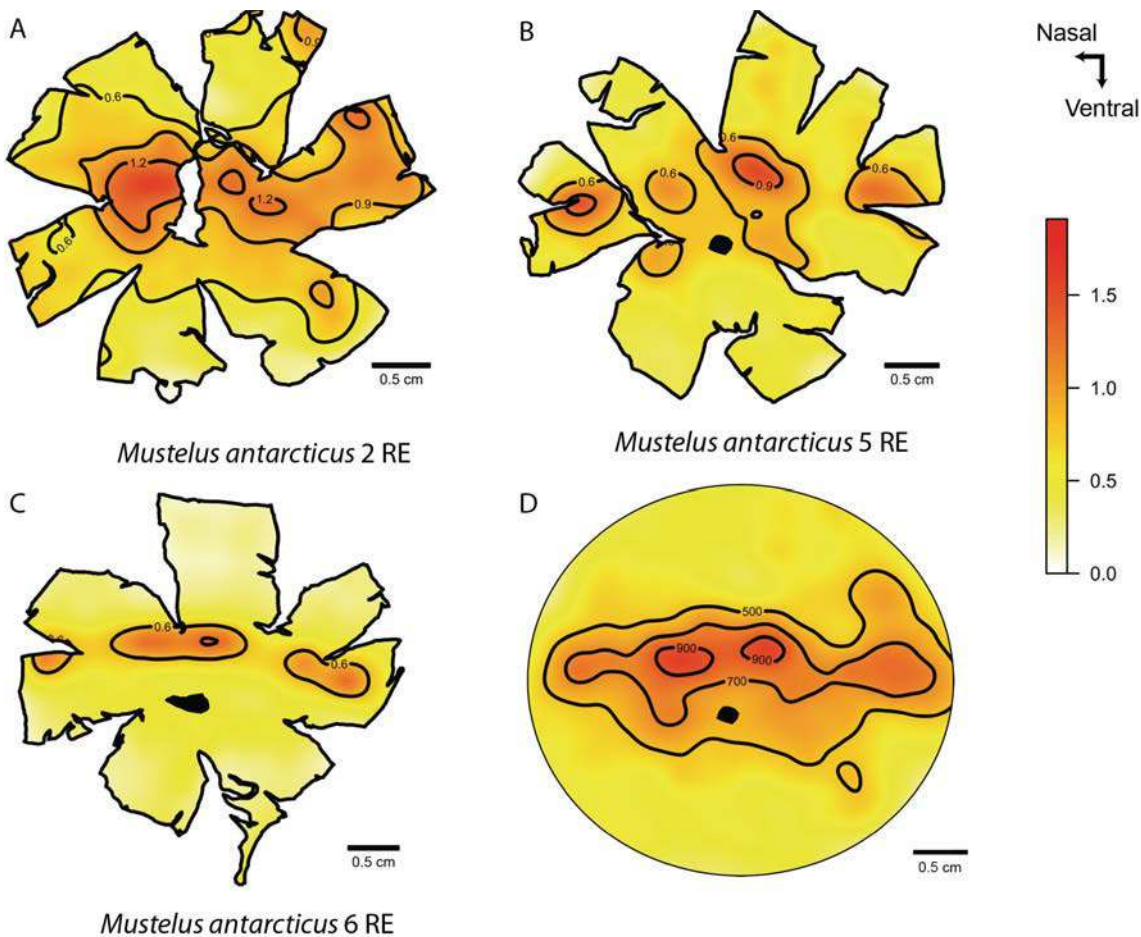


Figure 3.1 Ganglion cell density maps in the gummy shark, *Mustelus antarcticus*. A). Male 60 cm TL right eye. B). Male 62 cm TL right eye. C). Male 56 cm TL right eye. D) Average ganglion cell density map. The values are $\times 1000$ cells mm^{-2} .

The rod density maps showed a shallow streak in the dorsal retinal region. The left retina (20 LE) showed a portion of the ventral retina with values of $<60,000$ cells mm^{-2} (Figure 3.2C) that were different from the two other retinas. The average map showed a shallow dorsal streak of more than $100,000$ cells mm^{-2} and an area of $>80,000$ cells mm^{-2} was consistently found in the three individual retinas around the optic nerve head (Figure 3.2D). The total number of rods per retina varied from 41 million cells in 20 LE to 66 million cells in 2 RE.

The cone density maps showed a dorsal streak of more than $1,500$ cells mm^{-2} with a peak density of $>2,000$ cells mm^{-2} (Figure 3.3D). This regional peak is consistent in the three retinas but retina 6 RE (Figure

3.3B) showed a higher peak of $>2,500$ cells mm^{-2} in the central region and another one in the temporal region. The variation in the periphery of the retinas showed retina 20 LE with lower values of more than 500 cells mm^{-2} while the periphery of 6 RE had regions close to 1,000 cells mm^{-2} . The total number of cones varied from close to 428,000 cells (20 LE) to 1,037,000 cells (6 RE).

Table 3-1. Eye morphometrics and stereological data for the ganglion cells, rods and cones in the four retinas of the juvenile gummy shark, *Mustelus antarcticus*.

	Individual	2 Right Eye	5 Right Eye	6 Right Eye	20 Left Eye	Average
	Sex	Male	Male	Male	Female	
	Size cm	60	62	56	54	61
	Dorso-ventral mm	12.07	11.33	11.47	10.76	11.7
	Rostro-caudal mm	16.12	16.92	16.35	15.42	16.52
	Axial mm	16.19	16.79	16.95	16.7	16.49
	Average Lens Diameter	7.5	7.96	8.7	7.3	7.73
Ganglion cells	Counting frame	150*150	150*150	300*300		150*150
	Sampled sites	209	202	199		205.5
	Area	713,290,000	775,549,000	739,472,000		744419500
	Number of Cells	510,855	360,889	243,378		435872
	Peak 1000* cells mm^{-2}	1.625	1.077	0.922		1.4
	CE	0.038	0.037	0.052		0.0375
Rods	Counting frame	30*30		30*30	30*30	30*30
	Sampled sites	210		193	212	210
	Area	759,306,000		771,233,000	537,088,000	759306000
	Number of Cells	66,500,212		64,866,668	41,435,024	66500212
	Peak cells 1000* mm^{-2}	130.133		123.99	116.805	130.1
	CE	0.021		0.019	0.023	0.021
Cones	Counting frame	100*100		100*100	100*100	100*100
	Sampled sites	214		195	216	214
	Area	759,306,000		771,233,000	537,088,000	759306000
	Number of Cells	650,522		1,037,200	428,544	650522
	Peak*1000 cells mm^{-2}	2.707		3.324	2.433	2.7
	CE	0.049		0.049	0.039	0.049
	Focal length mm	9.57	10.15	11.11		9.86
	Spatial Resolving Power (cycles per degree)	3.62	3.12	3.16		3.37



The proportion of rods to cones was close to 50:1 in the dorsal streak and 60:1 around the periphery. The rod to ganglion cell summation ratio varied from less than 100:1 in the dorso-nasal part of central retina to 300:1 in the dorsal and ventral retina (Figure 3.4A). The cone to ganglion cell summation ratio was different across the retina with areas of 1:1 in the periphery and around the optic nerve head and a value of 3:1 in the dorsal retina (Figure 3.4B). The calculated spatial resolving power varied between 3.12 cycles per degree (5 RE) to 3.61 cycles per degree (2 RE) with mean of 3.37 (+/- 0.27) cycles per degree.

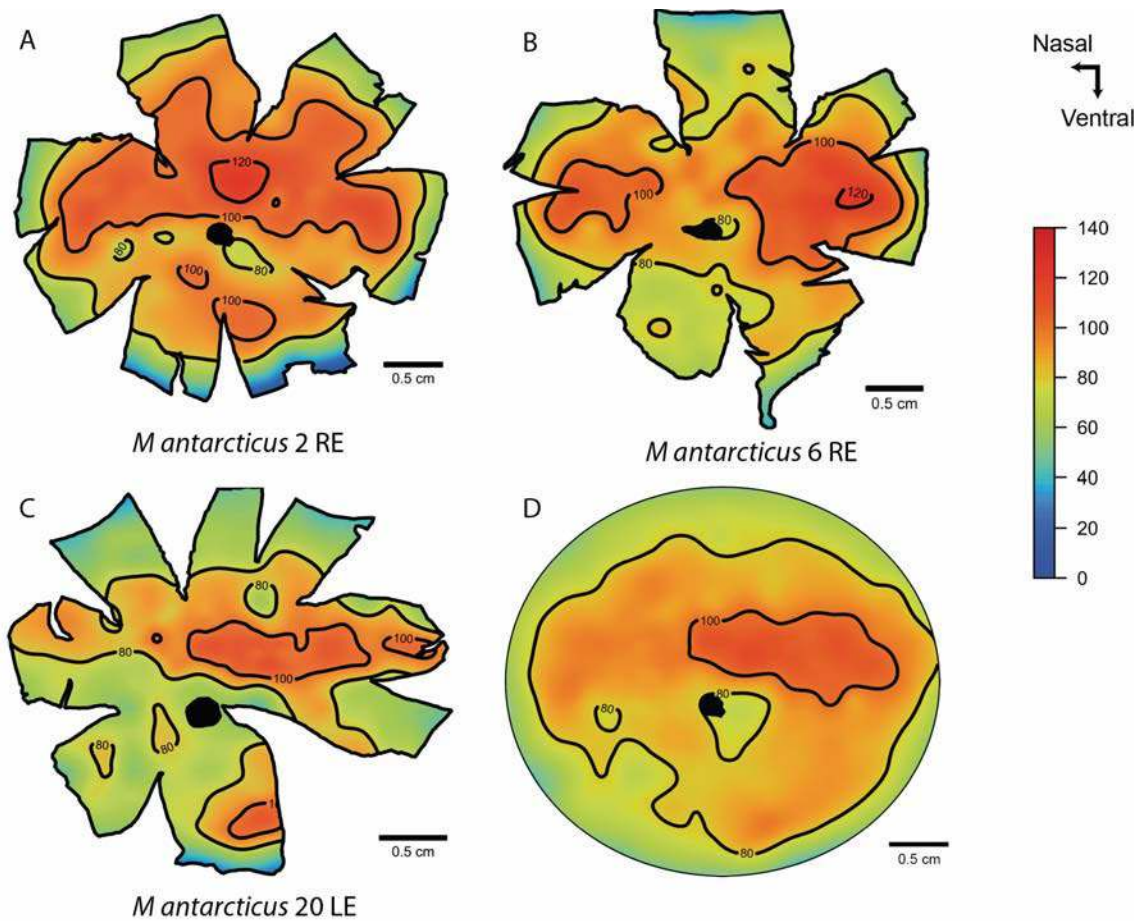


Figure 3.2 Rod cell density maps in the gummy shark, *Mustelus antarcticus*. A). Male 60 cm TL right eye. B). Male 56 cm TL right eye. C). Female 54 cm TL left eye. D) Average rod cell density map. The values are $\times 1000 \text{ cells mm}^{-2}$.

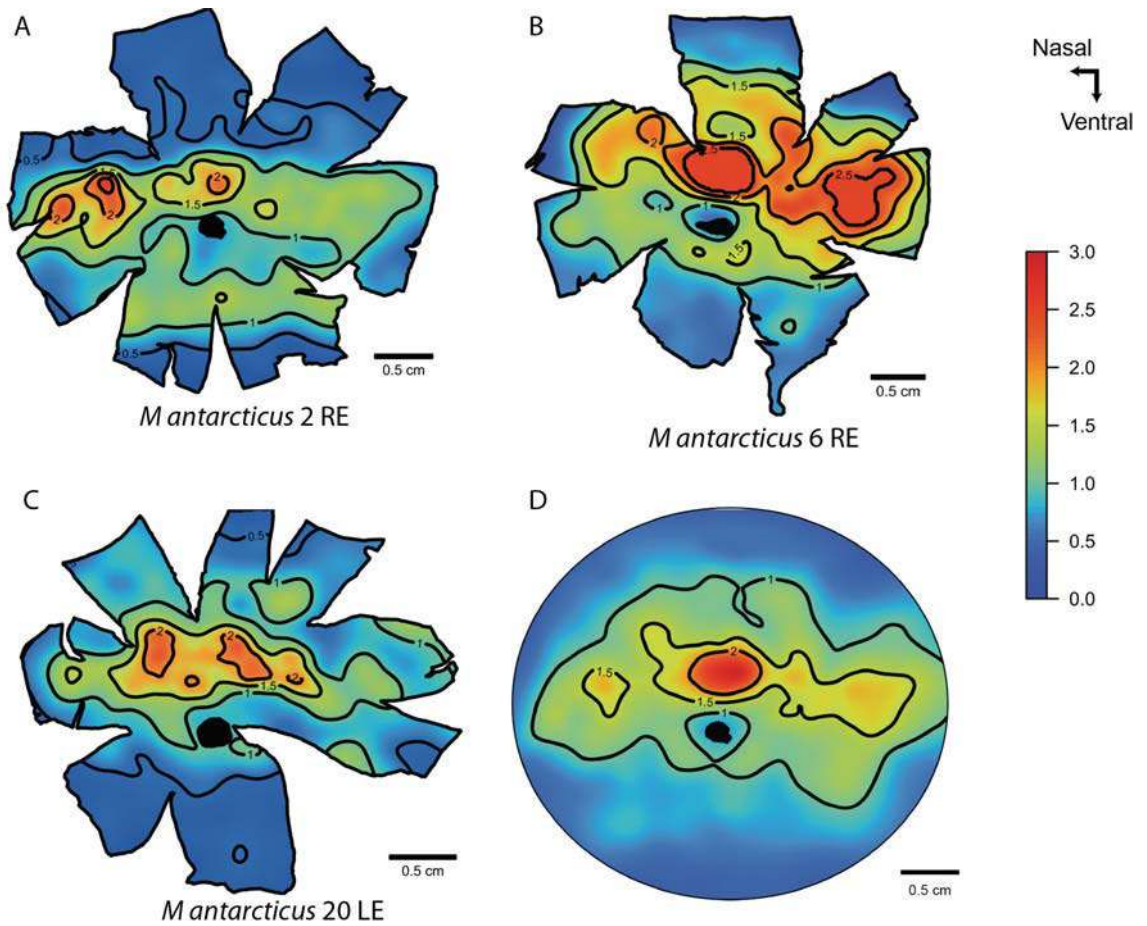


Figure 3.3 Cone cell density maps in the gummy shark, *Mustelus antarcticus*. A). Male 60 cm TL right eye. B). Male 56 cm TL right eye. C). Female 54 cm TL left eye D) Average cone cell density map. The values are $\times 1000$ cells mm^{-2} .

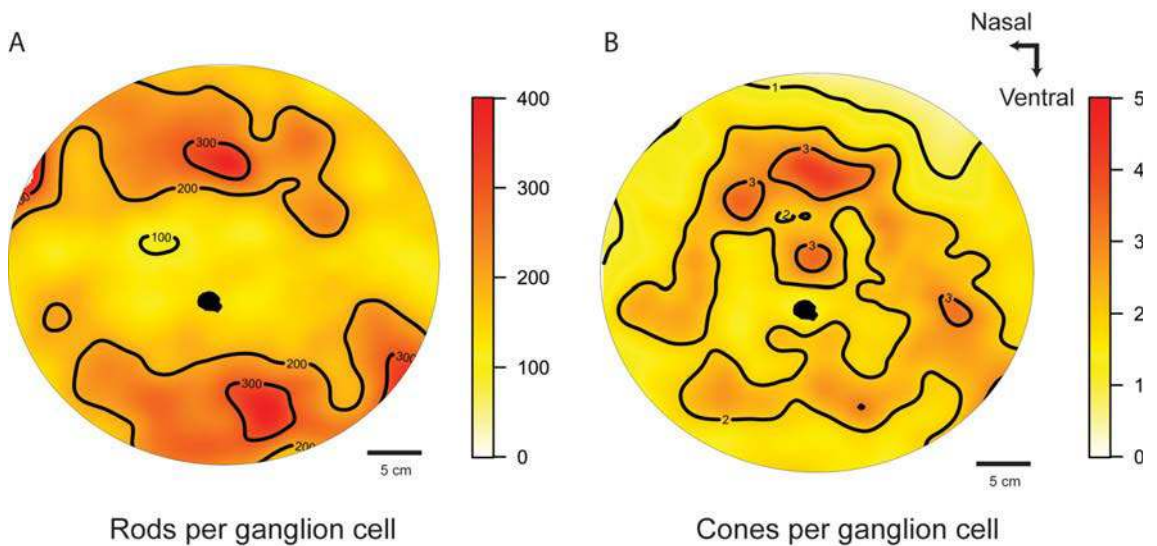


Figure 3.4 Summation maps between photoreceptor and ganglion cells in the retina of the gummy shark, *Mustelus antarcticus*. A). Number of rods per ganglion cell summation map. B). Number of cones per ganglion cell summation map.



Discussion

Both types of photoreceptors (rods and cones) were observed in the retina of the gummy shark, *Mustelus antarcticus*. The proportion of rods to cones in *M. antarcticus* is greater (50:1) than in some benthic shallow water sharks that have a range from 5:1 to 20:1 (see review from Hart et al, 2006). However, this species (with a depth range of 0-350 m) possesses a similar or lower rod to cone ration than other sharks that have a greater depth range (0 to 1,460 m) like the smooth dogfish, *Mustelus canis* (>100:1) (Stell and Witkovsky, 1973b); the birdbeak dogfish, *Deania calcea* (>100:1) (Kohbara et al., 1987) and the piked dogfish, *Squalus acanthias* (50:1) (Stell, 1972) The relatively high proportion of rods to cones in the retina of juvenile gummy sharks suggest a crepuscular to nocturnal activity pattern and/or an adaptation for vision in deep water, although the presence of cones suggests some capacity for photopic vision. It is unknown whether other species of sharks from the family Triakidae i.e. *Triakis semifasciata* and *Mustelus henlei* also possess a low proportion of cones since Sillman et al. (1996) admits that the number of cones was not quantified. The theoretical spatial resolving power at about three cycles per degree is consistent with values calculated for deep-sea species of elasmobranchs showing a shift from acute vision to a high sensitivity vision.

Differences in the topographic distribution and numbers of neurons in the retinas of elasmobranchs are subtle compared to other vertebrate groups. The use of average maps is a great tool to reduce the small intraspecific variation observed between similar-sized individuals in order to ascertain the major specializations in each species. Although providing a consistent set of results and revealing a common set of visual specialisations, all retinas showed some degree of variation. This intraspecific variability may be natural or may be due to retinal damage during dissection and/or the variations in the degree of staining with

cresyl violet (Stone, 1981). The use of the smoothing spatial analysis reduces the effect of artefacts in each retina and the creation of average maps can provide a more accurate topographic representation that encompasses the main specializations that are consistent across all retinas. Previous studies have shown only one representative of each species i.e. normally the retinal map with less convoluted iso-density lines, instead of showing an average map. The differences in the total cell number of neurons (photoreceptors or ganglion cells) might be the result of higher levels of intraspecific variation that would be expected during the development of any retina specializations in elasmobranchs (Harahush et al., 2009). The use of animals of similar size and age generally reduces ontogenic variability in the number and density of retinal neurons. In this study, all the sharks were juveniles where the retina is still developing and undergoing the rapid addition of new neurons (Harahush et al., 2009). Although the individuals used were all size matched, it was impossible to assess the age of each of these specimens, which could explain the variability in the total ganglion cell.

The dorsal streak, with characteristic regions of high cell density zones, is a specialization useful for scanning the horizon, and is observed in the retinas of a number of other species of elasmobranchs occupying a similar habitat. The peak density of rods in the gummy shark retina (113,000 cells mm^{-2}) is also similar to other species of sharks. According to Litherland and Collin (2008), the whitetip reef shark, *Triaenodon obesus*, possesses a similar but slightly lower peak of rods (104,100 cells mm^{-2}) and is reported to live at depths of between 5 and 40 meters but can venture to depths of 400 meters that corresponds to the depth range of the gummy shark (Last and Stevens, 2009). The distribution of cones shows a centro-dorsal acute zone, providing the ability to detect prey on the substrate. A dorsal streak of high ganglion cell density has been found to be present in a range of other species i.e. velvet belly dogfish, *Etmopterus spinax* (>900 cells mm^{-2}) (Bozzano and



Collin, 2000) and the brown-banded bamboo shark, *Chiloscyllium punctatum* ($>2,500$ cells mm^{-2}) (Lisney and Collin, 2008).

The anatomical spatial resolving power (SRP) calculated from the peak ganglion cell density should be a better indicator of visual acuity than using the peak of rod photoreceptor cell density because the ganglion cells are responsible for the output signal of the retina to the visual centres of the brain and receive signals from very many rods. Nevertheless, some ganglion cells might not be involved in the photoreceptor pathways and this might result in an overestimation of the spatial resolving power. The spatial resolving power of over 3 cycles per degree in *M. antarcticus* is similar to other species of coastal or demersal elasmobranchs, i.e. the velvet belly dogfish, *Etmopterus spinax* (3.07 cycles per degree, benthopelagic) (Bozzano and Collin, 2000) and the brown-banded bamboo shark, *Chiloscyllium punctatum* (2.02 cycles per degree, coastal) (Lisney and Collin, 2008).

The gummy shark, *M. antarcticus*, is a demersal species where juveniles are known to live from the shallow coastal zones to about 80 meters depth. Although some estuaries may be expected to provide some level of protection for juveniles, bycatch data does not support them occupying any specific areas of refuge (Williams and Schaap, 1992, Prince, 2005, Jones et al., 2010). Interestingly, Williams and Schaap (1992) found that, juveniles were predominantly caught during the night in Tasmania. This suggests that juvenile gummy sharks have nocturnal habits, which may confirm why crabs and octopuses, which are active in low light conditions, comprise such a large part of their diet (Simpfendorfer et al., 2001) and why predominantly rod-based vision might help them to detect prey moving over the substrate. Since the diet of the gummy shark shifts when they are adults (to other types of crustaceans such as lobster and larger bony fishes), a concomitant change in their visual ecology may also be predicted.

Some studies have attempted to design accessories for commercial fishing gear to help reduce bycatch of juvenile sharks. Future improvements could include visual deterrents such as reducing the contrast of any baits (Hart et al., 2007), the deployment of light sticks or photoluminescent nets that are visible to sharks (allowing them to avoid them in time) but may not be visible to other target fishes (Jordan et al., 2013). Other studies have suggested that predator shapes be used in nets to reduce bycatch, where knowledge of the spatial resolving power would be critical (Wang et al., 2010). Other design features for reducing bycatch could include understanding the limits of vision and spectral sensitivity—especially given that sharks appear to be cone monochromats and have a rather limited range of spectral sensitivities of both rods and cones (Hart et al. 2011) compared to fishes—and the influences of other senses (electroreception, chemoreception and audition) (Meredith and Kajiura, 2010, Collin, 2012, Kempster et al., 2012, Gardiner et al., 2013, Jordan et al., 2013).

Further studies comparing juveniles to adults might reveal an ontogenetic change in the development of the visual system in gummy sharks. The possible change in photoreceptor densities and proportions of rods and cones might be the result of a dietary shift with maturity. If juveniles have a higher sensitivity to light and because their activity patterns align with a nocturnal lifestyle then a bycatch reduction device producing a bright flashing light may be useful in deterring this species, thereby reducing bycatch.



Acknowledgements

We would like to thank Camila Martins, Richard Reyna (University of Melbourne) and Matt Cini (Reel Time Fishing Charters) for collecting samples of gummy sharks in Western Port Bay, Victoria. We are sincerely thankful to Joao Paulo Coimbra and Caroline Kerr for all the invaluable help in the laboratory. This research was supported by an Australian Research Council Discovery Project Grant (DP110103294) to SPC, NSH and others, and the Western Australian State Government (to SPC). EG-G was supported by the Mexican scholarship for Postgraduate studies (CONACyT) and an Ad-Hoc Top-Up Scholarship by the University of Western Australia.

Chapter 4 Retinal characteristics and visual specializations in three species of chimaeras, the deep sea *Rhinochimaera pacifica* and *Chimaera lignaria*, and the vertical migrator *Callorhinchus milii*

E. Garza-Gisholt, N.S. Hart and S. P. Collin

School of Animal Biology and The UWA Oceans Institute, The University of Western Australia, Crawley, 6009 W.A., Australia

Abstract

The order Holocephali is one of the most ancient groups of vertebrates but their biology and ecology are poorly studied. The majority of holocephalans live in the mesopelagic zone of the deep ocean, where there is little or no sunlight, but some species migrate to more brightly lit shallow waters to reproduce. The present study compares the retinal characteristics of two species of deep-sea chimaeras: the Pacific spookfish (*Rhinochimaera pacifica*) and the Carpenter's chimaera (*Chimaera lignaria*) with the elephant shark (*Callorhinchus milii*), a vertical migrator that lives in the mesopelagic zone but migrates to shallow waters to reproduce. The two species of deep-sea chimaeras possess pure rod retinae with long outer segments (mean 66 and 68 μm in *C. lignaria* and *R. pacifica*, respectively) that may serve to increase visual sensitivity. In contrast, the retina of the elephant shark possesses both rods, which are significantly shorter (mean 34 μm) than those found in the deep-sea species, and cones, and therefore the potential for color vision. Topographic maps of the photoreceptor distribution in the three species reveal a similar pattern with a dorsal horizontal streak (peak rod density ranging from 70,000 to 120,000 rods per mm^2) sampling the lower visual field with the peak density of



rods being much higher in the deep-sea chimaeras (80,000 to 120,000 rods per mm^2) than in the elephant shark (70,000 rods per mm^2). The ganglion cell distribution closely follows that of the photoreceptor populations in all three species but there is a lower peak density of ganglion cells in the deep-sea species of chimaeras (150 cells mm^{-2} compared to 400 cells mm^{-2} in the elephant shark), which represents a significant increase in the summation ratio of photoreceptors to ganglion cells. The theoretical maximum anatomical spatial resolving power calculated from the spacing of the ganglion cells is similar for all three species with values around 2.5 cycles per degree. Calculated optical sensitivity varies from $2.20 \mu\text{m}^{-2} \text{sr}^{-1}$ in *C. milii* to $4.42 \mu\text{m}^{-2} \text{sr}^{-1}$ in *R. pacifica*. It is evident that the eyes of deep-sea chimaeras increase sensitivity to detect objects under low light levels but at the expense of both resolution and the capacity for colour vision. In contrast, the elephant shark has lower sensitivity and the potential for colour discrimination.

Keywords

Chimaera; Holocephali; visual ecology; ganglion cell; photoreceptors; optical sensitivity; spatial resolving power; summation map

Introduction

Chimaeras, from the subclass Holocephali, are one of the most ancient groups of vertebrates. They are cartilaginous fishes, closely related to sharks and rays (subclass Elasmobranchii), which all belong to the Chondrichthyes, a class that evolved in the Silurian Period over 400 million years ago (Inoue et al., 2010). The holocephalians are a less diverse group than the elasmobranchs with only about 47 extant described species from the more than 1,200 species of chondrichthyans (Lund and Grogan, 1997, Last and Stevens, 2009, Lisney, 2010). There are three different families within the order Holocephali: Chimaeridae,

Rhinochimaeridae and Callorhinchidae. The present study analyses one member of each of these families; the Carpenter's chimaera, (*Chimaera lignaria*: Chimaeridae), the Pacific spookfish (*Rhinochimaera pacifica*: Rhinochimaeridae) and the elephant shark (*Callorhynchus milii*: Callorhinchidae).

In the last decades, the depletion of pelagic fish stocks has seen increased pressure placed on deep-sea fisheries including chimaeras, where they are now considered to be vulnerable to overfishing (Koslow et al., 2000, Devine et al., 2006, Morato et al., 2006, García et al., 2008, Norse et al., 2012). This is especially true for all three species of callorhinchids, which migrate to shallow estuaries to reproduce (Ebert, 2003, Didier, 2004, Lisney, 2010). Nevertheless, the abundance of the spotted ratfish, *Hydrolagus colliei* was reported to have increased in 1995 in Californian waters (Barnett, 2008). In some regions of Australia and New Zealand, chimaeras are consumed by humans as 'flake', often sold as fish and chips (Francis, 1997, Francis, 1998, Last and Stevens, 2009).

Their unique morphological characteristics and their relationship with basal vertebrates, makes the chimaeras one of the most interesting groups to study with respect to their visual system (Ebert, 2003, Compagno et al., 2005) since they live in the mesopelagic zone at more than 500 meters, where there are low levels of sunlight (Didier, 1998, Compagno, 2001, Didier, 2004, Last and Stevens, 2009) in addition to the bioluminescence produced by a large range of animals in the deep-sea (Herring, 1977, Herring, 2000, Warrant and Locket, 2004). Chimaeras living in this zone may have adaptations to either increase sensitivity, as the levels of sunlight diminish, while other species might shift to enhancing resolution to locate small sources of bioluminescence (Warrant and Locket, 2004). On the other hand, the elephant shark



(*Callorhinchus milii*) migrates to shallow, brightly-lit water to reproduce but otherwise lives in deep, dimly-lit, water (Last and Stevens, 2009).

Very little is known about the biology of chimaerids but, like sharks, they mature late, give birth to a small number of offspring and have no parental care (Compagno et al., 2005, García et al., 2008). Isolated reports on their diet reveal that *Chimaera monstrosa* (Ebert and Bizzarro, 2007), *Hydrolagus* species (Marques and Porteiro, 2000, Moura et al., 2005, Gonzalez et al., 2007), and *Harriota raleighana* (Dunn et al., 2010) all feed on benthic invertebrates like crustaceans, ophiurids, polychaetes and urchins. However, there is a dietary difference between *Harriota* sp. from the Rhinochimaeridae family that feed predominantly on benthic invertebrates and *Hydrolagus* sp. from the Chimaeridae family that feed primarily on pelagic molluscs like cephalopods (Gonzalez et al., 2007).

Chimaeras, like other elasmobranchs, have a large range of sensory systems that allow them to detect a range of environmental stimuli in relatively deep water. Over the last decade, vision has been studied more intensively in elasmobranchs but chimaeras have received little attention (Hart et al., 2006, Lisney, 2010). Despite living in low light environments, some species of chimaerids have prominent eyes, which are relatively large with respect to their body size (Didier, 2004, Lisney, 2010). Large eyes represent a specialization to increase sensitivity, especially in deep-sea species, where the amount of light available for vision is limited (Warrant and Locket, 2004, Lisney and Collin, 2007, Douglas, 2010). The pupil of most deep-sea elasmobranchs shows little or no ability to change size, remaining dilated to increase the amount of light entering the eye (Kuchnow, 1971, Maddock and Nicol, 1978, Bozzano et al., 2001). Some species of chimaeras also possess a *tapetum lucidum*, a reflective layer of cells behind the retina that increases sensitivity by reflecting light back through the photoreceptors (Denton

and Nicol, 1964, Maddock and Nicol, 1978, Didier, 2004). Additionally, species that live in the mesopelagic zone have specializations to optimize light absorption such as the elongation of the outer segments in the photoreceptor cells (Land, 1981, Warrant and Locket, 2004).

The analyses of retinal cell distribution remains a powerful technique to infer the visual ecology of species that are hard to observe in their natural environment (Collin, 1999, Collin, 2008). Photoreceptor cells (rods and cones) are responsible for light detection and phototransduction; rod photoreceptors possess long outer segments to enhance light capture and sensitivity and operate in dim light conditions, while cones possess smaller, tapered outer segments that and operate in high light intensities. If a species possesses more than one type of cone photoreceptor, each containing a visual pigment with a different peak spectral sensitivity, it has the potential for colour vision (Carter, 1948). Most chimaeras are reported to have a pure rod retina with a visual pigment tuned to maximally absorb the wavelengths of light available in deep water. The rod visual pigments of deep-sea fishes contain a chromophore based on vitamin A₁ that absorb wavelengths between 470 and 490 nm (Denton, 1963, Crescitelli, 1969, Beatty, 1969, Partridge et al., 1989, Douglas et al., 1995, Fröhlich et al., 1995). Although little is known about the photoreceptors in chimaerids, Vigh-Teichman et al (1990) characterised two types of rods based on immunohistochemical and ultrastructural criteria in the rabbit fish, *Chimaera monstrosa*. More recently, Davies et al (2009) showed that the retina of the elephant shark, *Callorhinchus milli*, possesses a single type of rod opsin gene (Rh1) and three cone opsin genes (Rh2, LWS1 and LWS2), thereby providing the potential for colour vision.

Many studies of the distribution of ganglion cells (total population or subtypes) in the retina of elasmobranchs reveal a range of specializations for acute vision subtending different regions of each



species' visual field (Hueter, 1991a, Bozzano and Collin, 2000, Bozzano, 2004, Theiss et al., 2007, Litherland and Collin, 2008). However, very few studies have concentrated on the topography of ganglion cells in chimaeras with the exception of the spotted ratfish, *Hydrolagus colliei* (Collin, 1999) and the large-eyed rabbitfish, *Hydrolagus mirabilis* (Bozzano and Collin, 2000), where both studies revealed a pronounced horizontal streak or elongated increase on cell density across the dorsal meridian of the retina. No studies have examined the convergence of photoreceptor cells on ganglion cells (convergence ratio) in the retina of chimaeras, which is a quantitative indicator of sensitivity/resolution (Litherland and Collin, 2008, Douglas, 2010). Another parameter that is useful to compare the level of visual specialization to different light intensities and habitats is the optical sensitivity. The amount of photons detected by each photoreceptor gives a measure of the sensitivity of the retina. Strategies to increase the photon collection by the photoreceptors include increasing the optical aperture. The elongation of the outer segments can be found in some teleost fishes that live in the mesopelagic zone like the blue marlin with an optical sensitivity of $1.5 \mu\text{m}^{-2} \text{sr}^{-1}$ (Fritsches et al., 2003). Sensitivity can vary greatly across groups of the organisms and comparisons should be treated carefully. For example teleost fishes have an optical sensitivity of around 1.5 to $6 \mu\text{m}^{-2} \text{sr}^{-1}$, while some marine invertebrates such as the deep-sea crustacean, *Oplophorus* sp. can reach up to $3300 \mu\text{m}^{-2} \text{sr}^{-1}$ (Land, 1981).

This study examines the visual ecology of three species of chimaeras from two different habitats (deep-sea and shallow water) and reveals specializations for higher sensitivity in the deep-sea species (*Rhinochimaera pacifica* and *Chimaera lignaria*) and specializations for enhanced resolution in the migratory species (*Callorhinchus milii*).

Methods

Collection of animals

Elephant sharks (*Callorhinchus milii*) were collected in shallow water off the coast of Victoria, Australia using rod and reel in Western Port Bay with the Department of Fisheries (Permit RP1041). The animals were transported to the Department of Primary Industries (DPI) facilities in Queenscliff for additional physiological experiments and were euthanized using an overdose of tricaine methane sulfonate (MS222; 1:2,000 in seawater) according to the Ethical guidelines of the University of Western Australia (AEC RA/3/100/917).

Deep-sea chimaeras (*Rhinochimaera pacifica* and *Chimaera lignaria*) were collected during a fishing trip off the coast of New Zealand in the fishing boat Sea Mount operated by Anton's Seafoods Ltd., a company based in Auckland, New Zealand that was targeting orange roughy and catching deep-sea sharks and chimaeras as bycatch. Animals were dead when brought onto the boat but sufficiently fresh for anatomical studies.

Eye dissection and visualization of photoreceptors and ganglion cells

The eyes of each individual were measured longitudinally (rostrally-caudally) and axially (medio-laterally) using a pair of digital calipers. A small lesion was made in the ventral part of the eyecup (prior to eye removal) for orientation. The eyes were then enucleated and the cornea, lens and iris removed to expose the fundus. The eyecup was submerged in 4% paraformaldehyde in 0.1 M sodium phosphate buffer (pH 7.2-7.4) for a maximum of 14 days and then transferred to a mixture of 0.1 M phosphate buffer and 1% sodium azide (pH 7.2-7.4) and stored at 4°C. Three retinas per species were carefully dissected free of the eyecup and radial cuts made to flatten the retina and aid in the removal of the



scleral and choroidal layers. The pigment epithelium was removed using fine forceps and a fine natural-hair paint brush.

The retina was first flattened onto a glass slide, photoreceptor layer facing up, and mounted under a cover slip in 100% glycerol. The cover slip was sealed using nail polish to prevent the retina from drying out. After two to three days, the retina had cleared sufficiently in the glycerol that the morphology and topographic density distribution of the photoreceptors could be analyzed using conventional transmitted light microscopy. The cones and rods were visible in axial view and could be distinguished (based on their position and size) by changing the fine focus on the microscope at 600X magnification.

After the completion of the photoreceptor analysis, the retina was washed in 0.1 M phosphate buffer (pH 7.2-7.4) to remove the glycerol. The retina was then mounted ganglion cell layer upwards on a gelatinized slide and consequently hydrated and Nissl stained with an aqueous solution of 0.1% cresyl violet (Sigma pH 3.8). The retina was then dehydrated using a graded series of ethanols (for details, see Garza-Gisholt et al., 2014 Chapter 3) (Stone, 1981, Coimbra et al., 2006, Coimbra et al., 2009). The retina was stained for 2 minutes and then dehydrated and washed in xylene to increase the contrast. The retina was coverslipped with Entellan (Merck Millipore) and allowed to set for 24 hours before counting.

Ganglion cells were distinguished by their large and irregularly-shaped somata and granular staining of the Nissl substance present in the cytoplasm, which is different to the smaller and more circular amacrine cell soma (Collin and Pettigrew, 1988a, Bozzano and Collin, 2000). Only orthotopic ganglion cells located in the ganglion cell layer were analyzed. In some cartilaginous fishes, a proportion of the ganglion cell

population is located in the inner plexiform and inner nuclear layers of the retina but as these are relatively sparsely distributed and can be difficult to stain and/or visualized we ignored these in the present study, although we recognize that this may result in an underestimation of ganglion cell density and thus spatial resolving power.

Assessment of the topographic distribution of photoreceptors and ganglion cells was conducted using a non-biased stereological method using a motorized compound microscope and StereoInvestigator software (Microbrightfields, USA) (for details see, Garza-Gisholt et al 2014, Chapter 3). The topographic maps were constructed using R (R Core Team, 2012) and the script described in Chapter 2 using the thin plate spline model (from the `sp` package with undersmoothing parameters (for details, see Chapter 2 and).

Retinal summation maps and calculations of spatial resolving power

Summation ratios comparing the density of rod photoreceptor cells and ganglion cells at each retinal locus were calculated using the average maps (see above) for each species. The two topography maps were aligned with the optic nerve head as a reference point, where the grid of calculated average cell densities were then used to obtain the number of rods per ganglion cell. These summation ratios were plotted and iso-density contours constructed using the same technique as for the single cell type maps.

The highest density of ganglion cells was used to calculate the spatial resolving power assuming a square mosaic distribution according to (Collin and Pettigrew, 1989, Fritsches et al., 2003):



$$\text{cycles per degree} = \left(\frac{1}{2}\right) \cdot \left(\frac{\sqrt{n}}{\arctan\left(\frac{1}{2.55 \cdot r}\right)}\right)$$

One can also make the calculation based on a hexagonal mosaic distribution of ganglion cells according to (Hart, 2002, Theiss et al., 2007):

$$\text{cycles per degree} = \left(\frac{1}{2}\right) \cdot \left(\frac{2\pi \cdot 2.55 \cdot r}{360}\right) \cdot \sqrt{\left(\frac{2n}{\sqrt{3}}\right)}$$

where r is the axial radius of the lens along the optical axis, which is multiplied by 2.55 according to Matthiessen's ratio to estimate the focal length and n is the highest cell density in the area centralis (Matthiessen, 1880).

Histology of the retina and the calculation of optical sensitivity

Small pieces of retina fixed in Karnovsky's solution (2.5% glutaraldehyde, 2% paraformaldehyde in 0.1 M cacodylate buffer pH 7.4) were dissected out of the eyecup, embedded in araldite and orientated for sectioning in the transverse plane. Using a microtome (LKB Bromma Ultratome Nova) transverse sections (1 μ m in thickness) were cut and mounted on a glass slide, stained using an aqueous solution of 1% Toluidine blue and coverslipped using Entellan (Merck Millipore). Stained sections were photographed using an Olympus BP70 Camera mounted on an Olympus BX50 compound microscope using 40X, 60X and 100X objectives. Images were edited using Adobe Photoshop CS5 (brightness and contrast only) and photoreceptor outer and inner segment measurements were obtained using Image J open access software (Schneider et al., 2012).

The optical sensitivity equation of Land (1981) was used to compare the relative light gathering ability of the rod photoreceptors between the three species. This calculation is based on the maximum absorption of monochromatic light by rod photoreceptors. The specific absorbance of the outer segment was calculated by (Partridge et al., 1989) for the narrownose chimaera, *Harriotta raleighana* (Rhinochimaeridae), ($k=0.0123 \cdot 2.303 = 0.028 \mu\text{m}^{-1}$), which was used for all species in the absence of actual microspectrophotometric measurements for these species. The absorptance F of monochromatic light at the wavelength of maximum sensitivity (λ_{max}) of the rod pigment is given by:

$$F\lambda_{\text{max}} = 1 - e^{(-kl)}$$

Where k is the naperian absorbance of the outer segment when illuminated axially and l is the length of the outer segment.

Assuming that these deep-sea chimaeras do not change the size of their pupillary aperture (Maddock and Nicol, 1978), the sensitivity of the rod photoreceptors at all depths is given by (Land 1981):

$$S(\mu\text{m}^2\text{sr}) = \left(\frac{\pi}{4}\right)^2 \cdot \left(\frac{A^2}{f}\right) \cdot d^2 \cdot F\lambda_{\text{max}}$$

where A is the diameter of the lens (as a proxy for the pupil diameter), f is the focal length (posterior nodal distance) of the eye calculated from Matthiessen's ratio: $2.55 \cdot$ lens radius (1880) and d is the inner segment diameter that acts as a light guide and is used as a proxy for the optical aperture. The units $\mu\text{m}^2\text{sr}$ refer to the spectral radiance that passes through a square micron of the retina.



Results

The choroidal layer in the back of the retina produced a bright green coloration (reflex) in the deep-sea chimaeras, *Rhinochimaera pacifica* and *Chimaera lignaria*. This layer corresponds to the *tapetum lucidum* that is comprised of guanine reflective crystals. The elephant shark, *Callorhynchus milii*, did not possess a *tapetum lucidum* like the deep-sea species (Figure 4.1).

Photoreceptor morphology and topographic distribution

Rods were observed in all three species of chimaeras and were characterised by their long cylindrical outer segments (as seen in transverse sections, Figure 4.2) and the tight packing of their slender inner segments when viewed in wholemound (Figure 4.3). The length of the rod outer segments varied between the deep-sea chimaeras (66-68 μm) and the elephant shark (34 μm). The diameter of the rod outer segments in the elephant shark is slightly smaller (mean of 2.8 μm) than the deep-sea sharks (*R. pacifica* 3.4 μm and *C. lignaria* 3.0 μm) (Table 4-1).

Cones were only observed in the retina of the elephant shark, *Callorhynchus milli*. Cones were characterized by the conical shape of their outer segments, the darkly-staining inner segment in transverse section compared to rods (Figure 4.2b) and by their larger inner segment (6.4 μm in diameter in cones compared to 3 μm in diameter in rods) when viewed in wholemound (Figure 4.3b, Table 4-1).

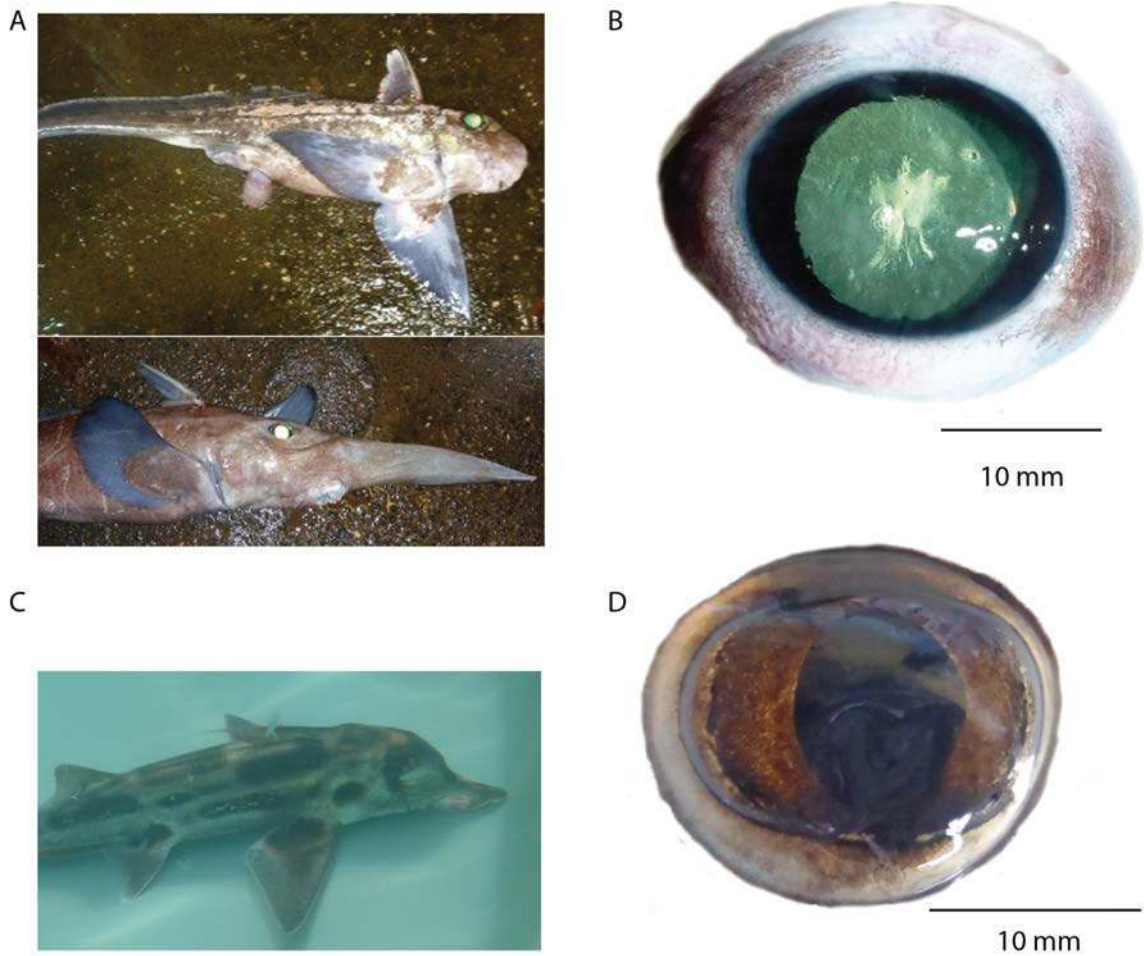


Figure 4.1 The eyes of chimaeras and their tapetal eyeshine. A). Two species of deep-sea chimaeras: Top: Carpenter's chimaera, *Chimaera lignaria*, Bottom: Pacific spookfish, *Rhinochimaera pacifica*. B) Enucleated eye of *R. pacifica* with the bright light reflex produced by the tapetum lucidum. C) Elephant shark, *Callorhynchus milii* in keeping tank. D) Eye of *C. milii* that does not show the bright colored reflex from the tapetum lucidum. Photos A and B courtesy of Amy Newman.

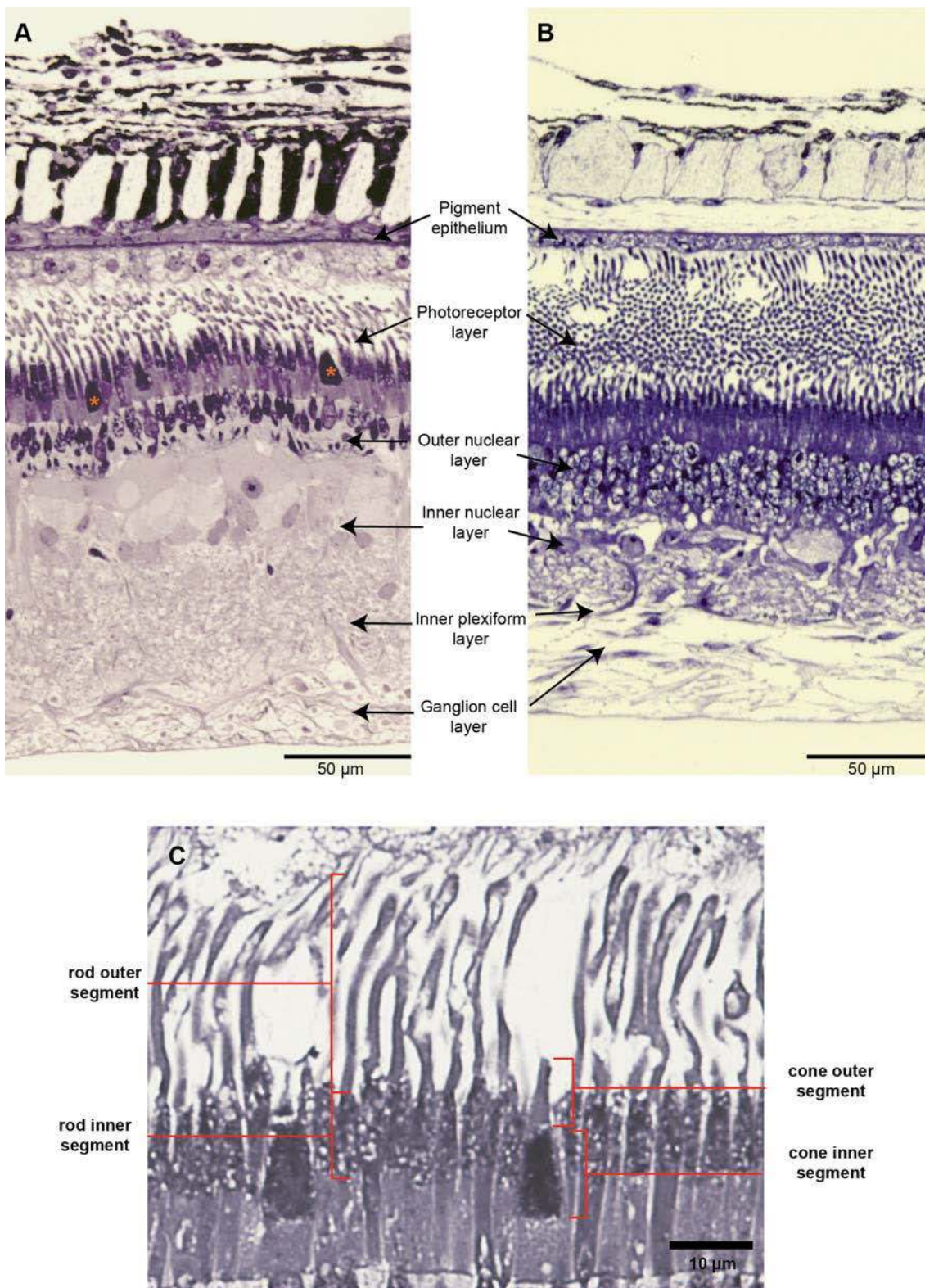


Figure 4.2 Retinal morphology. A). Transverse section of the retina of the elephant shark, *Callorhynchus milii*. Note the presence of cones marked with asterisks. B) Transverse section of the retina of the Carpenter's chimaera, *Chimaera lignaria*. Note the presence of only rods and the long outer segments compared to the elephant shark (A). C) Transverse section of the retina in the elephant shark at high magnification to show the cones and the division between the outer and inner segments of the photoreceptors.

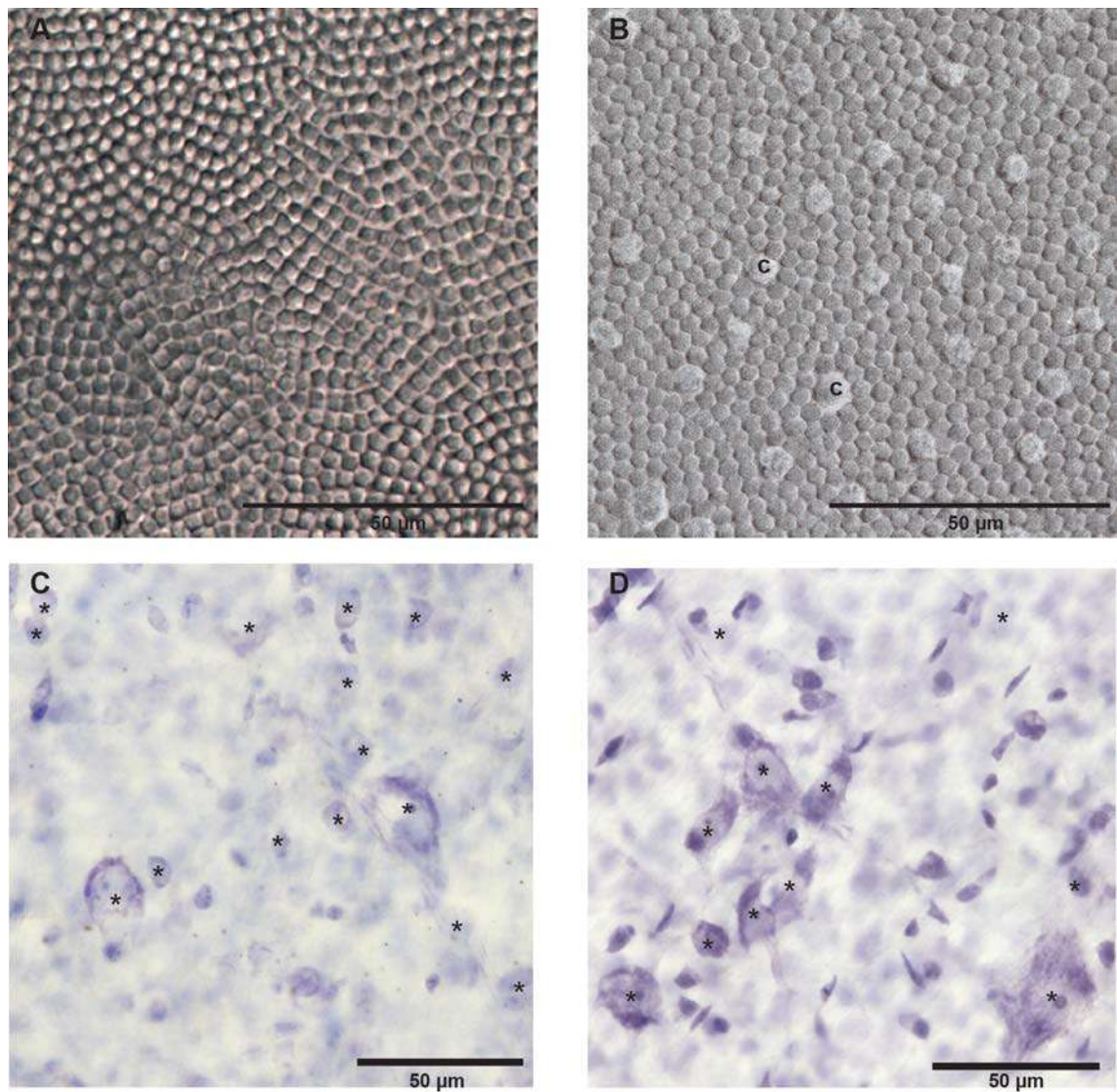


Figure 4.3 Axial view of the wholemounted retina. A). Photoreceptor cell layer of the Carpenter's chimaera, *Chimaera lignaria*, focused in the inner segments showing a rod-only retina. B). Photoreceptor cell layer in the elephant shark, *Callorhynchus milii*. Note the inner segments of the cones (c). C) Ganglion cell layer in the Carpenter's chimaera. D). Ganglion cell layer in the elephant shark, *= ganglion cells.



Table 4-1. Average total number of photoreceptors per retina and number of photoreceptors in the peak of the specialization. Rods (n=50) and cones (n=30). IS=inner segments, OS=outer segments.

	<i>Chimaera lignaria</i>	<i>Rhinochimaera pacifica</i>	<i>Callorhinchus milii</i>
Total Number of Rods (cells)	288,337,877	113,020,000	48,127,052
Peak Rod Density (cells mm ⁻²)	128,000	102,000	83,000
Rod IS diameter (μm)	3.46	3.87	3.01
Rod IS length (μm)	8.99	67.84	13.01
Rod OS diameter (μm)	3.032	3.43	2.84
Rod OS length (μm)	66.285	67.84	34.36
Total Number of Cones (cells)			2,095,804
Peak Cone Density (cells mm ⁻²)			5,896
Cone IS diameter (μm)			6.41
Cone IS length (μm)			11.07
Cone OS diameter (μm)			3.13
Cone OS length (μm)			6.64

The position of the eyes in the head of the three species is lateral so the nasal area of the retina is directed behind the animal, while the temporal area of the retina is directed in front of the animal. Cone distribution in the retina of the elephant shark shows a pronounced horizontal streak across the dorsal meridian of the retina that samples downwards into the lower frontal (eccentric) region of the visual field of the animal with two embedded areas of high density, one in the nasal retina and the other in the temporal retina. The peak density of cones in the nasal area is over 6,000 cells mm⁻², while the peak density falls to 5,000 cells mm⁻² in the temporal area (Figure 4.4). The cone density gradient (centro-peripheral gradient) is 6:1 and is steeper than the rod centro-peripheral gradient of 2:1. The rod to cone ratio within the horizontal streak of the elephant shark is around 12:1 rising to 60:1 in the periphery (Figure 4.4).

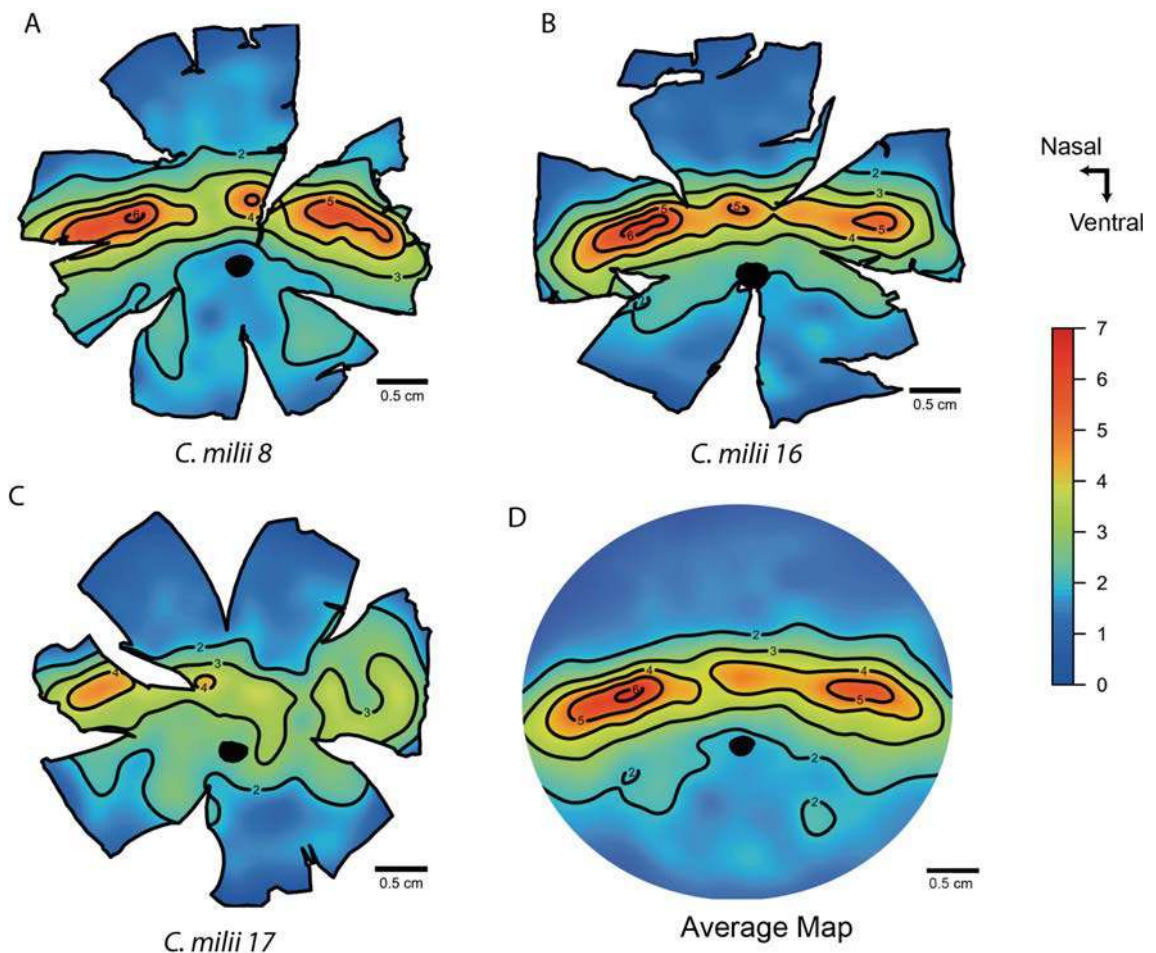


Figure 4.4 A), B) and C). Topographic maps of the individual cone photoreceptor distributions in three different individuals of elephant shark, *Callorhynchus milii* showing intraspecific variation and the original contour of the retinas including the radial cuts made to flatten the retina. D) Average cone topographic map in elephant shark. The values are $\times 1000$ cells mm^{-2} .

Rod density varied across the retina in a shallow gradient ranging from 60,000 to 119,000 cells mm^{-2} in *C. lignaria* and from 40,000 to 79,000 cells mm^{-2} in *R. pacifica* and revealed a weak specialization of increased cell density in the central retina (Figure 4.5A and B). The elephant shark, *C. milii*, shows a horizontal streak of more than 60,000 cells mm^{-2} and two areas, one nasal and the other temporal with a peak of more than 70,000 cells mm^{-2} (Figure 4.5C). The cumulative distribution function shows a steep slope in the mean of the cell densities confirming the shallow gradient. The rod density peaks in the deep-sea chimaeras reached around 100,000 cells mm^{-2} in the Carpenter's chimaera, *Chimarea lignaria* and 80,000 cells mm^{-2} in the Pacific spookfish, *Rhinochimaera pacifica*. Although the topographic



distribution of rods in the retinas of the deep-sea chimaeras did not show a pronounced specialization, the total number of rods was higher than in the retina of the elephant shark (Figure 4.5D).

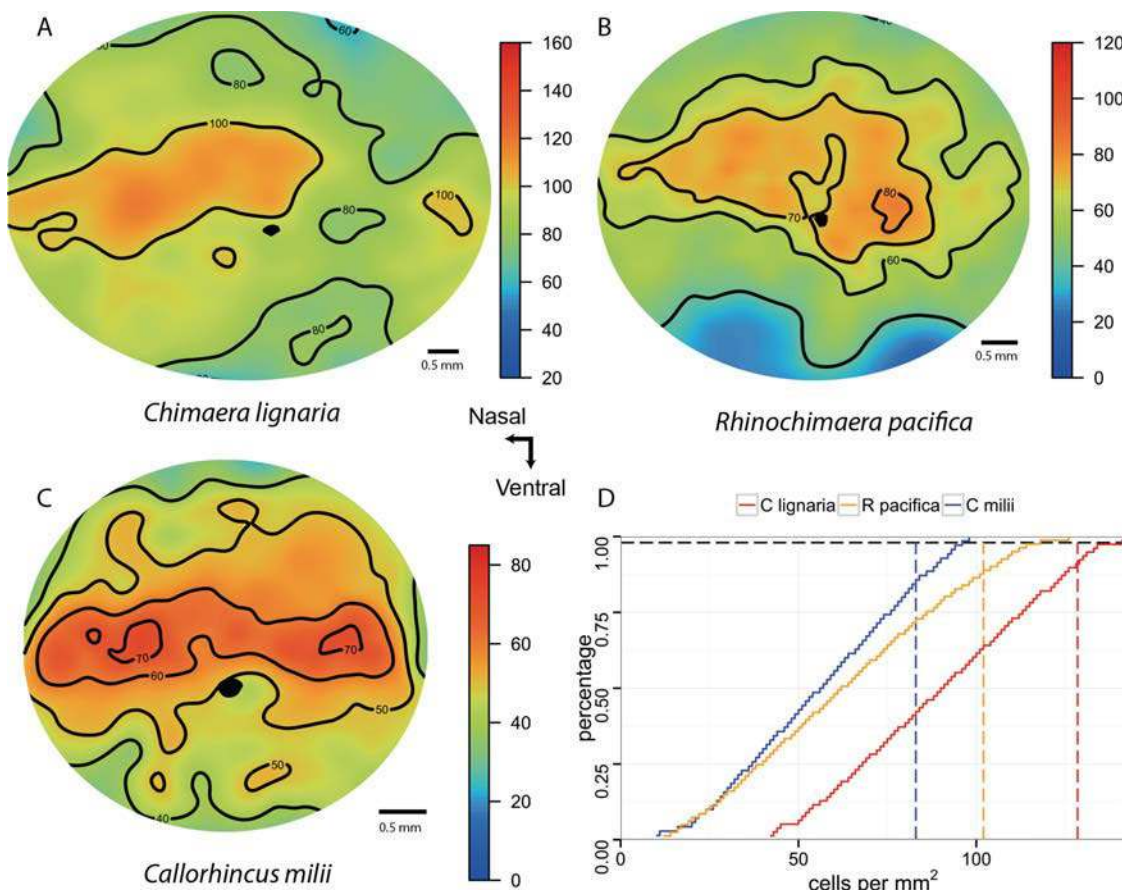


Figure 4.5 Isodensity contour maps of the rod photoreceptor distribution. A). Carpenter's chimaera (*C. lignaria*) average map, B) Pacific spookfish (*R. pacifica*) average map, C). Elephant shark (*C. milii*) average map, D) Empirical cumulative distribution function (ecdf) for the rod population of the three maps. Dashed lines represent the peak value at 98% of the distribution. The values are $\times 1000$ cells mm^{-2} .

Ganglion cell characterization and topography

The ganglion cell distribution shows a horizontal streak in the three species of chimaeras. Within the streak, there is/are specialized areas or secondary peak(s) in cell density in different parts of the retina in all three species. In the Carpenter's chimaera, *C. lignaria*, there is a nasal area (Figure 4.6A), while there are two areas in the Pacific spookfish, *R. pacifica*: one nasal and the other temporal (Figure 4.6B). These two

deep-sea species showed a similar peak cell density i.e. with *R. pacifica* having 200 cells mm^{-2} and *C. lignaria* having 150 cells mm^{-2} . In contrast, the elephant shark, *C. milii*, shows a temporal area with a peak cell density of more than 400 cells mm^{-2} and a dorsal specialization of lower magnitude of about 200 cells mm^{-2} (Figure 4.6C). The average size of the ganglion cells is similar in the three species at $200 \mu\text{m}^2$ but varied between $30 \mu\text{m}^2$ and almost $900 \mu\text{m}^2$ in area.

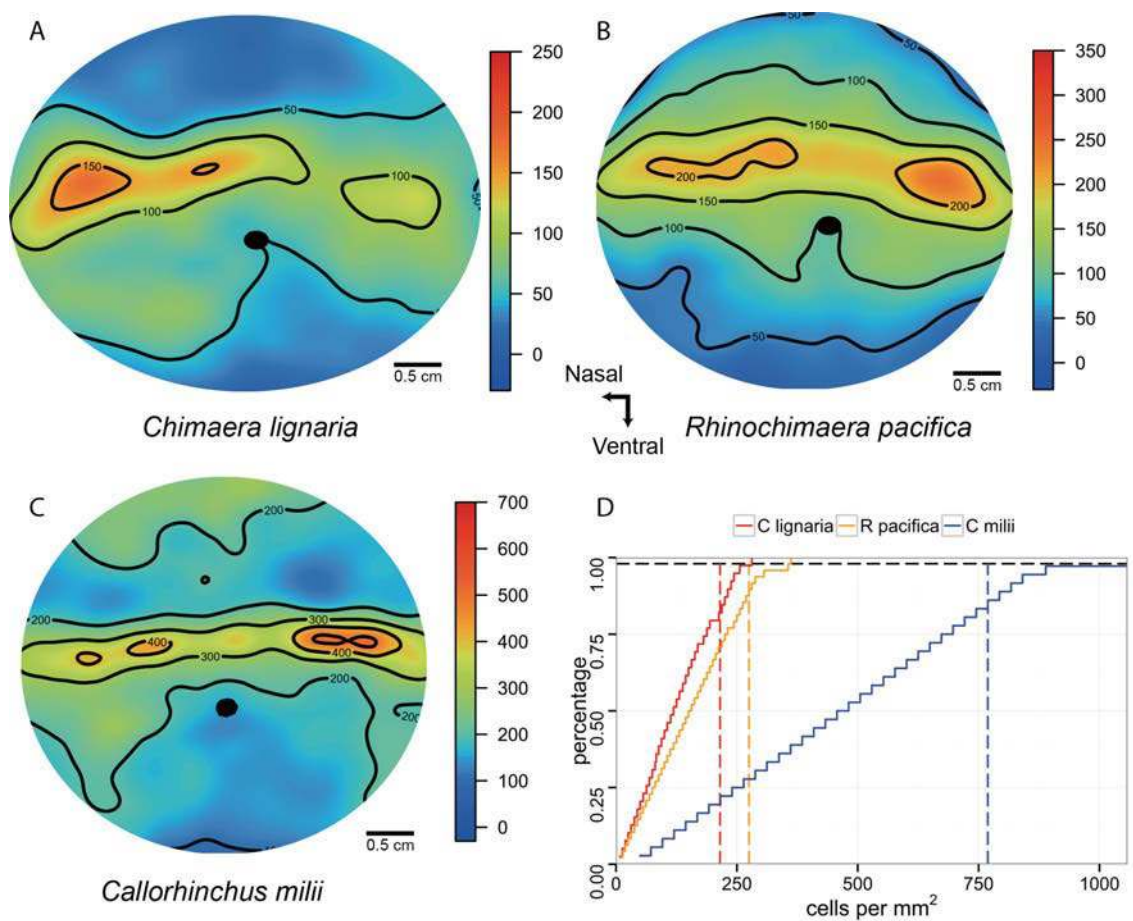


Figure 4.6 Isodensity contour maps of the ganglion cell distribution. A). Carpenter's chimaera (*C. lignaria*) average map, B) Pacific spookfish (*R. pacifica*) average map, C). Elephant shark (*C. milii*) average map, D) Empirical cumulative distribution function (ecdf) for the ganglion cell population of the three maps. Dashed lines represent the peak value at 98% of the distribution. The values are cells mm^{-2} .



Table 4-2. Average total number of ganglion cells per retina and number of ganglion cells in the peak of the specialization. Ganglion cell measurements in the three species in μm^2 .

	<i>Chimaera lignaria</i>	<i>Rhinochimaera pacifica</i>	<i>Callorhinchus milii</i>
Total Number of Ganglion Cells (cells)	176,498	217,144	220,166
Peak Ganglion Cell Density (cells mm^{-2})	215	275	769
Ganglion Cell area mean (μm^2)	183.84	194.96	178.46
Ganglion Cell area range (μm^2)	34-894	55-593	50-626

Summation maps

The retina of the elephant shark, *C. milii*, shows a lower summation ratio suggesting finer sampling (enhanced resolution) compared to the deep-sea chimaeras, which may rely more on sensitivity (Figure 4.7). The horizontal streak is pronounced in the three species with < 1,000 rods per ganglion cell in *C. lignaria*, 500 rods per ganglion cell in *R. pacifica* and < 200 rods per ganglion cells in *C. milii*. Interestingly, in the elephant shark, there is a high summation ratio in the dorso-temporal area with >500 rods per ganglion cell, indicative of a higher sensitivity area in the dorsal part of the retina, a region that subtends the substrate within the lower visual field (Figure 4.7C). *C. lignaria* has a higher mean summation ratio (1,750 rods per ganglion cell, calculated over the whole retina) than *R. pacifica* (700 rods per ganglion cell), while the elephant shark, *C. milii*, showed little variation in mean summation ratio (300 rods per ganglion cell) (Figure 4.7D).

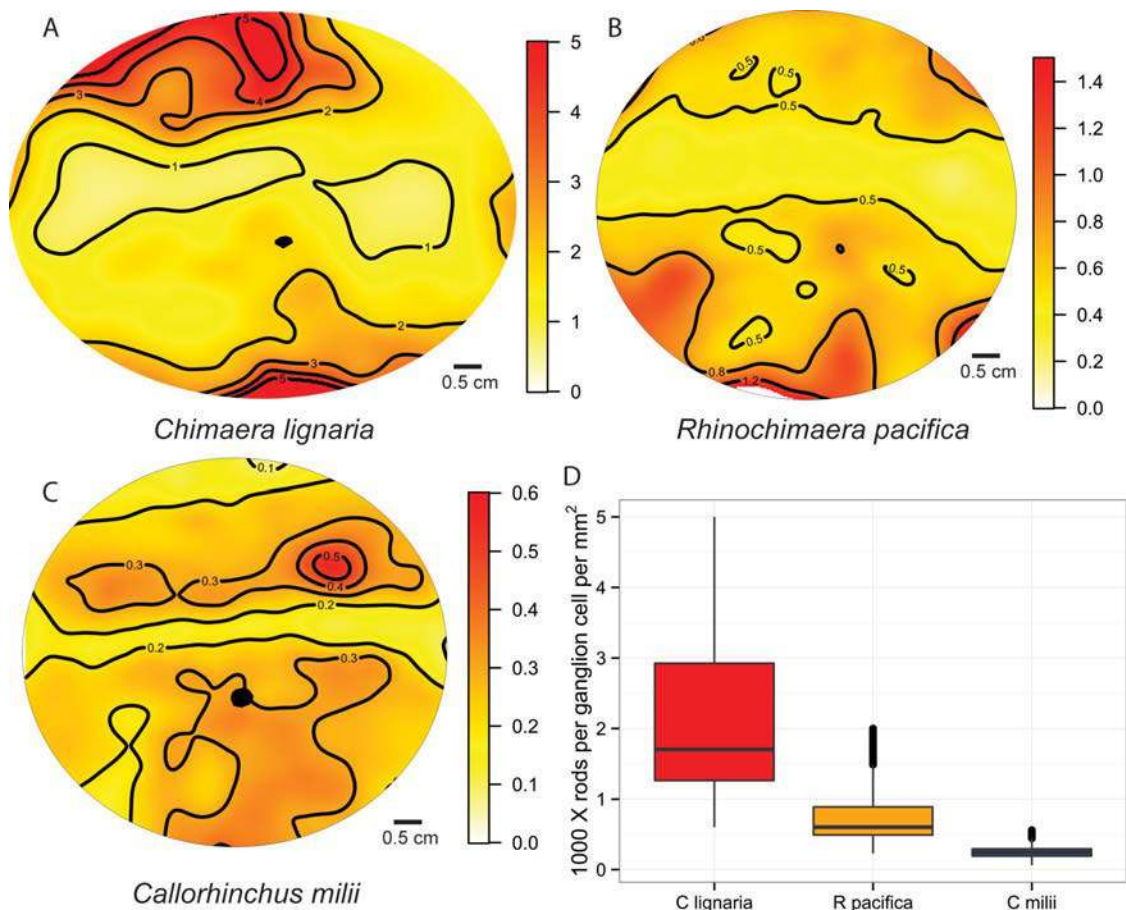


Figure 4.7 Summation maps showing the ratio of rod cells per ganglion cell (x1,000). A). Carpenter's chimaera (*C. lignaria*) map, B) Pacific spookfish (*R. pacifica*) map, C). Elephant shark (*C. milii*) map, D) Boxplot representing the frequency distribution of the summation ratios in the retinas of the three species. The values are x1000 rods per ganglion cell.

Spatial resolving power and optical sensitivity

The arrangement of the ganglion cells in the retina of the chimaeras is unknown so the square method and the hexagonal method were both used for comparison. The difference between the two methods was less than 10%, with the square method calculated to be lower using the peak in the ganglion cell population. The Carpenter's chimaera, *C. lignaria*, had a higher spatial resolving power (SRP) of almost 3 cycles per degree, while the Pacific spookfish *R. pacifica*, had an SRP of 2.6 cycles per degree and the elephant shark, *C. milii*, an SRP of 2.5 cycles per degree, calculated using a hexagonal cell distribution (Table 4-3).



Table 4-3. Anatomical characteristics of the lens, spatial resolving power and optical sensitivity for the three species of chimaeras.

	<i>Chimaera lignaria</i>	<i>Rhinochimaera pacifica</i>	<i>Callorhincus milii</i>
Lens diameter (A) (mm)	21.74	14.03	9.86
Focal length (f) (mm)	27.72	17.89	12.57
Spatial Resolving Power (square) (cycles deg ⁻¹)	2.74	2.44	2.35
Spatial Resolving Power (hexagonal) (cycles deg ⁻¹)	2.94	2.62	2.52
k (μm ⁻¹)	0.028*	0.028*	0.028*
F _{λmax}	0.84	0.85	0.62
Sensitivity(μm ² sr)	2.94	3.81	1.89

*From Partridge *et al* 1989

Both the optical sensitivity and light absorption levels revealed a higher value for the deep-sea chimaeras than the chimaera which ventures into shallow water to reproduce. The long rod outer segments increase photon absorption with F_{λmax} equal to 0.84 and 0.85 in the two species of deep-sea chimaeras, *C. lignaria* and *R. pacifica*, respectively. In contrast, the elephant shark, *C. milii* has a lower absorption of F_{λmax} (0.62). The optical sensitivity was higher in the two deep-sea chimaeras; *R. pacifica* with 3.8 μm⁻² sr⁻¹ and *C. lignaria* with 2.9 μm⁻² sr⁻¹, while the lowest value was found in *C. milii* with 1.9 μm⁻² sr⁻¹.

Discussion

The elephant shark, *Callorhincus milii*, displays visual specialisations that improve their ability to move between deep water (where the amount of sunlight is reduced) to shallow water (where bright light conditions prevail), to reproduce during autumn. The presence of cones and potentially colour vision, the lower number of rods, the smaller size of the rod outer segments and the higher number of ganglion cells are

all adaptations to optimize vision in the upper part of the water column, where light levels are higher than in the darker mesopelagic zone of the deep-sea. In contrast, the two species of deep-sea chimaeras show specializations that reflect the fact that they exclusively inhabit a much dimmer environment, where levels of sunlight are low and bioluminescent light sources predominate. These include the presence of a highly reflective, green coloured *tapetum lucidum*, higher rod densities, longer and wider rod outer segments and a higher summation ratio.

The mean length of the rod outer segments in the Carpenter's chimaera, *Chimaera lignaria*, and the pacific spookfish, *Rhinochimaera pacifica*, (~66-68 μm) are consistent with other deep-sea chimaeras such as *Hydrolagus mirabilis* (64 μm) (Fröhlich et al., 1995), *Hydrolagus affinis* (46.6 μm) (Denton and Nicol, 1964) and *Chimaera monstrosa* (50 μm) (Vigh-Teichmann et al., 1990) all of which live at more than 600 meters in depth. In contrast, the rod outer segments of the elephant shark, *Callorhynchus milii* (35 μm) are more similar to *Hydrolagus colliei* (22 μm) (Maddock and Nicol, 1978), which has been reported at depths of 80 meters but, like *C. milii*, also ventures into shallow water (Last and Stevens, 2009). Compared to some elasmobranchs, rod outer segment length in chimaerids is similar to some of the nocturnal, benthic elasmobranchs such as the Port Jackson shark (*Heterodontus potusjacksoni*), eastern shovelnose ray (*Aptychotrema rostrata*) and the pink whipray (*Himantura fai*), all of which possess outer segment lengths of about (35 μm) (Litherland and Collin, 2008, Schieber et al., 2012).

Few studies have mapped the topographic distribution of photoreceptors in elasmobranchs. The ornate wobbegong, *Orectolobus ornatus*, possesses a dorsal elongation with two peaks, one nasal and one temporal of about 50,000 rods mm^{-2} . The epaulette shark,



Hemiscyllium ocellatum, also has a horizontal streak with a temporal peak of about 80,000 rods mm^{-2} (Litherland and Collin, 2008). The horizontal streak is consistent with the topographic distribution in the elephant shark, *C. milii* (peak of 70,000 cells mm^{-2}). The number of rods is higher in the retina of purely deep-sea chimaeras, presumably as an adaptation to increase absolute sensitivity and, therefore, the detection of objects under low light conditions. The deep-sea chimaeras, *R. pacifica* and *C. lignaria* have rod peaks between 80,000 and 100,000 cells mm^{-2} that are consistent to some reports of rod density in *Chimaera monstrosa* around 100,000 cells mm^{-2} (Franz, 1905 cited in Lisney, 2010).

With the presence of three types of cone pigments in the elephant shark retina, *C. milii*, is similar to some species of rays that live in shallower water (Davies et al., 2009). The complement of cone receptor types extends sensitivity across more of the visible spectrum and provides the potential for colour vision. The ability to discriminate colour appears to have been lost in true sharks (Selachii), which possess only a single cone type in addition to a rod (Hart et al., 2011, Theiss et al., 2012). The low ratio of rods to cones (12:1) in the elephant shark is similar to species of sharks and rays that live in dim light conditions i.e. *Hemiscyllium ocellatum* (18:1), *Orectolobus ornatus* (19:1) (Litherland and Collin, 2008) and *Isurus oxyrinchus* (10:1) (Gruber et al., 1975a). This predicts that elephant sharks have high sensitivity vision in darker environments but can still see objects when they migrate into the shallow, brightly-lit estuaries to reproduce.

The calculated optical sensitivities of the deep-sea chimaeras are relatively high compared to the elephant shark because their rod outer segments are almost double their length. Optical sensitivity is a relative measure because other factors affect the total sensitivity of the eye (Land, 1981). The use of monochromatic light for the calculation is

adequate for the deep-sea species and for species that detect bioluminescence (Warrant and Locket, 2004). The values of optical sensitivity calculated for the chimaeras (range from 1.9 to 3.8 $\mu\text{m}^{-2} \text{sr}^{-1}$) are consistent to the values obtained for other bony fishes like the blue marlin and the blue tuskfish (2.8 and 1.4 $\mu\text{m}^{-2} \text{sr}^{-1}$, respectively) based on their double cones that are the largest photoreceptors in their retina (Fritsches et al., 2003).

All the topographic maps of ganglion cell density for the three species of chimaerids show a similar pattern to the large-eyed rabbitfish *Hydrolagus mirabilis* (Bozzano and Collin, 2000) and the spotted ratfish, *Hydrolagus colliei* (Collin, 1999), which possess a dorsal horizontal streak with both a nasal area and a temporal area of acute vision. In *H. colliei*, the density of cells in the temporal area (1,500 cells mm^{-2}) is higher than in the nasal area (1,300 cells mm^{-2}) (Bozzano and Collin, 2000) as is found in the elephant shark, *C. milii*, and the Pacific spookfish, *R. pacifica*. The presence of a dorsally located horizontal streak probably reflects the fact that they live in open areas near the substrate, where they need to sample objects at the sand-water interface across a large panoramic field (Hughes, 1975, Hughes, 1977, Collin and Pettigrew, 1988c). The peak ganglion cell density within this specialization varies within the Holocephali. *Hydrolagus mirabilis* and *Chimaera monstrosa* possess peaks of 1,600 ganglion cells mm^{-2} (Bozzano and Collin, 2000) and 600 ganglion cells mm^{-2} (Franz, 1905), compared to 153 ganglion cells mm^{-2} in *Chimaera lignaria*, 230 ganglion cells mm^{-2} in *Rhinochimaera pacifica* and ~460 ganglion cells mm^{-2} in *Callorhincus milii*.

The mean area of the ganglion cell somata is larger in chimaerids (with somata reaching nearly 900 μm^2), than any other species of Chondrichthyes, i.e. about three times larger than in the deep-sea shark *Etmopterus spinax* (Bozzano and Collin, 2000) and six times



larger than a range of elasmobranchs ($150 \mu\text{m}^2$, Bozzano and Collin, 2000). A greater proportion of large ganglion cells were observed than small ganglion cells, which could have been displaced to the inner nuclear layer or inner plexiform layers (Stell and Witkovsky, 1973a, Collin, 1988) and therefore not counted. These large ganglion cells may therefore represent a subpopulation of ganglion cells that also have large dendritic fields and may be involved in movement detection (Barlow, 1953, Boycott and Wässle, 1974). Another alternative is that giant ganglion cells provide a large visual angle like in the smooth dogfish, *Mustelus canis*, where the giant ganglion cells each occupying an area of more than $700 \mu\text{m}^2$, subtend a visual angle of 6° (Stell and Witkovsky, 1973a).

The anatomical spatial resolving power (SRP) calculated using ganglion cell density is arguably a better indicator than values calculated using photoreceptor density since the ganglion cells are the output neurons of the retina. The ratio of photoreceptors to ganglion cells (or convergence of information) represents a trade-off between spatial resolution and sensitivity (Pettigrew et al., 1988, Fritsches et al., 2003). The low spatial resolving power calculated for the three species of chimaeras (~2.6 cycles per degree) is similar and within range of that calculated for a number of elasmobranchs (2 to 11 cycles per degree, (Lisney and Collin, 2008)). It is possible that the estimates of SRP may be over-estimated because some of the smaller ganglion cells may have been omitted from counts (as they would have resembled amacrine cells) and/or because the inner nuclear and inner plexiform layers were not sampled. However, the error for the morphological estimate is unlikely to be larger than the error obtained when visual acuity is examined using behavioral methods (Collin and Pettigrew, 1989).

The presence of a dorsal horizontal streak in the elephant shark with a low number of rods per ganglion cell (summation ratio) is a

specialization allowing this species to distinguish objects on the substrate. The summation ratio in the deep-sea chimaeras is appreciably higher than in the elephant shark. A high summation ratio potentially increases sensitivity in the low light conditions of the deep-sea. Some teleost fishes possess other specializations to increase sensitivity like the grouping of photoreceptors to increase the ability to capture photons, but the chimaeras only have high number of photoreceptors with no grouping observed (Wagner et al., 1998, Warrant and Locket, 2004, Douglas, 2010). The high number of photoreceptors and their convergence on a relatively small number of large ganglion cells represents a specialization in dim light environments to increase sensitivity, a useful adaptation to allow these species to be alerted to the presence of potential prey or predators as soon as an object enters its visual field (Bozzano and Collin, 2000) .

The perception of environmental cues such as finding food, detecting possible predators and finding potential mates to reproduce is a complex interaction of many different senses. This study shows that vision plays an important role in each species' ability to navigate within their environment. Further studies require more attention on other senses and how they transmit sensory information to the central nervous system. Brain studies in Rhinochimaerids have revealed that the anterior lateral line lobe is well developed, where vision, lateral line and electroreception are important sources of sensory input for this group of early vertebrates (Yopak and Montgomery, 2008). All of these senses operate over relatively close range, which might be useful for both finding food and social communication. Chimaeras use mechanisms like spines on their claspers and head (in males) to attach to the female but they first need to get close enough to their reproductive partners (LaMarca, 1964). Feeding strategies vary in the Rhinochimaeridae and Chimaeridae, which feed on either benthic invertebrates or pelagic invertebrates, respectively, which may indicate the relative importance of different senses. Rhinochimaerid species have



a prominent snout and a relatively high number of electroreceptors with well developed lateral line canals that can be useful especially to detect buried, benthic prey. On the other hand, chimaerid species might rely more on vision to detect pelagic (possibly bioluminescent) prey (Gonzalez et al., 2007). The use of additional species of each family would also reveal more information of the phylogenetic relationships of the retinal specializations within the group. The callorhynchid family is basal compared to the rhinochimaerid and chimaerid families (Inoue et al., 2010, Didier et al., 2012). The presence of a more sensitive retina in chimaerids and rhinochimaerids may be a divergence in the evolution of the group, where they had to live in deeper waters. While the presence of colour vision in the more basal group may relate to the use of more shallow habitats from the more ancient species of holocephalians.

Acknowledgements

We would like to thank Amy Newman for her efforts to collect Carpenter's chimaera and Pacific spookfish. Also we would like to express our gratitude to Milan Barbarich, Managing Director of Anton's Seafoods Ltd in Auckland for allowing us access to the Seamount and to all the crew of the ship for facilitating the sampling of the species. We also appreciate help from Camila Martins, Richard Reyna and Matt Cini in collecting samples of elephant sharks in Queenscliff, Victoria. We are sincerely thankful to Joao Paulo Coimbra and Caroline Kerr for all the invaluable help in the lab. This research was supported by an Australian Research Council Discovery Project Grant (DP110103294) to SPC, NSH and others, and the Western Australian State Government (to SPC). EGG. was supported by the Mexican scholarship for Postgraduate studies (CONACyT) and the Ad-Hoc Top-Up Scholarship by the University of Western Australia.

**Chapter 5 Visual specializations in five sympatric species of
stingrays from the family Dasyatidae from Ningaloo Reef, Western
Australia**

Garza-Gisholt, E., Kempster, R.M., Hart, N.S., and Collin, S. P.

School of Animal Biology and The UWA Oceans Institute, The University of Western Australia, Crawley, 6009 W.A, Australia.

Abstract

The eyes of five ray species (*Taeniura lymma*, *Neotrygon kuhlii*, *Pastinachus atrus*, *Himantura uarnak* and *Urogymnus asperrimus*) from the same taxonomic family (Dasyatidae) and the same geographic region (Ningaloo Reef, Western Australia) were studied to identify differences in retinal specialisations that may reflect niche specialisation. The topographic distributions of photoreceptors (rods and all cones) and ganglion cells were assessed, and used to identify localised peaks in cell densities that indicate specialisations for acute vision. These data were also used to calculate summation ratios of photoreceptors to ganglion cells in each species, and estimate the anatomical spatial resolving power of the eye. Subtle differences in the distribution of retinal neurons appear to be related to the ecology of these closely-related species of stingrays. The main specialization in the retinal cell density distribution is the dorsal streak that allows these animals to scan the substrate for potential prey. The bluespotted fantail ray, *Taeniura lymma*, showed a higher peak density of rods (86,700 rods mm⁻²) suggesting a specialization for scotopic vision. The highest peak density of cones (9,970 cones mm⁻²) was found in *Himantura uarnak* and the highest peak density of ganglion cells (4,500 cells mm⁻²) was found in *Pastinachus atrus*. The proportion of rods to cones in the dorsal streak



was higher in the two smaller species (12.5-14:1 in the bluespotted stingrays *T. lymma* and *N. kuhlii*) than the larger stingrays (6-8:1 in *P. atrus*, *H. uarnak* and *U. asperrimus*). Visual specializations in different sympatric species are subtle but may reflect specializations to specific ecological niches.

Keywords

Visual specialization; retina; Dasyatidae; ganglion cells; photoreceptors; spatial resolving power; sympatric species; speciation

Introduction

Study of the visual ecology of elasmobranchs has intensified in recent decades, where broad comparisons of different species from different taxonomic groups have been previously examined (Gruber and Cohen, 1978, Bozzano and Collin, 2000, Hart et al., 2006, Lisney and Collin, 2007, Lisney and Collin, 2008, McComb and Kajiura, 2008, Schieber et al., 2012). However, there are few comparative studies of species from the same family that all live in a similar ecological niche, the study of which may reveal how sympatric species coexist without overlapping in the use of resources.

The subclass Elasmobranchii, which includes sharks, rays and skates, is one of the most ancient groups of vertebrates. Currently, more than 500 species of rays, divided into four orders, have been described with new species being reported every year (Nelson, 2006). One of the most diverse families of rays is the Dasyatidae (stingrays) with more than 70 species divided into nine genera that live in both tropical and temperate zones around the world, including some exclusively freshwater species. Their size varies from 20 to 200 cm disc width (DW) and most of the species are benthic (Last and Stevens, 2009). The diet of most stingrays consists of benthic invertebrates, mainly crustaceans and polychaetes,

but they can also consume molluscs and echinoderms (Last and Stevens, 2009, Jacobsen and Bennett, 2012, O'Shea et al., 2013). They protect themselves from predators by spending part of their time buried under the sand and, in some species, by the use of one or more venomous spines (Teaf and Lewis, 1987, Carpenter and Niem, 1999). Some common predators include different species of sharks, including the hammerhead, which has a special preference for biting off the pectoral fins of stingrays (Strong et al., 1990).

The coast of Western Australia exhibits a high diversity of stingray species living in a similar habitat (O'Shea et al., 2013). The five species within the family Dasyatidae investigated in this study were all collected from Ningaloo Reef and represent five different genera (*Neotrygon*, *Taeniura*, *Himantura*, *Pastinachus* and *Urogymnus*) within the family. Two of the species, the bluespotted maskray (*Neotrygon kuhlii*) and the bluespotted fantail ray (*Taeniura lymma*) are typically smaller with a maximum disc width of approximately 45 cm. In contrast, the three other species, the reticulated ray (*Himantura uarnak*), the porcupine ray (*Urogymnus asperrimus*) and the cow tail ray (*Pastinachus atrus*) all measure more than 90 cm in diameter when mature. The coloration and morphology of each species is also variable with *T. lymma* and *N. kuhlii* possessing distinctive blue spots over the body, *H. uarnak* having a whip-like tail with fine, dark bands, *U. asperrimus* having extremely rough skin (thereby protecting this species from predation and negating the need for a tail spine) and a grey colouration and *P. atrus* having a dark coloration with a broad flattened tail (Last and Stevens, 2009).

Previous studies have investigated the origins of speciation between different populations of rays and there are different theories as to what causes the gene barrier. Sympatric species, which live in the same area, should exploit different resources to avoid competitive exclusion and allow coexistence (West-Eberhard, 1986). Some ecological traits that



might shift between species are diet, the use of habitat subregions or temporal variation in activity. Some studies have tried to explain how this coexistence occurs in rays using diet shift (Platell et al., 1998, White et al., 2004, O'Shea et al., 2013) or the exploitation of habitat sub-regions (White and Potter, 2004, Marshall et al., 2008). Morphological (Rosenberger, 2001) and molecular (Puckridge et al., 2012) evidence suggests that the genera within the Dasyatidae family are evolutionarily polyphyletic and several geological events, such as the collision between the Australian and Eurasian Plates and subsequent sea-level changes in the mid-Miocene and Pleistocene, might have fragmented the habitat of larger populations and promoted speciation (Aschliman et al., 2012b).

The study of the visual ecology of the different sympatric ray species may provide insight into the nature of the ecological partitioning. Elasmobranchs have at least seven different senses (vision, olfaction, taste, hearing, touch, lateral line and electroreception) to perceive their environment. Vision is a sense that operates over relatively short distances (tens of metres) and allows the rays to detect prey, conspecifics and predators (Hueter et al., 2004, Compagno et al., 2005). A large number of studies involving many invertebrate and vertebrate animals shows that different visual traits relate directly to the ecology of each species, i.e. nocturnal species have adaptations for scotopic vision (Walls, 1942). However, there is generally a trade-off between sensitivity and resolution. Sensitivity is a very important feature for species that require good vision in dim light conditions, such as nocturnal and deep-sea animals. On the other hand, resolution is often an important feature for species that live in bright light conditions and need to optimise visual acuity (Sadler, 1973, Hueter, 1991b, Warrant and Locket, 2004, Douglas, 2010).

Coral reef ecosystems support a rich diversity of species, with their distribution restricted by physical factors like temperature, light and the availability of nutrients. With some exceptions, most coral reefs are found in a tropical range of latitudes and lie within the first 50 meters of depth (Hoegh-Guldberg, 1999, Kleypas et al., 1999). A coral reef supports many microhabitats that vary in light conditions (in both intensity and spectral composition). The wide spectrum of wavelengths present in the reef environment allows several specializations for the perception of colour; even allowing species-specific UV patterns in some teleost fishes to be recognized (Losey et al., 1999, Siebeck, 2004). Some microhabitats include low light areas such as caves and shaded areas that are illuminated by scattered light creating dim light conditions rich in medium wavelengths up to 500 nm (Marshall and Vorobyev, 2003). The temporal variation of light intensities in the reef ecosystem creates a diversity of feeding interactions between diurnal and nocturnal species. Some species of elasmobranch are crepuscular or nocturnal and have a visual system optimised for scotopic vision (Compagno et al., 2005, Lisney and Collin, 2007, Litherland and Collin, 2008).

The number, distribution, and ratio of cones (photopic vision) and rods (scotopic vision) relates directly to the light conditions in the habitat of each species (Litherland and Collin, 2008). Cone photoreceptors are adapted for bright light conditions, while rod photoreceptors operate only in dim light conditions. The proportion of rods and cones have been compared in diverse species of elasmobranchs (see review by Hart 2006) and more specifically in rays of the *Dasyatidae* family (Hamasaki and Gruber, 1965, Toyoda et al., 1978, Braekevelt, 1994a, Logiudice and Laird, 1994, Schieber et al., 2012). In the rod system, the convergence or summation of signals is high i.e. many rods connect to a single bipolar cell and many bipolar cells in turn connect to a single ganglion cell, thereby increasing absolute sensitivity (Sterling et al., 1986). In the cone system, there is usually less convergence, i.e. fewer cones connect to a given bipolar cell and fewer cone bipolar cells



connect to a given ganglion cell. Although, the bipolar cells might receive mixed signals from rod and cones in fishes (Connaughton et al., 2004). The cone pathway is less convergent onto ganglion cells (Kolb, 1995a), where the integrity of the signal is maintained throughout the visual pathway. The distribution of ganglion cells is important because it reveals much about how the eye is used and the relevance of different areas of the visual field (Lythgoe, 1979, Warrant, 1999) since the axons emanating from the ganglion cells constitute the final bottleneck of information that projects to the visual centres within the brain. Few studies have determined the level of summation between photoreceptors and ganglion cells in elasmobranchs (Litherland and Collin, 2008).

The morphological and physiological characteristics of the retina affect the sensitivity and resolution of the peripheral visual system and also subserve modalities such as motion detection and colour vision. The many subtypes of retinal neuron are not distributed evenly across the retina of most animals, and interspecific variation in their distribution is often related to specific aspects of the animal's visual ecology. The terrain theory proposed by Hughes (1975) states that animals which inhabit an open environment tend to have a horizontal streak of increased cell density across the retinal meridian, which allows the visual system to sample the visual horizon without having to make extensive movements of their eyes, head or body. In contrast, animals that live in enclosed environments like rainforests or coral reefs tend to have a concentric area of higher retinal cell density (Collin and Pettigrew, 1988b) that allows the sampling of a localised field of view in a complex environment in order to detect small organisms and discriminate objects that might camouflage themselves against the background. The concentric area increases spatial resolving power by increased image sampling within a localised retinal region. Previous studies of the topographic distribution of retinal ganglion cells in rays have revealed a dorsally-located streak of elevated cell density in the eyes of *N. kuhlii* (Theiss et al., 2007) and *T. lymma* (Lisney and Collin,

2008). The dorsal position of the streak in the retina provides enhanced visual acuity in the ventral visual field, enabling the animal to scan the substrate for prey during benthic feeding behaviour.

The study of the retinal specializations of these five species of rays will provide clues to how the different species might coexist in the same habitat. The goal of the present study is to determine if small variations in retinal specializations of closely-related sympatric species reflect niche partitioning. This is accomplished by assessing visual capabilities of the eye in bright light conditions (presence and position of cone photoreceptors), dim light conditions (presence and position of rod photoreceptors) and the summation of information transmitted to the brain. The relationship between photoreceptor density and ganglion cell density is examined to reveal whether resolution and visual acuity are more important than sensitivity in sympatric stingrays occupying a coral reef.

Methods

Ethics Statement

This study was carried out in strict accordance with the guidelines of the *Australian Code of Practice for the Care and Use of Animals for Scientific Purposes* (7th Edition 2004). All efforts were made to minimize the suffering of the animals.

Specimen Collection

Five species of adult stingrays from the family Dasyatidae: bluespotted fantail ray (*Taeniura lymma*, n=2, 25 and 27 cm DW), bluespotted maskray (*Neotrygon kuhlii*, n=2, 32 and 35 cm DW) reticulated whipray (*Himantura uarnak*, n=2, 89 and 120 cm DW), porcupine ray (*Urogamurus*



asperrimus, n=2, 105 and 122 cm DW) and cowtail ray (*Pastinachus atrus*, n=2, 109 and 145 cm DW) were collected in 2010 from Ningaloo reef in north Western Australia under WA fisheries permit (No. 1724-2010) as part of a large age, diet and growth study (O'Shea et al., 2013); material was acquired for this study to maximise the use of tissue. The animals were euthanized in the field by severing the spinal cord following the protocol approved by the Murdoch University Animal Ethics Committee (License: #U6/2010-2011); and Fisheries Collection Permit (No.: #R2275/09).

Eye enucleation and retinal dissection

Eyes were removed after making an incision in the ventral sclera for orientation and the cornea dissected away. The eye was inverted to remove the vitreous humour and the lens with the aid of gravity and by gently pulling the vitreous without introducing tweezers into the eyecup, thereby avoiding damage to the retina. Three different measurements of the lens were taken with a digital vernier caliper: rostro-caudal, dorso-ventral and axial diameters. The eye cup was fixed in 4% paraformaldehyde in 0.1 M sodium phosphate buffer (PB, pH 7.2-7.4) and stored until transported to the lab. After a few weeks, the tissue was transferred to 0.1 M PB containing 1% sodium azide and stored at 4°C until required. A similar procedure to that described in Chapter 2 was used to dissect out the retina with the exception that the retinas were dissected free by removing the sclera before making any radial cuts. This procedure was adopted since the scleral eyecup is thick and has extensive patches of connective tissue making it difficult to make the radial cuts. The choroidal layer is tightly attached to the sclera via numerous fibers in these species so it was necessary to use a scalpel blade to cut away the sclera and not damage the retina.

Assessment of the topographic distribution of photoreceptors and ganglion cells was conducted using a non-biased stereological method

using a compound microscope fitted with a motorized stage and StereoInvestigator software (Microbrightfields, USA) (for details see, Garza-Gisholt et al 2014, Chapter 3). The topographic maps were constructed using R (R Core Team, 2012) and the script described in Chapter 2 using the thin plate spline model (from the *sp* package using under-smoothing parameters (for details, see Garza-Gisholt et al 2014, Chapter 2).

Two retinas per species were used to assess the ratio and distribution of rods and cones following the same protocol as described in Chapter 3. The counting frame used for rods was 25 x 25 μm . Morphological criteria were used to discriminate between rods and cones. The smaller inner segments and long cylindrical outer segments distinguished rods. Cones, in contrast, present a thin profile in the apical portion of the outer segments, while they become wider close to the inner segments. The counting frame used for cones was 100 x 100 μm since the smaller counting frame would not detect the, often subtle, differences in cone cell density and the relative scarcity of cones across the retina. After counting both populations of photoreceptors, the retinas were floated free of the slides and washed in 0.1M phosphate buffer (pH 7.2-7.4), mounted on a gelatinized slide and stained for Nissl substance for two minutes (See details, Garza-Gisholt et al 2014, Chapter 3). Counts of ganglion cells were done using a counting frame of 100 x 100 μm . Ganglion cells located in both the inner plexiform and ganglion cell layers were counted without discriminating between these two populations. Ganglion cells were distinguished when possible by their large and irregularly-shaped somata and granular staining of the Nissl substance present in the cytoplasm, which is different to the smaller and more circular amacrine cell somata (Bozzano and Collin, 2000, Collin and Pettigrew, 1988a). Glial cells were identified by their darker coloration and elongated shape (Collin and Pettigrew, 1988a, Theiss et al., 2007) and excluded from all counts.



Average maps and transects

Each retina was analysed for the distribution of both photoreceptor and ganglion cell populations. However, in order to obtain an average map, all the topographic maps from similar-sized individual animals of the same species were aligned using the optic nerve head and opposite eyes were “mirrored” to match similar orientations considering symmetry in the two eyes. Any differences in the size of the retinas were corrected to the highest retinal size and maps were visually compared to assess orientational alignment. The under-smoothed thin plate spline was then used to obtain the krig function of the spatial analysis. A grid of coordinates spaced out every 200 μm was created using the minimum and maximum x and y coordinates and the values for each function were calculated (See details, Garza-Gisholt et al 2014, Chapter 3). Using the data frame obtained, a topographic map was constructed masking the data to an oval shape that loosely represents the original shape of the eye but it includes the values calculated in the radial cuts that are not in the same position for each retina.

To make transects of different species maps comparable, the retinal maps were standardized to a percentage of the distance between the optic nerve and the periphery, where the centre is 0 and the extremes are -1 and 1 in the horizontal and vertical axes. This is a requirement of the methodology in order to compare retinas of different sizes and shapes (batoid retinas are rostro-caudally elongated compared to shark retinas). The centre of the transect corresponds to the position of the optic nerve; the horizontal transects to the left of the centre (negative values) corresponds to the nasal retinal region, while to the right of the centre (positive values) corresponds to the temporal retinal region. In the vertical transects, negative values represent positions in the ventral retinal regions and positive values represent locations in the dorsal retinal regions.

Spatial resolving power and retinal summation

A comparison between the cone photoreceptor cell densities and ganglion cell densities was performed by overlapping the average photoreceptor map and the average ganglion cell map, making sure the orientation of each retina was aligned, and dividing the grid of photoreceptor values by the ganglion cell values using the R program. Spatial resolving power (SRP) was calculated assuming a hexagonal ganglion cell distribution as performed in previous studies (Hart, 2002, Theiss et al., 2007) :

$$d = \frac{2\pi f}{360}$$

$$S^2 = \frac{2}{D\sqrt{3}}$$

$$v = \frac{1}{S\sqrt{3}}$$

where d is the distance on the retina subtended by one degree, f is the focal length calculated by multiplying the axial radius of the lens along the optical axis by 2.55 according to Matthiessen's ratio (Matthiessen, 1880), D is the peak ganglion cell density in the area centralis, S is the cell to cell spacing and v is the maximum spatial frequency. The spatial resolving power in cycles per degree is then given by $v * d$ (Hart, 2002, Theiss et al., 2007).

Results

The retinas of the five species of stingrays examined possess different proportions of both cone and rod photoreceptors. Rods are more abundant than cones in all species and, in general, the distribution of photoreceptors is non-homogeneous across the retina, with shallow gradient changes in rod density and steep gradient changes in cone density. The topographic maps show a dorsal high density streak in the photoreceptor and ganglion cell distributions in all species, which is



more pronounced in the ganglion cell and cone distributions than in the rod distribution. However, small differences in cell density, topography and the magnitude (retinal coverage) of the specialization occurs between species.

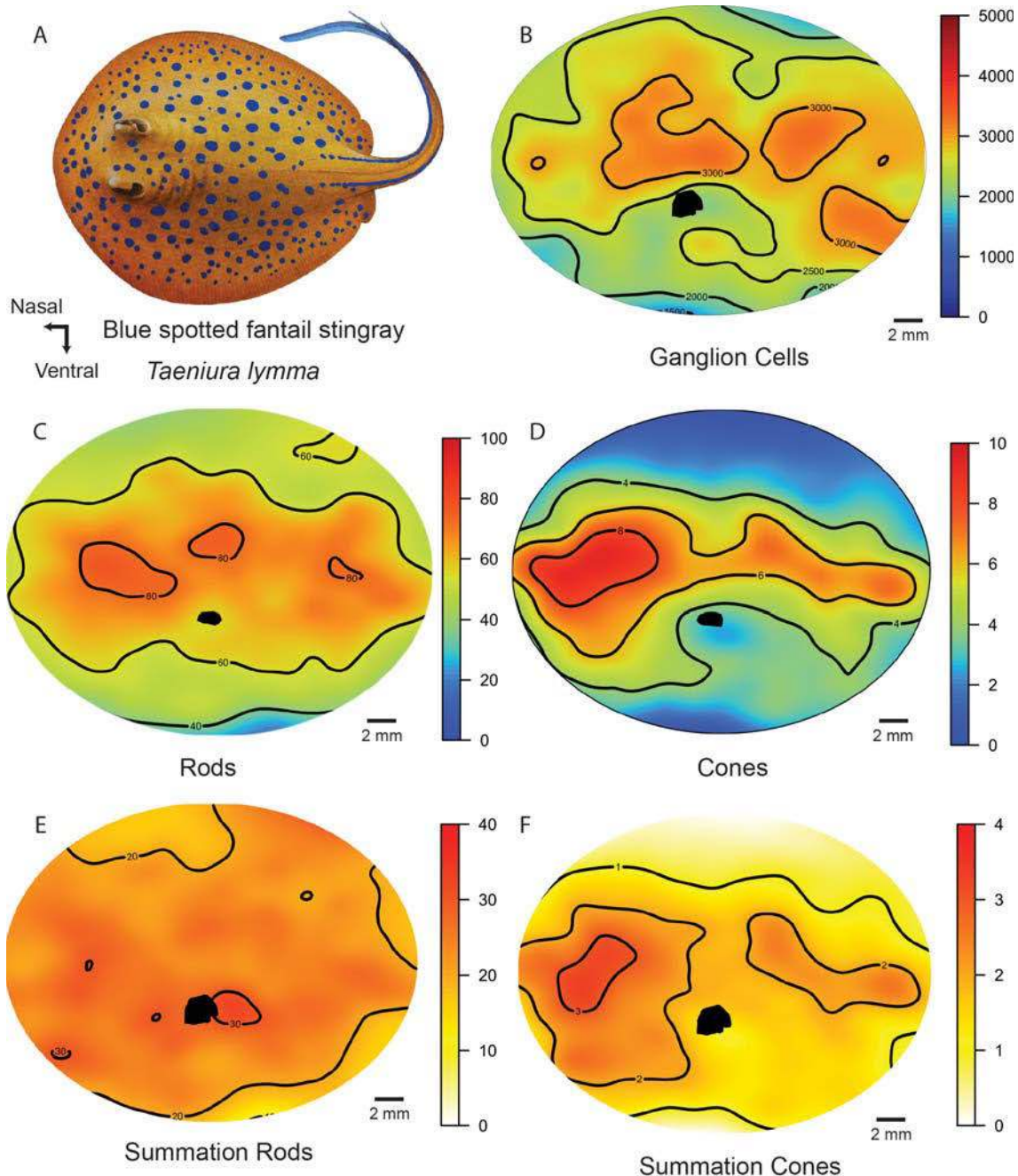


Figure 5.1 Average retinal cell density maps in the bluespotted fantail ray, *Taeniura lymma*. A). Diagram of the bluespotted fantail ray (25-27 cm DW) (adapted from Last and Stevens, 2009). B). Average ganglion cell density map (cells mm⁻²). C) Average rod cell density map (1000 x cells mm⁻²). D). Average cone cell density map (1000 x cells mm⁻²). E). Number of rods per ganglion cell summation map. F). Number of cones per ganglion cell summation map.

The bluespotted fantail ray, *Taeniura lymma* (Figure 5.1A), has a retinal ganglion cell distribution with some shallow, dorsal horizontal areas of more than 3,000 cells mm⁻². The lowest density region lies in the ventral retina with densities of less than 2,000 cells mm⁻² (Figure 5.1B). The rod distribution shows a gradient between 40,000 and 80,000 cells mm⁻², but the streak is not pronounced; instead it shows three areas of increased density of more than 80,000 cells mm⁻² with the largest area in the nasal retina (Figure 5.1C). The cone distribution shows a similar pattern with a gradient between 2,000 and 8,000 cells mm⁻² and a nasal area with densities higher than 8,000 cells mm⁻² (Figure 5.1D). The summation ratio of rods to ganglion cells is approximately 20:1 across the retina with a small area with a ratio higher of > 30:1 adjacent to the optic nerve (Figure 5.1E). The cone to ganglion cell summation map shows a region of higher ratios (~3:1) consistent with the nasal area of cone distribution although most of the dorsal and ventral periphery of the retina has a lower ratio of 1:1 (Figure 5.1F).

The bluespotted maskray, *Neotrygon kuhlii* (Figure 5.2A), possesses a specialised region of ganglion cells in a dorsal streak, reaching more than 2,500 cells mm⁻² in dorsal retina (Figure 5.2B) and rods without a well-defined specialization, reaching a density of more than 60,000 cells mm⁻² in similar regions of the dorsal retina (Figure 5.2C). These shallow gradient peaks are consistent between photoreceptor and ganglion cell maps as can be observed in the summation map, where a lower rod to ganglion cell ratio is observed over much of central retina with a ratio of less than 20:1 (Figure 5.2E). Cone densities, in contrast, show a distinctive pattern with a well-defined dorsal streak with a peak of more than 6,000 cells mm⁻² and central and nasal peaks of more than 8,000 cells mm⁻² (Figure 5.2D). The cone to ganglion cell ratio is low in the periphery with 1:1 ratio and high in the centre of the retina with a ratio of 3:1 (Figure 5.2F).

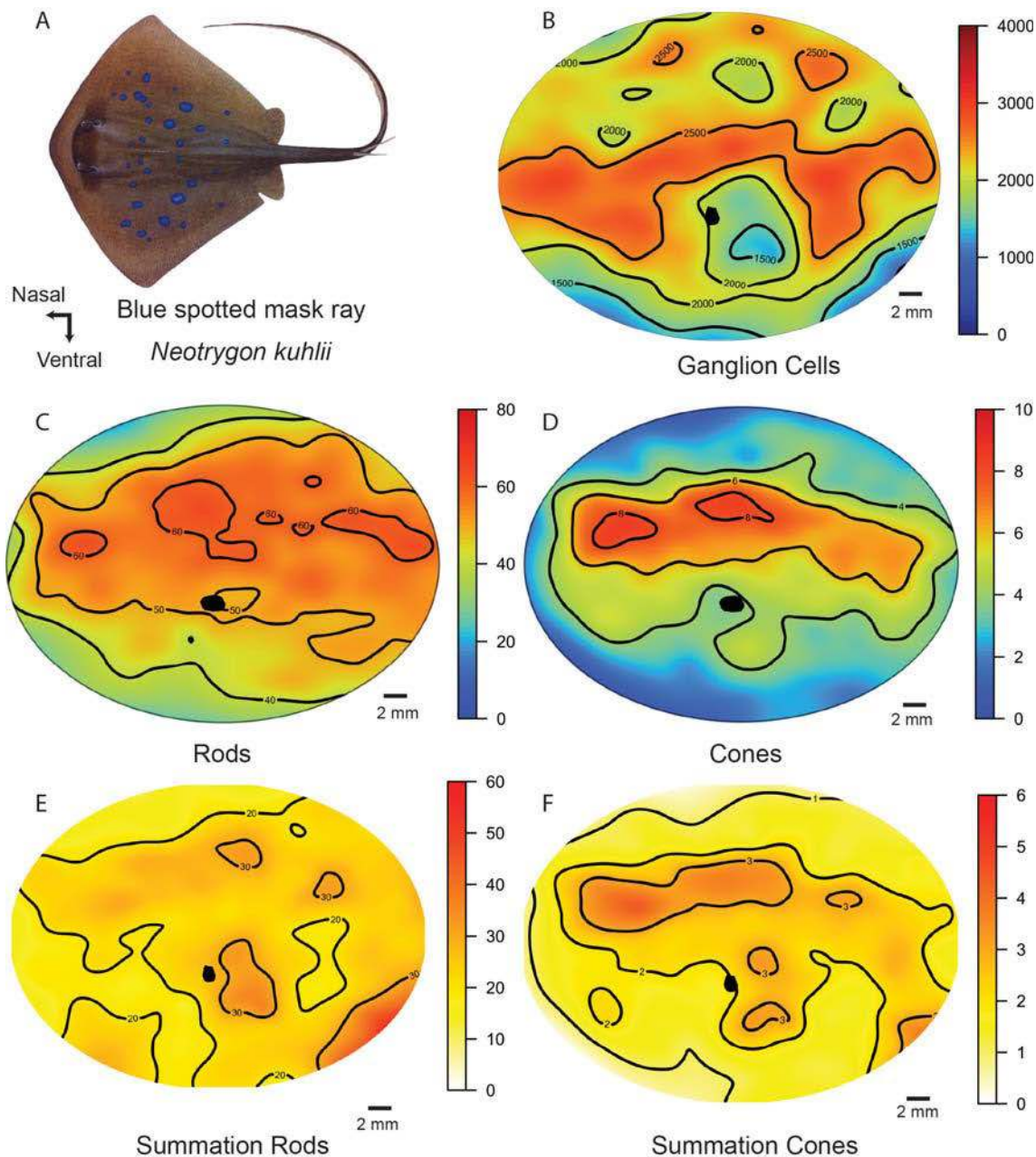


Figure 5.2 Average retinal cell density maps in the bluespotted maskray, *Neotrygon kuhlii*. A). Diagram of the bluespotted maskray (32-35 cm DW) (adapted from Last and Stevens, 2009). B). Average ganglion cell density map (cells mm⁻²). C) Average rod cell density map (1000 x cells mm⁻²). D). Average cone cell density map (1000 x cells mm⁻²). E). Number of rods per ganglion cell summation map. F). Number of cones per ganglion cell summation map.

The reticulated whipray, *Himantura uarnak* (Figure 5.3A), possesses an elongated horizontal specialization of increased photoreceptor and ganglion cell densities. Ganglion cell density increases in dorsal retina with a streak of 3,000 cells mm⁻² and a dorso-temporal area of more than 4,000 cells mm⁻² (Figure 5.3B). The region of peak rod density (<50,000 cells mm⁻²) is located closer to the equator of the retina with a shallow gradient from 30,000 to 60,000 cells

mm^{-2} (Figure 5.3C), while the cone distribution forms a dorsal arch $>8,000$ cells mm^{-2} with three peaks of more than $9,000$ cells mm^{-2} and a steeper gradient of change from $2,000$ to $10,000$ cells mm^{-2} (Figure 5.3D). The topography of the changes in summation ratio of the photoreceptors to ganglion cells is very similar between rods (high acute area less than 20:1) (Figure 5.3E) and cones (high acute area less than 3:1) (Figure 5.3F), both of which reveal a dorsal streak.

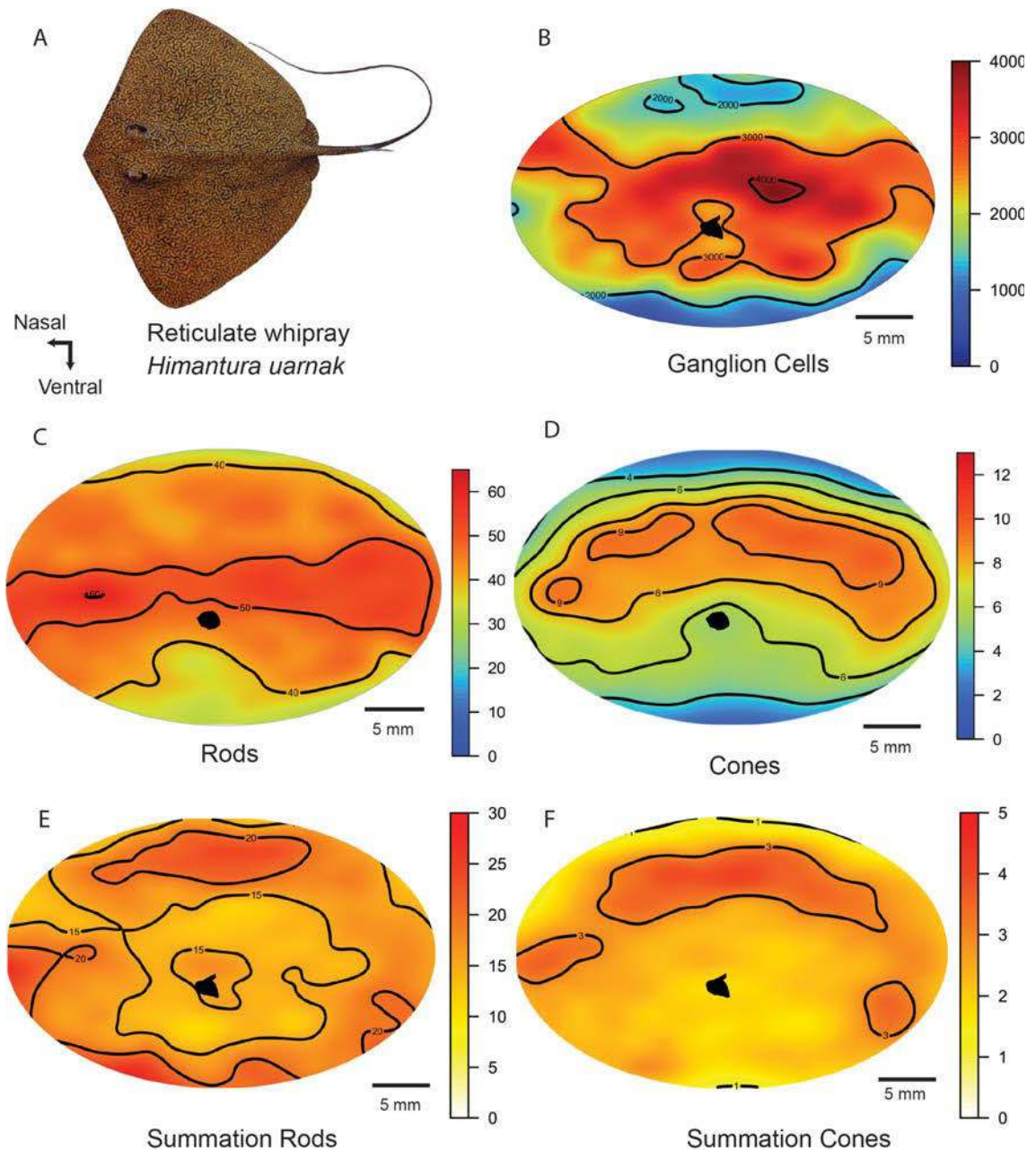


Figure 5.3 Average retinal cell density maps in the reticulated whipray, *Himantura uarnak*. A). Diagram of the reticulated whipray (89-120 cm DW) (adapted from Last and Stevens, 2009). B). Average ganglion cell density map (cells mm^{-2}). C) Average rod cell density map ($1000 \times$ cells mm^{-2}). D). Average cone cell density map ($1000 \times$ cells mm^{-2}). E). Number of rods per ganglion cell summation map. F). Number of cones per ganglion cell summation map.



The cowtail ray, *Pastinachus atrus* (Figure 5.4A), shows a ganglion cell distribution with a clear dorsal streak of more than 4,000 cells mm⁻² (Figure 5.4B). Rod density gradients are shallow and no streak pattern is consistently observed, where rods are distributed uniformly across most of the retina at a peak density of 40,000 cells mm⁻² with only temporal and nasal peaks reaching more than 50,000 cells mm⁻² (Figure 5.4C). The cone distribution shows a very similar pattern with a peak of more than 6,000 cells mm⁻² across the streak but without the temporal peak (Figure 5.4D). The summation maps also do not reveal a distinct streak, with the rod to ganglion cell summation map showing two peaks (both with a 20:1 ratio), one in the dorsal retina and the other in the ventral retina (Figure 5.4E). In contrast, the cone to ganglion cell summation ratio reveals that most of the retina has a 1:1 ratio with some small areas of more than 2:1 ratio in the dorsal retina and one area in the ventral retina (Figure 5.4F).

The porcupine ray, *Urogymnus asperrimus* (Figure 5.5A), shows a ganglion cell distribution with a shallow, dorsal streak of more than 3,000 cells mm⁻² (Figure 5.5B). Rod density gradients are shallow and similar to the other species but with a small peak of more than 60,000 cells mm⁻² close to the optic nerve (Figure 5.5C). The cone density map shows a more pronounced difference between the centre of the retina and the periphery ranging from 2,000 to 6,000 cells mm⁻² respectively (Figure 5.5D). The extended increase in cone cell density or streak in the porcupine ray is not as marked as in the other species of stingrays. The summation maps do show an area of higher summation (with a ratio of 20:1) in the dorsal region of the retina. In the rod to ganglion cell summation ratio map, most of the area has a ratio of 10:1 (Figure 5.5E), while the cone to ganglion cell summation map has a higher ratio of 2:1 in the dorsal streak with a small nasal area having a ratio of more than 3:1 (Figure 5.5F).

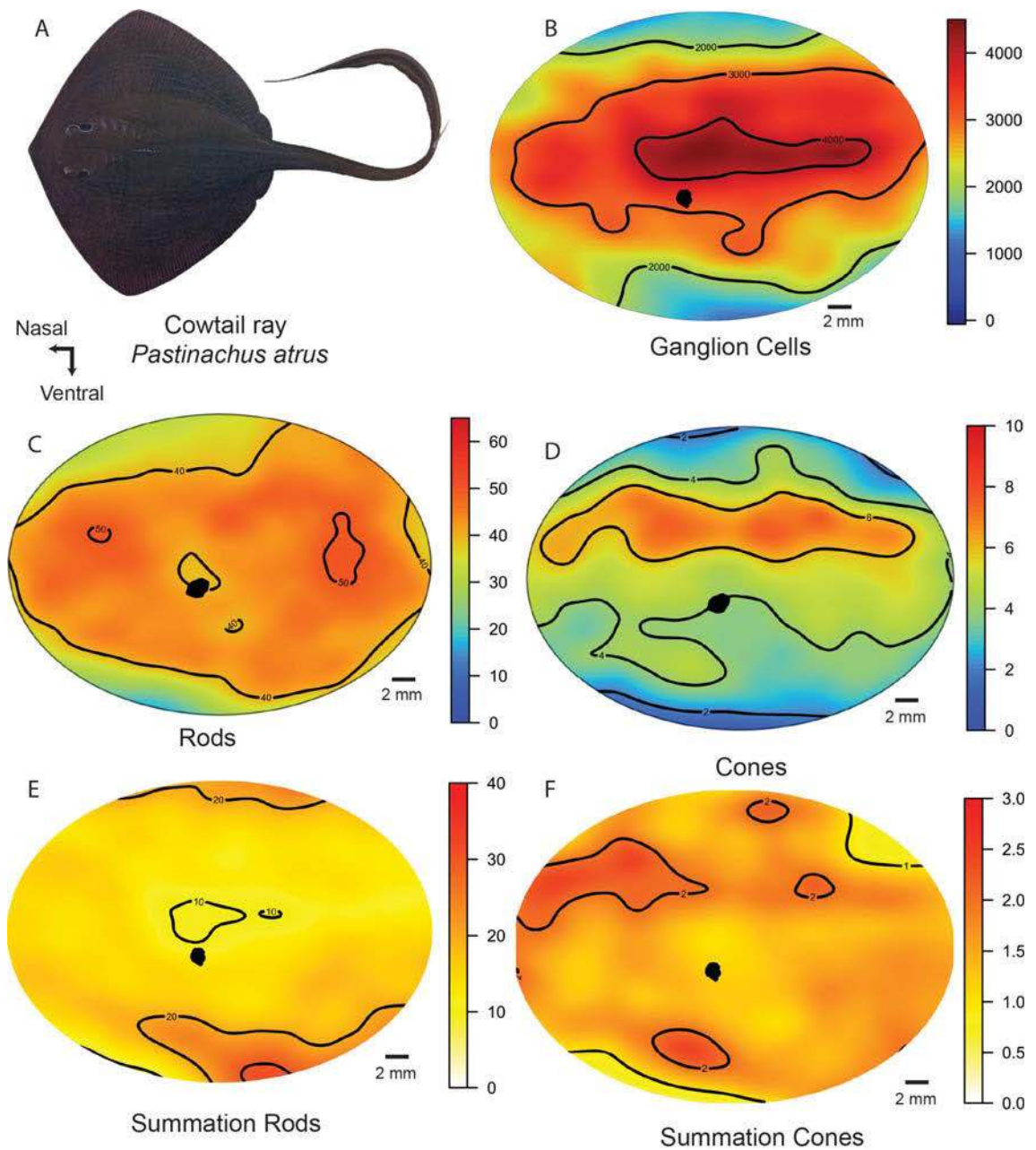


Figure 5.4 Average retinal cell density maps in the cowtail ray, *Pastinachus atrus*. A). Diagram of the cowtail ray (109-145 cm DW) (adapted from Last and Stevens, 2009). B). Average ganglion cell density map (cells mm⁻²). C) Average rods cell density map (1000 x cells mm⁻²). D). Average cone cell density map (1000 x cells mm⁻²). E). Number of rod per ganglion cell summation map. F). Number of cones per ganglion cell summation map.

A comparison of the position and magnitude (gradient and coverage) of the specializations was also assessed using horizontal and vertical transects of cell density. The peak ganglion cell densities varied between the five species of stingrays with only small variations (2,990 to 4,500 cells mm⁻²) revealed between the small rays (fantail and maskray) and the large stingrays (cowtail, reticulated and porcupine) (Table 5-1). All



the species showed a dorsal streak but the position of the peak ganglion cell density varied between species (Figure 5.6B). The cowtail and the reticulated ray possesses a temporal peak, which also represented the highest density in the cowtail ($>4,500$ cells mm^{-2}). In contrast, the maskray had peak ganglion cell density in nasal retina. The porcupine and mask rays had peaks in the central part of the retina (Figure 5.6A).

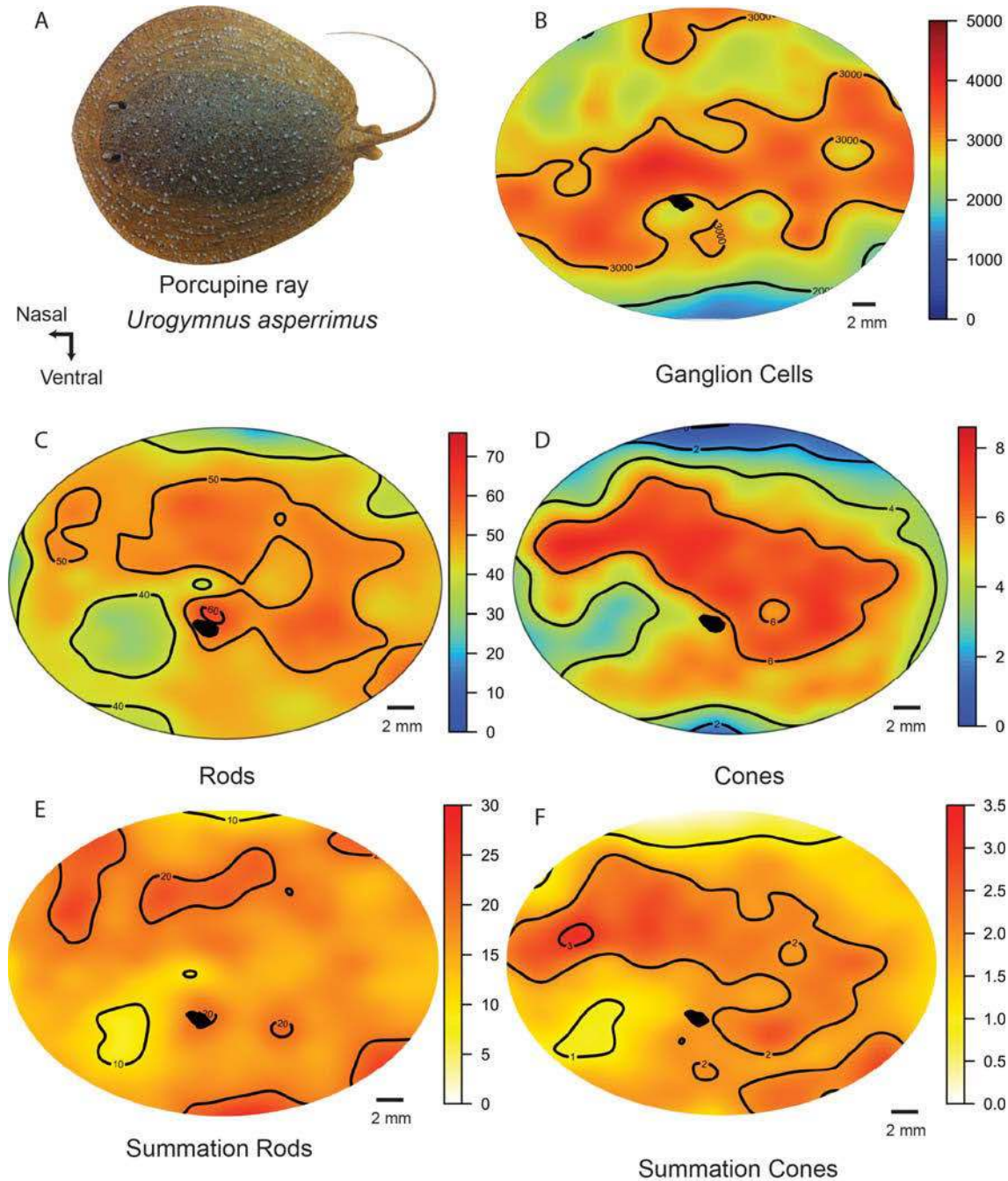


Figure 5.5 Average retinal cell density maps in the porcupine ray, *Urogymnus asperrimus*. A). Diagram of the porcupine ray (105-122 cm DW) (adapted from Last and Stevens, 2009). B). Average ganglion cell density map (cells mm^{-2}). C) Average rod cell density map (1000 x cells mm^{-2}). D). Average cone cell density map (1000 x cells mm^{-2}). E). Number of rods per ganglion cell summation map. F). Number of cones per ganglion cell summation map.

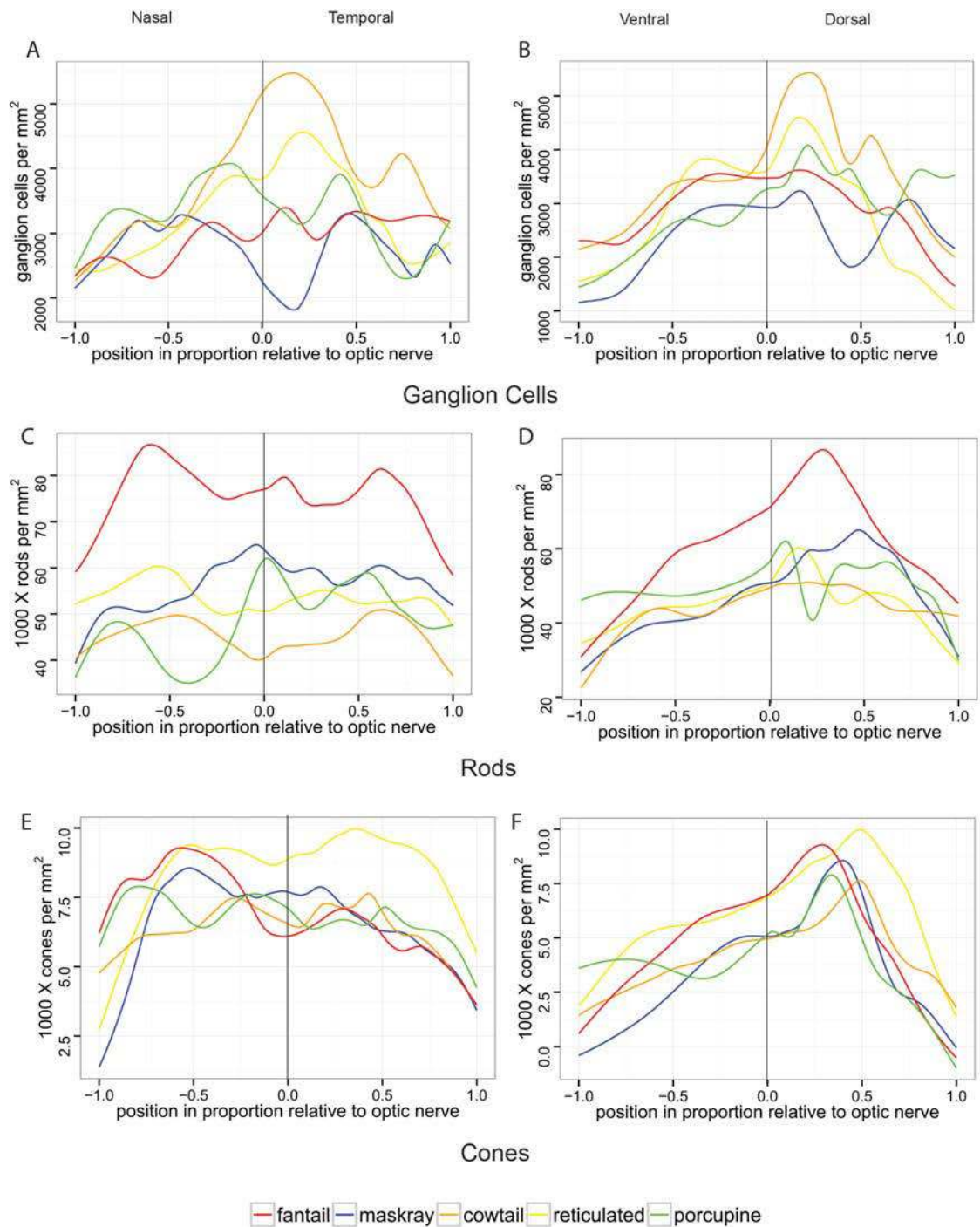


Figure 5.6 Transects across the retinal maps comparing cell density across the five species. A). Horizontal transects of the rod density maps. B). Vertical transects of the rod density maps. C). Horizontal transects of the cone density maps. D). Vertical transects of the cone density maps. E). Horizontal transects of the ganglion cell density maps. F). Vertical transects of the ganglion cell density maps. The horizontal transects (A, C, E) run through the highest peak in each average retina and are not in the same vertical position. The traces to the left of the 0.0 axis depict densities in nasal retinal regions, while traces to the right of the 0.0 axis depict densities in temporal retinal regions. The vertical transects (B, D, F) run to the highest peak in each average retina and are not in the same horizontal position. The line to the left of the 0.0 axis is in the ventral position and the line to the right is in the dorsal position of the retina.



Table 5-1. Retinal data of the specializations of the ganglion cells, rods and cones in the five species. Spatial resolving power values are in cycles per degree. The cell density values are in cells mm⁻². The position of the peaks are represented by the horizontal and vertical axes.

Scientific Name	<i>Taeniura lymma</i>	<i>Neotrygon kuhlii</i>	<i>Pastinachus atrus</i>	<i>Himantura uarnak</i>	<i>Urogymnus asperrimus</i>
Common Name	Bluespotted fantail ray	Bluespotted maskray	Cowtail ray	Reticulated whipray	Porcupine ray
Size (cm)	25-27	32-35	109-145	89-120	105-122
Focal length (mm)	10.17	11.05	10.96	10.91	11.41
Spatial resolving power (cycles per degree)	5.52	5.67	6.9	6.63	6.78
Peak Ganglion Cells (cells mm ⁻²)	3,350	2,990	4,500	4,200	4,020
Position Peak GC	(0.52, 0.35, 0.47)	(0.51, 0.18)	(0.08, 0.26)	(0.28, 0.24)	(-0.13, 0.20)
Peak Rods (cells mm ⁻²)	86,700	65,000	51,000	60,000	62,000
Position Peak Rods	(-0.6, 0.28)	(-0.04, 0.46)	(0.62, 0.21)	(-0.56, 0.15)	(0.02, 0.09)
Peak Cones (cells mm ⁻²)	9,280	8,560	7,640	9,970	7,890
Position Peak Cones	(-0.56, 0.29)	(-0.52, 0.4)	(0.42, 0.48)	(0.36, 0.48)	(-0.78, 0.33)
Rods: Cones ratio in Streak	14:1	12.5:1	6.6:1	6.25:1	8.3:1

The highest density of rod photoreceptors was observed in the fantail ray (86,700 cells mm⁻²) with almost 20,000 cells mm⁻² more than the maskray (65,000 cells mm⁻²). The lowest rod densities were found in the three larger species of stingrays: porcupine (62,000 cells mm⁻²) reticulated (60,000 cells mm⁻²) and cowtail (51,000 cells mm⁻²) (Table 5.1). The position of the peak rod density was always located in the dorsal hemiretina in all species (Figure 5.6D), but restricted to temporal (cowtail ray), nasal (fantail and reticulated stingrays) and central (maskray and porcupine ray) retina (Figure 5.6C). The peak cone photoreceptor density varied in the five species of stingrays ranging from 9,970 cells mm⁻² in the reticulated ray to 7,640 cells mm⁻² in the cowtail ray. The position of the peak cone density also varied from temporal (cowtail and reticulated rays) to nasal (fantail, mask and porcupine rays) retina (Figure 5.6E). The ratio of rod to cone photoreceptors in the streak was higher in the two species of bluespotted stingrays, *T. lymma* and *N. kuhlii* i.e. 14:1 and 12.5:1, respectively, than in the three species of larger stingrays, *P. atrus*, *H. uarnak* and *U. asperrimus* i.e. 6.6:1, 6.25:1 and 8.3:1, respectively (Table 5.1).

Visual Specializations and Light Detection in Chondrichthyes

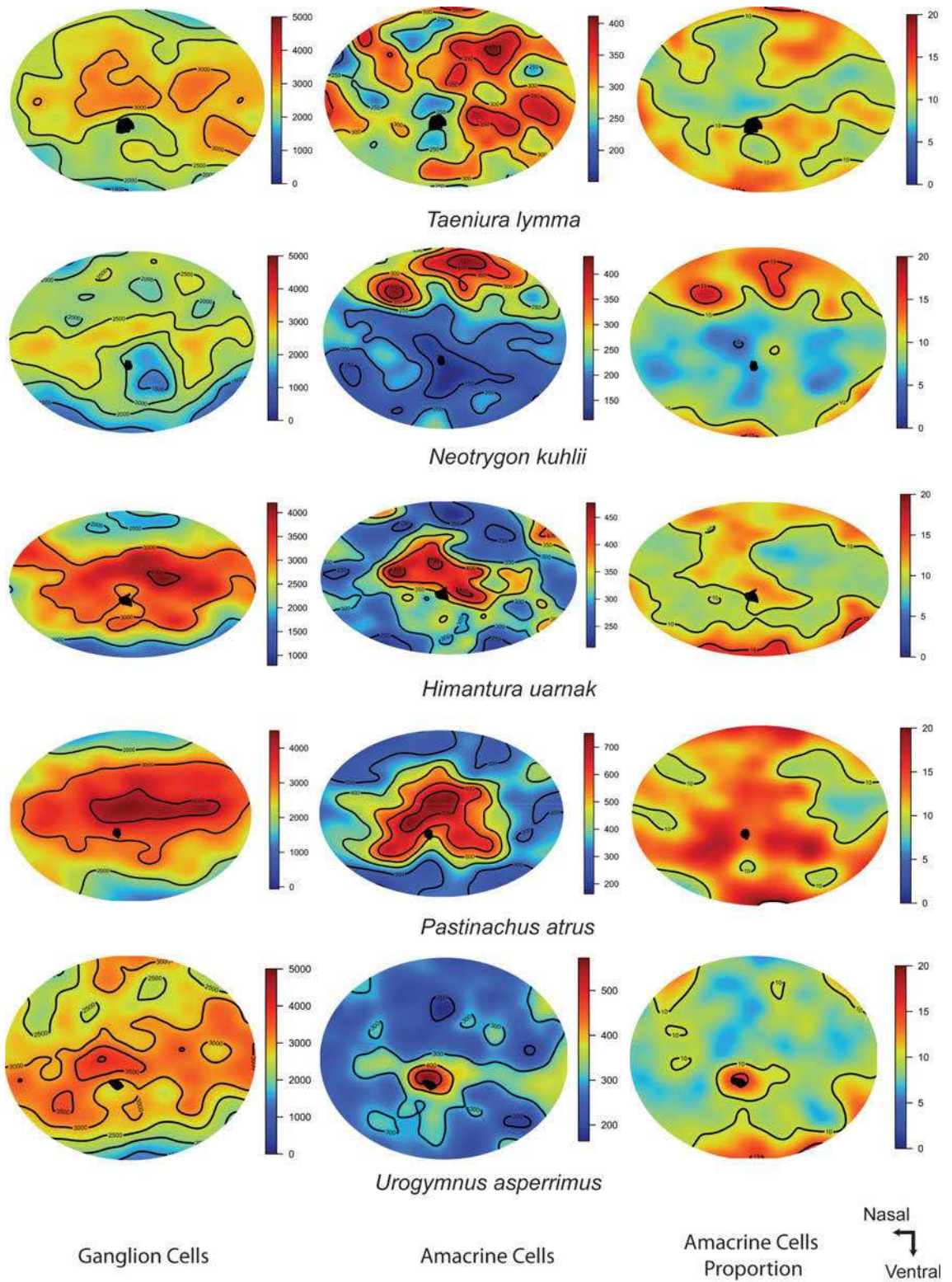


Figure 5.7 Ganglion cell, amacrine cell density distribution maps and amacrine cell proportions from the total cell numbers in the retina in the five species of rays



The proportion of amacrine cells in the ganglion cell layer of the retina was lower than 20% in the five species studied. Some species, like *N. kuhlii*, showed a steeper distribution of amacrine cells than ganglion cells. The other species, like *P. atrus*, *U asperrimus* and *H uarnak*, possessed a similar distribution of amacrine cells and ganglion cells. *T. lymma* possessed an irregular distribution of amacrine cells that is different to the distribution of ganglion cells (Figure 5.7).

The focal length of the eye was relatively similar between the five different species with a range between 10.17 and 11.41 mm (Table 5.1). Estimates of spatial resolving power using the peak ganglion cell density in the streak were also similar between the five different species of stingrays with the lowest value of 5.52 cycles per degree found in the bluespotted fantail *T. lymma*, and the highest value of 6.9 cycles per degree found in the cowtail, *P. atrus* (Table 5.1).

Discussion

In this study, we examined the topographic distribution of photoreceptors and ganglion cells in five sympatric species of stingrays from the same family in order to identify possible variations in retinal morphology that may reflect adaptations to specific ecological niches. The retinal topography of all five stingrays follows a similar general pattern with a dorsal horizontal streak across the retina. The most significant differences between species are the higher density of rods in the retina of *T. lymma* (by almost 30%), the higher density of cones in *H. uarnak* and the higher rod to cone ratio in the dorsal streak of smaller stingrays compared to larger stingrays.

The use of average topographic maps reflects the general pattern between different retinas of the same species. In the current study, all

the retinas used for the average were from adult animals of similar size and the size of the retina was standardized to the largest retina to match the different regions. Although not applicable here, since ontogenetic changes in the retinal topography are likely to occur it is strongly recommended not to use the average technique when retinas from different developmental stages are analysed (Bailes et al., 2006, Harahush et al., 2009, Litherland et al., 2009). The use of transects to compare the retinas provides a rapid method of visual assessment of the relative position and the magnitude of each specialization. It should be noted that the positions of the transects used in this study are not the same for each species, as each transect was aligned to fall across the peak in cell density. The use of a vertical and a horizontal transect intersecting at the highest cell density peak also gives the position of the specialization relative to the optic nerve head making transects of different species more comparable. The creation of a quadrature system, where the values represent the proportion of the distance from the optic nerve head to the periphery should be considered carefully because the shape of the retina and the position of the optic nerve head might be distorted. The optic nerve head in rays is located naso-ventrally so, when the distances to the periphery are standardized, the distance of the optic nerve head to the ventral edge should equate to the distance to the dorsal edge, but in reality it is smaller.

Ganglion cell distribution

Ganglion cells are the neurons responsible for transmitting information about the retinal image to the visual centres of the brain. For a given density of photoreceptors, lower densities of ganglion cells (indicating higher summation ratios) would increase retinal sensitivity, while higher densities of ganglion cells would increase retinal resolution. Higher sensitivity is an important feature for scotopic vision in deep-sea, nocturnal or crepuscular species (Lythgoe, 1979, Warrant and Locket, 2004). Previous studies of the ganglion cell distribution in the



bluespotted fantail rays and the bluespotted maskrays reported similar cell densities but the position of the specializations differ slightly. The bluespotted fantail, *T. lymma*, was described as having a dorso-central streak close to the optic nerve (Lisney and Collin, 2008). This finding differs from the dorsal streak found in the present study. The iso-density line representing 3,000 cells mm⁻² is present in topographic maps generated in both studies and occurs in a similar position but the current study shows a lower peak density in the dorsal part of the retina i.e. 3,350 cells mm⁻² compared to 4,290 cells mm⁻² found by Lisney and Collin (2008). A previous study of the ganglion cell topography in *Neotrygon kuhlii* (= *Dasyatis kuhlii*) shows a dorsal streak similar to the current study with most of the retinal regions with densities higher than 2,500 cells mm⁻² and several peaks within the streak (nasal, central and temporal) with densities greater than 3,500 cells mm⁻² with an average peak of 4,251 ± 720 cells mm⁻² (Theiss et al., 2007). The average map obtained in the present study shows the dorsal streak to be more than 2,500 cells mm⁻² with the highest peak at 2,990 cells mm⁻² but in a nasal position. The horizontally elongated streak located in the dorsal retina with multiple peaks in the nasal, central and temporal regions is consistent in the different studies but the position of the highest peak and the magnitude varies. The difference in the peak densities might be caused by the difference in the size of the animals analysed in the study (32-35 cm DW in present study compared to 23 cm DW in Theiss et al., 2007).

Other studies on shallow water rays present similar values for the peak ganglion cell densities i.e. in the giant shovelnose ray, *Glaucostegus typus* (= *Rhinobatos batillum*) with peaks at 5,500 cells mm⁻² (Collin, 1988). Some species of rays such as the Bigelow's ray, *Raja bigelowi* (Bozzano and Collin, 2000) and the eastern shovelnose ray, *Aptychotrema rostrata* (Litherland and Collin, 2008) possess peaks of 2,200 cells mm⁻² and 2,740 cells mm⁻², respectively, which are lower compared to the peak densities in the ray species examined in the

current study. Several studies in benthic species of sharks have found values for the peak density of ganglion cells that are lower than these species of rays i.e. the lemon shark, *Negaprion brevirostris* (1,600 cells mm⁻²)(Hueter, 1991a), the epaulette shark, *Hemiscyllium ocelatum* (central peak of 1,825 cells mm⁻²) and the small spotted catshark, *Scyliorhinus canicula* (with a temporal peak at 2,396 cells mm⁻²) (Bozzano and Collin, 2000).

The current study aimed to distinguish between ganglion cells and amacrine cells that were stained for Nissl substance. Distinguishing between amacrine cells and ganglion cells was more difficult in some sections of the retina, especially where cell densities were higher and the diameter of the cell profiles was similar. Previous studies have showed, using retrograde labelling from the optic nerve, that amacrine cells account for around 20% of the Nissl-stained neurons in the specialized areas of the retina, therefore the actual densities of ganglion cell densities may be somewhat less in the high density/specialized areas (Collin, 1988, Lisney and Collin, 2008). Ganglion cells in the inner plexiform layer were counted in this study, but we did not differentiate and count ganglion cells displaced to the inner nuclear layer (Stell and Witkovsky, 1973a, Peterson and Rowe, 1980).

Focal length and spatial resolving power

Matthiessen's ratio (or the constant relationship of 2.55 between the lens radius (r) and the distance from the lens centre to the retina (focal length/r)) has traditionally been used to calculate the focal length (Matthiessen, 1880) in the aquatic eye and this has similarly been used in calculations in this study of the five species of stingrays. The lens of the elasmobranch eye also varies from near spherical to elongated axially (Sivak, 1978, Sivak and Luer, 1991, Hueter et al., 2001, Theiss et al., 2007). The axial elongation of the lens was found to be around 10% in the different rays examined; but the orientation of the lens was



hard to maintain in the field so the correct orientation was not completely accurate, providing one source of error in the calculation of lens radius and thereby the calculation of focal length. Lisney and Collin (2008) used a higher ratio of 2.75 obtained from the mean of experimental measures of eight species of elasmobranchs, although it has been proposed that this ratio might diminish with developmental changes from juveniles to adults from 2.75 to 2.55 (Sivak and Luer, 1991). It is interesting to note that besides the difference in the size of the five stingrays, i.e. the small species: bluespotted rays, *T. lymma* and *N. kuhlii*, with a disc width of 25 and 35 cm, respectively and the large species: reticulated whipray, cowtail ray, and porcupine ray with a disc width between 89 and 145 cm, the focal length of the five species does not vary much (between 10.17 and 10.47 mm for the small stingrays and between 10.91 and 11.41 mm in the large stingrays). These values suggest that the eyes of the smaller stingrays are relatively large compared to the eyes of the larger stingrays.

The spatial resolving power in the five species of stingrays varies from 5.52 to 6.9 cycles per degree. A previous study by Lisney and Collin (2008) calculated the spatial resolving power in the bluespotted fantail, *Taeniura lymma*, and found a slightly higher value than the current study (7.50 compared to 5.52 cycles per degree) but this value was still within the range obtained for the five species of the same family. This is interesting considering that the peak density of ganglion cells is higher in the current study but the use of a higher Matthiessen ratio by Lisney and Collin gave a higher spatial resolving power. Another study by Theiss et al. (2007) found a lower value for *N. kuhlii* (4.10 ± 0.69 cycles per degree) compared to the present study (5.67 cycles per degree). The focal length was also higher in the current study (11.17 mm) compared to the range previously calculated (5.6 to 10.4 mm). Another possible explanation of this discrepancy is the use of adult animals in the current study with a size range between 32 to 35 cm DW (8.67 mm lens diameter average), where Theiss et al. (2007) used smaller animals of 21

to 30 cm DW obtaining lens diameters of 5.2 to 6.5 mm. Other studies suggest that juveniles might have a lower spatial resolving power as a consequence of having smaller eyes and lenses and thus a shorter focal length (Collin and Pettigrew, 1989, Lisney and Collin, 2008).

Spatial resolving power in elasmobranchs has previously been calculated as between 2 and 11 cycles per degree (Stell and Witkovsky, 1973a, Hueter, 1991a, Bozzano and Collin, 2000, Bozzano, 2004, Theiss et al., 2007, Lisney and Collin, 2008, Litherland and Collin, 2008). The most significant observation is that the relatively high value for the spatial resolving power of the eye in the stingrays was only reported previously in *T. lymma*, and it was considered abnormal for a benthic species (Lisney and Collin, 2008).

The range of the peak of rod cells to the peak of cone cells ratios in the five species of stingrays varied from 6.2:1 to 14.0:1 and may reflect an adaptation to different ambient light environments from dim/nocturnal to bright/diurnal (Yokoyama and Yokoyama, 1996, Pankhurst and Hilder, 1998, Hart et al., 2006). Other studies have quantified the proportion of cones and rods in stingrays using different techniques, such as light microscopic examination of radial and transverse sections of the retina in the pink whipray, *Himantura fai* (3:1) (Schieber et al., 2012), the Atlantic stingray, *Dasyatis sabina* (3:1) (Logiudice and Laird, 1994), the red stingray, *Dasyatis akajei* (5:1) (Toyoda et al., 1978); the bluntnose stingray, *Dasyatis sayi* (Yokoyama and Yokoyama, 1996) (5:1) (Hamasaki and Gruber, 1965) and the short-tail stingray, *Dasyatis brevicauda* (10:1) (Braekevelt, 1994a). It is important to note that the method of using radial sections to estimate the differences in rod and cone densities may underestimate the ratio of rods to cones. The stereological technique in wholemounted retinas considers different counting frames for rods and cones and the different sampling design improves the optimal assessment of the two densities within the retina.



Litherland and Collin (2008) used the whole-mounted retina to calculate the ratio between the peak density of rod and cone cells in the Australian shovelnose ray, *Aptychotrema rostrata* and found a ratio of 5:1.

Topographic studies of photoreceptor distribution have not typically been presented for elasmobranchs although they provide important ecological information and have received more attention in other groups of animals like mammals (Packer et al., 1989, Curcio et al., 1990, Andrade da Costa and Hokoç, 2000, Franco et al., 2000, Ahnelt et al., 2006, Schiviz et al., 2008). The range of peak cone photoreceptor densities in the stingrays varied from 7,640 to 9,970 cells mm⁻² and falls within the range reported by Litherland and Collin (2008), where they mapped rod and cone densities of four species of elasmobranchs: the ornate wobbegong (*Orectolobus ornatus*), the whitetip reef shark (*Triaenodon obesus*), the epaulette shark (*Hemiscyllium ocellatum*) and the eastern shovelnose ray (*Aptychotrema rostrata*). The peak number of cones between 3,600 and 18,200 cells mm⁻² is similar to the numbers obtained in the present study.

Summation ratio of photoreceptors to ganglion cells

The summation ratio maps were constructed separately for cones and rods because, in most animals, these subserve vision under different levels of ambient illumination. A high number of photoreceptors per ganglion cell will increase the absolute sensitivity of the retina in certain areas at the cost of spatial resolving power, as observed for the rods with typical ratios around 20:1. On the contrary, if fewer photoreceptors converge onto individual ganglion cells then there is the potential for higher spatial resolving power, albeit at the cost of absolute sensitivity. Litherland and Collin (2008) previously analysed the summation between photoreceptor cells and ganglion cells without discriminating between the cone and rod populations. They found that areas of high

photoreceptor density usually overlap with areas of high ganglion cell density resulting in lower summation ratios. However, the proportions of cones and rods in the retina are not uniform. In the present study, the cowtail and reticulated rays show lower summation ratios in the specialized zones for acute vision than in the periphery. On the other hand, the bluespotted maskray, the fantail and the porcupine rays all show higher summation in the periphery for enhanced sensitivity.

The stingray eye is elongated in the rostro-caudal axis and thus somewhat ovoid rather than spherical in shape. The flattened shape of the body is reflected in the hemispherical shape of the eye, thereby permitting the sampling of light (and its visual field) in the horizontal axis more efficiently. The lens of the eye is closer to spherical in contrast to the shape of the eye. The pupil plays an important role as the iris regulates the light that enters the eye (Kuchnow, 1971). Elasmobranchs have a wide variety of pupil shapes, where stingrays, in particular, have peculiar designs like crescent-shaped apertures (Murphy and Howland, 1991, Schwab and Hart, 2006). It is suggested that multiple pupillary apertures are formed from the crescent-shaped pupil and are useful for species that are active at low light levels but also need good vision during photopic conditions when the multiple pupillary apertures reduce the light flux into the retina (Murphy and Howland, 1991). It is possible that the shape of the pupil in the rays examined corresponds to the position of the retinal specializations as found in other species of fishes (Douglas et al., 2002). The lens of the elasmobranch eye varies from near spherical to elongated axially (Sivak, 1978, Sivak and Luer, 1991, Hueter et al., 2001, Theiss et al., 2007). The axial elongation of the lens was found to be around 10% in the different rays examined; but the orientation of the lens was hard to maintain in the field so the correct orientation was not completely accurate, providing one source of error in the calculation of lens radius.



Visual ecology

Rays from the family Dasyatidae generally have a diet consisting of benthic invertebrates. Small variations in the diet of the different species of rays might facilitate their sympatric existence. A previous study with the same five species of rays showed that the only species that shows dietary partitioning is the reticulated whipray, *Himantura uarnak*, which predares more on crustaceans, while the other four species have a diet composed predominantly of annelids (O'Shea et al., 2013). Crustaceans normally move over the surface of the sand and enhanced visual acuity in the central part of the retina (subtending lateral or eccentric visual space) may facilitate the detection of this type of prey. On the other hand, buried animals like polychaete worms might be detected by other senses such as olfaction (Heupel and Bennett, 1998, Meredith and Kajiura, 2010) and electroreception (Blonder and Alevizon, 1988, Collin and Whitehead, 2004, McGowan and Kajiura, 2009, Kempster et al., 2013).

Taeniura lymma has a synchronised movement pattern, where they move to sand flats during high tide to feed on polychaete worms, molluscs and/or fishes, and move back to the protection of caves and rocks when the tide is low (Jonna, 2003, Last and Stevens, 2009). We observed that *T. lymma* was found under rocks and in shaded areas most of the time. It is possible that they stay there to rest waiting for the opportune moment to feed. This behaviour may be mediated by the high number of rods (30% more than other species) localised within a specialised retinal region of high sensitivity given the dim light conditions found in caves (Marshall et al., 2003). In contrast, the other four species were found most of the time in sandy flats in open areas, where the use of rods is restricted during bright light conditions and higher number of cones might be preferable.

Other behaviours in the different species of rays may be mediated by the visual system. Grouping behaviour has been observed in different stingrays possibly because groups of animals can maximize feeding opportunities and increase the chances of detecting predators (Semeniuk and Dill, 2005, Semeniuk and Dill, 2006). Some species of Dasyatidae have been reported to form groups comprised of different species (reticulated whipray and cowtail ray). It has been reported that the success of escaping predators in low light conditions is increased when the whipray, *H. uarnak*, is present with groups of a different species of cowtail i.e. *Pastinachus sephen*. (Semeniuk and Dill, 2006). The low levels of summation in central retina may mediate acute vision for interspecific identification, while the high levels of summation in the periphery may enable the detection of approaching predators.

Analysis of the topographic distribution of photoreceptor and ganglion cells has revealed subtle differences that reflect ecological differences in some of the five stingray species examined. The bluespotted fantail ray shows some specializations for vision in dim light conditions, perhaps due to the time they spend in caves and/or because they are more active during crepuscular periods of the day than the other species. The higher cone numbers and the low levels of summation (mediating acute vision) in the reticulated whipray may be related to its diet of crustaceans. Further work to examine physiological visual characteristics and photoreceptor spectral sensitivity may validate some of the assumptions made with morphological characteristic. Additionally, the use of other sensory modalities may reveal more information about how these closely-related species might perceive their environment and if any specific ecological traits have promoted speciation and/or further ecological partitioning.



Acknowledgements

We would like to thank all the field volunteers: Owen O'Shea, Thomas Espeland, Kim Brooks, Mark Meekan and Channing Egeberg for their in collecting the samples. We are sincerely thankful to Joao Paulo Coimbra and Caroline Kerr for all the invaluable help in the lab. This research was supported by an Australian Research Council Discovery Project Grant (DP110103294) to SPC, NSH, and others; and the Western Australian State Government (to SPC). EGG was supported by the Mexican scholarship for Postgraduate studies (CONACyT) and the Ad-Hoc Top-Up Scholarship by the University of Western Australia.

Chapter 6 Immunohistochemical labelling of a long wavelength-sensitive cone opsin in the retina of three species of cartilaginous fishes (Chondrichthyes)

Garza-Gisholt, E, Kempster, R.M., Hart, N.S. and Collin, S.P.

School of Animal Biology and The UWA Oceans Institute, The University of Western Australia, Crawley, 6009 W.A.

Abstract

The anatomical identification of spectrally-distinct cone types is a very useful tool for assessing the capacity of vertebrate animals to see colour and establishing which parts of the visual field are sampled differentially. Representatives of the two major groups of cartilaginous fishes or Chondrichthyes, i.e. the Elamobranchii (gummy shark, *Mustelus antarcticus*, bluespotted maskray, *Neotrygon kuhlii* and bluespotted fantail ray, *Taeniura lymma*) and the Holocephali (elephant shark, *Callorhynchus milii* and deep-sea chimaera *Rhinochimaera pacifica*) were examined for the presence of positive immunoreactivity to an anti-long-wavelength-sensitive (LWS) cone opsin antibody in the retina. The different proportions and distribution of LWS cones (where present) to the total number of cones was established by comparing positively-labelled cones, to the total population of cones (labelled plus unlabelled cone profiles) using stereological methods. Species that frequent brightly lit environments possessed high proportions of LWS cones distributed in a dorsal horizontal streak i.e. the rays, *N. kuhlii* (93%) and *T. lymma* (73%) and the elephant shark *C. milii* (72%). Species considered to be deep water inhabitants, i.e. *R. pacifica* and *M. antarcticus*, did not show any immunoreactivity to the LWS opsin antibody. These results may reflect differences in the relative availability



of long wavelength light in each species' habitat and/or the identity of the cone opsins present in the retina of each species. The higher density of LWS cones and total cones in the dorsal retina also reveals a specialisation for high acuity vision in the ventral visual field that may be adaptive for the detection and identification of prey on or near the substrate within each species' benthic/benthopelagic habitat. These findings support those of previous studies that have shown large variations in the spectral sensitivity of the eyes of cartilaginous fishes and the influence of the light environment on the sensory ecology of these early vertebrates.

Keywords

LWS cones; immunohistochemistry; *Neotrygon kuhlii*; *Taeniura lymma*; *Callorhinchus milii*; photoreceptors; deep-sea

Introduction

Vertebrate photoreceptors respond to light via a phototransduction process initiated by a visual pigment embedded within the membranous discs of the outer segments. The spectral sensitivity of a visual pigment is determined by the amino acid sequence of the opsin protein and the type of chromophore molecule of which it consists. (Kolb, 1995b, Shichida and Matsuyama, 2009). The sensitivity hypothesis proposes that visual pigments in fishes should have wavelengths of maximum absorbance (λ_{\max}) that are matched to the most abundant wavelengths of light in their habitat (Loew and Lythgoe, 1978, Crescitelli et al., 1985). However, the contrast hypothesis states that the maximum absorption of a visual pigment that is offset from the wavelengths of light penetrating the water column has the advantage of detecting an object depending on its radiance relative to the background (McFarland and Munz, 1975, Loew and Lythgoe, 1978, Bowmaker, 1995). Fishes appear to follow both strategies, where visual pigment absorption is

either matched to the ambient light of the habitat, as in deep-sea fishes (Douglas et al., 1995, Douglas and Partridge, 1997) or in some lakes, where the water clarity is high (Muntz, 1976, Bowmaker et al., 1994, Bowmaker, 1995) or offset like shallow water fishes (Lythgoe, 1984) such as cichlids (Fernald and Liebman, 1980).

Cones can vary by virtue of their peak spectral sensitivity due to differences in the amino acid sequence of their visual pigment and the relative proportion of the chromophore it uses to initiate the biochemical phototransduction cascade (retinal and dehydroretinal). The possession of multiple visual pigments is an adaptation for detecting a broader range of wavelengths of light that penetrate the water column and for discriminating between colours (Bowmaker, 1995).

Previous studies using microspectrophotometry (MSP) have shown that rays possess multiple cone visual pigments in addition to a single rod pigment. Hart et al. (2004) found three spectrally-distinct cone types in the retina of the giant shovelnose ray, *Glaucostegus typus* (477, 502 and 561 nm λ_{\max}) and the Eastern shovelnose ray, *Aptychotrema rostrata* (459, 492 and 553 nm λ_{\max}) and Theiss et al (2007) found three different cone pigments in the retina of the bluespotted maskray, *Neotrygon kuhlii* (476, 498 and 552 nm λ_{\max}). Behavioural studies have confirmed that rays have colour vision (Van-Eyk et al., 2011). In contrast, all shark species studied thus far possess only one type of cone pigment (Hart et al., 2006, Hart et al., 2011, Theiss et al., 2012) in addition to a rod pigment, meaning that they are cone monochromats and potentially colour blind. Rod opsin sequences have been established for the small-spotted catshark, *Scyliorhinus canicula* and blackmouth catshark, *Galeus mesastomus* (Bozzano et al., 2001) and the ray *Raja erinacea* (see review Hart et al 2006). However, few studies have examined the cone opsin sequences of sharks and rays, with the exception of the ornate



wobbegong, *Orectolobus ornatus*, the spotted wobbegong, *Orectolobus maculatus*, (Theiss et al., 2012) and the bluespotted maskray *Neotrygon kuhlii* (Lisney, 2004), all of which revealed an LWS opsin. Davies et al. (2009) found three types of cone opsins (Rh2, LWS1 and LWS2) in the retina of the elephant shark, *Callorhinchus milii*.

Although molecular characterisation of opsin genes is a powerful method in establishing the complement of visual pigments expressed in the retina, immunohistochemistry enables specific photoreceptor subtypes to be characterised based on their specificity to an antibody, with the possibility of revealing the proportion of cone photoreceptors and their distribution across the retina. Although there are few examples of this approach in the cartilaginous fishes, studies on the lesser spotted dogfish, *Scyliorhinus canicula*, and the brown shyshark *Haploblepharus fuscus* have shown cell proliferation using antibodies raised against proliferating cell nuclear antigen (PCNA) and against rod opsin (Ferreiro-Galve et al., 2010). Immunohistochemistry has been used extensively for characterising the distribution of cone visual pigments in a large range of vertebrates, including mammals (Araki et al., 1987, Ahnelt et al., 1995, Hemmi and Grünert, 1999, Ahnelt et al., 2006), amphibians (Röhlich et al., 1989) and teleost fishes (Vihtelic et al., 1999, Fuller et al., 2003) but this has never been attempted in the chondrichthyan retina to our knowledge.

Different species of chondrichthyans were collected based on their variable habitats i.e. from shallow coral reefs (two species of stingrays) to temperate demersal waters (one species of gummy shark and the elephant shark) to the deep-sea (the long-nose chimaera). The intensity and spectral composition of light varies with depth due to differential absorption and scattering of light within the water column (Jerlov and Nielsen, 1974, McFarland, 1986, McFarland, 1991, Jonasz and Fournier, 2011). Long wavelengths are known to attenuate more rapidly

than short wavelengths with increasing depth, so we predicted that shallow water species may retain long wavelength sensitivity within their cone photoreceptors for operating in photopic conditions, while the deep-sea species will have lost this ability, relying predominantly on rod-based scotopic vision.

Methods

This study was carried out in strict accordance with the guidelines of the *Australian Code of Practice for the Care and Use of Animals for Scientific Purposes* (7th Edition 2004). All efforts were made to minimize the suffering of the animals.

Bluespotted fantail rays, *Taeniura lymma*, (n=3, 27 to 29 cm DW) and bluespotted maskrays, *Neotrygon kuhlii*, (n=3, 37 to 43 cm DW) were collected in Ningaloo reef under WA fisheries permit (No. 1724-2010) and under the approval of the Murdoch University Animal Ethics Committee (License: #U6/2010-2011); and Fisheries Collection Permit (No.: #R2275/09). (see Chapter 5 for further details). Gummy sharks, *Mustelus antarcticus*, (see Chapter 3 for further details) and elephant shark, *Callorhynchus milii*, (n=3, 81 to 90 cm TL) were collected in Western Port Bay, Victoria under DEC Fisheries permit (P1041). Pacific spookfish, *Rhinochimaera pacifica*, were donated from a commercial fishing boat targeting orange roughy off the New Zealand coast. All the animals were euthanized with an overdose of tricaine methane sulfonate (MS222; 1:2,000 in seawater) or by severing the spinal cord according to the Ethical guidelines of the University of Western Australia (AEC RA/3/100/917).

Eyes were removed after making an incision in the ventral sclera for orientation and the cornea dissected away. The eye cup was fixed in 4% paraformaldehyde in 0.1 M sodium phosphate buffer (PB, pH 7.2-7.4)



and stored until transported to the lab. After a few weeks, the tissue was transferred to 0.1 M PB containing 1% sodium azide and stored at 4°C until required. The retinas were carefully dissected free of the eyecup and radial cuts made to flatten the retina and aid in the removal of the scleral and choroidal layers. One retina of each species was then divided into six smaller pieces for immunohistochemical analyses using one anti-long-wavelength-sensitive (LWS, CERN 956 provided by Prof. W. DeGrip) and three different anti-short-wavelength-sensitive antibodies; (SWS, CERN 933 provided by Prof. W. DeGrip) antibodies, SC-14363 SWS opsin antibodies (Santa Cruz Biotechnology Inc.) and anti-opsin antibody blue ab5407 (Millipore). Appropriate controls that excluded the primary antibody or the secondary antibody were applied with negative staining results.

No positive labelling was observed to the SWS-opsin antibodies in any of the five species examined. However, the retinas of three species (*C. milii*, *N. kuhlii* and *T. lymma*) showed positive labelling to the LWS antibody in wholemount. Retinal dissection and the preparation of retinal wholemounts has been described previously (see Chapter 3; Garza-Gisholt, et al., 2015) but each retina was placed flat on top of a plastic mesh with a plastic holder for easy manipulation (Figure 6.1). The mesh fitted the petri dish used for staining so the retina could be transferred between different solutions without damage, while keeping the retina flat and enabling easy immersion. Antigen retrieval was performed by incubating the retina in 0.2 M boric acid in 0.1 M phosphate buffer (PB) (pH 7.0) at 60°C for 30 minutes and then a solution of 10% methanol and 10% hydrogen peroxide solution in 0.1 PB (pH 7.4) for 20 minutes (Wilson et al., 2007). The isolated retina was then washed in a 5% Triton X-100 (Sigma) solution in 0.1 M PB (pH 7.4) (2 times for 5 minutes each) and one time for 20 minutes.



Figure 6.1 Petri dish set for change of solutions for the immunohistochemical protocol with the plastic mesh designed for handling the free floating retinal wholemounts.

After antigen retrieval, the retina was rinsed three times for 5 minutes each in 0.1 M phosphate buffer (pH=7.4) and in a solution containing the anti-LWS opsin primary antibody; 1:1000, CERN 956 raised in rabbit against the peptide of mammalian long-wavelength sensitive (LWS) cone pigment (generously provided by Prof. W. DeGrip, Radboud University Nijmegen), 5% normal donkey serum (Millipore) and 0.3% Triton X-100 in 0.1 M phosphate buffer (pH 7.4) overnight. The retina was then rinsed in 0.1 M PB (pH 7.4) three times for five minutes each. The retina was then incubated with biotin-SP-conjugated anti-rabbit secondary antibody (Jackson ImmunoResearch 711-065-152, 1:1000) with 0.3% Triton in 0.1 M PB (pH 7.4) for two hours. Then the retina was incubated for one hour in a solution of avidin-biotin complex (Vectastain ABC kit, Vector Laboratories). The retina was then rinsed in 0.1 M PB three times for five minutes before reacting with the chromogen VIP (Vector SK 4600 Purple) for three minutes or with DAB with nickel (Vector) for two minutes. Retinas were mounted photoreceptor side up on a gelatinized slide and allowed to dry at room temperature to attach to the slide, rehydrated and then dehydrated in an ascending alcohol series (50%, 70% and two 100% solutions). Slides were coverslipped with Entellan/New medium (Merck Millipore) and allowed to dry.



Assessment of the topographic distribution of labelled outer segments was conducted using a non-biased stereological method using a compound microscope fitted with a motorized stage and StereoInvestigator software (Microbrightfield, USA) (for details see, Garza-Gisholt et al 2015, Chapter 3). The average topographic maps were constructed using R (R Core Team, 2012) and the script described in Chapter 2 using the thin plate spline model (from the *sp* package using under-smoothing parameters; for details, see Garza-Gisholt et al. 2015, Chapter 2) and the averaging technique described in Chapter 3. Cones labelled with anti-LWS opsin antibodies were identified by the distinct labelling of their outer segments. Unlabelled cones were not easily discernible in the immunolabelled retinas because the chromogen labels the outer segments and it partially blocks the inner segment plane that is necessary to identify cones from rods. Instead, the average retinal maps of the total cones in the bluespotted stingrays, *N. kuhlii* and *T. lymma* from Chapter 5 and the average map of the total cones in the elephant shark, *C. milii*, from Chapter 4 were used to calculate the proportion of unlabelled cones. The total cones maps were overlapped with the immunolabelled cones map and the difference was plotted in a third topographic map assuming that the remaining cones have a different pigment identity.

Results

The anti-LWS cone-specific antibody labelled outer segments in the two species of stingrays, *Taeniura lymma* and *Neotrygon kuhlii* and the elephant shark, *Callorhinchus milii* (Figure 6.2). No positive labelling of LWS immunoreactive photoreceptors was observed for any of the other two species (the deep-sea chimaera, *Rhinochimaera pacifica* and the gummy shark, *Mustelus antarcticus*). The SWS cone-specific antibodies failed to label any photoreceptors in all five species of Chondrichthyes.

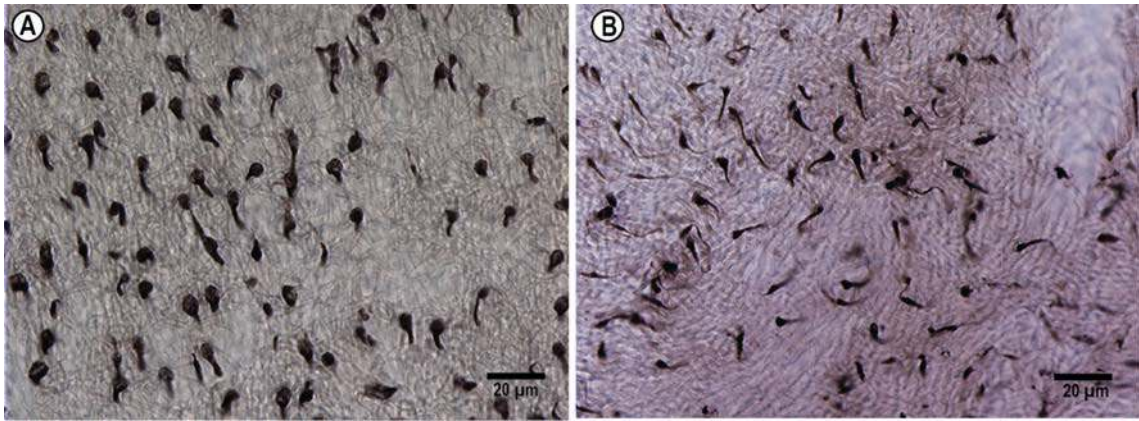


Figure 6.2 Light micrographs of the positive immunolabelling for LWS opsin in the outer segments of the retinal cones in wholmount using CERN 956 (1:1000 generously provided by Prof. W. DeGrip, Radboud University Nijmegen) and reacted with DAB with a nickel chromogen
 A) Bluespotted maskray, *Neotrygon kuhlii*. B). Bluespotted fantail ray, *Taeniura lymma*.

The elephant shark, *C. milii*, showed an elongated dorsal streak of LWS cones with a density of more than 2,000 cells mm^{-2} with a peak of 4,400 cells mm^{-2} slightly temporo-central (Figure 6.3B). The map of the calculated unlabelled cones showed two areas of more than 2,000 cells mm^{-2} in dorso-nasal and dorso-temporal retinal regions with a peak of 3,200 cells mm^{-2} (Figure 6.3C). The proportion of LWS cones compared to the total cone population (based on the larger axial diameter of the unlabelled cones) was estimated to be 72% (Table 6-1).

The bluespotted fantail ray, *T. lymma* (Figure 6.3A), showed a wide, dorsal streak of LWS cones with an elongated zone of more than 4,000 cells mm^{-2} reaching a peak of 5,700 cells mm^{-2} in temporal retina. The map of the calculated unlabelled cones showed a high density area in the dorso-nasal region with a density of more than 4,000 cells mm^{-2} and reaching a peak of 5,900 cells mm^{-2} in temporal retina (Figure 6.3C). The proportion of LWS cones compared to the total cone population was similar to *C. milii* at 73% (Table 6-1)(Figure 6.3E). The bluespotted maskray, *N. kuhlii*, showed a discontinuous dorsal streak with a density of LWS cones of more than 6,000 cells mm^{-2} reaching a peak of 7,100 cells mm^{-2} (Figure 6.3H). The map of the unlabelled cones showed three smaller acute zones in the dorsal region of the retina reaching a peak of



2,500 cells mm^{-2} (Figure 6.3I). The percentage of LWS cones as a proportion of the total cone population was 93%

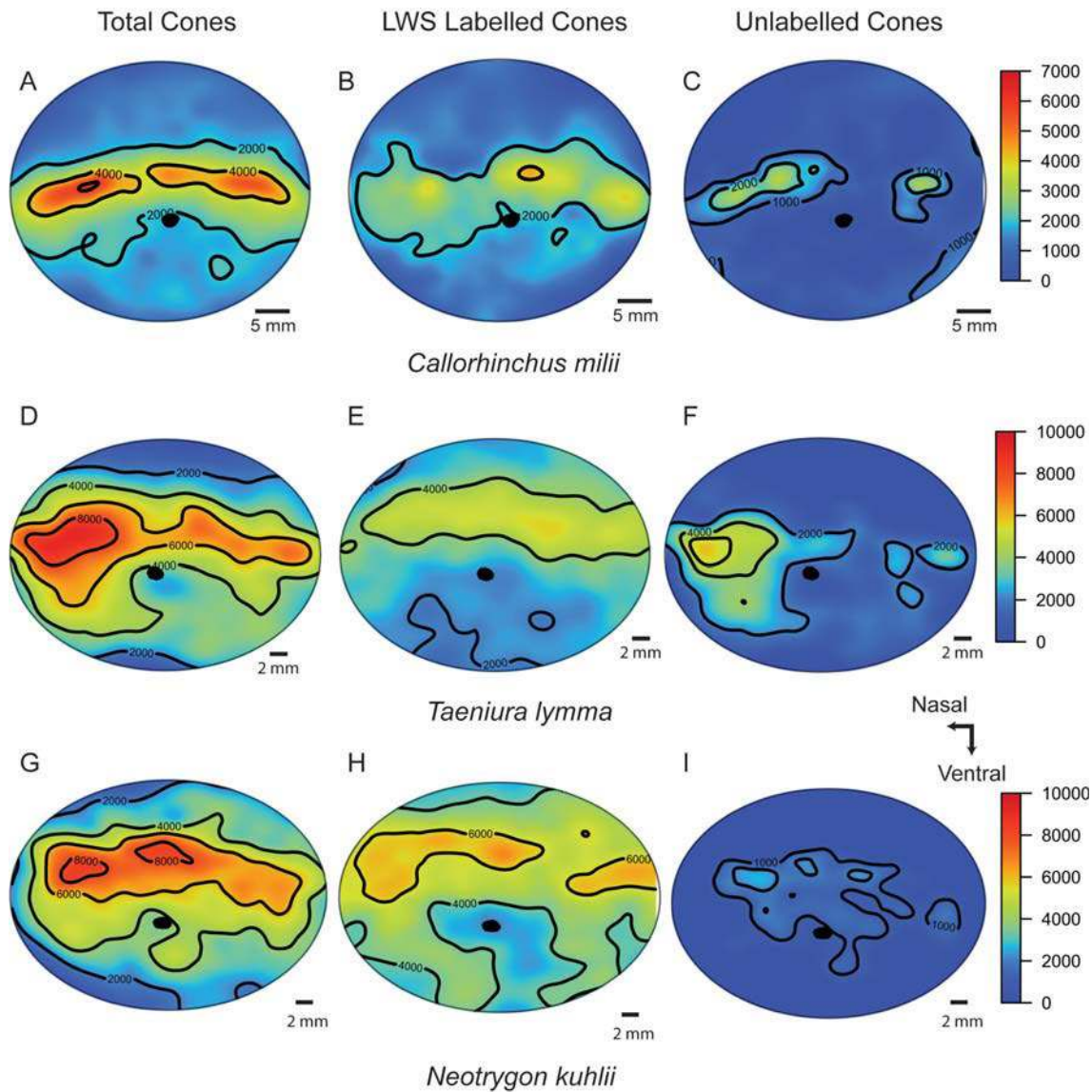


Figure 6.3 Average topographic density maps of the cone distribution in the three species that showed LWS antibody labelling. A) Total cone distribution in *Callorhinchus milii* (Chapter 3 Garza-Gisholt et al 2015). B) Total LWS labelled cone distribution in *Callorhinchus milii*. C). Distribution of unlabelled cones (total minus LWS immunoreactive) in *Callorhinchus milii*. D) Total cone distribution in *Taeniura lymma* (Chapter 4 Garza-Gisholt et al 2015). E) Total LWS labelled cone distribution in *Taeniura lymma*. F). *Taeniura lymma* difference of the total cones to the LWS labelled cones. G) Total cone distribution in *Neotrygon kuhlii* (Chapter 4 Garza-Gisholt et al 2015). H) Total LWS labelled cone distribution in *Neotrygon kuhlii*. I). Distribution of unlabelled cones (total minus LWS immunoreactive) in *Neotrygon kuhlii*.

Table 6-1. Size, depth range and cone photoreceptor data for three species with positive immunoreactivity to the LWS antibody: *Callorhynchus milii*, *Taeniura lymma* and *Neotrygon kuhlii* for each species. Size in *C. milii* is total length, while size in *N. kuhlii* and *T. lymma* is disc width. Depths obtained from Last and Stevens (2009).

Species	<i>Callorhynchus milii</i>	<i>Taeniura lymma</i>	<i>Neotrygon kuhlii</i>
Common name	Elephant Shark	Bluespotted Fantail Ray	Bluespotted Maskray
Size (cm)	81-90	27-29	37-44
Depth range (m)	0-200	0-20	0-90
Peak total cones (cells mm ⁻²)	6,177	9,258	8,558
Peak LWS cones (cells mm ⁻²)	4,479	5,705	7,097
Peak unlabelled cones (cells mm ⁻²)	3,205	5,978	2,553
Percentage LWS cones	71.88	72.97	93.14
Percentage unlabelled cones	28.12	27.03	6.86

Discussion

This study is the first to show specific immunoreactivity to any cone visual pigment in retinal photoreceptors in the Class Chondrichthyes. CERN 956 is an antibody raised against a peptide fragment from the human LWS cone. It has specificity for LWS cone pigment in non-mammalian species such as chicken, lizard and salamander but it has never been tested in cartilaginous fishes (Vissers and DeGrip, 1996, Sherry et al., 1998). The positive labelling of a subpopulation of photoreceptors using this antibody raised in mammals reveals the conservative nature of at least the LWS opsins in vertebrates (Collin et al., 2009).



The two species of stingrays and the elephant shark showed specific antibody labelling for the LWS visual pigment, which appeared to be restricted to retinal cones, revealing the existence of at least two types of cone photoreceptors (based on the presence of a proportion of unlabelled cone photoreceptors). However, the proportion of LWS cones and unlabelled cones varied between these three species.

The bluespotted maskray, *Neotrygon kuhlii* possesses a high proportion of LWS cones compared to the bluespotted fantail ray (93% to 73%) and the peak density of unlabelled cones is higher in the fantail than in the maskray (6,000 to 2,500 cells mm⁻²), suggesting that *N. kuhlii* might rely more on longer wavelength light than *T. lymma*. An increased dependence on long wavelengths of light may be related to the use of a different sub-habitat or differences in the timing of peak activity periods. One previous microspectrophotometric study on the bluespotted maskray reveals three visual pigments with peak spectral sensitivities (λ_{\max} values) at 476, 498 and 552 nm (Theiss et al., 2007). It is likely that the anti-LWS antibody used in this study labels at least the cones containing the 552nm pigment in *N. kuhlii*, although the opsin genes expressed within the retina of this species have been cloned only partially presenting an alignment to LWS and Rh1 vertebrate opsins (Lisney, 2004). The high proportion of cones labelled by the LWS antibody (93%) correlates to the light environment where these species live, i.e. shallow water, bright light coral reef environments rich in all wavelengths of the visible spectrum including long wavelengths (red). The dorsal increase in the density of LWS cones (streak) also indicates that long wavelength sensitivity directed towards the substrate may be an ecological adaptation for prey capture and predator avoidance (Logiudice and Laird, 1994, Bozzano and Collin, 2000, Theiss et al., 2007). In contrast, the bluespotted fantail ray, *Taeniura lymma*, shows a lower proportion of LWS cones (73%). The position and magnitude of the specialization is also different between the two species of stingrays; *T.*

lymma has fewer LWS cones in the dorsal streak (4,000 cells mm⁻²) compared to the *N. kuhlii* (6,000 cells mm⁻²) and a higher proportion of unidentified cones in the nasal position (4,000 cells mm⁻² and <1,000 cells mm⁻², respectively). The nasal region of the retina receives light from behind the animal, and, as such, is perhaps an important specialisation for detecting predators in eccentric visual space. The difference in the proportion of LWS cones between the two species of ray also aligns with the difference of their microhabitats. *T. lymma* has been observed to migrate into open areas at high tide in search of benthic prey, retreating at low tide to rest in caves and under coral overhangs (Jonna, 2003, Last and Stevens, 2009). The lower proportion of LWS cones may reflect this species propensity to spend long periods of time in shaded areas, which are richer in shorter wavelengths (Marshall et al., 2003). On the other hand, *N. kuhlii*, which feeds at high tide but remains in open areas at low tide, preferring to bury itself to avoid predation, may require more LWS cones.

The elephant shark *Callorhinchus milii* showed a high proportion of unlabelled cones (28%) that is consistent with its migratory habits of moving into shallow water to reproduce, although it can live up to 200 meters in depth. Three cone pigments have been identified in the elephant shark from molecular expression studies that revealed a LWS1 (499 nm λ_{\max}), a LWS2 (548 nm λ_{\max}) and a Rh2 (442 nm λ_{\max}) visual pigment in addition to a rod pigment (Davies et al., 2009). According to Davies et al (2009), the LWS1 and LWS2 opsin genes share 77% of their nucleotides and 79% of their amino acids, so the LWS antibody used in this study would probably label both types of pigments, expressed in two morphological types of cone photoreceptors. If this is the case, the unlabelled cone population might represent the cones expressing the Rh2 pigment. The light intensity of the habitat of *C. milii* varies markedly since it is predominantly a deep-sea species but migrates to shallow estuaries to reproduce. In the dim light environment of the deep-sea, vision will be rod dominated, therefore the three different cone



pigments will only operate as this species moves into shallower, brightly lit water, where colour vision will provide a selective advantage for finding mates and feeding within a photic environment. This level of adaptation may extend to the young hatchlings (elephant sharks are oviparous), where the newborn pups lack any parental care, (Wourms, 1977, Last and Stevens, 2009). Further analysis on the eyes of juvenile specimens might reveal if they migrate to deep water to grow and eventually reproduce but this may be difficult since there is very little information on where the hatchlings aggregate.

Long wavelengths are absorbed rapidly in the water column with increasing depth and most deep-sea species possess pure-rod retinas for scotopic vision. It was therefore expected that the retinas of the purely deep-sea chimaera, *Rhinochimaera pacifica* and the gummy shark, *Mustelus antarcticus* (both demersal species) would not possess any LWS immunoreactive cones. *R. pacifica* possesses a rod-only retina based on morphological criteria (see Chapter 3 Garza-Gisholt et al 2015) but the gummy shark was found to possess a duplex retina containing both cones and rods (Chapter 2 Garza-Gisholt, et al 2015). Based on the lack of immunoreactivity to both the LWS and SWS opsin antibodies, the unlabelled population of cones in the gummy shark may contain a Rh2 visual pigment.

The SWS1 and SWS2 cone visual pigments are sensitive within the ultraviolet and violet regions of the spectrum and have been confirmed to be present in most classes of vertebrates (Takahashi et al., 2001, Collin et al., 2009, Hunt et al., 2009, Hunt and Peichl, 2013). However, this study reveals that these short wavelength-sensitive pigments may be absent in the chondrichthyan retina (although there is the possibility that the antibodies used were not class-specific enough to yield positive labelling) (Hart et al., 2004, Theiss et al., 2007, Hunt and Peichl, 2013) as is the case for a number of marine mammals (Peichl et al., 2001,

Levenson and Dizon, 2003, Newman and Robinson, 2005). Further research is required to confirm these findings at the molecular level and explore whether more than one visual pigment may be expressed within a single photoreceptor type (co-expression), as has been confirmed in mammals (Röhlich et al., 1994, Szél et al., 1998, Peichl et al., 2004, Lukats et al., 2005) .

Acknowledgements

We are sincerely thankful to William De Grip for generously providing the opsin antibodies. We also are thankful to Joao Paulo Coimbra and Caroline Kerr for all their invaluable assistance. This research was supported by an Australian Research Council Discovery Project Grant (DP110103294) to SPC, NSH, and others; and the Western Australian State Government (to SPC). This research was also supported by the Sea World Research and Rescue Foundation (SWR/3/2012) to SPC, NSH and EGG. EGG was supported by a Mexican scholarship for Postgraduate studies (CONACyT) and an Ad-Hoc Top-Up Scholarship from The University of Western Australia.

**Chapter 7 The morphology of the pineal organ in Chondrichthyes:
a comparison between the elephant shark (*Callorhinchus milii*:
Holocephali) and the bluespotted maskray (*Neotrygon kuhlii*:
Elasmobranchii)**

Garza-Gisholt, E., Hart, N.S. and Collin, S.P.

School of Animal Biology and The UWA Oceans Institute, The University of Western Australia, Crawley, 6009 W.A.

Abstract

The morphology of the pineal organ was compared between two species of cartilaginous fish: the elephant shark, *Callorhinchus milii* (Holocephali) and the bluespotted maskray, *Neotrygon kuhlii* (Elasmobranchii) using light microscopy. Both species possess a prominent pineal organ. In *C. milii*, the pineal vesicle lies within a deep recess in the ventral surface of the dorsal chondrocranium, whereas in *N. kuhlii* the pineal sits in a shallow v-shaped superficial fissure. These differences in pineal pit morphology are probably related to the relative thickness of the chondrocranium, which is much thicker in *C. milii* than *N. kuhlii*. *C. milii* also has a patch of skin above the pineal that is devoid of pigmentation and probably acts as a pineal 'window' to let more light penetrate to the pineal photoreceptors. In contrast, the location of the pineal in *N. kuhlii* is not apparent from external examination. The pineal vesicle is stratified into two layers of photoreceptors and support cells in the pineal parenchyma and the neural layer with bipolar and ganglion cells in both species. The pineal lumen in *C. milii* is larger and the walls are more convoluted than in *N. kuhlii*, thereby providing a means to increase the overall number of rod-like photoreceptors that line the entire lumen. The photoreceptors in



N. kuhlii have a more cone-like shape and the outer segments are not continuous in the lumen of the vesicle. The difference in habitat may directly affect the morphology of the pineal organ, where *C. milii* migrates from deeper waters to reproduce in estuaries, thereby requiring a more sensitive pineal with an increased photoreceptor surface, a clear pineal window and rod-like photoreceptors. In contrast, *N. kuhlii* lives in bright light conditions year round in temperate water sand flats and coral reef areas, where the lack of a pineal window, fewer photoreceptors and cone-shaped photoreceptors may represent an adaptation for life in higher light conditions.

Keywords

Pineal gland; epiphysis; light detection; pineal stalk; *Neotrygon kuhlii*; *Callorhinchus milii*; Chondrichthyes

Introduction

Light detection in many vertebrates is mediated via image-forming structures such as the eye and also non-imaging structures such as the pineal organ (epiphysis), the epithalamus and the anterior hypothalamus (Philp et al., 2000, Vigh et al., 2002). The pineal organ is a photoreceptive structure part of the epithalamus located dorsal of the telencephalon and connected to the diencephalon via a stalk (Mandado et al., 2001, Vigh et al., 2002) and is responsible for regulating a range of homeostatic functions and behaviours in most vertebrates, although its photoreceptive function is diminished in mammals. The pineal organ has a dual function: it is responsible for the initial phototransduction of light energy and subsequent transmission of neural signals to other parts of the central nervous system in addition to hormonal regulation via the production of melatonin. Melatonin is responsible for regulating the circadian rhythms in many species of vertebrates that have a daily cycle of hormonal production (Fenwick, 1970, Cassone, 1990).

Previous studies have described the pineal organ in different species of Chondrichthyes. In 1919, Tilney and Warren reviewed the available knowledge of the pineal complex in elasmobranchs and compared this to cyclostomes (Agnatha) and bony fishes (Teleostei) and noted the absence of the parapineal in elasmobranchs for the first time. The pineal organ was described as a projection extending from the roof of the interbrain terminating in the surface of the skull. Later, Rudeberg (1968, 1969) described the ultrastructure of the pineal in the small spotted catshark, *Scyliorhinus canicula*, and revealed the presence of receptor cells in the pineal vesicle with a cone-like shape, irregularly-developed outer segments and support cells with characteristically high concentrations of smooth endoplasmic reticulum. Molecular studies by Hamasaki and Streck (1971) analysed the photopigment housed within the pineal photoreceptors of *S. canicula* and found, despite the cone-like appearance of the photoreceptors, that the photopigment was a rhodopsin (Rh1) with a similar spectral sensitivity to the rhodopsin found in the retina (λ_{max} of 500 nm). Immunohistochemical studies to identify the opsin protein in the rabbit fish, *Chimaera monstrosa* using antigen-photoexcited and phosphorylated rhodopsin was positive in the pineal gland and retina (Vigh-Teichmann et al., 1990, Vigh et al., 2002).

Tract tracing techniques have been used to follow the neural pathways from the output cells in the pineal (ganglion cells) to their targets in the brain of a few species of elasmobranchs. The pineal projections to the CNS of the small spotted catshark, *S. canicula* and the skate, *Raja montagui*, were traced using the carbocyanine dye Dil and revealed a multitude of targets within the midbrain (Mandado et al., 2001). Immunohistochemistry also revealed strong immunoreactivity to choline acetyltransferase (ChAT) in the photoreceptors of the pineal gland (Anadon et al., 2000) and rich GABAergic innervation in the pineal organ (Carrera et al., 2006) in *S. canicula*. The hormonal output of the pineal organ has been studied in different species of Chondrichthyes



specifically for the production of melatonin (Demski, 1991, Vernadakis et al., 1998, Davies et al., 2012). The behaviour and change of colouration in the small spotted catshark, *S. canicula*, was also analysed after removing the pineal gland by pinealectomy (Wilson and Dodd, 1973).

This study represents the first morphological description and comparison of the pineal organ of a migratory species of chondrichthian—the elephant shark, *Callorhinchus milii*, which migrates from its deep-sea habitat to shallow water estuaries to reproduce in autumn and a sedentary species, the bluespotted maskray, *Neotrygon kuhlii*, which inhabits shallow water coral reefs and sand flats year round. The aim of this study was to investigate the morphological differences in the pineal organ between the two species. These differences might reveal some clues as to the role that the pineal gland plays in triggering the migration for reproduction. The morphology of the pineal organ in each species, as with the remainder of the CNS, is found to differ markedly, reflecting both environmental and phylogenetic variation.

Methods

Bluespotted maskrays, *Neotrygon kuhlii*, (2 adults, 35 and 43 cm disc width, DW) were collected in 2010 from Ningaloo reef in north Western Australia under WA Fisheries permit (No. 1724-2010) as part of a large age, diet and growth study (O'Shea et al., 2013); material was acquired for this study to maximise the use of tissue. The animals were euthanized in the field by severing the spinal cord following the protocol approved by the Murdoch University Animal Ethics Committee (License: #U6/2010-2011); Fisheries Collection Permit (No.: #R2275/09). Elephant sharks, *Callorhinchus milii*, (2 adults, 69 and 90 cm total length, TL) were collected during May, 2011 from Western Port Bay, Victoria under the Department of Fisheries Permit (RP 1041) and

transported to the Department of Primary Industries facilities in Queenscliff, Victoria. The animals were euthanized using an overdose of tricaine methanesulfonate salt (MS222) according to the protocol approved for the University of Western Australia Animal Ethics Committee (RA/3/100/917).

After euthanasia, the head of the animals was severed and the brain was ventrally exposed by removing the skin, connective tissue and cartilage from the skull using a scalpel blade. The head was immersed in fixative for a couple of weeks until transport to the laboratory, where the heads were transferred to 0.1 M phosphate buffer (pH 7.2-7.4) with 0.1% sodium azide (as an antifungal/antibacterial agent) until dissection and processing. Half of the heads were preserved in 4% paraformaldehyde in 0.1 M phosphate buffer (pH 7.2-7.4) for the proposed immunohistochemical analyses and the other half of the heads were fixed in 2.5% glutaraldehyde and 2% paraformaldehyde in 0.1 M cacodylate buffer (pH 7.2-7.4) for future ultrastructural studies using electron microscopy.

In order to expose the pineal gland, all the cartilage of the braincase was removed from the ventral and lateral regions first, followed finally by the removal of the dorsal cartilage, being careful to keep the pineal vesicle and the pineal stalk still attached to the skull. This approach was effective but time consuming. Therefore, after the first few individuals and the correct location of the pineal was identified for each species, only the top of the skull was removed. The pineal gland is difficult to locate within the infolding of the cartilage that forms the cavity where the pineal sits. On some occasions, an aqueous solution of 1% Toluidine blue was administered to the area for a few seconds and then washed clear with 0.1 M phosphate buffer to increase the contrast of the pineal vesicle and its associated stalk.



In order to isolate the pineal for morphological examination, the skin and the connective tissue were removed and the cartilage was trimmed around the pineal to leave a small block of about 2 mm X 2 mm. The cartilage immediately surrounding the pineal cavity was left intact in order to identify any possible invagination of pineal tissue within the cartilage. The tissue was post-fixed on a shaking table in 1% osmium tetroxide in 0.15 M phosphate buffer (PB, pH 7.4) for two hours. Then, the tissue was washed in 0.1 M PB (pH 7.4) (3 x 5 minutes each). The tissue was embedded in araldite by dehydrating through a series of alcohols (20%, 40%, 60%, 80% and 100% ethanol; 100% pure grade ethanol twice and 100% propylene oxide) for 30 minutes each and then infiltrated with a series of epoxy resins (25% for 1 hour, 50% for 2 hours and 100% (x3) for 2 hours followed by araldite in propylene oxide) and finally embedded in pure araldite overnight at 60°C. Using a microtome (LKB Bromma Ultratome Nova), transverse sections (1µm in thickness) were cut and mounted on a glass slide, stained using an aqueous solution of 1% Toluidine blue and coverslipped using Entellan (Merck Millipore). Stained sections were photographed using an Olympus DP70 Camera mounted on an Olympus BX50 compound microscope using 10X, 40X and 100X objectives. The brightness and contrast of the micrographs were edited using Adobe Photoshop CS5 and measurements were obtained using Image J open access software (Schneider et al., 2012).

Results

The pineal organ of the two species is comprised of a pineal bulb vesicle located in the dorsal part of the brain and a pineal stalk that connects the vesicle to the brain. The pineal vesicle is located at the end of a long, thin, tubular stalk adjacent to the inner surface of the skull, with its long axis oriented approximately parallel to the rostral-caudal axis of the animal (Figure 7.1). The proximal part of the pineal stalk is attached at the juncture of the optic tectum (mesencephalon) and the forebrain

(diencephalon) and extends into the cranial roof. When the top of the skull is removed, the pineal stalk often detaches from the brain, which may account for the paucity of information of this organ in this class of vertebrates.

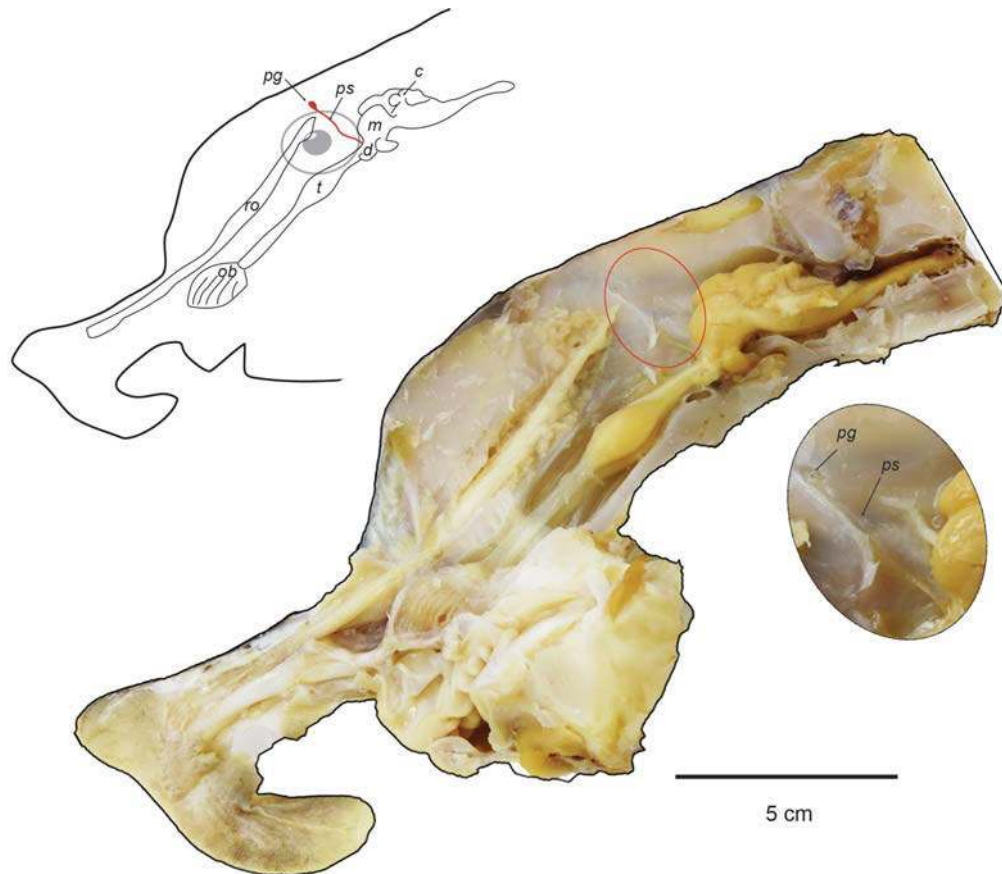


Figure 7.1 Position of the pineal gland in the brain of the elephant shark, *Callorhynchus milii*. Detail of the attachment of the pineal gland between the mesencephalon and the diencephalon. *pg* pineal gland, *ps* pineal stalk, *c* cerebellum, *m* mesencephalon, *d* diencephalon, *t* telencephalon, *ob* olfactory bulb, *ro* ramus ophthalmicus.

The position of the pineal organ in the bluespotted maskray, *Neotrygon kuhlii* is difficult to see since the underlying cartilage and skin is homogenous in colour, while the location of the pineal organ in the elephant shark, *Callorhynchus milii* is more easily identified since the skin overlying the part of the chondrocranium containing the pineal



organ lacks the silver coloration of the rest of the head. This clear patch creates a pineal window characteristic of *C. milii*. The portion of the chondrocranium that protects the pineal vesicle also has a different shape and thickness between the two species. The skull of *N. kuhlii* has a v-shaped cleft in the cartilage forming a pineal notch that is less than one third of the thickness of the adjacent cartilage (Figure 7.2). In contrast, the skull of *C. milii* forms a cavity, where the pineal vesicle sits completely within the depression. The skull thickness adjacent to the pineal pit in *C. milii* is 4.5 mm compared to 0.7 mm in *N. kuhlii*; the thickness of the cartilage overlying the pineal in *C. milii* is 0.6 mm, compared to 0.2 mm in *N. kuhlii* (Table 7-1).

Table 7-1. Measurements of the pineal gland, pineal stalk and cartilage thickness in the two species of Chondrichthyes, the bluespotted maskray *Netorygon kuhlii* and the elephant shark, *Callorhinchus milii*. The pineal and lumen measurements were taken in the largest section of the pineal and represent the maximum values.

	<i>Callorhinchus milii</i>	<i>Netorygon kuhlii</i>
Pineal width (μm)	626.67	407.15
Pineal height (μm)	417.49	210.70
Lumen width (μm)	491.17	317.13
Lumen height (μm)	236.94	92.09
Stalk width (μm)	571.5	140
Cartilage thickness adjacent (μm)	4472.97	681.86
Cartilage thickness above the pineal (μm)	586.31	234.62

The pineal stalk is a thin tubular structure composed of nerve fibers (ganglion cell axons) that connects the pineal vesicle to the roof of the diencephalon with a continuous lumen that is thinner in *N. kuhlii* compared to *C. milii* (140 to 371 μm , respectively). The pineal vesicle is smaller and more dorso-ventrally flattened in the bluespotted maskray, *N. kuhlii*, than the elephant shark, *C. milii* (407 to 626 μm diameter, respectively). In *C. milii*, the lumen of the pineal gland at its widest point

is more convoluted and free of debris. On the other hand, the lumen surface in *N. kuhlii* is almost flat and the lumen contains more debris that may represent an aggregation of biological products of the pineal such as melatonin, macrophage cells or detached outer segments. Close to the distal end of the gland, the lumen is convoluted in both species.

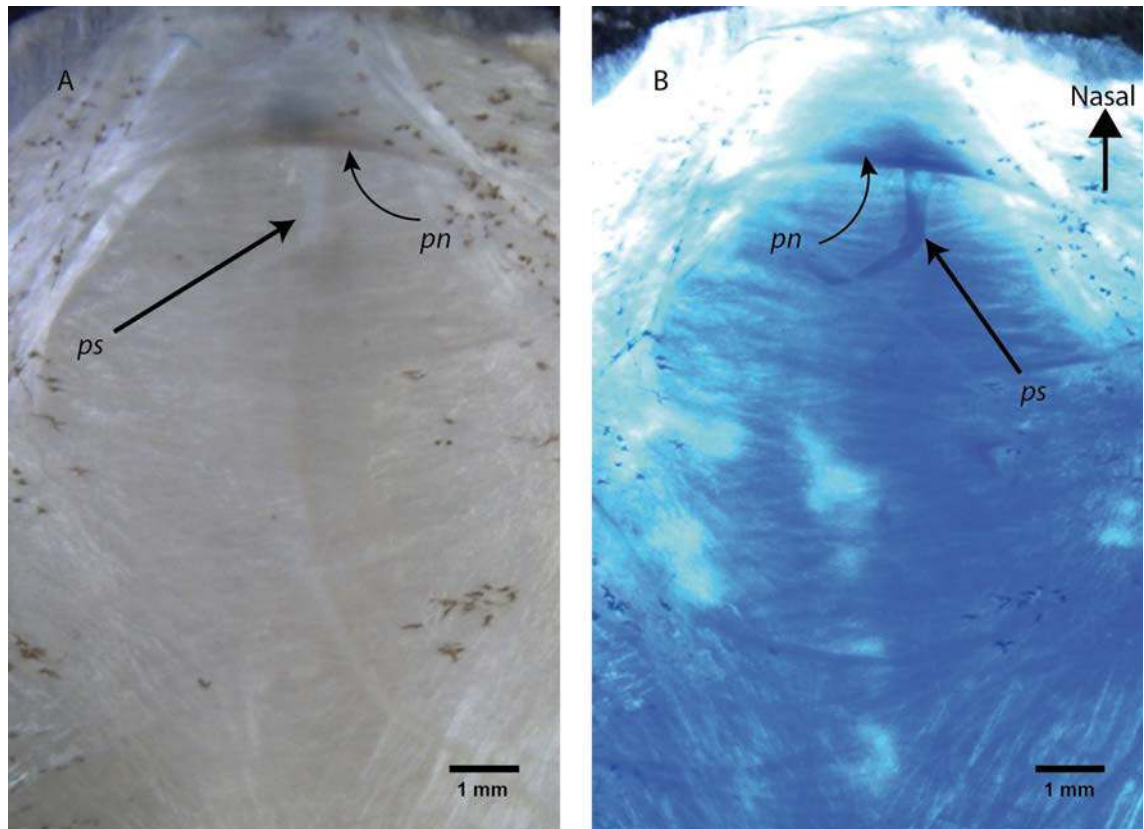


Figure 7.2 Position of the pineal gland in the ventral portion of the cartilage in the skull of the bluespotted maskray, *Neotrygon kuhlii* (Male, 35 cm DW). A). Pineal fissure and pineal stalk in unstained sample. B). Pineal fissure and pineal stalk after 10 seconds staining in Toluidine blue. *ps* pineal stalk, *pn* pineal notch.

The cellular morphology of the pineal gland of both species shows a laminated structure of at least two cell layers (Figures 7.3A and C). The inner layer that opposes the lumen—also referred as the pineal parenchyma—is composed by photoreceptor-like cells and support cells. The photoreceptor cells in *C. milii* appear more abundant with cylindrical and relatively larger outer segments resembling retinal rods lining the lumen and elongated inner segments (Figure 7.3B). In contrast, the photoreceptor cells in *N. kuhlii* occur in patches and



appear smaller with a slight tapering of the outer segments resembling retinal cones and thicker inner segments (Figure 7.3D). The photoreceptor cells are surrounded by elongated support cells, which appear as darkly-stained, elongated cells adjacent to the photoreceptors that do not protrude into the lumen of the pineal. Beneath the layer of photoreceptor nuclei, there is a fibrous zone that contains bipolar cells, which are obvious in *N. kuhlii* but less distinct in *C. milii* and presumably ganglion cells, but these are not evident in the light micrographs. The pineal vesicle is surrounded by an area of connective tissue that contains a bed of capillaries that never enters the gland (Figure 7.3).

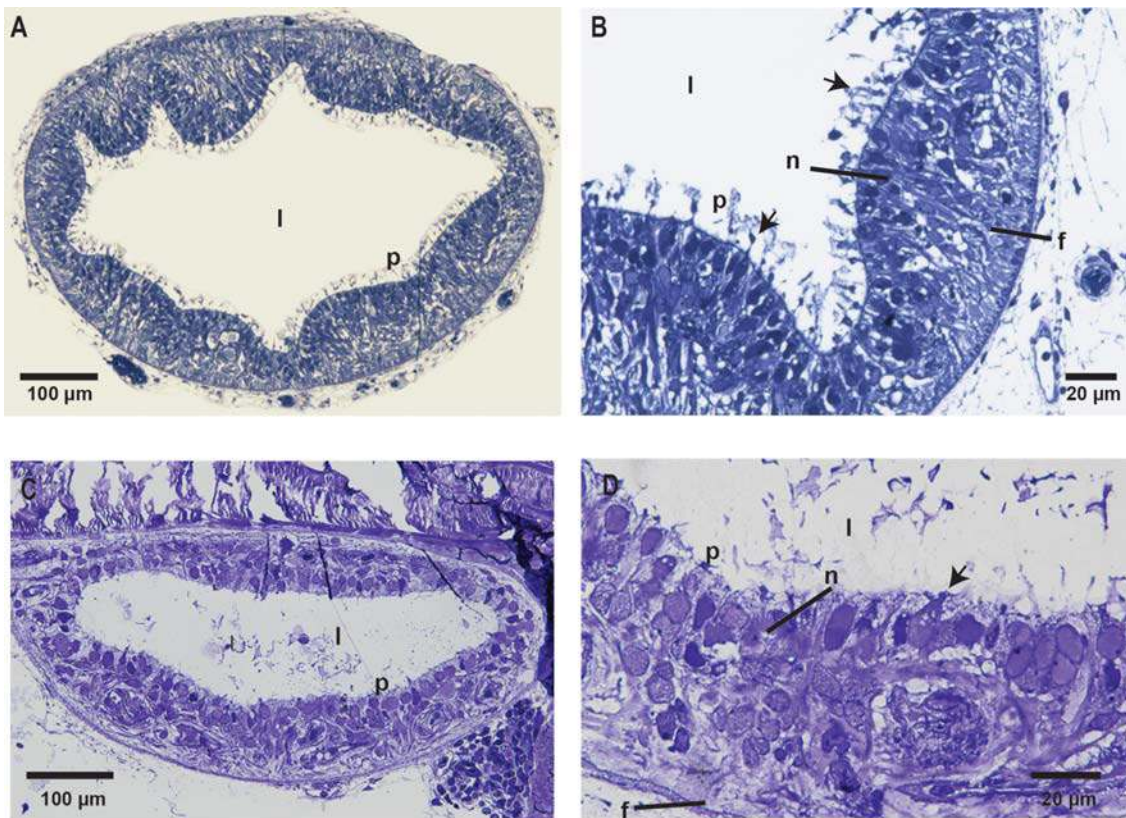


Figure 7.3 Light micrographs of the pineal gland in a 2 μm thick transverse section of the pineal gland A) Elephant shark, *C. milii* at low magnification. B). Elephant shark, *C. milii* at high magnification. C) Bluespotted maskray, *N. kuhlii* at low magnification. D) Bluespotted maskray, *N. kuhlii* at high magnification. *l* lumen, *p* photoreceptor, *n* nuclear layer, *f* fiber layer. The arrows indicate the position of photoreceptor outer segments.

Discussion

The morphology of the vesicle at the end of the pineal stalk was similar in both species. The migratory elephant shark, *C. milii* (0 - 200 m depth range), possesses a larger pineal vesicle with a more convoluted lumen, thereby increasing the surface area and potentially supporting a larger number of photoreceptors, a specialization that could increase sensitivity. The shape of the photoreceptors also suggests they are more rod-like and therefore may be more sensitive to light, which would penetrate the skin through the clear pineal window. In contrast, the shallow water maskray, *N. kuhlii* (depth range 0-90 m), which inhabits coral reef areas and estuaries, possesses a smaller pineal gland with a less-convoluted lumen supporting a lower number of cone-like photoreceptors. The skin overlying the cranium in *N. kuhlii* has the same colouration as the rest of the head, and therefore lacks a pineal window (although transmission was not measured formally in this study), reflecting the higher ambient light intensities where this species lives.

The roof of the skull in Chondrichthyes varies markedly between the Holocephali (chimaeras) and the Elasmobranchii (sharks and rays) (Schultze, 1993). Based on early studies, a portion of the roof of the skull in selachians (sharks) is unchondrified forming a “prefrontal epiphysial fontanelle or “fenestra praecerebralis” (Allis, 1923), which appears similar to the pineal notch found in the bluespotted maskray, *N. kuhlii* (Batoidea). Additionally, some studies have noticed that the infolding in the roof plate might be more conspicuous in some selachians such as the six gill shark *Hexanchus* genus (= *Notidianus*) (Tilney and Warren, 1919). In contrast, the pineal cavity in the elephant shark, *C. milii* has previously been described as a pineal foramen that is different to the original epiphysial fontanelle thought to divide and



protect the ethmoidal canal in the nasal capsule (De Beer and Moy-Thomas, 1935, Smeets, 1998).

The pineal complex has been described for several chondrichthyans and has consistently been found to comprise a pineal vesicle supported by a pineal stalk and the two species examined here do not deviate from this arrangement (Tilney and Warren, 1919, Rudeberg, 1968, Rudeberg, 1969, Gruber et al., 1975b). However, a different morphology is found in other vertebrate classes i.e. lampreys and bony fishes, which also possess a parapineal structure (Vigh et al., 2002).

The photoreceptors in the pineal of the small-spotted catshark, *Scyliorhinus canicula* were described as cone-shaped with irregularly-developed outer segments projecting into the lumen (Rudeberg, 1968, Rudeberg, 1969) and appear to be more similar to the photoreceptors found in *N. kuhlii*. Rod-shaped pineal photoreceptors have been described in the deep-sea chimaera, *Chimaera monstrosa* (Vigh-Teichmann et al., 1990) that resemble more closely the photoreceptors observed in *C. milii*. Support cells rich in smooth endoplasmic reticulum have also been characterized using electron microscopy in *S. canicula* (Rudeberg, 1969). Using light stimulation of the pineal, Hamasaki and Streck (1971) revealed that the pineal organ in *S. canicula* shows a similar photosensitivity to the retina, where light is able to penetrate the skin and overlying cartilage to stimulate the photoreceptors lining the pineal lumen (Hamasaki and Streck, 1971, Gruber et al., 1975b, Meissl and Yañez, 1994). Signals generated at the level of the photoreceptors are conveyed to the ganglion cells via multipolar or bipolar cells that terminate on dendrites via synaptic contacts (Vigh et al., 2002). Differences in the staining patterns of neurons in *C. milii* and *N. kuhlii*, as observed by Toluidine blue staining in semi-thin resin sections, suggest there may be at least two types of photoreceptors, as revealed immunohistochemically by Vigh-Teichmann et al. (1990).

Further study is required to characterise the spectral identity of the pineal photoreceptors based on immunohistochemical methods (Vigh-Teichmann et al., 1983a, Vigh-Teichmann et al., 1983b, Vigh-Teichmann et al., 1990), peak absorption sensitivity using microspectrophotometry (Kusmic et al., 1993, Bowmaker and Wagner, 2004) and visual pigment (opsin) complement (Forsell et al., 2001, Philp et al., 2000). Moreover, *in situ* hybridization can be used to integrate molecular and morphological studies to better understand the function of the pineal in this class of vertebrate. The influences of the pineal input to other neural systems (and ultimately behaviour) can also be revealed by tracing the projections of the pineal complex to other parts of the CNS as previously examined in *S. canicula* (Mandado et al., 2001, Carrera et al., 2006). Therefore, there is still much to be done with respect to understanding the influence(s) of light (intensity and spectral composition) on circadian rhythms and the production of melatonin in this group. The influences of the pineal on melatonin and reproductive hormones are also likely to affect sexual development, which, in turn, is affected by environmental conditions (Wilson and Dodd, 1973, Demski, 1991, Morgan et al., 1994, Vernadakis et al., 1998). We hope this study stimulates further investigations on the pineal complex in chondrichthyans, including the critical environmental cues that govern the setting of circadian rhythms in both deep and shallow water.



Acknowledgements

We are sincerely thankful to Rachael Warrington, Carlos Salas, Jessica Leask, Michael Archer and Caroline Kerr for all their invaluable help in the lab. This research was supported by an Australian Research Council Discovery Project Grant (DP110103294) to SPC, NSH, and others; and the Western Australian State Government (to SPC). This research was also supported by the Sea World Research and Rescue Foundation (SWR/3/2012) to SPC, NSH and EGG. EGG was supported by the Mexican scholarship for Postgraduate studies (CONACyT) and the Ad-Hoc Top-Up Scholarship by the University of Western Australia.

Chapter 8 General Discussion

Visual neuroecology represents the integration of the morphological and physiological characteristics of the visual system with the ecology and behaviour of a species. The different species studied in this thesis represent the two groups of Chondrichthyes (Elasmobranchii: selachians and batoideans; and Holocephali: chimaeras). The species analysed display visual specializations according to the habitat where they live; if the light is scarce in deep water then the species tend to have adaptations for higher sensitivity, such as a rod-only retina, longer photoreceptor outer segments, the presence of a *tapetum lucidum* and lower resolution. In contrast, species that live in shallow water have a duplex retina with cones and rods, higher spatial resolving power, multiple types of cones and, therefore, the potential colour discrimination.

The topographic distribution of photoreceptor (rods and cones) and ganglion cells reveals a mild dorsal streak or specialization that is commonly found in Chondrichthyes species (Collin, 1988, Bozzano and Collin, 2000, Lisney and Collin, 2008, Schieber et al., 2012). The dorsal streak arrangement permits the animal to efficiently sample the visual horizon to detect predators, possible prey items and for social interactions (Hughes and Whitteridge, 1973, Collin and Shand, 2003). Other groups of aquatic vertebrates possess a higher variability in retinal specializations. Multiple studies have demonstrated a high level of retinal variability with different types of streaks (dorsal, ventral, peripheral), *areae centrales* and even multiple *areae* in different retinal regions i.e. in teleosts (Collin and Pettigrew, 1988c, Collin and Pettigrew, 1988b, Collin and Partridge, 1996), marine mammals (Mass and Supin, 1995, Mass and Supin, 1997, Mass and Supin, 2003), birds (Coimbra et al., 2012b) and reptiles (Hart et al., 2012).

After testing a variety of methods to construct and compare topographic maps, the thin plate spline method is the most useful method to display the density distribution of the retinal cells and an under-smoothed function is found to resolve any inherent specialisations, especially in retinas with shallow density gradients where an over-smoothed function would neglect the small differences as often is observed in Chondrichthyes. In all species, the rods showed a consistently shallower gradient of cell density change across the retina of no more than 2.2:1 cells from the specialization to the periphery, while the cones revealed a more pronounced gradient of cell densities of about 3:1 cells in the stingrays from the specialization to the periphery with even higher gradients in the demersal species (*C. milii* = 5:1 and *M. antarcticus* = 6:1). The shallow gradient of rods may reflect the lack of importance of high spatial resolution under scotopic conditions. The more pronounced streak of cones and ganglion cells provides better resolution in a specific region of the visual field of view in bright light (photopic) conditions.

Two species of chimaeras (the Pacific spookfish, *Rhinochimaera pacifica* and the longeye chimaera, *Chimaera lignaria*) live exclusively in the deep-sea at more than 500 meters depth, where there is virtually no sunlight (Warrant and Locket, 2004). Accordingly, the two species of chimaeras possess most visual specializations to increase the sensitivity of the retina at the cost of high resolving power and colour vision. The findings of a rod-only retina with long, thin outer segments, and the presence of a brightly coloured green *tapetum lucidum*, that reflects the light back onto the photoreceptors, are adaptations to increase the sensitivity of the eye and are consistent with other species of deep-sea teleosts (Denton and Nicol, 1964, Best and Nicol, 1967, Collin and Partridge, 1996, Warrant, 2000). Some deep-sea animals like teleost fishes and some crustaceans have photopigments in the retina that are tuned to the predominant wavelengths of the bioluminescent emissions produced by other organisms (prey detection) or by the same species (to find reproductive partners) (O'Day and Fernandez, 1974,

Partridge et al., 1988, Warrant, 2000, Turner et al., 2009). Some deep-sea teleosts may have other adaptations like the presence of a fovea, which is a pit in the retina within an increased density of cells or area centralis, but a fovea is not present in the species analysed and has not been recorded for any species of Chondrichthyes. In the deep-sea, the presence of a fovea is an adaptation to detect point sources of bioluminescence at depths of over 1000 meters (Collin and Collin, 1999, Collin et al., 2000, Warrant, 2000). The absence of a fovea might reflect that the deep-sea chimaeras use other senses like olfaction and electroreception to detect benthic prey. Vision will be more useful when these species frequent mesopelagic regions of the water column between 500 and 1000 meters in depth, where some sunlight is known to penetrate (Warrant, 2000, Douglas et al., 2003).

The five species of rays within the family Dasyatidae (*Neotrygon kuhlii*, *Taeniura lymma*, *Himantura huarnak*, *Pastinachus atrus* and *Urogymnus asperrimus*) live in shallow waters in bright light conditions. The stingrays' visual ecology (photopic vision) represents an adaptation to much higher visual acuity and the presence of colour vision compared to the deep-sea chimaeras (rod-only scotopic vision). The five species of stingrays possess a duplex retina (rod and cone photoreceptors) and the photoreceptors have a lower degree of convergence onto the ganglion cells that will enhance visual acuity. Enhanced visual acuity improves the capacity to cope in coral reef environments that are visually complex compared to the deep-sea and comprise a number of complex microhabitats and differ in the intensity and spectral distribution of light (Marshall et al., 2003). The diversity of animals and ecological niches encourages specializations in coral reef species (Hughes et al., 2002, Barber and Bellwood, 2005). The visual ecology of the five species of stingrays shows some differences that relate to their different use of the habitat. The bluespotted maskray, *N. kuhlii*, possesses higher visual acuity and a higher proportion of long wavelength-sensitive (LWS) cones than the bluespotted fantail ray, *T. lymma*. *N. kuhlii* spends most of its time in brightly-lit, sandy, flat patches while *T. lymma* hides in caves or

under rocks before moving to sandy patches in high tides to feed (Jonna, 2003). The different habitats of these two species appear to be reflected in their visual ecology both with regard to the intensity and spectral composition of the ambient light environment.

The elephant shark, *Callorhinchus milii*, (Holocephali) has a similar visual ecology to the gummy shark, *Mustelus antarcticus* (Elasmobranchii) and can be considered as a transitional species. Both species are demersal with a distribution between shallow estuarine waters to more than 200 meters depth. The light conditions in the habitat of both species vary from bright light at the surface to dim light at the deepest part of their depth range, so the visual demands may change accordingly (Collin and Shand, 2003). The visual specialisations have characteristics for high sensitivity in dim light conditions with a rod-dominant retina but the presence of cones suggests a visual specialization for photopic conditions. The spatial resolving power i.e. the capacity of the organism to resolve detail in an object against the background shows a lower value in demersal species (gummy shark and elephant shark) and is similar to the deep-sea chimaeras which vary between 2.53 and 3.37 cycles per degree. In contrast, all the species of stingrays have a spatial resolving power in the range of 5.94 to 7.66 cycles per degree. This range is similar to other elasmobranchs as discussed previously (Chapters 2, 3 and 4) but also to other marine species with a range between 2 and 14 cycles per degree as in teleosts (Nakamura, 1968, Collin and Pettigrew, 1989, Fritsches et al., 2003), marine mammals (Schusterman and Balliet, 1970, Watkins and Wartzok, 1985, Bauer et al., 2003), reptiles (Bartol et al., 2002, Hart et al., 2012) and invertebrates (Muntz and Gwyther, 1989).

The characterisation of the LWS cone photopigment and the inference of multiple pigments in the elephant shark and the stingrays reveal the potential for colour vision in both species. Thus far, the evidence in the

literature and the negative immunohistochemical results in the retinas of gummy sharks shown here might indicate that selachians possess only one type of cone photopigment making them cone monochromats (Hart et al., 2011, Theiss et al., 2012). This poses an interesting question of why the two sister taxa (Batoidea and Holocephali) have the potential for colour vision, while the sharks (that live in similar habitats) have lost the ability to discriminate colours. The use of immunohistochemistry also supports the idea of the absence of the SWS cone opsin in the retina of chondrichthyans, a finding that is similar to studies in marine mammals (Peichl et al., 2001, Hunt and Peichl, 2013, Meredith et al., 2013) but is different to other groups like teleost fishes (Cummings and Partridge, 2001, Bailes et al., 2007, Collin et al., 2009) and marine reptiles (Levenson et al., 2004, Hart et al., 2012).

The study of the pineal gland comparing the elephant shark, *C. milii*, and the bluespotted maskray, *N. kuhlii*, represents the first comparison of the morphology of the pineal in two species of Chondrichthyes with different habitats. The preliminary results using light microscopical analyses of the type and number of pineal photoreceptors reveal that the pineal organ in *C. milii* has a higher sensitivity than *N. kuhlii*. The surface of the vesicle in *C. milii* is covered by long photoreceptors and the presence of a pineal window in the overlying skin and cartilage affirms the important role of the pineal in this group (Gruber et al., 1975b, Clark and Kristof, 1990). The similarity between the specializations in the retina and the pineal, where *C. milii* has adaptations for greater sensitivity and *N. kuhlii* has adaptations for better acuity and chromatic processing, suggest that other experiments that we did in the retina might be useful to perform in the pineal to reveal more information about the non-visual systems of Chondrichthyans. For example, the use of different anti-opsin antibodies might reveal the types of visual pigment(s) expressed in the pineal, which could be compared to that expressed in the retina, as has been done in *Chimaera monstrosa* (Vigh-Teichmann et al., 1990). A three dimensional study of the density of photoreceptors in the pineal in these species would reveal important

information of how this organ responds to environmental light and how circadian rhythms are set.

Future research should include elucidating the mechanisms underlying the production of melatonin in the pineal and the seasonality of reproduction, both of which should be influenced by the amount and spectral quality of light experienced by the animals. Additionally, identifying the neural connections of the pineal organ and the retina to different areas of the brain will be critical for interpreting the use of visual and non-visual information by these fascinating animals.. The integration of the sensory information in different regions of the brain can be studied to assess the importance of each sense in the ecology of each species (Yopak et al., 2007, Lisney et al., 2008, Yopak and Montgomery, 2008, Yopak et al., 2010). Ultimately, the animal integrates information from different senses and according to how they perceive their environment and their sensory demands.

References

- Ahnelt PK, Hokoç JN, Röhlich P. 1995. Photoreceptors in a primitive mammal, the South American opossum, *Didelphis marsupialis aurita*: Characterization with anti-opsin immunolabeling. *Visual Neuroscience* 12(05):793-804.
- Ahnelt PK, Schubert C, Kubber-heiss A, Schiviz A, Anger E. 2006. Independent variation of retinal S and M cone photoreceptor topographies: A survey of four families of mammals. *Visual Neuroscience* 23(3-4):429-435.
- Akima H. 1978. A method of bivariate interpolation and smooth surface fitting for irregularly distributed data points. *ACM Trans Math Softw* 4(2):148-159.
- Akima H, Gebhardt A, Petzoldt T, Maechler M. 2012. Akima: Interpolation of irregularly spaced data: R package
- Allis EP. 1923. The cranial anatomy of *Chlamydoselachus anguineus*. *Acta Zoologica* 4(2-3):123-221.
- Anadon R, Molist P, Rodriguez-Moldes I, Lopez JM, Quintela I, Cervino MC, Barja P, Gonzalez A. 2000. Distribution of choline acetyltransferase immunoreactivity in the brain of an elasmobranch, the lesser spotted dogfish (*Scyliorhinus canicula*). *Journal of Comparative Neurology* 420(2):139-170.
- Andrade da Costa BLS, Hokoç JN. 2000. Photoreceptor topography of the retina in the New World monkey *Cebus apella*. *Vision Research* 40(18):2395-2409.
- Araki M, Iida Y, Taketani S, Watanabe K, Ohta T, Saito T. 1987. Characterization of photoreceptor cell differentiation in the rat retinal cell culture. *Developmental Biology* 124(1):239-247.
- Arnason U, Gullberg A, Janke A. 2001. Molecular phylogenetics of gnathostomous (jawed) fishes: old bones, new cartilage. *The Norwegian Academy of Science and Letters* 30(4):249-255.
- Aschliman NC, Claeson KM, McEachran JD. 2012a. Phylogeny of the Batoidea. In: Carrier JC, Musick JA, Heithaus MR, eds. *Biology of sharks and their relatives*. Second Edition ed: CRC press. p 57-95.
- Aschliman NC, Nishida M, Miya M, Inoue JG, Rosana KM, Naylor GJ. 2012b. Body plan convergence in the evolution of skates and rays (Chondrichthyes: Batoidea). *Molecular Phylogenetics and Evolution* 63(1):28-42.
- Baddeley A. 2008. Analysing spatial point patterns in R. Technical report, CSIRO, 2010. Version 4. Available at www.csiro.au/resources/pf16h.html. 232 p.
- Baddeley A, Turner R. 2005. spatstat: An R package for analyzing spatial point patterns. *J Stat Softw* 12(6):1-42.
- Bailes HJ, Davies WL, Trezise AEO, Collin SP. 2007. Visual pigments in a living fossil, the Australian lungfish *Neoceratodus forsteri*. *BMC Evolutionary Biology* 7(1):200.
- Bailes HJ, Robinson SR, Trezise AEO, Collin SP. 2006. Morphology, characterization, and distribution of retinal photoreceptors in the

- Australian lungfish *Neoceratodus forsteri* (Krefft, 1870). *Journal of Comparative Neurology* 494(3):381-397.
- Barber PH, Bellwood DR. 2005. Biodiversity hotspots: evolutionary origins of biodiversity in wrasses (*Halichoeres*: Labridae) in the Indo-Pacific and new world tropics. *Molecular Phylogenetics and Evolution* 35:235-253.
- Barker MJ, Schluessel V. 2005. Managing global shark fisheries: suggestions for prioritizing management strategies. *Aquatic Conservation: Marine and Freshwater Ecosystems* 15:325-347.
- Barlow HB. 1953. Summation and inhibition in the frog's retina. *The Journal of physiology* 119(1):69-88.
- Barnett LAK. 2008. Life History, Abundance, and Distribution of the Spotted Ratfish, *Hydrolagus colliei*. Monterey Bay, California: California State University. 155 p.
- Bartol S, Musick JA, Ochs AL. 2002. Visual acuity thresholds of juvenile loggerhead sea turtles (*Caretta caretta*): an electrophysiological approach. *Journal of Comparative Physiology A* 187(12):953-960.
- Bauer GB, Colbert DE, Gaspard Iii JC, Littlefield B, Fellner W. 2003. Underwater visual acuity of Florida manatees (*Trichechus manatus latirostris*). *International journal of comparative psychology* 16(2):130-142.
- Beatty DD. 1969. Visual pigments of three species of cartilaginous fishes. *Nature* 222:285.
- Beazley LD, Dunlop SA. 1983. The evolution of an area and visual streak in the marsupial *Setonix brachyurus*. *The Journal of Comparative Neurology* 216(2):211-231.
- Berkley MA. 1976. Some comments on visual acuity and its relation to eye structure. In: Masterton RB, Campbell CBG, Bitterman ME, Hotton N, eds. *Evolution of Brain and Behavior in Vertebrates*. Hillsdale, New Jersey: Lawrence Erlbaum Associates Inc. Publishers. p 73-87.
- Best ACG, Nicol JAC. 1967. Reflecting cells of the elasmobranch *tapetum lucidum*. *Contributions in Marine Science* 12:172-201.
- Bivand RS, Pebesma EJ, Gómez-Rubio V. 2008. *Applied spatial data analysis with R*: Springer. 390 p.
- Blonder BI, Alevizon WS. 1988. Prey discrimination and electroreception in the stingray *Dasyatis sabina*. *Copeia* 1988(1):33-36.
- Bowmaker JK. 1995. The visual pigments of fish. *Progress in Retinal and Eye Research* 15(1):1-31.
- Bowmaker JK. 2008. Evolution of vertebrate visual pigments. *Vision Research* 48(20):2022-2041.
- Bowmaker JK, Govardovskii VI, Shukolyukov SA, L.V. Zueva J, Hunt DM, Sideleva VG, Smirnova OG. 1994. Visual pigments and the photic environment: The cottoid fish of Lake Baikal. *Vision Research* 34(5):591-605.
- Bowmaker JK, Wagner HJ. 2004. Pineal organs of deep-sea fish: photopigments and structure. *The Journal of Experimental Biology* 207:2379-2387.
- Boycott B, Wässle H. 1974. The morphological types of ganglion cells of the domestic cat's retina. *The Journal of physiology* 240(2):397-419.

- Bozzano A. 2004. Retinal specialisations in the dogfish *Centroscymnus coelolepis* from the Mediterranean deep-sea. *Scientia Marina* 68:185-195.
- Bozzano A, Collin SP. 2000. Retinal ganglion cell topography in elasmobranchs. *Brain Behavior and Evolution* 55(4):191-208.
- Bozzano A, Murgia R, Vallerga S, Hirano J, Archer S. 2001. The photoreceptor system in the retinae of two dogfishes, *Scyliorhinus canicula* and *Galeus melastomus*: possible relationship with depth distribution and predatory lifestyle. *Journal of Fish Biology* 59:1258-1278.
- Braekevelt C. 1994a. Retinal photoreceptor fine structure in the short-tailed stingray. *Dasyatis brevicaudata*. *Histology and Histopathology* 9:507-514.
- Braekevelt CR. 1994b. Fine-Structure of the Retinal-pigment epithelium in the Port Jackson Shark (*Heterodontus phillipi*). *Anatomy and Embryology* 190(5):501-506.
- Bres M. 1993. The behaviour of sharks. *Reviews in Fish Biology and Fisheries* 3(2):133-159.
- Carpenter KE, Niem VH. 1999. The living resources of the Western Central Pacific Volume 3 Batoid fishes, chimaeras and bony fishes part 1 (Elopidae to Linophrynidae). FAO, ed. Rome: FOOD AND AGRICULTURE ORGANIZATION OF THE UNITED NATIONS.
- Carrera I, Sueiro C, Molist P, Holstein GR, Martinelli G, Rodriguez-Moldes I, Anadon R. 2006. GABAergic system of the pineal organ of an elasmobranch (*Scyliorhinus canicula*): a developmental immunocytochemical study. *Cell and Tissue Research* 323(2):273-281.
- Carter GS. 1948. Colour and Colour Vision in Animals. *Nature* 4120:600-601.
- Cassone VM. 1990. Effects of melatonin on vertebrate circadian systems. *Trends Neurosci* 13(11):457-464.
- Clark E, Kristof E. 1990. Deep-sea elasmobranchs observed from submersibles off Bermuda, Grand Cayman, and Freeport, Bahamas. In: Pratt Jr HL, Gruber SH, Taniuchi T, eds. *Elasmobranchs as living resources: Advances in the Biology, Ecology, Systematics, and the status of the fisheries*. Vol NOAA Technical Report NMFS 90. Honolulu, Hawaii: National Oceanic and Atmospheric Administration. p 269-284.
- Clarke SC, McAllister MK, Michielsens CGJ. 2005. Estimates of shark species composition and numbers associated with the shark fin trade based on Hong Kong auction data. *J Northw Atl Fish Sci* 35:453-465.
- Coimbra JP, Hart NS, Collin SP, Manger PR. 2012a. Scene from above: Retinal ganglion cell topography and spatial resolving power in the giraffe (*Giraffa camelopardalis*). *Journal of Comparative Neurology* 521(9):2042-2057.
- Coimbra JP, Marceliano MLV, Andrade-da-Costa BLD, Yamada ES. 2006. The retina of tyrant flycatchers: Topographic organization of neuronal density and size in the ganglion cell layer of the great kiskadee *Pitangus sulphuratus* and the rusty margined flycatcher *Myiozetetes*

- cayanensis* (Aves : Tyrannidae). *Brain, Behavior and Evolution* 68(1):15-25.
- Coimbra JP, Nolan PM, Collin SP, Hart NS. 2012b. Retinal ganglion cell topography and spatial resolving power in penguins. *Brain, Behavior and Evolution* 80(4):254-268.
- Coimbra JP, Trevia N, Marceliano MLV, Andrade-Da-Costa BLD, Picanco-Diniz CW, Yamada ES. 2009. Number and distribution of neurons in the retinal ganglion cell layer in relation to foraging behaviors of tyrant flycatchers. *Journal of Comparative Neurology* 514(1):66-73.
- Collin SP. 1988. The retina of the shovel-nosed ray, *Rhinobatos batillum* (Rhinobatidae): morphology and quantitative analysis of the ganglion, amacrine and bipolar cell populations. *Experimental Biology* 47(4):195.
- Collin SP. 1997. Specialisations of the teleost visual system: adaptive diversity from shallow-water to deep-sea. *Acta physiologica Scandinavica Supplementum* 638:5-24.
- Collin SP. 1999. Behavioural ecology and retinal cell topography. *Adaptive mechanisms in the ecology of vision*:509-535.
- Collin SP. 2008. A web-based archive for topographic maps of retinal cell distribution in vertebrates. *Clinical and Experimental Optometry* 91(1):85-95.
- Collin SP. 2009. Early evolution of vertebrate photoreception: lessons from lampreys and lungfishes. *Integrative Zoology* 4(1):87-98.
- Collin SP. 2010. Evolution and Ecology of Retinal Photoreception in Early Vertebrates. *Brain Behavior and Evolution* 75(3):174-185.
- Collin SP. 2012. The neuroecology of cartilaginous fishes: sensory strategies for survival. *Brain, Behavior and Evolution* 80(2):80-96.
- Collin SP, Collin HB. 1999. The foveal photoreceptor mosaic in the pipefish, *Corythoichthyes paxtoni* Syngnathidae, Teleostei. *Histology and Histopathology* 14:369-382.
- Collin SP, Davies WL, Hart NS, Hunt DM. 2009. The evolution of early vertebrate photoreceptors. *Philosophical Transactions of the Royal Society B: Biological Sciences* 364(1531):2925-2940.
- Collin SP, Knight MA, Davies WL, Potter IC, Hunt DM, Trezise AEO. 2003. Ancient colour vision: multiple opsin genes in the ancestral vertebrates. *Current Biology* 13(22):R864-R865.
- Collin SP, Lloyd DJ, Wagner HJ. 2000. Foveate vision in deep-sea teleosts: a comparison of primary visual and olfactory inputs. *Philosophical Transactions of the Royal Society of London Series B-Biological Sciences* 355(1401):1315-1320.
- Collin SP, Partridge JC. 1996. Retinal specializations in the eyes of deep-sea teleosts. *Journal of Fish Biology* 49:157-174.
- Collin SP, Pettigrew JD. 1988a. Retinal ganglion-cell topography in teleosts- a comparison between nissl-stained material and retrograde labeling from the optic-nerve. *Journal of Comparative Neurology* 276(3):412-422.
- Collin SP, Pettigrew JD. 1988b. Retinal topography in reef teleosts I. Some species with well-developed areae but poorly-developed streaks. *Brain, Behavior and Evolution* 31(5):269-282.

- Collin SP, Pettigrew JD. 1988c. Retinal topography in reef teleosts II. Some species with prominent horizontal streaks and high-density areas. *Brain, Behavior and Evolution* 31(5):283-295.
- Collin SP, Pettigrew JD. 1989. Quantitative comparison of the limits on visual spatial resolution set by the ganglion cell layer in 12 species of reef teleosts. *Brain Behavior and Evolution* 34(3):184-192.
- Collin SP, Shand J. 2003. Retinal sampling and the visual field in fishes. In: Collin S, Marshall NJ, eds. *Sensory processing in aquatic environments*: Springer New York. p 139-169.
- Collin SP, Whitehead D. 2004. The functional roles of passive electroreception in non-electric fishes. *Anim Biol* 54(1):1-25.
- Compagno LJV. 2001. *Sharks of the world : an annotated and illustrated catalogue of shark species known to date*. Rome: FAO Food and Agriculture Organization of the United Nations. 269 p.
- Compagno LJV, Dando M, Fowler S. 2005. *Sharks of the world*. Princeton, New Jersey: Princeton University Press.
- Connaughton V, Graham D, Nelson R. 2004. Identification and morphological classification of horizontal, bipolar, and amacrine cells within the zebrafish retina. *Journal of Comparative Neurology* 477(4):371-385.
- Crescitelli F. 1969. The visual pigment of a chimaeroid fish. *Vision Research* 9(12):1407-1414.
- Crescitelli F, McFallngai M, Horwitz J. 1985. The visual pigment sensitivity hypothesis- Further evidence from fishes varying habitats. *Journal of Comparative Physiology a-Sensory Neural and Behavioral Physiology* 157(3):323-333.
- Cummings ME, Partridge JC. 2001. Visual pigments and optical habitats of surfperch (Embiotocidae) in the California kelp forest. *J Comp Physiol A -Neuroethol Sens Neural Behav Physiol* 187(11):875-889.
- Curcio CA, Sloan KR, Kalina RE, Hendrickson AE. 1990. Human photoreceptor topography. *The Journal of Comparative Neurology* 292(4):497-523.
- Chelvanayagam DK. 2000. Interpreting the distortion associated with a retinal wholemount. *Journal of Theoretical Biology* 205(3):443-455.
- Davies WIL, Tay B-H, Zheng L, Danks JA, Brenner S, Foster RG, Collin SP, Hankins MW, Venkatesh B, Hunt DM. 2012. Evolution and functional characterisation of melanopsins in a deep-sea chimaera (elephant shark, *Callorhinchus milii*). *PLoS ONE* 7(12):e51276.
- Davies WL, Carvalho LS, Tay BH, Brenner S, Hunt DM, Venkatesh B. 2009. Into the blue: Gene duplication and loss underlie color vision adaptations in a deep-sea chimaera, the elephant shark *Callorhinchus milii*. *Genome Research* 19(3):415-426.
- Davies WL, Hankins MW, Foster RG. 2010. Vertebrate ancient opsin and melanopsin: divergent irradiance detectors. *Photochemical & Photobiological Sciences* 9(11):1444-1457.
- De Beer G, Moy-Thomas J. 1935. On the skull of Holocephali. *Philosophical Transactions of the Royal Society of London Series B, Biological Sciences* 224(514):287-312.

- Demski LS. 1991. Neural substrates for photic control of Elasmobranch sexual development and behavior. *Journal of Experimental Zoology* 256(S5 Supplement: Vision in Elasmobranchs: A Comparative and Ecological Perspective):121-129.
- Denton EJ. 1963. The visual pigments of some deep-sea elasmobranchs. *Journal of the Marine Biological Association of the UK* 43:65-70.
- Denton EJ, Nicol JAC. 1964. The chodioid tapeta of some cartilaginous fishes (Chondrichthyes). *Journal of the Marine Biological Association of the UK* 44:219-258.
- Devine JA, Baker KD, Haedrich RL. 2006. Fisheries: deep-sea fishes qualify as endangered. *Nature* 439(7072):29-29.
- Didier DA. 1998. The leopard Chimaera, a new species of chimaeroid fish from New Zealand (Holocephali, Chimaeriformes, Chimaeridae). *Ichthyol Res* 5(3):281-289.
- Didier DA. 2004. Phylogeny and classification of extant Holocephali. In: Carrier JC, Musick JA, Heithaus MR, eds. *Biology of sharks and their relatives*. Boca Raton: CRC Press. p 115-136.
- Didier DA, Kemper JM, Ebert DA. 2012. Phylogeny, biology and classification of extant holocephalans. In: Carrier JC, Musick JA, Heithaus MR, eds. *Biology of sharks and their relatives*. Second Edition ed: CRC press. p 97-123.
- Do-Nascimento J, Do-Nascimento R, Damasceno B, Silveira L. 1991. The neurons of the retinal ganglion cell layer of the guinea pig: quantitative analysis of their distribution and size. *Brazilian journal of medical and biological research= Revista brasileira de pesquisas medicas e biologicas/Sociedade Brasileira de Biofisica[et al]* 24(2):199-214.
- Dolan T, Fernandez-Juricic E. 2010. Retinal ganglion cell topography of five species of ground-foraging birds. *Brain Behavior and Evolution* 75:111-121.
- Douglas RH. 2010. Vision: Vertebrates. In: Breed MD, Moore J, eds. *Encyclopedia of Animal Behavior*. Oxford: Academic Press. p 525-542.
- Douglas RH, Collin SP, Corrigan J. 2002. The eyes of suckermouth armoured catfish (Loricariidae, subfamily Hypostomus): pupil response, lenticular longitudinal spherical aberration and retinal topography. *Journal of Experimental Biology* 205(22):3425-3433.
- Douglas RH, Hunt DM, Bowmaker JK. 2003. Spectral Sensitivity Tuning in the Deep-Sea. In: Collin SP, Marshall NJ, eds. *Sensory Processing in Aquatic Environments* New York: Springer Verlag. p 323-342.
- Douglas RH, Partridge JC. 1997. On the visual pigments of deep-sea fish. *Journal of Fish Biology* 50(1):68-85.
- Douglas RH, Partridge JC, Hope AJ. 1995. Visual and lenticular pigments in the eyes of demersal deep-sea fishes. *Journal of Comparative Physiology A* 177(1):111-122.
- Dowling JE. 1997. *Encyclopedia of human biology*. San Diego: Academic Press.
- Dowling JE, Ripps H. 1991. On the duplex nature of the skate retina. *Journal of Experimental Zoology* 256(S5 Supplement: Vision in Elasmobranchs: A Comparative and Ecological PerspectiveS5):55-65.

- Duchon J. 1977. Splines minimizing rotation-invariant semi-norms in Sobolev spaces. *Constructive theory of functions of several variables*: Springer. p 85-100.
- Dunn KA, Morrissey JF. 1995. Molecular phylogeny of elasmobranchs. *Copeia* 1995(3):526-531.
- Dunn MR, Griggs L, Forman J, Horn P. 2010. Feeding habits and niche separation among the deep-sea chimaeroid fishes *Harriotta raleighana*, *Hydrolagus bemisi* and *Hydrolagus novaezealandiae*. *Marine Ecology-Progress Series* 407:209-225.
- Ebert DA. 2003. *Sharks, rays, and chimaeras of California*. Los Angeles, CA: University of California Press. 284 p.
- Ebert DA, Bizzarro J. 2007. Standardized diet compositions and trophic levels of skates (Chondrichthyes: Rajiformes: Rajoidei). *Environmental Biology of Fishes* 80(2):221-237.
- Famiglietti EV, Sharpe SJ. 1995. Regional topography of rod and immunocytochemically characterized “blue” and “green” cone photoreceptors in rabbit retina. *Visual Neuroscience* 12(06):1151-1175.
- Fenwick JC. 1970. Demonstration and effect of melatonin in fish. *General and Comparative Endocrinology* 14(1):86-97.
- Fernald RD, Liebman PA. 1980. Visual receptor pigments in the African cichlid fish, *Haplochromis burtoni*. *Vision Research* 20(10):857-864.
- Ferreiro-Galve S, Rodríguez-Moldes I, Anadón R, Candal E. 2010. Patterns of cell proliferation and rod photoreceptor differentiation in shark retinas. *Journal of Chemical Neuroanatomy* 39:1-14.
- Fields R, Lange G. 1980. Electroreception in the ratfish (*Hydrolagus colliei*). *SCIENCE* 207(4430):547-548.
- Fischer QS, Kirby M. 1991. Number and distribution of retinal ganglion cells in Anubis baboons (*Papio anubis*). *Brain, Behavior and Evolution* 37(4):189-203.
- Fong QSW, Anderson JL. 2002. International shark fin markets and shark management: an integrated market preference-cohort analysis of the blacktip shark (*Carcharhinus limbatus*). *Ecological Economics* 40:117-130.
- Forsell J, Ekström P, Flamarique IN, Holmqvist B. 2001. Expression of pineal ultraviolet-and green-like opsins in the pineal organ and retina of teleosts. *Journal of Experimental Biology* 204(14):2517-2525.
- Fox DL, Kuchnow KP. 1965. Reversible light-screening pigment of elasmobranch eyes- Chemical identity with melanin. *Science* 150(3696):612-614.
- Francis MP. 1997. Reproductive Strategy of White Sharks, *Carcharodon carcharias*. *Shark News* 9:1-3.
- Francis MP. 1998. New Zealand shark fisheries: development, size and management. *Marine and Freshwater Research* 49:579-591.
- Franco ECS, Finlay BL, Silveira LCL, Yamada ES, Crowley JC. 2000. Conservation of absolute foveal area in New World monkeys. *Brain, Behavior and Evolution* 56(5):276-286.

- Freitas R, Zhang GJ, Albert JS, Evans DH, Cohn MJ. 2006. Developmental origin of shark electrosensory organs. *Evolution & Development* 8(1):74-80.
- Fritsches KA, Marshall NJ, Warrant EJ. 2003. Retinal specializations in the blue marlin: eyes designed for sensitivity to low light levels. *Marine and Freshwater Research* 54(4):333-341.
- Fröhlich E, Negishi K, Wagner H-J. 1995. Patterns of rod proliferation in deep-sea fish retinae. *Vision Research* 35(13):1799-1811.
- Fuller RC, Fleishman LJ, Leal M, Travis J, Loew E. 2003. Intraspecific variation in retinal cone distribution in the bluefin killifish, *Lucania goodei*. *Journal of Comparative Physiology A* 189(8):609-616.
- García VB, Lucifora LO, Myers RA. 2008. The importance of habitat and life history to extinction risk in sharks, skates, rays and chimaeras. *Proceedings of the Royal Society B: Biological Sciences* 275(1630):83-89.
- Gardiner JM, Atema J, Hueter RE, Motta PJ. 2013. Sensory switching in sharks: the role of multimodal stimuli in prey tracking and capture. *Integrative and Comparative Biology* 53:E74-E74.
- Gardner MG, Ward RD. 1998. Population structure of the Australian gummy shark (*Mustelus antarcticus* Günther) inferred from allozymes, mitochondrial DNA and vertebrae counts. *Marine and Freshwater Research* 49:733-745.
- Garza-Gisholt E, Hemmi JM, Hart NS, Collin SP. 2014. A comparison of spatial analysis methods for the construction of topographic maps of retinal cell density. *PLoS ONE* 9(4):e93485.
- Glickstein M. 1976. The vertebrate eye. In: Masterton RB, Campbell CBG, Bitterman ME, Hotton N, eds. *Evolution of brain and behavior in Vertebrates*. Hillsdale, New Jersey: Lawrence Erlbaum Associates, Inc. Publishers. p 53-71.
- Gonzalez C, Teruel J, López E, Paz X. Feeding habits and biological features of deep-sea species of the Northwest Atlantic: large-eyed Rabbitfish (*Hydrolagus mirabilis*), narrownose chimaera (*Harriotta raleighana*) and black dogfish (*Centroscyllium fabricii*). 2007. Northwest Atlantic Fisheries Organization. p 9.
- Gouras P. 1991. Color vision. In: Kandel ER, Schwartz JH, Jessell TM, eds. *Principles of Neural Science*. Vol 3. New York: Elsevier Science Publishers. p 467-479.
- Grogan ED, Lund R, Greenfest-Allen E. 2012. The Origin and Relationships of Early Chondrichthyans. In: Carrier JC, Musick JA, Heithaus MR, eds. *Biology of sharks and their relatives*. Second Edition ed: CRC press. p 3-30.
- Gruber SH, Cohen JL. 1978. Visual system of the elasmobranchs: State of the Art 1960-1975. In: Hodgson ES, Mathewson RF, eds. *Sensory Biology of Sharks, Skates and Rays*: Technical Information Division, Naval Research Laboratory. p 11-105.
- Gruber SH, Gulley RL, Brandon J. 1975a. Duplex retina in 7 elasmobranch species. *Bulletin of Marine Science* 25(3):353-358.
- Gruber SH, Hamasaki DI, Davis BL. 1975b. Window to the epiphysis in sharks. *Copeia* 1975(2):378-380.

- Gruber SH, Loew ER, McFarland WN. 1991. Rod and cone pigments of the Atlantic guitarfish, *Rhinobatos lentiginos* Garman. *Journal of Experimental Zoology* 256(S5 Supplement: Vision in Elasmobranchs: A Comparative and Ecological Perspective):85-87.
- Hamasaki D, Gruber S. 1965. The photoreceptors of the nurse shark, *Ginglymostoma cirratum* and the sting ray, *Dasyatis sayi*. *Bulletin of Marine Science* 15(4):1051-1059.
- Hamasaki DI, Streck P. 1971. Properties of epiphysis-cerebri of small spotted dogfish shark, *Scyliorhinus caniculus* L. *Vision Research* 11(3):189-198.
- Hancock PA, Hutchinson MF. 2006. Spatial interpolation of large climate data sets using bivariate thin plate smoothing splines. *Environmental Modelling & Software* 21(12):1684-1694.
- Hankins MW, Peirson SN, Foster RG. 2008. Melanopsin: an exciting photopigment. *Trends Neurosci* 31(1):27-36.
- Harahush BK, Hart NS, Green K, Collin SP. 2009. Retinal neurogenesis and ontogenetic changes in the visual system of the brown banded bamboo shark, *Chiloscyllium punctatum* (Hemiscyllidae, Elasmobranchii). *The Journal of Comparative Neurology* 513(1):83-97.
- Harman A, Dann J, Ahmat A, Macuda T, Johnston K, Timney B. 2001. The retinal ganglion cell layer and visual acuity of the camel. *Brain Behavior and Evolution* 58(1):15-27.
- Hart NS. 2002. Vision in the peafowl (Aves: *Pavo cristatus*). *The Journal of Experimental Biology* 205:3295-3935.
- Hart NS, Coimbra JP, Collin SP, Westhoff G. 2012. Photoreceptor types, visual pigments, and topographic specializations in the retinas of hydrophiid sea snakes. *The Journal of Comparative Neurology* 520(6):1246-1261.
- Hart NS, Lisney TJ, Collin SP. 2006. Visual Communication in Elasmobranchs. In: Ladich F, Collin SP, Moller P, Kapoor BG, eds. *Communication in Fishes*. Vol 2. Enfield, New Hampshire: Science Publishers. p 337-392.
- Hart NS, Lisney TJ, Marshall NJ, Collin SP. 2004. Multiple cone visual pigments and the potential for trichromatic colour vision in two species of elasmobranch. *Journal of Experimental Biology* 207(26):4587-4594.
- Hart NS, Theiss SM, Harahush BK, Collin SP. 2011. Microspectrophotometric evidence for cone monochromacy in sharks. *Naturwissenschaften* 98(3):193-201.
- Heath AR. 1991. The ocular tapetum lucidum- A model system for interdisciplinary studies in elasmobranch biology. *Journal of Experimental Zoology* 256(S5 Supplement: Vision in Elasmobranchs: A Comparative and Ecological Perspective):41-45.
- Hemmi JM, Grünert U. 1999. Distribution of photoreceptor types in the retina of a marsupial, the tammar wallaby (*Macropus eugenii*). *Visual Neuroscience* 16(02):291-302.
- Hengl T. 2007. A practical guide to geostatistical mapping and environmental variables. Italy: European Commission. Joint Research Centre. Institute for Environment and Sustainability. 291 p.

- Herring PJ. 1977. Bioluminescence of marine organisms. *Nature* 267(5614):788-793.
- Herring PJ. 2000. Bioluminescent signals and the role of reflectors. *Journal of Optics a-Pure and Applied Optics* 2(6):R29-R38.
- Heupel MR, Bennett MB. 1998. Observations on the diet and feeding habits of the epaulette shark, *Hemiscyllium ocellatum* (Bonnaterre), on Heron Island Reef, Great Barrier Reef, Australia. *Marine and Freshwater Research* 49:753-756.
- Heupel MR, Carlson JK, Simpfendorfer CA. 2007. Shark nursery areas: concepts, definition, characterization and assumptions. *Marine Ecology-Progress Series* 337:287-297.
- Hijmans RJ, van Etten J. 2012. raster: Geographic analysis and modeling with raster data. Version 2.0-12: R package.
- Hodgson ES, Mathewson RF. 1978. Electrophysiological studies of chemoreception in Elasmobranchs. In: Hodgson ES, Mathewson RF, eds. *Sensory Biology of Sharks, Skates and Rays: Technical Information Division, Naval Research Laboratory*. p 227-267.
- Hoegh-Guldberg O. 1999. Climate change, coral bleaching and the future of the world's coral reefs. *Marine and Freshwater Research* 50:839-866.
- Hoelzel AR. 2001. Shark fishing in fin soup. *Conservation Genetics* V2(1):69-72.
- Hofer H, Carroll J, Neitz J, Neitz M, Williams DR. 2005. Organization of the human trichromatic cone mosaic. *The Journal of Neuroscience* 25(42):9669-9679.
- Holts DB. 1988. Review of US west coast commercial shark fisheries. *Marine Fisheries Review* 50(1):1-8.
- Hueter RE. 1991a. Adaptations for spatial vision in sharks. *Journal of Experimental Zoology* 256(S5 Supplement: Vision in Elasmobranchs: A Comparative and Ecological Perspective):130-141.
- Hueter RE. 1991b. Vision in Elasmobranchs- Introduction. *Journal of Experimental Zoology* 256(S5 Supplement: Vision in Elasmobranchs: A Comparative and Ecological Perspective):1-2.
- Hueter RE, Gruber SH. 1980. Retinoscopy of aquatic eyes. *Vision Research* 20(3):197-200.
- Hueter RE, Mann DA, Maruska KP, Sisneros JA, Demski LS. 2004. Sensory biology of elasmobranchs. *Biology of sharks and their relatives*:325-368.
- Hueter RE, Murphy CJ, Howland M, Sivak JG, Paul-Murphy JR, Howland HC. 2001. Refractive state and accommodation in the eyes of free-swimming versus restrained juvenile lemon sharks (*Negaprion brevirostris*). *Vision Research* 41(15):1885-1889.
- Hughes A. 1975. A comparison of retinal ganglion cell topography in the plains and tree kangaroo. *The Journal of physiology* 244(1):61P.
- Hughes A. 1977. The topography of vision in mammals of contrasting life style: Comparative optics and retinal organization. In: Crescitelli F, ed. *The Visual System in Vertebrates*. Vol VII. Berlin: Springer Verlag. p 613-756.

- Hughes A, Whitteridge D. 1973. The receptive fields and topographical organization of goat retinal ganglion cells. *Vision Research* 13(6):1101-1114.
- Hughes TP, Bellwood DR, Connolly SR. 2002. Biodiversity hotspots, centres of endemism, and the conservation of coral reefs. *Ecology Letters* 5:775-784.
- Hunt DM, Carvalho LS, Cowing JA, Davies WL. 2009. Evolution and spectral tuning of visual pigments in birds and mammals. *Philosophical Transactions of the Royal Society B: Biological Sciences* 364(1531):2941-2955.
- Hunt DM, Peichl L. 2013. S cones: Evolution, retinal distribution, development, and spectral sensitivity. *Visual Neuroscience* FirstView:1-24.
- Inoue JG, Miya M, Lam K, Tay BH, Danks JA, Bell J, Walker TI, Venkatesh B. 2010. Evolutionary origin and phylogeny of the modern holocephalans (Chondrichthyes: Chimaeriformes): A mitogenomic perspective. *Molecular Biology and Evolution* 27(11):2576-2586.
- Jacobsen IP, Bennett MB. 2012. Feeding ecology and dietary comparisons among three sympatric *Neotrygon* (Myliobatoidei: Dasyatidae) species. *Journal of Fish Biology* 80(5):1580-1594.
- Jerlov NG, Nielsen ES. 1974. *Optical aspects of Oceanography*: Academic Press.
- Jonasz M, Fournier G. 2011. *Light Scattering by Particles in Water: Theoretical and Experimental Foundations*: Theoretical and Experimental Foundations: Access Online via Elsevier.
- Jones AA, Hall NG, Potter IC. 2010. Species compositions of elasmobranchs caught by three different commercial fishing methods off southwestern Australia, and biological data for four abundant bycatch species. *Fishery Bulletin* 108(4):365-381.
- Jonna R. 2003. *Dasyatidae*. *Animal Diversity Web*. Vol 2013: University of Michigan.
- Jordan LK, Mandelman JW, McComb DM, Fordham SV, Carlson JK, Werner TB. 2013. Linking sensory biology and fisheries bycatch reduction in elasmobranch fishes: a review with new directions for research. *Conservation Physiology* 1(1):1-20.
- Kalmijn AJ. 1982. Electric and magnetic field detection in Elasmobranch fishes. *Science* 218:916-918.
- Kempster R, McCarthy I, Collin S. 2012. Phylogenetic and ecological factors influencing the number and distribution of electroreceptors in elasmobranchs. *Journal of Fish Biology* 80(5):2055-2088.
- Kempster RM, Garza-Gisholt E, Egeberg CA, Hart NS, O'Shea OR, Collin SP. 2013. Sexual dimorphism of the electrosensory system: A quantitative analysis of nerve axons in the dorsal anterior lateral line nerve of the blue-spotted fantail stingray (*Taeniura lymma*). *Brain, Behavior and Evolution* 81(4):226-235.
- Kim DE. 2007. Prey detection mechanism of elasmobranchs. *Biosystems* 87(2-3):322-331.

- Kirkwood GP, Walker TI. 1986. Gill net mesh selectivities for gummy shark, *Mustelus antarcticus* Günther, taken in south-eastern Australian waters. *Marine and Freshwater Research* 37(6):689-697.
- Kleypas JA, McManus JW, Menez LAB. 1999. Environmental limits to coral reef development: Where do we draw the line? *American Zoologist* 39(1):146-159.
- Kohbara J, Niwa H, Oguri M. 1987. Comparative light microscopic studies on the retina of some elasmobranch fishes. *Nippon Suisan Gakkaishi* 53(12):2117-2125.
- Kolb H. 1995a. Cone pathways through the retina. In: Kolb H, Fernandez E, Nelson R, eds. *eWebvision: The Organization of the Retina and Visual System* (Internet). Salt Lake City: University of Utah Health Sciences Center.
- Kolb H. 1995b. Photoreceptors. In: Kolb H, Fernandez E, Nelson R, eds. *Webvision: The Organization of the Retina and Visual System* (Internet). Salt Lake City: University of Utah Health Sciences Center.
- Koslow JA, Boehlert GW, Gordon JDM, Haedrich RL, Lorance P, Parin N. 2000. Continental slope and deep-sea fisheries: implications for a fragile ecosystem. *ICES Journal of Marine Science: Journal du Conseil* 57(3):548-557.
- Kuchnow KP. 1971. The elasmobranch pupillary response. *Vision Research* 11(12):1395-1406.
- Kuchnow KP, Martin R. 1970. Pigment migration in tapetum lucidum of elasmobranch eye - Evidence for a nervous mechanism. *Vision Research* 10(9):825-828.
- Kusmic C, Barsanti L, Passarelli V, Gualtieri P. 1993. Photoreceptor morphology and visual pigment content in the pineal organ and in the retina of juvenile and adult trout, *Salmo irideus*. *Micron* 24(3):279-286.
- LaMarca MJ. 1964. The functional anatomy of the clasper and clasper gland of the yellow stingray, *Urolophus jamaicensis* (Cuvier). *Journal of Morphology* 114(2):303-323.
- Lamb TD, Collin SP, Pugh EN. 2007. Evolution of the vertebrate eye: opsins, photoreceptors, retina and eye cup. *Nature Reviews Neuroscience* 8(12):960-975.
- Land MF. 1981. Optics and vision in invertebrates. In: Autrum H, ed. *Handbook of sensory physiology*. Vol Vol. VII/6B. Berlin: Springer. p 471-592.
- Last PR, Stevens JD. 2009. *Sharks and rays of Australia*. Collingwood, VIC: CSIRO Publishing. 644 p.
- Lenanton RCJ, Heald DI, Platell M, Cliff M, Shaw J. 1990. Aspect of the reproductive biology of the Gummy Shark, *Mustelus antarcticus* Gunther, from waters off the South coast of Western Australia. *Marine and Freshwater Research* 41(6):807-822.
- Levenson DH, Dizon A. 2003. Genetic evidence for the ancestral loss of short-wavelength-sensitive cone pigments in mysticete and odontocete cetaceans. *Proceedings of the Royal Society of London Series B: Biological Sciences* 270(1516):673-679.

- Levenson DH, Eckert SA, Crognale MA, Deegan II JF, Jacobs GH. 2004. Photopic spectral sensitivity of green and loggerhead sea turtles. *Journal Information* 2004(4):908-914.
- Lisney T. 2010. A review of the sensory biology of chimaeroid fishes (Chondrichthyes; Holocephali). *Reviews in Fish Biology and Fisheries* 20:571-590.
- Lisney TJ. 2004. *Neuroethology and vision in elasmobranchs*. Brisbane: University of Queensland. 281 p.
- Lisney TJ, Collin SP. 2007. Relative eye size in elasmobranchs. *Brain Behavior and Evolution* 69:266-279.
- Lisney TJ, Collin SP. 2008. Retinal ganglion cell distribution and spatial resolving power in elasmobranchs. *Brain Behavior and Evolution* 72:59-77.
- Lisney TJ, Yopak KE, Montgomery JC, Collin SP. 2008. Variation in brain organization and cerebellar foliation in Chondrichthyans: Batoids. *Brain Behavior and Evolution* 72(4):262-282.
- Litherland L, Collin SP. 2008. Comparative visual function in elasmobranchs: Spatial arrangement and ecological correlates of photoreceptor and ganglion cell distributions. *Visual Neuroscience* 25(04):549-561.
- Litherland L, Collin SP, Fritsches KA. 2009. Eye growth in sharks: Ecological implications for changes in retinal topography and visual resolution. *Visual Neuroscience* 26(4):397-409.
- Locket NA. 1971. Retinal structure in *Platytrichtes apus*, a deep-sea fish with a pure rod fovea. *J Mar Biol Assoc UK* 51:79-91.
- Locket NA. 1977. Adaptations to the deep-sea environment. *Handbook of sensory physiology* 7(5):67-192.
- Loew ER, Lythgoe JN. 1978. The ecology of cone pigments in teleost fishes. *Vision Research* 18(6):715-722.
- Logiudice FT, Laird RJ. 1994. Morphology and density distribution of cone photoreceptor in the retina of the atlantic stingray, *Dasyatis sabina*. *Journal of Morphology* 221(3):277-289.
- Losey GS, Cronin TW, Goldsmith TH, Hyde D, Marshall NJ, McFarland WN. 1999. The UV visual world of fishes: a review. *Journal of Fish Biology* 54(5):921-943.
- Lukats A, Szabo A, Röhlich P, Vigh B, Szel A. 2005. Photopigment coexpression in mammals: comparative and developmental aspects. *Histology and Histopathology*:87.
- Lund R, Grogan ED. 1997. Relationships of the Chimaeriformes and the basal radiation of the Chondrichthyes. *Reviews in Fish Biology and Fisheries* 7:65-123.
- Lythgoe JN. 1979. *The ecology of vision*: Clarendon Press Oxford.
- Lythgoe JN. 1984. Visual pigments and environmental light. *Vision Research* 24(11):1539-1550.
- Maddock RG, Nicol JAC. 1978. Studies on the eyes of *Hydrolagus* (Pisces: Chimaeridae). *Contrib Mar Sci* 21:77-87.
- Mandado M, Molist P, Anadon R, Yanez J. 2001. A Dil-tracing study of the neural connections of the pineal organ in two elasmobranchs (*Scyliorhinus canicula* and *Raja montagui*) suggests a pineal projection

- to the midbrain GnRH-immunoreactive nucleus. *Cell and Tissue Research* 303(3):391-401.
- Marques A, Porteiro F. 2000. Hydrothermal vent mussel *Bathymodiolus* sp (Mollusca : Mytilidae): Diet item of *Hydrolagus affinis* (Pisces : Chimaeridae). *Copeia*(3):806-807.
- Marshall AD, Kyne PM, Bennett MB. 2008. Comparing the diet of two sympatric urolophid elasmobranchs (*Trygonoptera testacea* Müller & Henle and *Urolophus kapalensis* Yearsley & Last): evidence of ontogenetic shifts and possible resource partitioning. *Journal of Fish Biology* 72(4):883-898.
- Marshall NJ, Jennings K, McFarland WN, Loew ER, Losey GS, Montgomery WL. 2003. Visual biology of hawaiian coral Reef fishes. III. Environmental light and an integrated approach to the ecology of reef fish vision. *Copeia* 2003(3):467-480.
- Marshall NJ, Vorobyev M. 2003. The design of color signals and color vision in fishes. In: Collin SP, Marshall NJ, eds. *Sensory Processing in Aquatic Environments* New York: Springer Verlag. p 194-222.
- Maruska KP. 2001. Morphology of the mechanosensory lateral line system in elasmobranch fishes: ecological and behavioral considerations. *Environmental Biology of Fishes* 60:47-75.
- Mass A, Supin AY. 1992. Peak density, size and regional distribution of ganglion cells in the retina of the fur seal *Callorhinus ursinus*. *Brain, Behavior and Evolution* 39(2):69-76.
- Mass A, Supin AY. 1995. Ganglion cell topography of the retina in the bottlenosed dolphin, *Tursiops truncatus*. *Brain, Behavior and Evolution* 45(5):257-265.
- Mass AM, Supin AY. 1997. Ocular anatomy, retinal ganglion cell distribution, and visual resolution in the gray whale, *Eschrichtius gibbosus*. *Aquatic Mammals* 23:17-28.
- Mass AM, Supin AY. 1999. Retinal topography and visual acuity in the riverine tucuxi (*Sotalia fluviatilis*). *Marine Mammal Science* 15(2):351-365.
- Mass AM, Supin AY. 2003. Retinal topography of the harp seal *Pagophilus groenlandicus*. *Brain, Behavior and Evolution* 62(4):212-222.
- Matthiessen L. 1880. Untersuchungen über den aplanatismus und die periscopie der krystalllinsen in den augen der fische. *Pflügers Archiv European Journal of Physiology* 21(1):287-307.
- McComb D, Tricas T, Kajiura S. 2009. Enhanced visual fields in hammerhead sharks. *The Journal of Experimental Biology* 212(24):4010-4018.
- McComb DM, Frank TM, Hueter RE, Kajiura SM. 2010. Temporal resolution and spectral sensitivity of the visual system of three coastal shark species from different light environments. *Physiological and Biochemical Zoology* 83(2):299-307.
- McComb DM, Kajiura SM. 2008. Visual fields of four batoid fishes: a comparative study. *J Exp Biol* 211(4):482-490.
- McFarland WN. 1986. Light in the sea—Correlations with behaviors of fishes and invertebrates. *American Zoologist* 26(2):389-401.

- McFarland WN. 1991. Light in the sea: The optical world of elasmobranchs. *Journal of Experimental Zoology* 256(S5 Supplement: Vision in Elasmobranchs: A Comparative and Ecological Perspective):3-12.
- McFarland WN, Munz FW. 1975. Part III: The evolution of photopic visual pigments in fishes. *Vision Research* 15(10):1071-1080.
- McGowan DW, Kajiura SM. 2009. Electroreception in the euryhaline stingray, *Dasyatis sabina*. *Journal of Experimental Biology* 212(10):1544-1552.
- Meissl H, Yañez J. 1994. Pineal photosensitivity. A comparison with retinal photoreception. *Acta Neurobiol* 54:19-29.
- Meredith RW, Gatesy J, Emerling CA, York VM, Springer MS. 2013. Rod monochromacy and the coevolution of cetacean retinal opsins. *Plos Genetics* 9(4).
- Meredith TL, Kajiura SM. 2010. Olfactory morphology and physiology of elasmobranchs. *The Journal of Experimental Biology* 213(20):3449-3456.
- Moore BA, Kamilar JM, Collin SP, Bininda-Emonds ORP, Dominy NJ, Hall MI, Heesy CP, Johnsen S, Lisney TJ, Loew ER, Moritz G, Nava SS, Warrant E, Yopak KE, Fernández-Juricic E. 2012. A novel method for comparative analysis of retinal specialization traits from topographic maps. *Journal of Vision* 12(12):1-24.
- Morato T, Watson R, Pitcher TJ, Pauly D. 2006. Fishing down the deep. *Fish and Fisheries* 7(1):24-34.
- Morgan PJ, Barrett P, Howell HE, Helliwell R. 1994. Melatonin receptors: Localization, molecular pharmacology and physiological significance. *Neurochemistry International* 24(2):101-146.
- Moulton P, Walker T, Saddler S. 1992. Age and growth studies of Gummy Shark, *Mustelus antarcticus* Gunther, and School Shark, *Galeorhinus galeus* (Linnaeus), from Southern Australian Waters. *Marine and Freshwater Research* 43(5):1241-1267.
- Moura T, Figueiredo I, Bordalo-Machado P, Almeida C, Gordo LS. 2005. A new deep-water chimaerid species, *Hydrolagus lusitanicus* n. sp., from off mainland Portugal with a proposal of a new identification key for the genus *Hydrolagus* (Holocephali: Chimaeridae) in the north-east Atlantic. *Journal of Fish Biology* 67(3):742-751.
- Moyle PB, Cech JJ. 1988. *Fishes an introduction to Ichthyology*. NJ: Prentice-Hall.
- Muntz W, Gwyther J. 1989. Short communication: The visual acuity of octopuses for gratings of different orientations. *Journal of Experimental Biology* 142(1):461-464.
- Muntz WRA. 1976. Visual pigments of cichlid fishes from Malawi. *Vision Research* 16(9):897-903.
- Murphy CJ, Howland HC. 1991. The functional significance of crescent-shaped pupils and multiple pupillary apertures. *Journal of Experimental Zoology* 256(S5 Supplement: Vision in Elasmobranchs: A Comparative and Ecological Perspective):22-28.
- Myrberg Jr AA. 1991. Distinctive markings of sharks: Ethological considerations of visual function. *Journal of Experimental Zoology*

- 256(S5 Supplement: Vision in Elasmobranchs: A Comparative and Ecological PerspectiveS5):156-166.
- Nakamura EL. 1968. Visual acuity of two tunas, *Katsuwonus pelamis* and *Euthynnus affinis*. *Copeia*:41-49.
- Naylor GJP, Caira JN, Jensen K, Rosana KAM, Straube N, Lakner C. 2012. Elasmobranch phylogeny: A mitochondrial estimate based on 595 species. In: Carrier JC, Musick JA, Heithaus MR, eds. *Biology of sharks and their relatives*. Second Edition ed: CRC press. p 31-56.
- Naylor GJP, Ryburn JA, Fedrigo O, Lopez JA. 2005. Phylogenetic Relationships among the major lineages of modern elasmobranchs. In: Hamlett WC, ed. *Reproductive biology and phylogeny*. Vol 3. Enfield, NH: Science Publishers, Inc. p 1-25.
- Nelson JS. 2006. *Fishes of the World*: Wiley. com.
- Neuwirth E. 2012. RColorBrewer: Color Brewer palettes. Version 1.0-5: CRAN.
- Newman LA, Robinson PR. 2005. Cone visual pigments of aquatic mammals. *Visual Neuroscience* 22(6):873-879.
- Norse EA, Brooke S, Cheung WWL, Clark MR, Ekeland I, Froese R, Gjerde KM, Haedrich RL, Heppell SS, Morato T, Morgan LE, Pauly D, Sumaila R, Watson R. 2012. Sustainability of deep-sea fisheries. *Mar Pol* 36(2):307-320.
- Nychka D, Furrer R, Sain S. 2012. *fields: Tools for spatial data.*: National Center for Atmospheric Research
- O'Day WT, Fernandez HR. 1974. *Aristostomias scintillans* (Malacosteidae): A deep-sea fish with visual pigments apparently adapted to its own bioluminescence. *Vision Research* 14(7):545-550.
- O'Shea OR, Thums M, van Keulen M, Kempster RM, Meekan MG. 2013. Dietary partitioning by five sympatric species of stingray (Dasyatidae) on coral reefs. *Journal of Fish Biology* 82(6):1805-1820.
- Packer O, Hendrickson AE, Curcio CA. 1989. Photoreceptor topography of the retina in the adult pigtail macaque (*Macaca nemestrina*). *The Journal of Comparative Neurology* 288(1):165-183.
- Pankhurst PM, Hilder PE. 1998. Effect of light intensity on feeding of striped trumpeter *Latris lineata* larvae. *Marine and Freshwater Research* 49(5):363-368.
- Partridge JC, Archer SN, Lythgoe JN. 1988. Visual pigments in the individual rods of deep-sea fishes. *Journal of Comparative Physiology A* 162(4):543-550.
- Partridge JC, Shand J, Archer SN, Lythgoe JN, Groningen-Luyben WAHM. 1989. Interspecific variation in the visual pigments of deep-sea fishes. *Journal of Comparative Physiology A: Neuroethology, Sensory, Neural, and Behavioral Physiology* 164(4):513-529.
- Peach MB, Marshall NJ. 2009. The comparative morphology of pit organs in elasmobranchs. *Journal of Morphology* 270(6):688-701.
- Peichl L, Behrmann G, Kroeger RH. 2001. For whales and seals the ocean is not blue: a visual pigment loss in marine mammals*. *European Journal of Neuroscience* 13(8):1520-1528.

- Peichl L, Nèmec P, Burda H. 2004. Unusual cone and rod properties in subterranean African mole-rats (Rodentia, Bathyergidae). *European Journal of Neuroscience* 19(6):1545-1558.
- Peterson EH, Rowe MH. 1980. Different regional specializations of neurons in the ganglion cell layer and inner plexiform layer of the California horned shark, *Heterodontus francisci*. *Brain Research* 201(1):195-201.
- Pettigrew JD, Dreher B, Hopkins CS, McCall MJ, Brown M. 1988. Peak density and distribution of ganglion cells in the retinae of microchiropteran bats: implications for visual acuity. *Brain Behav Evol* 32(1):39-56.
- Philp AR, Garcia-Fernandez JM, Soni BG, Lucas RJ, Bellingham J, Foster RG. 2000. Vertebrate ancient (VA) opsin and extraretinal photoreception in the Atlantic salmon (*Salmo salar*). *Journal of Experimental Biology* 203(12):1925-1936.
- Platell ME, Potter IC, Clarke KR. 1998. Resource partitioning by four species of elasmobranchs (Batoidea: Urolophidae) in coastal waters of temperate Australia. *Marine Biology* 131(4):719-734.
- Pribac F, Punt AE, Taylor BL, Walker TI. 2005. Using length, age and tagging data in a stock assessment of a length selective fishery for Gummy Shark (*Mustelus antarcticus*). *J Northw Atl Fish Sci* 35:267-290.
- Prince JD. 2005. Gauntlet fisheries for elasmobranchs – the secret of sustainable shark fisheries. *J Northw Atl Fish Sci* 35:407-416.
- Puckridge M, Last PR, White WT, Andreakis N. 2012. Phylogeography of the Indo-West Pacific maskrays (Dasyatidae, *Neotrygon*): a complex example of chondrichthyan radiation in the Cenozoic. *Ecology and Evolution* 3(2):217-232.
- Pumphrey R. 1948. The theory of the fovea. *Journal of Experimental Biology* 25(3):299-312.
- R Core Team. 2012. R: A language and environment for statistical computing. Vienna, Austria: R Foundation for Statistical Computing.
- R Studio. 2012. R Studio. Boston, MA.
- Ramon y Cajal S. 1972. The structure of the retina: Charles C. Thomas Publisher.
- Ripps H, Weale RA. 1969. Color vision. *Annu Rev Psychol* 20:193-216.
- Roberts BL. 1978. Mechanoreception and the behavior of elasmobranch fishes with special reference to the acustico-lateralis system. In: Hodgson ES, Mathewson RF, eds. *Sensory Biology of Sharks, Skates and Rays: Technical Information Division, Naval Research Laboratory*. p 331-389.
- Rocha FA, Ahnelt PK, Peichl L, Saito CA, Silveira LCL, de Lima SMA. 2009. The topography of cone photoreceptors in the retina of a diurnal rodent, the agouti (*Dasyprocta aguti*). *Visual Neuroscience* 26(02):167-175.
- Röhlich P, Szél Á, Papermaster DS. 1989. Immunocytochemical reactivity of *Xenopus laevis* retinal rods and cones with several monoclonal antibodies to visual pigments. *The Journal of Comparative Neurology* 290(1):105-117.

- Röhlich P, van Veen T, Szél Á. 1994. Two different visual pigments in one retinal cone cell. *Neuron* 13(5):1159-1166.
- Rosenberger LJ. 2001. Phylogenetic relationships within the stingray genus *Dasyatis* (Chondrichthyes : Dasyatidae). *Copeia* 2001(3):615-627.
- Royer F, Fromentin J-M, Gaspar P. 2004. Association between bluefin tuna schools and oceanic features in the western Mediterranean. *Marine Ecology Progress Series* 269:249-263.
- Rudeberg C. 1968. Receptor cells in pineal organ of dogfish *Scyliorhinus canicula* Linne. *Zeitschrift Fur Zellforschung Und Mikroskopische Anatomie* 85(4):521-526.
- Rudeberg C. 1969. Light and electron microscopic studies on pineal organ of dogfish *Scyliorhinus canicula* L. *Zeitschrift Fur Zellforschung Und Mikroskopische Anatomie* 96(4):548-581.
- Sadler JD. 1973. The focal length of the fish eye lens and visual acuity. *Vision Research* 13(2):417-423.
- Schieber NL, Collin SP, Hart NS. 2012. Comparative retinal anatomy in four species of elasmobranch. *Journal of Morphology* 273(4):423-440.
- Schiviz AN, Ruf T, Kuebber-Heiss A, Schubert C, Ahnelt PK. 2008. Retinal cone topography of artiodactyl mammals: Influence of body height and habitat. *The Journal of Comparative Neurology* 507(3):1336-1350.
- Schluessel V, Bennett MB, Bleckmann H, Blomberg S, Collin SP. 2008. Morphometric and ultrastructural comparison of the olfactory system in elasmobranchs: The significance of structure-function relationships based on phylogeny and ecology. *Journal of Morphology* 269(11):1365-1386.
- Schneider CA, Rasband WS, Eliceiri KW. 2012. NIH Image to ImageJ: 25 years of image analysis. *Nat Methods* 9(7):671-675.
- Schultze HP. 1993. Patterns of diversity in the skulls of jawed fishes. In: Hanken J, Hall BK, eds. *The Skull. Vol 2 Patterns of Structural and Systematic Diversity*. Chicago: University of Chicago Press. p 580.
- Schusterman RJ, Balliet RF. 1970. Visual acuity of the harbour seal and the Steller sea lion under water. *Nature* 226(5245):563-564.
- Schwab I, Hart N. 2006. More than black and white. *British journal of ophthalmology* 90(4):406-406.
- Semeniuk CAD, Dill LM. 2005. Cost/benefit analysis of group and solitary resting in the cowtail stingray, *Pastinachus sephen*. *Behavioral Ecology* 16(2):417-426.
- Semeniuk CAD, Dill LM. 2006. Anti-predator benefits of mixed-species groups of cowtail stingrays (*Pastinachus sephen*) and whipsnays (*Himantura uarnak*) at rest. *Ethology* 112(1):33-43.
- Sherry DM, Bui DD, DeGrip WJ. 1998. Identification and distribution of photoreceptor subtypes in the neotenic tiger salamander retina. *Visual Neuroscience* 15(06):1175-1187.
- Shichida Y, Matsuyama T. 2009. Evolution of opsins and phototransduction. *Philosophical Transactions of the Royal Society B: Biological Sciences* 364(1531):2881-2895.
- Siebeck UE. 2004. Communication in coral reef fish: the role of ultraviolet colour patterns in damselfish territorial behaviour. *Animal Behaviour* 68(2):273-282.

- Silveira L, Picanço-Diniz C, Oswaldo-Cruz E. 1989. Distribution and size of ganglion cells in the retinae of large Amazon rodents. *Visual Neuroscience* 2(03):221-235.
- Sillman AJ, Letsinger GA, Patel S, Loew ER, Klimley AP. 1996. Visual pigments and photoreceptors in two species of shark, *Triakis semifasciata* and *Mustelus henlei*. *Journal of Experimental Zoology* 276(1):1-10.
- Simonoff JS. 1996. *Smoothing methods in statistics*: Springer.
- Simpfendorfer CA, Goodreid A, McAuley RB. 2001. Diet of three commercially important shark species from Western Australian waters. *Marine and Freshwater Research* 52(7):975-985.
- Sisneros JA, Tricas TC. 2002. Neuroethology and life history adaptations of the elasmobranch electric sense. *Journal of Physiology- Paris* 96:379-389.
- Sivak JG. 1978. Refraction and accommodations of the Elasmobranch eye. In: Hodgson ES, Mathewson RF, eds. *Sensory Biology of Sharks, Skates and Rays*: Technical Information Division, Naval Research Laboratory. p 107-115.
- Sivak JG, Luer CA. 1991. Optical development of the ocular lens of an elasmobranch, *Raja elantera*. *Vision Research* 31(3):373-382.
- Smeets WJAJ. 1998. Cartilaginous Fishes. In: Nieuwenhuyis R, ten Donkelaar HJ, Nicholson C, eds. *The Central Nervous System of Vertebrates: With Posters. Vol 1*. Heidelberg: Springer. p 544-646.
- Stell WK. 1972. The structure and morphologic relations of rods and cones in the retina of the spiny dogfish, *Squalus*. *Comparative Biochemistry and Physiology Part A: Physiology* 42(1):141-151.
- Stell WK, Witkovsky P. 1973a. Retinal structure in the smooth dogfish, *Mustelus canis*: General description and light microscopy of giant ganglion cells. *The Journal of Comparative Neurology* 148(1):1-31.
- Stell WK, Witkovsky P. 1973b. Retinal structure in the smooth dogfish, *Mustelus canis*: Light microscopy of photoreceptor and horizontal cells. *The Journal of Comparative Neurology* 148(1):33-45.
- Sterling P, Freed M, Smith RG. 1986. Microcircuitry and functional architecture of the cat retina. *Trends Neurosci* 9(0):186-192.
- Stevens JD, Bonfil R, Dulvy NK, Walker PA. 2000. The effects of fishing on sharks, rays, and chimaeras (chondrichthyans), and the implications for marine ecosystems. *ICES Journal of Marine Science* 57(3):476-494.
- Stevenson M. 2009. Investigation of spatial patterns of animal disease. In: EpiCentre I, ed. *Advanced Analysis and Interpretation of Animal Health Data*. Palmerston North, New Zealand. p 97.
- Stone J. 1981. *The whole mount handbook: A guide to the preparation and analysis of retinal whole mounts*: Maitland Publications.
- Stone J, Halasz P. 1989. Topography of the retina in the elephant *Loxodonta africana*. *Brain, Behavior and Evolution* 34(2):84-95.
- Strong WR, Snelson FF, Gruber SH. 1990. Hammerhead shark predation on stingrays- An observation of prey handling by *Sphyrna mokarran*. *Copeia* 1990(3):836-840.

- SurrIDGE AK, Osorio D, Mundy NI. 2003. Evolution and selection of trichromatic vision in primates. *Trends in Ecology & Evolution* 18(4):198-205.
- Szél Á, Lukáts Á, Fekete T, Somogyi J, Petry H, Cooper H, Röhlich P. 1998. Visual pigment coexpression in cone cells. *Med Sci Mon* 4:46-56.
- Takahashi Y, Hisatomi O, Sakakibara S, Tokunaga F, Tsukahara Y. 2001. Distribution of blue-sensitive photoreceptors in amphibian retinas. *FEBS Letters* 501(2-3):151-155.
- Teaf CM, Lewis TC. 1987. Seasonal occurrence of multiple caudal spines in the Atlantic Stingray, *Dasyatis sabina* (Pisces: Dasyatidae). *Copeia* 1987(1):224-227.
- Theiss SM, Collin SP, Hart NS. 2010. Interspecific visual adaptations among Wobbegong Sharks (Orectolobidae). *Brain Behavior and Evolution* 76(3-4):248-260.
- Theiss SM, Davies WIL, Collin SP, Hunt DM, Hart NS. 2012. Cone monochromacy and visual pigment spectral tuning in wobbegong sharks. *Biology Letters* 8(6):1019-1022.
- Theiss SM, Lisney TJ, Collin SP, Hart NS. 2007. Colour vision and visual ecology of the blue-spotted maskray, *Dasyatis kuhlii* Müller & Henle, 1814. *Journal of Comparative Physiology A* 193(1):67-79.
- Tilney F, Warren LF. 1919. The morphology and evolutionary significance of the pineal body. Philadelphia: The Wistar Institute of Anatomy and Biology. 257 p.
- Toyoda J-I, Saito T, Kondo H. 1978. Three types of horizontal cells in the stingray retina: Their morphology and physiology. *The Journal of Comparative Neurology* 179(3):569-579.
- Turner JR, White EM, Collins MA, Partridge JC, Douglas RH. 2009. Vision in lanternfish (Myctophidae): Adaptations for viewing bioluminescence in the deep-sea. *Deep Sea Research Part I: Oceanographic Research Papers* 56(6):1003-1017.
- Ullmann JFP, Moore BA, Temple SE, Fernández-Juricic E, Collin SP. 2012. The retinal wholemount technique: A window to understanding the brain and behaviour. *Brain, Behavior and Evolution* 79(1):26-44.
- Van-Eyk SM, Siebeck UE, Champ CM, Marshall J, Hart NS. 2011. Behavioural evidence for colour vision in an elasmobranch. *The Journal of Experimental Biology* 214(24):4186-4192.
- Vernadakis AJ, Bemis WE, Bittman EL. 1998. Localization and partial characterization of melatonin receptors in amphioxus, hagfish, lamprey, and skate. *General and Comparative Endocrinology* 110(1):67-78.
- Vigh B, Manzano MJ, Zadori A, Frank CL, Lukats A, Rohlich P, Szel A, David C. 2002. Nonvisual photoreceptors of the deep brain, pineal organs and retina. *Histology and Histopathology* 17(2):555-590.
- Vigh-Teichmann I, Korf HW, Nurnberger F, Oksche A, Vigh B, Olsson R. 1983a. Opsin-immunoreactive outer segments in the pineal and parapineal organs of the lamprey (*Lampetra fluviatilis*), the eel (*Anguilla anguilla*), and the rainbow trout (*Salmo gairdneri*). *Cell and Tissue Research* 230:289-307.

- Vigh-Teichmann I, Szel A, Rohlich P, Vigh B. 1990. A comparison of the ultrastructure and opsin immunocytochemistry of the pineal organ and retina of the deep-sea fish *Chimaera monstrosa*. *Experimental Biology* 48:361-371.
- Vigh-Teichmann I, Vigh B, Manzano e Silva MJ, Aros B. 1983b. The pineal organ of *Raja clavata* - Opsin immunoreactivity and ultrastructure. *Cell and Tissue Research* 228(1):139-148.
- Vihhtelic TS, Doro CJ, Hyde DR. 1999. Cloning and characterization of six zebrafish photoreceptor opsin cDNAs and immunolocalization of their corresponding proteins. *Visual Neuroscience* 16(03):571-585.
- Vissers PM, DeGrip WJ. 1996. Functional expression of human cone pigments using recombinant baculovirus: compatibility with histidine tagging and evidence for N-glycosylation. *FEBS Lett* 396(1):26-30.
- Vorobyev M, Osorio D, Bennett ATD, Marshall NJ, Cuthill IC. 1998. Tetrachromacy, oil droplets and bird plumage colours. *Journal of Comparative Physiology A* 183(5):621-633.
- Wagner HJ, Frohlich E, Negishi K, Collin SP. 1998. The eyes of deep-sea fish II. Functional morphology of the retina. *Progress in Retinal and Eye Research* 17(4):637-685.
- Walker T, Moulton P, Dow N, Saddler S. 1994. Stock assessments of the gummy shark, *Mustelus antarcticus* Gunther, in Bass Strait and off South Australia. Hancock, DA (ed):173-187.
- Walker TI. 1998. Can shark resources be harvested sustainably? A question revisited with a review of shark fisheries. *Marine and Freshwater Research* 49(7):553-572.
- Walls GL. 1942. The vertebrate size and its adaptive radiation. New York: Hafner.
- Wang JH, Fisler S, Swimmer Y. 2010. Developing visual deterrents to reduce sea turtle bycatch in gill net fisheries. *Marine Ecology-Progress Series* 408:241-250.
- Warrant E. 2000. The eyes of deep-sea fishes and the changing nature of visual scenes with depth. *Philosophical Transactions of the Royal Society of London Series B: Biological Sciences* 355(1401):1155-1159.
- Warrant EJ. 1999. Seeing better at night: life style, eye design and the optimum strategy of spatial and temporal summation. *Vision Research* 39(9):1611-1630.
- Warrant EJ, Lockett AN. 2004. Vision in the deep sea. *Biological Reviews* 79(03):671-712.
- Watkins WA, Wartzok D. 1985. Sensory biophysics of marine mammals. *Marine Mammal Science* 1(3):219-260.
- West MJ, Slomianka L, Gundersen HJG. 1991. Unbiased stereological estimation of the total number of neurons in the subdivisions of the rat hippocampus using the optical fractionator. *The Anatomical Record* 231(4):482-497.
- West-Eberhard MJ. 1986. Alternative adaptations, speciation, and phylogeny (A Review). *Proceedings of the National Academy of Sciences of the United States of America* 83(5):1388-1392.

- White WT, Platell ME, Potter IC. 2004. Comparisons between the diets of four abundant species of elasmobranchs in a subtropical embayment: implications for resource partitioning. *Marine Biology* 144(3):439-448.
- White WT, Potter IC. 2004. Habitat partitioning among four elasmobranch species in nearshore, shallow waters of a subtropical embayment in Western Australia. *Marine Biology* 145(5):1023-1032.
- Wickham H. 2009. *ggplot2: Elegant graphics for data analysis*. New York: Springer.
- Wickham H. 2011. The Split-Aply-Combine strategy for data analysis. *J Stat Softw* 40(1):1-29.
- Wickham H. 2012. *Stringr: Make it easier to work with strings*. Version 0.6.1.
- Wilson E, Jackson S, Cruwys S, Kerry P. 2007. An evaluation of the immunohistochemistry benefits of boric acid antigen retrieval on rat decalcified joint tissues. *Journal of immunological methods* 322(1):137-142.
- Wilson JF, Dodd JM. 1973. The role of the pineal complex and lateral eyes in the colour change response of the dogfish, *Scyliorhinus canicula* L. *Journal of Endocrinology* 58:591-598.
- Williams H, Schaap AH. 1992. Preliminary results of a study into the incidental mortality of sharks in Gill-nets in two Tasmanian Shark Nursery Areas. *Marine and Freshwater Research* 43(1):237-250.
- Wourms JP. 1977. Reproduction and development in Chondrichthyan Fishes. *American Zoologist* 17(2):379-410.
- Yokoyama S, Yokoyama R. 1996. Adaptive evolution of photoreceptors and visual pigments in vertebrates. *Annual Review of Ecology and Systematics*:543-567.
- Yopak KE, Lisney TJ, Collin SP, Montgomery JC. 2007. Variation in brain organization and cerebellar foliation in chondrichthyans: Sharks and holocephalans. *Brain Behavior and Evolution* 69(4):280-300.
- Yopak KE, Lisney TJ, Darlington RB, Collin SP, Montgomery JC, Finlay BL. 2010. A conserved pattern of brain scaling from sharks to primates. *Proceedings of the National Academy of Sciences of the United States of America* 107(29):12946-12951.
- Yopak KE, Montgomery JC. 2008. Brain organization and specialization in deep-sea chondrichthyans. *Brain Behavior and Evolution* 71(4):287-307.
- Zaviezo T, Grez AA, Estades CF, PÉRez A. 2006. Effects of habitat loss, habitat fragmentation, and isolation on the density, species richness, and distribution of ladybeetles in manipulated alfalfa landscapes. *Ecological Entomology* 31(6):646-656.

Appendix I

Original R Script to extract information from Stereoinvestigator in xml format,

All the electronic files can be found in PLoS One publication:

<http://journals.plos.org/plosone/article?id=10.1371/journal.pone.0093485>

Garza-Gisholt E, Hemmi JM, Hart NS, Collin SP. 2014. A comparison of spatial analysis methods for the construction of topographic maps of retinal cell density. PLoS ONE 9(4):e93485.

```
#####Comparison of spatial analysis methods to construct
topographic cell densities maps. Xml version.
##### Garza-Gisholt, E., Hemmi, J.M., Hart, N.S. and Collin,
S.P.
```

```
###This version extracts the information from an xml file exported from
StereoInvestigator. If you have your information in illustrator or other
graphical program, then run the script to extract information from svg
file
```

```
###We recommend using R Studio especially if you are novice in the use of
R
```

```
### To download R Studio for any platform, go to http://www.rstudio.com.
```

```
### You have to press Ctrl + Enter or Cmd + Enter in Mac to run a command.
```

```
###The symbol "#" before any line in R corresponds to notes. Some commands
that do not need to run every time have the # symbol; if you need to run
them just delete the # and run the command
```

```
### If you have an error message don't panic, instead read what the error
says and try to figure out what is wrong with the file or with the
commands
```

```
### You can always go back and run the commands until you find where the
problem is. Also you can reset the values with the button "Clear All" in
the workspace.
```

```
### To look for help with specific commands you can run the help from R
with ? and the function you want to know for example ?library
```

```
### The first part of the script extracts the information from the xml
file
```

```
### It is good idea to open the xml file to familiarize yourself with the
structure of the file and the data that have to be extracted.
```

```
### The extraction of the information from the xml file was done with the
collaboration of Duncan Temple Lang, Dec 14, 2011. He is the creator of
the XML package for R
```

```
### It is necessary that you save a file with the name retina.xml
exporting the tracing points from Stereo Investigator. This is done by
File->Export tracing-> then name the file and select the xml extension.
```

###we suggest you to use the same contour to count rods, cones and subsampling. We also recommend you to have a directory for each retina and copy this script into it. When you run the script all the images will be saved in the directory where the script is located.

###First set your directory to where you opened the file. A copy of the script should be copied to the directory of your retina, open that copy and then in the menu "Session" select "Set working Directory" the option "To source file location"

The first part recalls the x and y coordinates for the contour, optic nerve and each of the markers. It extracts the "Site" where the marker was placed.

###The packages needed to run the script can be installed for the first time using the next command deleting the "#" sign and pressing ctrl+Enter

```
#install.packages(c("XML", "plyr", "stringr", "spatstat", "ggplot2", "fields", "Akima", "sp", "RColorBrewer", "raster", "maptools"))
```

```
library(XML)
doc = xmlParse("retina.xml")
nsURI = c(n = "http://www.mbfbioscience.com/2007/neuroLucida")
contours = getNodeSet(doc, "//n:contour", nsURI)
contour = getNodeSet(doc, "//n:contour[1]/n:point", nsURI)
opticnerve = getNodeSet(doc, "//n:contour[2]/n:point", nsURI)
markers = getNodeSet(doc, "//n:marker/n:point", nsURI)
getXY =
  function(node)
  {
    as(xmlAttrs(node)[c("x", "y")], "numeric")
  }
}
```

```
contour.xy=as.data.frame(t(sapply(contour, getXY)))
opticnerve.xy=as.data.frame(t(sapply(opticnerve, getXY)))
markers.xy = as.data.frame(t(sapply(markers, getXY)))
```

```
names(markers.xy) = c("x", "y")
names(contour.xy)=c("x", "y")
names(opticnerve.xy)=c("x", "y")
```

###If the retina needs to be rotated, it is better to do it mathematically from the coordinates with the following commands. In this example, the retina is rotated 180 degrees but some cases you will not need rotation. To select a different angle just change "angled=180" to the degrees that you need.

###In that case it is possible to select all the rotate data commands and comment on them using Ctr+Shift+C

###Rotate the data

```
names(markers.xy) = c("xn", "yn")
names(contour.xy)=c("xn", "yn")
names(opticnerve.xy)=c("xn", "yn")
```

```
angled=180
angle=angled/180*pi
rotcentre=c((mean(opticnerve.xy$xn)), (mean(opticnerve.xy$yn)))
```

```
contour.xy[, "xn"] <- contour.xy$xn+rotcentre[1]
contour.xy[, "yn"]<- contour.xy$yn+rotcentre[2]
opticnerve.xy[, "xn"] <- opticnerve.xy$xn+rotcentre[1]
opticnerve.xy[, "yn"]<- opticnerve.xy$yn+rotcentre[2]
markers.xy[, "xn"] <- markers.xy$xn+rotcentre[1]
markers.xy[, "yn"]<- markers.xy$yn+rotcentre[2]
```

```
contour.xy[, "x"] <- contour.xy$xn*cos(angle)-contour.xy$yn*sin(angle)
contour.xy[, "y"]<- contour.xy$xn*sin(angle)+contour.xy$yn*cos(angle)
```

```

opticnerve.xy[, "x"] <- opticnerve.xy$xn*cos(angle)-
opticnerve.xy$yn*sin(angle)
opticnerve.xy[, "y"] <-
opticnerve.xy$xn*sin(angle)+opticnerve.xy$yn*cos(angle)
markers.xy[, "x"] <- markers.xy$xn*cos(angle)-markers.xy$yn*sin(angle)
markers.xy[, "y"] <- markers.xy$xn*sin(angle)+markers.xy$yn*cos(angle)

#####End of rotate

markers.xy$Site = factor(xpathSApply(doc, "//n:marker/n:property",
xmlValue, namespaces = nsURI))
# detach("package:raster")
library(plyr)
library(ggplot2)
library(stringr)

###The ggplot helps to graphically observe if the contours and the markers
are correct. If you do not get any plot, check the xml structure again to
see that you are extracting the right information and you do not have any
errors.

ggplot(data = contour.xy, aes(x, y)) +
  geom_path(data= contour.xy, aes(x, y)) +
  geom_path(data= opticnerve.xy, aes(x, y)) +
  geom_point(data=markers.xy, col = "blue") +
  coord_equal()

###The next commands configure the data to be analysed. The markers are
counted and the x and y coordinates for each Site is obtained by averaging
all the markers.

counts<-data.frame(count(markers.xy, "Site"))
counts$x<-with(markers.xy, tapply(x, Site, mean))
counts$y<-with(markers.xy, tapply(y, Site, mean))

counts$Site= substring (counts$Site, 2)

counts$freq=as.numeric(counts$freq)
counts$Site=as.numeric(counts$Site)
sapply(counts, class)
counts[, "Site"] <- counts$Site+1
counts<-counts[with(counts, order(Site)), ]

### Now that the data frame is complete, the next step is to convert the
number of cells counted to a standard value, in this case the number of
cells per square millimetre. First, you need to change the counting frame
value to the counting frame you used. Remember that this is a variable
number and you have to change it for each retina analysed. In some cases,
for example, when you count photoreceptors it is necessary to express the
result in thousands of cells per square millimetre; in this case you need
to divide the number of cells by 1000 and express the values in the right
units.
counting.frame<- 400*400
counts = transform(counts, cells = (counts$freq *
(1000000/counting.frame)))
counts$cells<- round(counts$cells, digits = 0)
head(counts)

###If you want to manually remove any outliers that you identified before,
it is possible to do this with the command:

#counts<- subset(counts, !(Site %in% c(1,2,3,4)))

###This way it is possible to delete more than one row.

library(spatstat)
library(fields)
library(akima)

```

```

library(RColorBrewer)
library(sp)

###The next part of the script will set up the graphical parameters to
construct the maps. The package spatstat creates a "window" with the
function owin that is the area that will be analysed.
### The contour of the retina should be drawn in anticlockwise direction
and the optic nerve in a clockwise direction. Otherwise, if the owin
command marks an error then the nod direction should be reversed as
"list(x=rev(xp), y=rev(yp))"

xp<- as.vector(contour.xy$x)
yp<- as.vector(contour.xy$y)
xd<-as.vector(opticnerve.xy$x)
yd<-as.vector(opticnerve.xy$y)

retina <- owin(poly=list(list(x=rev(xp), y=rev(yp)), list(x=xd, y=yd)))
par(mar=c(0.6, 0.6, 0.6, 0.6))

###Other possible sources of error are if the contour self intersects. In
this case, it is recommend identifying the nods where it intersects and
deleting them.

plot(retina, hatch=TRUE)

retinamask<-as.mask(retina)

### The next commands set up the graphical parameters for the maps like
the colors, the mask and the scale bar.
### The three color gradients that we use are grey gradient, rainbow
gradient but cutting the darker blues from the spectrum or the heat
gradient (maps published).

bw<-rev(gray.colors(256))
color<-designer.colors( 256, tim.colors(5), x= c(-0.2, 0.2, 0.4, 0.7,
1.2))
heat<-rev(heat.colors(256))

xs<-as.vector(counts$x)
ys<-as.vector(counts$y)
cells<-as.vector(counts$cells)
samcells<-ppp(xs, ys, window=retina, marks=cells)
plot(unmark(samcells), main='', pch=".")
text(samcells, labels=marks(samcells), cex=0.7)

xrange <- range(xp, na.rm=TRUE)
yrange <- range(yp, na.rm=TRUE)
zrange <- c(30, 1.04*max(cells))

###The xbox and ybox ranges are used for the mask of the maps. Sometimes
it does not cover enough area and in that case you can increase the value
that extends the range.

xbox<-xrange + c((if(xrange[1]<0) (0.02*xrange[1]) else (-
0.02*xrange[1])),
(if(xrange[2]>0)
(0.02*xrange[2]) else (-0.02*xrange[2])))

ybox<-yrange + c((if(yrange[1]<0) (0.02*yrange[1]) else (-
0.02*yrange[1])),
(if(yrange[2]>0)
(0.02*yrange[2]) else (-0.02*yrange[2])))

###The scale bar can be modified to millimetres changing unit="mm" and
then reducing the scale to 0.001. The size of the scale bar is specified
with the size at the end of the function.

```

```

scalebar<-function (size, unit="cm", scale=.0001, t.cex= 0.8)
{
  x=0.98*xrange[2]-size
  y=yrange[1]+(0.06*(yrange[2]-yrange[1]))
  xvals=size * c(0, 0.5, 1) + x
  yvals=c(0, 0.01*(yrange[2]-yrange[1]), 0.03*(yrange[2]-yrange[1]),
0.04*(yrange[2]-yrange[1]))+ y
  for (i in 1:2) rect(xvals[i], yvals[3], xvals[i + 2], yvals[4],
col =
"black")
  labels <- c(paste(size*scale, unit))
  text(xvals[c(2)], yvals[1], labels = labels, adj = 0.5,
cex = t.cex)
}

```

```
size<-10000
```

```

mask<-function()
{
  polypath(c(xp, NA, c(xbox, rev(xbox))),
c(y, NA, rep(ybox, each=2)),
col="white", rule="evenodd", lty=0)
  polypath(xd, yd, col="black")
  plot(retina, main='', add=TRUE, lwd=2, scalebar(size))
}

```

###The first map is the Gaussian Kernel Smoother from the spatstat package. The sigma value can be adjusted to the distance between points. If it is omitted, the smoothing kernel bandwidth is chosen by least squares cross-validation.

###It is possible to change graphic parameters in the plot and contour functions. The col= can be changed to bw for black and white. nlevels is the number of contours but levels=c() and allows you to specify what contours will be plotted. For more options look ?contour and ?plot

```

dens<-Smooth.ppp(samcells, sigma = 2000)
plot(dens, main='', col=heat, win=retina, zlim=zrange)
contour(dens, add=TRUE, nlevels=5, asp=1, drawlabels=TRUE, levels=c(50,
100, 150, 200, 250), labcex=0.7, lwd=2)
mask()

```

The second map is the akima linear interpolation. The sequence of values can be modified in the "by=". In the example, a value is calculated every 200 microns. In this case, the command to plot the map is surface.

```

akimalin<-interp(xs, ys, cells,
xrange[2], by=200),
yrange[2], by=200),
linear=TRUE)
surface(akimalin, asp=1, col=heat, axes=FALSE, levels=c(50, 100, 150, 200,
250), ylim=yrange, xlim=xrange, zlim=zrange)
mask()

```

The third and fourth maps both work with the function Tps from the package fields. It gives a krig object that allows predicting values with the function. To calculate values every 200 microns, a grid is created with the following command.

```

grid<- make.surface.grid( list( seq((xrange[1]), (xrange[2]), by=200),
seq((yrange[1]), (yrange[2]), by=200)))
coord<-cbind(xs, ys)

```

The third map is a spline cubic interpolation. It uses the Tps function with a lambda value of 0.

```
kinterp<-Tps(coord, cells, lambda=0)
```

```

look<- predict(kinterp, grid)
out.p<-as.surface( grid, look)
surface(out.p, asp=1, col=heat, axes=FALSE, levels=c(50, 100, 150, 200,
250), zlim=zrange)
mask()

```

The fourth map is the Tps with the generalized cross validation (GCV) smoothing value. It is possible to change the smoothing with the degrees of freedom (df=) in the Tps function.

```

k<-Tps(coord, cells)
look2<- predict(k, grid)
out.p2<-as.surface( grid, look2)
surface(out.p2, asp=1, col=heat, levels=c(50, 100, 150, 200, 250),
axes=FALSE, zlim=zrange)
mask()

```

#####RESIDUALS#####

###The next list of commands will analyse the residuals of the two smoothing models Gks and Tps comparing the observed values to the modelled values. The maps show the position of the variation and the plots show the variation in the x and y axes.

```

library(raster)
library(maptools)

```

```

denssp<-as.SpatialGridDataFrame.im(dens)
densspras <- raster(denssp)

```

```

coords<-as.data.frame(coord)
coords$observed<-counts$cells
coords$tpsinterp<-predict(kinterp)
coords$tps<-predict(k)
coords$gks<-extract(densspras, as.data.frame(coord))

```

```

coords$tps.res<-(abs(coords$observed-coords$tps)*100/(coords$observed))
coords$gks.res<-(abs(coords$observed-coords$gks)*100/(coords$observed))

```

```

par(mar=c(2.5, 2.5, 2.5, 2.5))

```

```

res.tps.diff<-as.vector(coords$tps.res)
kinterp.tps<-Tps(coord, res.tps.diff, lambda=0)
surface(kinterp.tps, asp=1, col=color, axes=TRUE, labcex=0.8,
ylim=yrange, levels=c(10,50,100), zlim=c(-50,800))
mask()

```

```

res.gks.diff<-as.vector(coords$gks.res)
kinterp.gks<-Tps(coord, res.gks.diff, lambda=0)
surface(kinterp.gks, asp=1, col=color, axes=TRUE, labcex=0.8,
ylim=yrange, levels=c(10,50,100))
mask()

```

#####TRANSECTS#####

It is very useful to draw transects in the maps and extract the data from those transects.

```

y= rep(akimalin$y, each = length(akimalin$x))
x= rep(akimalin$x, length(akimalin$y))
z = as.numeric(akimalin$z)
akimalinsp = data.frame(x, y, z)

```

```

coords.long<-as.data.frame(grid)
coords.long$akimalin<-akimalinsp$z
coords.long$tpsinterp<-predict(kinterp, grid)
coords.long$tps<-predict(k, grid)
coords.long$gks<-extract(densspras, grid)
names(coords.long)<-c("xs", "ys", "observed", "tpslinear", "tps", "gks")

```



```

coords.long$xs<- round(coords.long$xs, digits = 0)
coords.long$ys<- round(coords.long$ys, digits = 0)
coords.long<-coords.long[!duplicated(coords.long$gks),]

par(mar=c(1.5, 1.5, 1.5, 1.5))
plot(dens, main='', col=bw, win=retina, bty="n", axes=TRUE)
plot(retina, main='', add=TRUE, lwd=2)

### The next commands help to decide where to place transects. The first
command will provide the coordinates with the highest x and y values. The
tables show the coordinates and the numbers of sites per coordinate.

coords.long[which.max(coords.long$tpslinear), ]

table(coords.long$xs)
table(coords.long$ys)

transectx1.val<--32078
transecty1.val<--19550

transectx1<-subset(coords.long, ys==transectx1.val)
transecty1<-subset(coords.long, xs==transecty1.val)

transectx1.observations<-subset(coords,          ys>=(transectx1.val-500)&
ys<=(transectx1.val+500))
transecty1.observations<-subset(coords,          xs>=(transecty1.val-500)&
xs<=(transecty1.val+500))

plot(dens, main='', col=bw, win=retina, bty="n", axes=TRUE)
plot(retina, main='', add=TRUE, lwd=2)
lines(transectx1$ys~transectx1$xs, lwd=2, col="red")
lines(transecty1$ys~transecty1$xs, lwd=2, col="blue")

ggplot(transectx1, aes(xs)) +
  geom_line(aes(y = observed))+
  geom_point(data=transectx1.observations, aes(y=observed), col =
"blue") +
  scale_x_continuous(limits=c(min(coords$xs), max(coords$xs)), "")+
  scale_y_continuous(limits=c(0, 300), "")+
  theme_bw()+
  theme(legend.position="top")

ggplot(transectx1, aes(xs)) +
  geom_line(aes(y = tpslinear))+
  geom_point(data=transectx1.observations, aes(y=observed), col =
"blue") +
  scale_x_continuous(limits=c(min(coords$xs), max(coords$xs)), "")+
  scale_y_continuous(limits=c(0, 300), "")+
  theme_bw()+
  theme(legend.position="top")

ggplot(transectx1, aes(xs)) +
  geom_line(aes(y = tps))+
  geom_point(data=transectx1.observations, aes(y=observed), col =
"blue") +
  scale_x_continuous(limits=c(min(coords$xs), max(coords$xs)), "")+
  scale_y_continuous(limits=c(0, 300), "")+
  theme_bw()+
  theme(legend.position="top")

ggplot(transectx1, aes(xs)) +
  geom_line(aes(y = gks))+
  geom_point(data=transectx1.observations, aes(y=observed), col =
"blue") +
  scale_x_continuous(limits=c(min(coords$xs), max(coords$xs)), "")+
  scale_y_continuous(limits=c(0, 300), "")+
  theme_bw()+
  theme(legend.position="top")

```

```
#####DISTRIBUTION FUNCTIONS#####
```

```
###It is possible to create the density distribution curves to compare
the functions. Also it is possible to create the empirical cumulative
distribution function (ecdf).
```

```
ggplot(coords.long)+
  geom_density(aes(x=gks, colour="Gks"))+
  geom_density(aes(x=observed, colour="Akimainterp"))+
  geom_density(aes(x=tpslinear, colour="Tpsinterp"))+
  geom_density(aes(x=tps, colour = "Tps"))+
  scale_colour_manual("",values=c("Akimainterp"="black",
  "Tpsinterp"="orange", "Tps"="blue", "Gks"= "red"), breaks =
  c("Akimainterp", "Tpsinterp", "Tps", "Gks"))+
  scale_x_continuous(expand = c(0, 0), limits=c(0, max(coords$tps)) )+
  xlab(expression("cells per " * mm^2))+
  scale_y_continuous(expand = c(0, 0), "")+
  theme_bw()+
  theme(legend.position="top")+
  theme(axis.text.y = element_text(angle = 90, hjust = 1))
```

```
coords.long<-na.omit(coords.long)
```

```
tpsinterpolation.ecdf<-ecdf(coords.long$tpslinear)
akima.ecdf<-ecdf(coords.long$observed)
tps.ecdf<-ecdf(coords.long$tps)
gks.ecdf<-ecdf(coords.long$gks)
```

```
tps.95<-quantile(tps.ecdf, c(.95))
gks.95<-quantile(gks.ecdf, c(.95))
tpsinterp.95<-quantile(tpsinterpolation.ecdf, c(.95))
akima.95<-quantile(akima.ecdf, c(.95))
```

```
table.ecdf.obs<-as.data.frame(coords.long$observed)
names(table.ecdf.obs)<-"cells"
table.ecdf.obs$model<-"akima"
```

```
table.ecdf.tpsint<-as.data.frame(coords.long$tpslinear)
names(table.ecdf.tpsint)<-"cells"
table.ecdf.tpsint$model<-"tpsint"
```

```
table.ecdf.tps<-as.data.frame(coords.long$tps)
names(table.ecdf.tps)<-"cells"
table.ecdf.tps$model<-"tps"
```

```
table.ecdf.gks<-as.data.frame(coords.long$gks)
names(table.ecdf.gks)<-"cells"
table.ecdf.gks$model<-"gks"
```

```
table.ecdf<-rbind(table.ecdf.obs, table.ecdf.tpsint, table.ecdf.tps,
table.ecdf.gks)
```

```
ecdf <- ddply(table.ecdf, .(model), summarize,
              cells = unique(cells),
              ecdf =
ecdf(cells)(unique(cells)))
```

```
ggplot(ecdf, aes(cells, ecdf, color = model)) +
  geom_hline(yintercept=0.95, linetype = "longdash")+
  geom_segment(aes(x=tpsinterp.95, y=0, xend=tpsinterp.95, yend=0.95),
              colour="orange", linetype =
"longdash")+
  geom_segment(aes(x=tps.95, y=0, xend=tps.95, yend=0.95),
              colour="blue", linetype =
"longdash")+
  geom_segment(aes(x=gks.95, y=0, xend=gks.95, yend=0.95),
```

```

                                colour="red",    linetype    =
"longdash")+
  geom_segment(aes(x=akima.95, y=0, xend=akima.95, yend=0.95),
                                colour="black",    linetype    =
"longdash")+
  scale_colour_manual("", values=c("akima"="black",
"tpsint"="orange","tps"="blue", "gks"="red"), breaks = c("akima",
"tpsint", "tps", "gks"))+
  scale_x_continuous(expand = c(0, 0), limits=c(0, max(coords$tps)) )+
  xlab(expression("cells per "*mm^2))+
  scale_y_continuous(expand = c(0, 0), "")+
  theme_bw()+
  theme(legend.position="top")+
  geom_step()+
  theme(axis.text.y = element_text(angle = 90, hjust = 1))

```

###Finally, maps can be exported in pdf, jpeg, tiff and other formats. For pdf:

```

#pdf('name.pdf')
#All the lines of the plots that want to be added (can be more than one
plot)
#dev.off()

```

###For publication, using Arial font is good to follow instructions from the blog: <http://r.789695.n4.nabble.com/How-to-enable-Arial-font-for-postscript-pdf-figure-on-windows-td3017809.html> and additionally the "extrafont" package includes many different types of fonts.

Alternative method to extract information from .svg file

```

## using svg to extract path
library(RCurl)
url <- "P cylindrica 14.svg"

# Parse the file
library(XML)
doc <- htmlParse(url)

# Extract the coordinates, as strings
opticnerve <- xpathSApply(doc, "//polyline[2]", xmlGetAttr, "points")
contour<- xpathSApply(doc, "//polyline[1]", xmlGetAttr, "points")

opticnerve<-sub("[[:blank:]]+$", "", opticnerve)
contour<-sub("[[:blank:]]+$", "", contour)
# Convert them to numbers
opticnerve <- lapply( strsplit(opticnerve, " "), function(u)
  matrix(as.numeric(unlist(strsplit(u, ","))),ncol=2,byrow=TRUE) )
contour<- lapply( strsplit(contour, " "), function(u)
  matrix(as.numeric(unlist(strsplit(u, ","))),ncol=2,byrow=TRUE) )
opticnerve.xy <- as.data.frame(opticnerve)
contour.xy<- as.data.frame(contour)

names(opticnerve.xy) = c("x", "y")
names(contour.xy) = c("x", "y")

library(plyr)
library(stringr)
markers<- xpathSApply(doc, "//text", xmlGetAttr, "transform")
markers<-as.data.frame(strsplit(markers, " +"), rownames=NULL)
markers<-as.data.frame(t(markers))
markers[c(1,2,3,4)]<-list(NULL)
names(markers) <- c("x", "y")
markers$y<- str_extract(markers$y, "[[:digit:]]+.[[:digit:]]+")

```

```

markers$x<- str_extract(markers$x, "[[:digit:]]+.[[:digit:]]+")
markers$y<- as.numeric(markers$y)
markers$x<- as.numeric(markers$x)
markers$cells<- xpathSApply(doc, "//text", xmlValue)
markers$cells<- as.numeric(markers$cells)
sapply(markers, class)

###Mirror image in the y values
contour.xy$y<--(contour.xy$y)
opticnerve.xy$y<--(opticnerve.xy$y)
markers$y<--(markers$y)

###Rotate the data
names(markers) = c("xn", "yn", "cells")
names(contour.xy)=c("xn", "yn")
names(opticnerve.xy)=c("xn", "yn")

angled=210
angle=angled/180*pi

contour.xy[,"x"] <- contour.xy$xn*cos(angle)-contour.xy$yn*sin(angle)
contour.xy[,"y"]<- contour.xy$xn*sin(angle)+contour.xy$yn*cos(angle)
opticnerve.xy[,"x"]<-
                                     opticnerve.xy$xn*cos(angle)-
opticnerve.xy$yn*sin(angle)
opticnerve.xy[,"y"]<-
opticnerve.xy$xn*sin(angle)+opticnerve.xy$yn*cos(angle)
markers[,"x"] <- markers$xn*cos(angle)-markers$yn*sin(angle)
markers[,"y"]<- markers$xn*sin(angle)+markers$yn*cos(angle)

#####End of rotate

rotcentre=c(-310, 50)

contour.xy[, "x"] <- contour.xy$x-rotcentre[1]
contour.xy[, "y"]<- contour.xy$y-rotcentre[2]
opticnerve.xy[, "x"] <- opticnerve.xy$x-rotcentre[1]
opticnerve.xy[, "y"]<- opticnerve.xy$y-rotcentre[2]
markers[, "x"] <- markers$x-rotcentre[1]
markers[, "y"]<- markers$y-rotcentre[2]

library(ggplot2)

ggplot(data = contour.xy, aes(x, y)) +
  geom_path(data= contour.xy, aes(x, y)) +
  geom_path(data= opticnerve.xy, aes(x, y)) +
  coord_equal()

```

Hybrid method to combine thin plate spline with interpolation for a fovea from

Chapter 2

```

fovea<- xpathSApply(doc, "//polyline[3]", xmlGetAttr, "points")
fovea<-sub("[[:blank:]]+$", "", fovea)
fovea<- lapply( strsplit(fovea, " "), function(u)
  matrix(as.numeric(unlist(strsplit(u, ","))), ncol=2, byrow=TRUE) )
fovea.xy<- as.data.frame(fovea)
foveawin<-
  owin(xrange=c(min(fovea.xy$x), max(fovea.xy$x)),
  yrange=c(min(fovea.xy$y), max(fovea.xy$y)))

plot(dens, main='', col=color, win=fovea, xlim=zrange, axes=TRUE)
polygon(fovea.xy$x, fovea.xy$y, lwd=2)

```

```

coord<-cbind(xs, ys)
foveapol<-in.poly(coord, fovea.xy)
fov<-counts
fov$cells[!foveapol] <- NA
fov<-na.omit(fov)

x.fovea<-as.vector(fov$x)
y.fovea<-as.vector(fov$y)
cells.fovea<-as.vector(fov$cells)
samcells.fovea<-ppp(x.fovea, y.fovea, window=foveawin, marks=cells.fovea)
dens.fovea<-smooth.ppp(samcells.fovea, sigma=150)

plot(dens, main='', col=color, win=fovea, zlim=zrange, axes=FALSE)
plot(dens.fovea, main='', col=color, win=retina, zlim=zrange, add=TRUE)
contour(dens, add=TRUE, nlevels=5, asp=1, levels=c(0.5,1,2,3,4),
labcex=0.7, lwd=2)
mask()

grid<- make.surface.grid(list( seq((xrange[1]), (xrange[2]), by=200),
seq((yrange[1]), (yrange[2]), by=200)))
grid<-grid/10
grid<-round(grid, digits=0)
grid<-grid*10

xf<-as.vector(fov$x)
yf<-as.vector(fov$y)
fcells<-as.vector(fov$cells)
fovcoord<-cbind(xf, yf)

fov.xrange <- range(fovea.xy$x, na.rm=TRUE)
fov.yrange <- range(fovea.xy$y, na.rm=TRUE)

fov.xrange
fov.yrange

grid.fov<-make.surface.grid( list( seq((fov.xrange[1]), (fov.xrange[2]),
by=200), seq((fov.yrange[1]), (fov.yrange[2]), by=200)))
grid.fov<-grid.fov/10
grid.fov<-round(grid.fov, digits=0)
grid.fov<-grid.fov*10

coord<-cbind(xs, ys)

kinterp<-Tps(coord, cells, lambda=0)
look<- predict(kinterp, grid)
out.p<-as.surface( grid, look)

surface(out.p, asp=1, col=color, axes=FALSE, labcex=0.8,
levels=c(0.5,1,2,3,4), zlim=zrange)
mask()

k<-Tps(coord, cells)
look2<- predict(k, grid)
out.p2<-as.surface( grid, look2)

out.p2$x<-out.p2$x/10
out.p2$x<-round(out.p2$x, digits=0)
out.p2$x<-out.p2$x*10
out.p2$y<-out.p2$y/10
out.p2$y<-round(out.p2$y, digits=0)
out.p2$y<-out.p2$y*10
kfov<-Tps(fovcoord, fcells, lambda=0)
lookfov<- predict(kfov, grid.fov)
out.pfov<-as.surface( grid.fov, lookfov)

out.pfov$x<-out.pfov$x/100
out.pfov$x<-round(out.pfov$x, digits=0)
out.pfov$x<-out.pfov$x*100
out.pfov$y<-out.pfov$y/100

```

```

out.pfov$y<-round(out.pfov$y, digits=0)
out.pfov$y<-out.pfov$y*100

out.pfov$z[out.pfov$z<2.5]<-2.5

coords.fov<-as.data.frame(grid.fov)
coords.fov<-coords.fov/100
coords.fov<-round(coords.fov, digits=0)
coords.fov<-coords.fov*100
coords.fov$cells<-predict(kfov, grid.fov)
names(coords.fov)<-c("x", "y", "z")
coords.tps<-as.data.frame(grid)
coords.tps$cells<-predict(k, grid)
names(coords.tps)<-c("x", "y", "z")
foveapol2<-in.poly(grid, fovea.xy)
coords.tps$z[foveapol2]<- NA
# coords.tps<-na.omit(coords.tps)

coords.tps$x<-coords.tps$x/100
coords.tps$x<-round(coords.tps$x, digits=0)
coords.tps$x<-coords.tps$x*100
coords.tps$y<-coords.tps$y/100
coords.tps$y<-round(coords.tps$y, digits=0)
coords.tps$y<-coords.tps$y*100

tmp <- merge(coords.tps, coords.fov, all.x = TRUE, by = c('x','y'))
tmp$z.x[!is.na(tmp$z.y)] <- tmp$z.y[!is.na(tmp$z.y)]
tmp$z.y<-NULL
names(tmp)<-c("x", "y", "z")

summary(tmp$z)
# listmp<-split(tmp, 3)
xsp<-as.vector(tmp$x)
yvsp<-as.vector(tmp$y)
z<-as.vector(tmp$z)
tmpcoord<-cbind(xsp, yvsp)

surface(out.pfov, asp=1, col=color, levels=c(3,4,6,7,8, 9, 10),
axes=FALSE, labcex=0.8, zlim=zrange)
surface(out.p2, asp=1, col=color, levels=c(0.5,1,2,3), axes=FALSE,
labcex=0.8, zlim=zrange)

image(out.p2, asp=1, col=color, zlim=zrange, axes=FALSE)
image(out.pfov, asp=1, col=color, add=TRUE, zlim=zrange, axes=FALSE,
bty="n")
contour(out.p2, add=TRUE, nlevels=5, asp=1, levels=c(0.5,1,2, 3),
labcex=0.7, lwd=2)
mask()

```

Script to separate different population of cells (rods, cones of cone subtypes).

```

counts$freq=as.numeric(counts$freq)
counts$Site=as.numeric(counts$Site)
sapply(counts, class)
counts[, "Site"] <- counts$Site+1
counts<-counts[with(counts, order(Site)), ]

counts$type= (sub("1", "rods", counts$type))
counts$type= (sub("3", "rods", counts$type))
counts$type= (sub("4", "rods", counts$type))

```



```

counts$type= (sub("2", "cones", counts$type))
counts$type= (sub("5", "cones", counts$type))
counts$type= (sub("6", "cones", counts$type))

counts.rods<-subset(counts, type == "rods")
counts.cones<-subset(counts, type=="cones")

### Now that the dataframe is complete, the next step is to convert the
number of cells counted to a standard value, in this case is number of
cells per square millimeter. First you need to change the counting frame
value to reflect the counting frame you used in Stereology. Remember that
it is a variable number and you have to change it for each retina
analysed.

rods.counting.frame<-30*30

counts.rods = transform(counts.rods, cells = (counts.rods$freq *
(1000/rods.counting.frame)))
counts.rods$cells<- round(counts.rods$cells, digits = 0)
head(counts.rods)

cones.counting.frame<-100*100

counts.cones = transform(counts.cones, cells = (counts.cones$freq *
(1000/cones.counting.frame)))
counts.cones$cells<- round(counts.cones$cells, digits = 2)
head(counts.cones)

library(spatstat)
library(fields)
library(akima)
library(RColorBrewer)
library(sp)

```

Method to combine and average multiple retinas

```

load("M antarcticus 2 RE GC.rda")
load("M antarcticus 5 RE GC.rda")
load("M antarcticus 6 RE GC.rda")

retina1.contour<-Ma2RE.contour
# retina1.opticnerve<-Ma2RE.opticnerve
retina1.counts<-Ma2RE.GC
retina2.contour<-Ma5RE.contour
retina2.opticnerve<-Ma5RE.opticnerve
retina2.counts<-Ma5RE.GC
retina3.contour<-Ma6RE.contour
retina3.opticnerve<-Ma6RE.opticnerve
retina3.counts<-Ma6RE.GC

library(ggplot2)
ggplot() +
  geom_path(data= retina1.contour, aes(x, y, col="red")) +
#   geom_path(data= retina1.opticnerve, aes(x, y, col="red"))+
  geom_path(data= retina2.contour, aes(x, y, col="blue")) +
  geom_path(data= retina2.opticnerve, aes(x, y, col="blue"))+
  geom_path(data= retina3.contour, aes(x, y, col="orange")) +
  geom_path(data= retina3.opticnerve, aes(x, y, col="blue"))+
  coord_equal()

retina1.contour$ind<-c("retina1")
retina2.contour$ind<-c("retina2")
retina3.contour$ind<-c("retina3")

```

```

retina1.contour$xn<-NULL
retina1.contour$yn<-NULL

retina2.contour$xn<-NULL
retina2.contour$yn<-NULL

retina3.contour$xn<-NULL
retina3.contour$yn<-NULL

retina3.counts$xn<-NULL
retina3.counts$yn<-NULL

contourmax<-rbind(retina1.contour, retina2.contour)

#
xrange<-c(min(contourmax$x), max(contourmax$x))
yrange<-c(min(contourmax$y), max(contourmax$y))
zrange <- c(0, 1.5)

standarize<-function(dataframe)
{
  dataframe$x2<-dataframe$x
  dataframe$y2<-dataframe$y
  dataframe$x<- ifelse(dataframe$x2<0,
(dataframe$x2*xrange[1]/min(dataframe$x2)),
(dataframe$x2*xrange[2]/max(dataframe$x2)))
  dataframe$y<- ifelse(dataframe$y2<0,
(dataframe$y2*yrange[1]/min(dataframe$y2)),
(dataframe$y2*yrange[2]/max(dataframe$y2)))
  output<-dataframe
  return(dataframe)
}

retina1.contour<-standarize(retina1.contour)
retina2.contour<-standarize(retina2.contour)
# retina3.contour<-standarize(retina3.contour)

retina1.counts<-standarize(retina1.counts)
retina2.counts<-standarize(retina2.counts)
# retina3.counts<-standarize(retina3.counts)

retina3.counts$x2<-retina3.counts$x
retina3.counts$y2<-retina3.counts$y

ggplot() +
  geom_path(data= retina1.contour, aes(x, y, col="red")) +
#   geom_path(data= retina1.opticnerve, aes(x, y, col="red"))+
  geom_path(data= retina2.contour, aes(x, y, col="orange")) +
  geom_path(data= retina2.opticnerve, aes(x, y, col="orange"))+
  geom_path(data= retina3.contour, aes(x, y, col="blue")) +
  geom_path(data= retina3.opticnerve, aes(x, y, col="blue"))+
  coord_equal()

retina1.counts$sp<-"retina1"
retina2.counts$sp<-"retina2"
retina3.counts$sp<-"retina3"

```

```

retina1.counts$type<-NULL
retina2.counts$type<-NULL
retina3.counts$type<-NULL

all.data<-rbind(retina1.counts, retina2.counts, retina3.counts)
kruskal.test(sp ~ cells, data = all.data)

ggplot(all.data, aes(x=sp, y=cells)) + geom_boxplot()+
#   geom_boxplot(outlier.shape=NA)+
#   scale_y_continuous(limits = quantile(all.data$cells, c(0.1, 0.9)))+
#   scale_x_discrete(name="")+
#   scale_y_continuous("cells / mm^2")+
#   theme_bw()

library(fields)

grid<- make.surface.grid( list( seq((xrange[1]), (xrange[2]), by=200),
seq((yrange[1]), (yrange[2]), by=200)))

color<-designer.colors( 256, tim.colors(5), x= c(-0.2, 0.2, 0.4, 0.7,
1.2))
heat<-rev(heat.colors(256))

xbox<-xrange + c((if(xrange[1]<0) (0.05*xrange[1]) else (-
0.05*xrange[1])),
(if(xrange[2]>0)
(0.05*xrange[2]) else (-0.05*xrange[2])))

ybox<-yrange + c((if(yrange[1]<0) (0.02*yrange[1]) else (-
0.02*yrange[1])),
(if(yrange[2]>0)
(0.02*yrange[2]) else (-0.02*yrange[2])))

scalebar<-function (size, unit="mm", scale=.001, t.cex= 0.8)
{
  x=0.98*xrange[2]-size
  y=yrange[1]+(0.06*(yrange[2]-yrange[1]))
  xvals=size * c(0, 0.5, 1) + x
  yvals=c(0, 0.01*(yrange[2]-yrange[1]), 0.03*(yrange[2]-yrange[1]),
0.04*(yrange[2]-yrange[1]))+ y
  for (i in 1:2) rect(xvals[i], yvals[3], xvals[i + 2], yvals[4],
col =
"black")
  labels <- c(paste(size*scale, unit))
  text(xvals[c(2)], yvals[1], labels = labels, adj = 0.5,
cex = t.cex)
}

size<-5000

#####
##### Spline smoothed data#####

Tps.ret<-function(dataframe)
{
  color<-designer.colors( 256, tim.colors(5), x= c(-0.2, 0.2, 0.4,
0.7, 1.2))
  grid<- make.surface.grid( list( seq((xrange[1]), (xrange[2]),
by=200), seq((yrange[1]), (yrange[2]), by=200)))
  coord<-cbind(dataframe$x, dataframe$y)
  # kinterp<-Tps(coord, dataframe$cells, lambda=0)
  # kinterp<-Tps(coord, dataframe$cells, df=nrow(dataframe)/2)
  # look<- predict(kinterp, grid)
  # out.p<-as.surface( grid, look)
  # surface(out.p, asp=1, col=color, axes=FALSE, levels=c(100, 200, 300,
400, 500))
  # # mask()
}

```

```

Tps.retina1<-      Tps.ret(retina1.counts)
Tps.retina2<-      Tps.ret(retina2.counts)
Tps.retina3<-      Tps.ret(retina3.counts)

coord<-as.data.frame(grid)
coord$retina1<-predict(Tps.retina1, grid)
coord$retina2<-predict(Tps.retina2, grid)
coord$retina3<-predict(Tps.retina3, grid)

tps.ecdf1<-ecdf(coord$retina1)
tps.ecdf2<-ecdf(coord$retina2)
tps.ecdf3<-ecdf(coord$retina3)

quantile(tps.ecdf1, c(.98))
quantile(tps.ecdf2, c(.98))
quantile(tps.ecdf3, c(.98))

quantile(tps.ecdf1, c(.95))
quantile(tps.ecdf2, c(.95))
quantile(tps.ecdf3, c(.95))

quantile(tps.ecdf1, c(.90))
quantile(tps.ecdf2, c(.90))
quantile(tps.ecdf3, c(.90))

coord<-as.data.frame(grid)
all.data.int<-coord
names(all.data.int)<-c("x", "y")
coord$retina1<-predict(Tps.retina1, grid)
coord$retina2<-predict(Tps.retina2, grid)
coord$retina3<-predict(Tps.retina3, grid)

Tps.Ma2RE.GC<-Tps.retina1
Tps.Ma5RE.GC<-Tps.retina2
Tps.Ma6RE.GC<-Tps.retina3
grid.Ma.GC<-grid
coord.Ma.GC<-coord

save(Tps.Ma2RE.GC, Tps.Ma5RE.GC, Tps.Ma6RE.GC, grid.Ma.GC, coord.Ma.GC,
file="M antarcticus GC.rda")

all.data.int1<-cbind(all.data.int, "cells"=coord$retina1)
all.data.int2<-cbind(all.data.int, "cells"=coord$retina2)
all.data.int3<-cbind(all.data.int, "cells"=coord$retina3)

all.data.int1$retina<-"retina1"
all.data.int2$retina<-"retina2"
all.data.int3$retina<-"retina3"

all.data.int<-rbind(all.data.int1, all.data.int2, all.data.int3)
kruskal.test(retina ~ cells, data = all.data.int)

ggplot(all.data.int, aes(x=retina, y=cells)) + geom_boxplot()+
  geom_boxplot(outlier.shape=NA)+
  scale_y_continuous(limits = quantile(all.data$cells, c(0.1,
0.9)))+
  scale_x_discrete(name="", labels = c("retina1" = "2RE","retina2"
="5RE", "retina3"="6RE", "retina4" ="20LE"))+
#   scale_y_continuous("cells / mm^2")+
  theme_bw()

library(grid)

xd<-as.vector(retina2.opticnerve$x)
yd<-as.vector(retina2.opticnerve$y)

coord$average<-(coord$retina1+coord$retina2+coord$retina3)/3
out.p2<-as.surface(grid, coord$average)

```

```

surface(out.p2, asp=1, col=color, lwd.poly=0.8, levels=c(0.5, 0.7, 0.9),
axes=FALSE, zlim=zrange)
scalebar(size)
polypath(xd, yd, col="black")

names(coord)<-c("x", "y", "retina1", "retina2", "retina3", "average")

GC.Ma.avg<-coord

save(GC.Ma.avg, file="M antarcticus GC average.rda")

tps.ecdf<-ecdf(coord$average)
quantile(tps.ecdf, c(.90))

#####
#####Interpolation#####
#####

Tps.int<-function(dataframe)
{
  color<-designer.colors( 256, tim.colors(5), x= c(-0.2, 0.2, 0.4,
0.7, 1.2))
  grid<- make.surface.grid( list( seq((xrange[1]), (xrange[2]),
by=200), seq((yrange[1]), (yrange[2]), by=200)))
  coord<-cbind(dataframe$x, dataframe$y)
  kinterp<-Tps(coord, dataframe$cells, lambda=0)
}

Tps.int.retina1<- Tps.int(retina1.counts)
Tps.int.retina2<- Tps.int(retina2.counts)
Tps.int.retina3<- Tps.int(retina3.counts)

coord$retina1.int<-predict(Tps.int.retina1, grid)
coord$retina2.int<-predict(Tps.int.retina2, grid)
coord$retina3.int<-predict(Tps.int.retina3, grid)

coord$average.int<-
(coord$retina1.int+coord$retina2.int+coord$retina3.int)/3
out.p3<-as.surface(grid, coord$average.int)
surface(out.p3, asp=1, col=color, lwd.poly=0.8, levels=c(500, 700, 900,
1100), axes=FALSE, zlim=zrange)
scalebar(size)
polypath(xd, yd, col="black")

```

Method to calculate the summation ratio between photoreceptors and ganglion cells.

###This method works for any comparison of different types of cells like rod and cone ratios, and the difference between total cones and LWS cones in Chapter 6

```

load("M antarcticus 2 RE GC.rda")
load("M antarcticus 5 RE GC.rda")
load("M antarcticus 6 RE GC.rda")

retina1.contour.GC<-Ma2RE.contour
# retina1.opticnerve<-Ma2RE.opticnerve
retina1.counts.GC<-Ma2RE.GC
retina2.contour.GC<-Ma5RE.contour
retina2.opticnerve.GC<-Ma5RE.opticnerve
retina2.counts.GC<-Ma5RE.GC

```

```

retina3.contour.GC<-Ma6RE.contour
retina3.opticnerve.GC<-Ma6RE.opticnerve
retina3.counts.GC<-Ma6RE.GC

load("M antarcticus 2 RE cones.rda")
load("M antarcticus 6 RE cones.rda")
load("M antarcticus 20 LE cones.rda")

retina1.contour.cones<-Ma2RE.contour
retina1.opticnerve.cones<-Ma2RE.opticnerve
retina1.counts.cones<-Ma2RE.cones
retina3.contour.cones<-Ma6RE.contour
retina3.opticnerve.cones<-Ma6RE.opticnerve
retina3.counts.cones<-Ma6RE.cones
retina4.contour.cones<-Ma20LE.contour
retina4.opticnerve.cones<-Ma20LE.opticnerve
retina4.counts.cones<-Ma20LE.cones

load("M antarcticus 2 RE rods.rda")
load("M antarcticus 6 RE rods.rda")
load("M antarcticus 20 LE rods.rda")

retina1.contour.rods<-Ma2RE.contour
retina1.opticnerve.rods<-Ma2RE.opticnerve
retina1.counts.rods<-Ma2RE.rods
retina3.contour.rods<-Ma6RE.contour
retina3.opticnerve.rods<-Ma6RE.opticnerve
retina3.counts.rods<-Ma6RE.rods
retina4.contour.rods<-Ma20LE.contour
retina4.opticnerve.rods<-Ma20LE.opticnerve
retina4.counts.rods<-Ma20LE.rods

library(ggplot2)
ggplot() +
  geom_path(data= retina1.contour.GC, aes(x, y)) +
  # geom_path(data= retina1.opticnerve, aes(x, y, col="red"))+
  geom_path(data= retina2.contour.GC, aes(x, y)) +
  geom_path(data= retina2.opticnerve.GC, aes(x, y))+
  geom_path(data= retina3.contour.GC, aes(x, y)) +
  geom_path(data= retina3.opticnerve.GC, aes(x, y))+
  geom_path(data= retina1.contour.cones, aes(x, y)) +
  geom_path(data= retina1.opticnerve.cones, aes(x, y))+
  geom_path(data= retina3.contour.cones, aes(x, y)) +
  geom_path(data= retina3.opticnerve.cones, aes(x, y))+
  geom_path(data= retina4.contour.cones, aes(x, y)) +
  geom_path(data= retina4.opticnerve.cones, aes(x, y))+
  coord_equal()

retina1.contour.GC$ind<-c("retina1.GC")
retina2.contour.GC$ind<-c("retina2.GC")
retina3.contour.GC$ind<-c("retina3.GC")

retina1.contour.cones$ind<-c("retina1.PR")
retina3.contour.cones$ind<-c("retina2.PR")
retina4.contour.cones$ind<-c("retina3.PR")

retina1.contour.GC$xn<-NULL
retina1.contour.GC$yn<-NULL
retina2.contour.GC$xn<-NULL
retina2.contour.GC$yn<-NULL
retina3.contour.GC$xn<-NULL
retina3.contour.GC$yn<-NULL
retina1.contour.cones$xn<-NULL
retina1.contour.cones$yn<-NULL
retina3.contour.cones$xn<-NULL
retina3.contour.cones$yn<-NULL
retina4.contour.cones$xn<-NULL
retina4.contour.cones$yn<-NULL

```



```

contourmax<-rbind(retina1.contour.GC, retina2.contour.GC,
retina1.contour.cones, retina4.contour.cones)

xrange<-c(min(contourmax$x), max(contourmax$x))
yrange<-c(min(contourmax$y), max(contourmax$y))

standarize<-function(dataframe)
{
  dataframe$x2<-dataframe$x
  dataframe$y2<-dataframe$y
  dataframe$x<- ifelse(dataframe$x2<0,
(dataframe$x2*xrange[1]/min(dataframe$x2)),
(dataframe$x2*xrange[2]/max(dataframe$x2)))
  dataframe$y<- ifelse(dataframe$y2<0,
(dataframe$y2*yrange[1]/min(dataframe$y2)),
(dataframe$y2*yrange[2]/max(dataframe$y2)))

  output<-dataframe
  return(dataframe)
}

retina1.contour.GC<-standarize(retina1.contour.GC)
retina2.contour.GC<-standarize(retina2.contour.GC)
retina1.contour.cones<-standarize(retina1.contour.cones)
retina4.contour.cones<-standarize(retina4.contour.cones)
retina1.contour.rods<-standarize(retina1.contour.rods)
retina4.contour.rods<-standarize(retina4.contour.rods)

retina1.counts.GC<-standarize(retina1.counts.GC)
retina2.counts.GC<-standarize(retina2.counts.GC)
retina1.counts.cones<-standarize(retina1.counts.cones)
retina4.counts.cones<-standarize(retina4.counts.cones)
retina1.counts.rods<-standarize(retina1.counts.rods)
retina4.counts.rods<-standarize(retina4.counts.rods)

library(ggplot2)
ggplot() +
  geom_path(data= retina1.contour.GC, aes(x, y)) +
  # geom_path(data= retina1.opticnerve, aes(x, y, col="red"))+
  geom_path(data= retina2.contour.GC, aes(x, y)) +
  geom_path(data= retina2.opticnerve.GC, aes(x, y))+
  geom_path(data= retina3.contour.GC, aes(x, y)) +
  geom_path(data= retina3.opticnerve.GC, aes(x, y))+
  geom_path(data= retina1.opticnerve.cones, aes(x, y))+
  geom_path(data= retina3.contour.cones, aes(x, y)) +
  geom_path(data= retina3.opticnerve.cones, aes(x, y))+
  geom_path(data= retina4.contour.cones, aes(x, y)) +
  geom_path(data= retina4.opticnerve.cones, aes(x, y))+
  coord_equal()

retina1.counts.cones$type<-NULL
retina3.counts.cones$type<-NULL
retina4.counts.cones$type<-NULL

library(fields)

grid<- make.surface.grid( list( seq((xrange[1]), (xrange[2]), by=200),
seq((yrange[1]), (yrange[2]), by=200)))
color<-designer.colors( 256, tim.colors(5), x= c(-0.2, 0.2, 0.4, 0.7,
1.2))

```

```

heat<-heat.colors(256)

xbox<-xrange + c((if(xrange[1]<0) (0.05*xrange[1]) else (-
0.05*xrange[1])),
                (if(xrange[2]>0)
(0.05*xrange[2]) else (-0.05*xrange[2])))

ybox<-yrange + c((if(yrange[1]<0) (0.02*yrange[1]) else (-
0.02*yrange[1])),
                (if(yrange[2]>0)
(0.02*yrange[2]) else (-0.02*yrange[2])))

scalebar<-function (size, unit="mm", scale=.001, t.cex= 0.8)
{
  x=0.98*xrange[2]-size
  y=yrange[1]+(0.06*(yrange[2]-yrange[1]))
  xvals=size * c(0, 0.5, 1) + x
  yvals=c(0, 0.01*(yrange[2]-yrange[1]), 0.03*(yrange[2]-yrange[1]),
0.04*(yrange[2]-yrange[1]))+ y
  for (i in 1:2) rect(xvals[i], yvals[3], xvals[i + 2], yvals[4],
col =
"black")
  labels <- c(paste(size*scale, unit))
  text(xvals[c(2)], yvals[1], labels = labels, adj = 0.5,
cex = t.cex)
}

size<-5000

Tps.ret<-function(dataframe)
{
  color<-designer.colors( 256, tim.colors(5), x= c(-0.2, 0.2, 0.4,
0.7, 1.2))
  grid<- make.surface.grid( list( seq((xrange[1]), (xrange[2]),
by=200), seq((yrange[1]), (yrange[2]), by=200)))
  coord<-cbind(dataframe$x, dataframe$y)
  kinterp<-Tps(coord, dataframe$cells, df=nrow(dataframe)/2)
}

Tps.retina1.GC<- Tps.ret(retina1.counts.GC)
Tps.retina2.GC<- Tps.ret(retina2.counts.GC)
Tps.retina3.GC<- Tps.ret(retina3.counts.GC)

Tps.retina1.cones<- Tps.ret(retina1.counts.cones)
Tps.retina3.cones<- Tps.ret(retina3.counts.cones)
Tps.retina4.cones<- Tps.ret(retina4.counts.cones)

Tps.retina1.rods<- Tps.ret(retina1.counts.rods)
Tps.retina3.rods<- Tps.ret(retina3.counts.rods)
Tps.retina4.rods<- Tps.ret(retina4.counts.rods)

coord.GC<-as.data.frame(grid)
coord.GC$retina1<-predict(Tps.retina1.GC, grid)
coord.GC$retina2<-predict(Tps.retina2.GC, grid)
coord.GC$retina3<-predict(Tps.retina3.GC, grid)

coord.cones<-as.data.frame(grid)
coord.cones$retina1<-predict(Tps.retina1.cones, grid)
coord.cones$retina3<-predict(Tps.retina3.cones, grid)
coord.cones$retina4<-predict(Tps.retina4.cones, grid)

coord.rods<-as.data.frame(grid)
coord.rods$retina1<-predict(Tps.retina1.rods, grid)
coord.rods$retina3<-predict(Tps.retina3.rods, grid)
coord.rods$retina4<-predict(Tps.retina4.rods, grid)

max(coord.rods$retina1)
max(coord.rods$retina3)

```

```

max(coord.rods$retina4)

max(coord.cones$retina1)
max(coord.cones$retina3)
max(coord.cones$retina4)

max(coord.GC$retina1)
max(coord.GC$retina2)
max(coord.GC$retina3)

library(grid)

xd<-as.vector(retinal.opticnerve.cones$x)
yd<-as.vector(retinal.opticnerve.cones$y)

coord.cones$average<-
(coord.cones$retina1+coord.cones$retina3+coord.cones$retina4)/3
out.p<-as.surface(grid, coord.cones$average)
surface(out.p, asp=1, col=color, lwd.poly=0.8, levels=c(1, 1.5, 2),
axes=FALSE, zlim=c(0, 3))
scalebar(size)
polypath(xd, yd, col="black")

coord.rods$average<-
(coord.rods$retina1+coord.rods$retina3+coord.rods$retina4)/3
out.rods<-as.surface(grid, coord.rods$average)
surface(out.rods, asp=1, col=color, lwd.poly=0.8, levels=c(60, 80, 100),
axes=FALSE, zlim=c(0, 140))
scalebar(size)
polypath(xd, yd, col="black")

coord.GC$average<-(coord.GC$retina1+coord.GC$retina2+coord.GC$retina3)/3
out.p2<-as.surface(grid, coord.GC$average)
surface(out.p2, asp=1, col=color, lwd.poly=0.8, levels=c(0.5, 0.7, 0.9),
axes=FALSE)
scalebar(size)
polypath(xd, yd, col="black")

coord.sum<-as.data.frame(cbind(x=coord.GC$V1, y=coord.GC$V2,
gc=coord.GC$average, cones=coord.cones$average, rods=coord.rods$average))

coord.sum$GC<-ifelse(coord.sum$V3<=0, 0.1, coord.sum$V3)
coord.sum$cones<-ifelse(coord.sum$V4<=0, 0.1, coord.sum$V4)
coord.sum$rods<-ifelse(coord.sum$V5<=0, 0.1, coord.sum$V5)

coord.sum$sumation.cones<-coord.sum$cones/coord.sum$GC
coord.sum$sumation.rods<-coord.sum$rods/coord.sum$GC

Ma.out.cones.sum<-as.surface(grid, coord.sum$sumation.cones)
surface(Ma.out.cones.sum, asp=1, lwd.poly=0.8, col=heat, axes=FALSE,
levels=c(1, 2, 3), zlim=c(0, 5))
scalebar(size)
polypath(xd, yd, col="black")

Ma.out.rods.sum<-as.surface(grid, coord.sum$sumation.rods)
surface(Ma.out.rods.sum, asp=1, lwd.poly=0.8, col=heat, axes=FALSE,
zlim=c(0, 400), levels=c(100, 200, 300))
scalebar(size)
polypath(xd, yd, col="black")

```

Method to save plots with Arial font for publications

```
postscript(file="summation rods.ps", horizontal=F,  
           onefile=F,  
           width=4.5, height=3.5,  
           family=c("C:/Arial/arial.afm",  
                   "C:/Arial/arial-Bold.afm",  
                   "C:/Arial/arial-Oblique.afm",  
                   "C:/Arial/arial-BoldOblique.afm"),  
           pointsize=8)  
surface(Ma.out.rods.sum, asp=1, lwd.poly=0.8, col=heat, axes=FALSE,  
        zlim=c(0, 400), levels=c(100, 200, 300))  
scalebar(size)  
polypath(xd, yd, col="black")  
dev.off()
```